

Ecole doctorale n° 432 : Sciences des Métiers de l'Ingénieur

Doctorat ParisTech

T H È S E

pour obtenir le grade de docteur délivré par

l'École nationale supérieure des mines de Paris

Spécialité “Energétique ”

présentée et soutenue publiquement par

Ana RENGEL

le 3 décembre 2010

**Conception et analyses énergétique et environnementale d'un bioréacteur
à microalgues pour la production d'énergie**

**Energy and environmental analyses of a bioreactor
for microalgae culture for energy production**

CONFIDENTIELLE

Directeur de thèse : **Denis CLODIC**

Co-encadrement de la thèse : **Dominique DRON**

Jury

M. Didier MAYER, Directeur de recherche, MINES ParisTech
M. Jocelyn BONJOUR, Professeur, INSA Lyon
M. Pierre NEVEU, Professeur, Université de Perpignan
M. Jean-Paul CADORET, Directeur de laboratoire, IFREMER
M. Denis CLODIC, Directeur de recherche, MINES ParisTech
Mme Dominique DRON, Directrice générale déléguée, IFREMER
M. Joseph SPADARO, Consultant

Président
Rapporteur
Rapporteur
Examineur
Examineur
Examineur
Examineur

ACKNOWLEDGMENTS

It is always difficult to start with...so many people involved in these three years...

First, I would like to thank Denis Clodic and Dominique Dron for giving me the opportunity to belong to the group “Centre Energétique et des Procédés” CEP and the group “Nouvelles Stratégies Energétiques”. I want to thank you for saying “Yes” after the question “Could my thesis be oriented to the design of a photobioreactor for microalgae culture?” I want to thank you for trusting me to develop “a very different subject” under the direction of both groups.

My gratitude is also for all the members of the jury for their interest and taking the time to examine this work.

I would like to thank the members of the group “Nouvelles Stratégies Energétiques”, PhD students and the enterprises for their questions and comments during the presentations. As well, my gratitude is for all the professors who were involved in my academic formation Assaad Zougahib, Dominique Marchio, Khalil El Khoury, Alain Gaunand.

I really want to thank to other people, outside of CEP, who allowed me to be in direct contact with algae: Pierre Metzger, Sebastián Sánchez...

Likewise, I would to thank Anne-Marie Bonnet for her help and guidance in this work and during my stay in CEP.

I would like to say “esker mila” to Peio Arribillaga for ALL his help constructing the two reactors. Thank you for all the advices and for teaching me so many technical things. I also would like to thank Franck Fayolle, David Sousa, Yu Yingzhong, Gérard, and Philippe for all their help.

I would like to thank all the people at CEP. Thank you for all the excellent moments, for smiling and always making the days better...Anthony, Arnaud, Baptiste, Benoît, Bruno, Carol, David D., David S., Erwan, Guillaume G., Guillaume K., Joelle, Julien, Laurent, Marcello, Masha, Olivier, Peio, Rabih, Rocío, Sabine, Sorina, Yannick, Yoann, Yussef, Yingzhong...

Here I would like to include Therese and Jocelyn...thank you for spoiling me!

And here, I don't really know how to start...my family. The word “gracias” is very small to thank to my mom for being my pillar. Thank you for always asking me if everything is all right...cómo va ese trabajo?, for listening to me so many times and always saying “tranquila hija, todo va a salir bien, tu puedes”. Thank to you, mom, I am here presenting this work. I want to say “muchas gracias tías” to my grandaunts (Berenice, Francia, Marucha, Astrid, Marianela, Esperanza, Trina, Anyolina, Cristina) and my grandma, all great women who always gave me the best example and the best company. I want to thank my cousins Brigido and Mariana for always listening me and making all the possible to make me laugh (I think I cannot delete from my mind, you both talking to me, with one glass of whiskey in the hand)...AND I want to say “merci” to a new member of the family (I hope he won't run away for this

phrase) Olivier Mathey, my boyfriend, who had a LOT of patience during the hard times, who advised me, who always tried to make me laugh, who fed me.....merci mi lindo!

I want to thank all my friends around the world. Even though they are far away, many times they supported me, they always trusted me, they always were there to say “come on Ana, you know you always arrive...you just complain” (I thank to all of you even though I didn’t like the last phrase). Muchas gracias a mis amigos Abraham, Adolfo, Augustin, Andrés, Carolina S., Dave, Eduardo, Elif, Gael, Ivona, Johanna F., Jose Alejandro, Jose Luis, Klaybert, Laura O., Laura S., Luciane, Luis Alfredo, Maral, Mariana, Nahir, Nicole, Oscar, Pancho, Rafa, Ricardo, Roselia, Usman, Wilian.....

*Thank to each one of you,
Merci beaucoup à chacun d’entre vous,
Muchas gracias a cada uno de ustedes.....!!!*

Ana A. Rengel I.

Introduction

Les algues sont des organismes photosynthétiques cultivés pour produire des composants utilisables dans l'industrie alimentaire ainsi que dans les industries pharmaceutique et cosmétique. L'intérêt de la culture des microalgues s'est manifesté dans les années 40 pour la production des protéines aux Etats Unis, en Allemagne et au Japon. Dans les années 80, le laboratoire NREL aux Etats Unis a réalisé une étude pour identifier les espèces de microalgues les plus prometteuses pour la production de lipides. Aujourd'hui cette étude est considérée comme le point de départ de la recherche de nouvelles pistes pour la production à grande échelle.

La production d'agro-carburants est aujourd'hui très controversée parce qu'il a été constaté une augmentation de la déforestation des forêts tropicales, de la pollution des eaux et des sols ainsi qu'une augmentation des émissions de gaz tels que le CO₂ et le N₂O. De plus, la compétition avec les terres cultivables s'est récemment accélérée.

Dans ce contexte, l'utilisation de microalgues pour la production d'énergie suscite un intérêt croissant. Les procédés de transformation tels que la digestion anaérobique, la fermentation, la liquéfaction hydrothermale, la pyrolyse et la gazéification sont entre autres étudiés pour l'exploitation de la biomasse algale. La comparaison avec les plantes terrestres permet d'identifier de nombreux avantages parmi lesquels :

- une productivité plus élevée ;
- selon l'espèce, les algues peuvent être cultivées dans des eaux douces ou salées et, potentiellement, dans des eaux usées ;
- les algues peuvent absorber des métaux lourds ; puisque les algues utilisent de l'azote et du phosphore pour se reproduire, elles peuvent traiter les eaux usées ;
- les fumées de centrales électriques peuvent être utilisées dans la culture de microalgues ;
- les systèmes de culture peuvent être installés sur des surfaces qui ne sont pas cultivables, par exemple les zones autour de sites industriels.

Par conséquent, plusieurs recherches ont pour objet de trouver des systèmes de culture à productivités élevées. D'une part, les bassins ouverts du type « raceway » sont les systèmes à ciel ouvert les plus connus et utilisés jusqu'à présent. D'autre part, il existe les photobioréacteurs qui sont des systèmes fermés de géométries variées. Les photobioréacteurs actuels sont à l'échelle de laboratoire et sont capables de produire de la biomasse avec un haut rendement.

Dans ce contexte, l'objectif principal de ce travail est l'étude hydrodynamique de deux photobioréacteurs afin d'évaluer leur faisabilité pour réaliser la culture de microalgues. Parallèlement, les avantages et les inconvénients de la culture de microalgues à grand échelle sont identifiés.

Dans le chapitre I, une synthèse générale de la biologie des algues, de leurs besoins ainsi que l'influence des conditions environnementales est présentée. Cette section présente les avantages et les inconvénients des systèmes de culture les plus prometteurs ainsi que l'intérêt des microalgues pour la production d'énergie.

Le chapitre II présente une étude hydrodynamique d'un réacteur airlift à circulation interne. La caractérisation du réacteur inclut le développement d'un modèle en réalisant un bilan d'énergie et en appliquant un modèle diphasique. Le modèle sera validé et complété par la construction d'un banc d'essais.

Dans le chapitre III, la distribution et la disponibilité de l'énergie lumineuse sont modélisées dans le réacteur airlift. Des modèles biologiques sont utilisés pour estimer la croissance de l'espèce *Chlamydomonas reinhardtii* dans deux situations différentes : culture sous un éclairage en continu et culture soumise à un cycle de lumière/obscurité. Selon les résultats à obtenir, la capacité du réacteur à dégager de l'oxygène et à absorber du CO₂ est également déterminée.

Le chapitre IV présente une étude hydrodynamique d'un réacteur hélicoïdal du type airlift. Un modèle est développé en suivant les mêmes principes que ceux du réacteur airlift étudié précédemment. Ce modèle est validé par une étude expérimentale. Les résultats hydrodynamiques de deux réacteurs sont comparés, ce qui permet d'identifier les limites et les potentiels de ces systèmes.

Finalement, le chapitre V synthétise l'analyse des avantages et des inconvénients de la culture de microalgues à grande échelle. Les impacts environnementaux, notamment liés à l'utilisation des nutriments et la consommation d'eau, sont présentés.

Chapitre I : Les besoins des algues pour la croissance dans des systèmes de culture

Les algues sont des organismes végétaux et aquatiques sans tiges, ni racines, ni feuilles. Dans un milieu liquide, les algues utilisent l'énergie solaire et l'eau pour transformer les composés organiques en biomasse et oxygène, en effectuant le procédé de photosynthèse. On peut différencier les algues en micro et macroalgues, classifiées selon leurs pigments, les caractéristiques de leurs parois et leurs compositions.

Les macroalgues peuvent atteindre des tailles de 60 m dont les plus connues sont les « seaweeds ». Elles sont cultivées pour produire des composants destinés aux industries cosmétique, alimentaire, pharmaceutique, etc. Aujourd'hui les macroalgues sont utilisées dans des procédés de transformation tels que la combustion, la pyrolyse et la digestion anaérobie pour produire de l'énergie, dont le biogaz.

Les microalgues sont des microorganismes qui peuvent habiter dans des eaux salées, douces, saumâtres et même dans des eaux usées. A l'échelle microscopique, elles peuvent être observées séparément ou en formant des colonies. Selon leurs types et les conditions environnementales, les microalgues peuvent produire des quantités importantes de lipides, de sucres et de protéines grâce à la photosynthèse.

La photosynthèse est réalisée par plusieurs réactions qui utilisent l'énergie solaire, le dioxyde de carbone et l'eau pour transformer les composés organiques en biomasse et oxygène. Les pigments récoltent la lumière et les réactions chimiques sont effectuées par les enzymes. L'efficacité photosynthétique est définie comme le rapport entre la biomasse produite et la lumière absorbée. L'efficacité photosynthétique des algues est estimée à 9 %, ce qui est beaucoup plus élevé que celles des plantes terrestres (entre 1 et 2 %).

Pour réaliser la photosynthèse et se reproduire, les algues ont besoin de nutriments, de lumière et de conditions détaillées dans les sections suivantes.

I.1. Les besoins pour la croissance des microalgues

I.1. L'énergie lumineuse

Dans tout le spectre de rayonnement électromagnétique, la photosynthèse est effectuée dans la gamme du « Rayonnement photosynthétiquement actif » entre 400 et 700 nm. Des études montrent que les algues nécessitent entre 6 et 16 photons pour réaliser la photosynthèse (8 photons constitue la référence usuelle des auteurs). L'énergie lumineuse ou l'irradiance est exprimée en *densité de flux de photons* ($\mu\text{mol}/\text{m}^2.\text{s}$).

Les pigments des algues absorbent les photons qui transportent l'énergie lumineuse. Les types de pigments et leurs concentrations définissent la largeur et le positionnement du spectre d'absorption d'une espèce d'algue. Si une culture de microalgues est exposée à la lumière artificielle, la source peut être sélectionnée pour fournir le spectre de lumière correspondant à l'absorption spécifique des pigments.

Selon la densité de flux de photons, les algues ont des réponses différentes. Si on veut étudier l'influence de l'éclairement sur la photosynthèse, on compare le taux de croissance avec la densité de flux de photons, en obtenant une courbe divisée en trois régions. Dans la première région, il existe une relation linéaire entre l'activité photosynthétique et l'éclairement (la lumière est un facteur limitant). Pour des intensités lumineuses plus élevées, on observe un plateau où l'éclairement est saturant ou optimal. Dans la troisième région, les intensités lumineuses sont très élevées et l'activité photosynthétique diminue ; il existe donc une photoinhibition de la photosynthèse.

Si la culture de microalgues est réalisée dans des bassins ouverts ou dans des photobioréacteurs, il existe une atténuation de la lumière le long de la culture en fonction de la concentration de la biomasse. Cette atténuation va affecter la productivité de la culture, d'où l'importance de créer une agitation adéquate dans le système de culture.

I.2. Le dioxyde de carbone

Le dioxyde de carbone est un élément nécessaire pour l'activité photosynthétique. Il est généralement admis qu'un kg d'algues absorbe entre 1,65 et 1,8 kg de CO_2 , car la biomasse des algues est composée de 45 % à 50 % de carbone. Selon plusieurs études expérimentales, une injection d'air enrichi en CO_2 dans la culture favorise la croissance des algues. Des concentrations de CO_2 , de 1 à 15 v/v% ont été testées sur plusieurs espèces telles que *Chlorella vulgaris*, *Monoruphidium minutum*, *Scenedesmus obliquus*, et *Dunaliella tertiolecta*. Actuellement, des études proposent l'utilisation de fumées de centrales électriques pour récupérer principalement le CO_2 et potentiellement d'autres gaz tels que le NO_x et le SO_x . Néanmoins, il faut traiter les fumées avant de les injecter dans la culture (e.g. en contrôlant la température).

I.3. L'eau et les nutriments

L'eau est le milieu liquide qui contient les nutriments nécessaires à la croissance des algues. Selon les espèces de microalgues, le milieu doit présenter certaines conditions de pH, de salinité, de température, et de concentration en nutriments. Le pH dépend principalement de la concentration de carbone existant dans le milieu, en forme de CO_2 , acide carbonique (H_2CO_3), bicarbonate (HCO_3^-), et

carbonate (CO_3^{2-}). La résistance des algues à une salinité élevée dépend de l'espèce. D'autres changent leur composition finale en modifiant leur teneur en lipides, en caroténoïdes ou en acides gras insaturés. Enfin, la plage de température la plus appropriée dépend de l'espèce à cultiver.

Les éléments nutritifs tels que le carbone, l'azote et le phosphore jouent un rôle important dans le métabolisme cellulaire et la composition biochimique des algues. Une altération de concentration de ces nutriments peut provoquer une teneur plus ou moins importante de lipides, de sucres ou des éléments tels que le β -carotène ou l'astaxanthine.

1.2. Les modes de culture – Le taux de croissance et le temps de doublement

D'une façon générale, il existe deux modes d'opération pour réaliser la culture de microalgues : en mode batch ou en continu. En mode continu, un volume de milieu frais est ajouté à la culture tandis que le même volume est retiré de la culture. Dans ce cas, le paramètre le plus important à vérifier est le taux de dilution.

En mode batch, un inoculum de microalgues est ajouté à un volume du milieu. Une fois que la concentration de biomasse désirée est atteinte, la culture est complètement arrêtée et la biomasse est récoltée. Dans ce mode opératoire, on peut observer cinq phases de croissance : *la phase de latence* où les cellules s'adaptent aux nouvelles conditions de culture ; *la phase exponentielle* où les cellules se multiplient très vite en observant une croissance exponentielle en fonction du temps ; *la phase linéaire (ou de ralentissement)* où la vitesse de croissance diminue ; *la phase stationnaire* où la croissance est nulle et finalement *la phase de déclin* où le taux de croissance est négatif, donc il existe une diminution de cellules viables pour la reproduction.

Le taux de croissance est défini comme la variation du nombre de cellules ou le poids de la biomasse dans une période de temps. Jusqu'à présent, différents modèles ont été développés pour estimer le taux de croissance. Le modèle le plus reconnu est basé sur la loi de Monod dans le cas d'une limitation de la croissance par la lumière. Des auteurs expliquent que ce modèle ne prend pas en compte l'effet de la photoinhibition. De ce fait, d'autres modèles sont étudiés actuellement.

Le temps de doublement est défini comme le temps nécessaire à un nombre de cellules pour doubler leur nombre ou leur poids.

1.3. Les systèmes de culture de microalgues

Les systèmes de production de microalgues sont des systèmes artificiels contrôlés afin d'obtenir des productivités élevées. Aujourd'hui, les systèmes de culture de microalgues peuvent être divisés en systèmes de culture à ciel ouvert ou « open ponds » et systèmes fermés appelés photobioréacteurs.

Les systèmes à ciel ouvert sont des bassins peu profonds, principalement classés en deux types : les bassins circulaires et les bassins du type « raceway ». Les bassins du type « raceway » sont formés par une série de canaux où le milieu liquide est agité par une roue à aubes. Ces bassins sont les systèmes les plus utilisés pour réaliser la culture de microalgues, dont les espèces les plus cultivées sont *Dunaliella salina*.

Dans les photobioréacteurs, la culture n'est pas en contact direct avec l'environnement. Actuellement, ils existent plusieurs configurations telles que les réacteurs tubulaires du type serpents, les réacteurs

du type panneaux rigides, les réacteurs du type sacs plastiques (ou « sleeves »), les colonnes à bulles, les réacteurs annulaires et les réacteurs du type « airlift » (colonne à bulles).

Une comparaison entre les systèmes de culture existant jusqu'à présent, permet d'observer que les photobioréacteurs ont des productivités plus élevées puisque :

- le taux de gaz d'injection, les concentrations de nutriments, la température, le pH, l'oxygène dissout sont mieux surveillés et contrôlés
- les microalgues peuvent être maintenues isolées d'autres organismes qui sont considérés comme des contaminants indésirables
- le rapport entre la surface et le volume du réacteur est plus élevé par rapport aux bassins à ciel ouvert, ce qui signifie une plus grande productivité de la biomasse algale
- les pertes d'eau par évaporation sont moins importantes ou nulles en comparaison avec les bassins à ciel ouvert. Dans des systèmes ouverts, l'évaporation provoque des changements dans la composition ionique du milieu liquide.

Cependant, les photobioréacteurs sont plus coûteux que les bassins en raison des matériaux de construction, de leur installation et de leur maintenance. Ils présentent des contraintes par rapport à l'accumulation d'oxygène, abîment des cellules à cause de fortes turbulences et de l'accumulation de biomasse sur les parois du réacteur, en provoquant une diminution de photons transmis vers la culture. Puisqu'une grande variété d'espèces peut être cultivée dans des photobioréacteurs, plusieurs études sont réalisées aujourd'hui pour vaincre ces contraintes.

1.4. La récolte de microalgues et la production d'huile algale

Une fois que la concentration de biomasse désirée est atteinte, la récolte peut être réalisée avec des méthodes telles que la floculation, la sédimentation, la filtration et la centrifugation. Dans la floculation une masse plus dense (des flocons) est formée par l'addition des produits (e.g. polymères) ou par la modification du pH. Dans la sédimentation, la biomasse flottante est déposée par l'action de la gravité, ce qui crée une masse concentrée plus facile à récolter.

La filtration est une méthode de récolte ou de déshydratation dont l'efficacité est fonction de la taille des cellules. Actuellement, il existe plusieurs équipements à grande échelle dessinés pour une certaine plage de tailles de cellules, dont les filtres rotatifs, les filtres à membranes, les filtres-presses à chambres, etc. La centrifugation est une méthode très intéressante pour diminuer l'humidité de la biomasse, cependant les centrifugeuses ont une consommation d'énergie élevée.

Afin d'obtenir de plus grandes efficacités de récoltes, il est nécessaire de combiner les méthodes de récolte et de déshydratation en suivant, par exemple, les procédés dans des stations d'épuration.

Selon les produits de la biomasse algale à exploiter, il est peut être nécessaire de sécher la biomasse une fois récoltée. Pour cela, la biomasse peut être séchée soit en l'exposant au soleil ou en utilisant des équipements de séchage. Le choix va dépendre de la qualité et du prix des produits.

Les lipides contenus dans la biomasse algale présentent un grand intérêt ; ils peuvent, entre autres, être transformés en biodiesel en réalisant une réaction appelée transestérification. Dans cette réaction, les triglycérides réagissent avec du méthanol ou de l'éthanol pour produire des esters d'éthyle (m) et du glycérol. Une tonne d'huile produit une tonne de biodiesel.

L'accumulation des lipides dans les cellules algales dépend de l'espèce ainsi que des conditions d'environnement. Certaines espèces peuvent accumuler jusqu'à 75 % de matière sèche. Selon plusieurs études, il est estimé que certaines espèces algales peuvent produire environ trente fois plus que la palme (~50 t/ha.an). Actuellement, le défi est d'atteindre une production de 100 t/ha.an.

Les lipides sont extraits selon deux méthodes : par pressage mécanique ou par addition de solvants. L'utilisation du solvant n-hexane est la technique la plus classique, avec laquelle on peut extraire 90 % de lipides contenus dans la biomasse.

1.5. Conversion thermochimique et biologique de microalgues

Pour produire de l'énergie, d'autres procédés de conversion peuvent être appliqués sur la biomasse algale. Ces procédés de transformation de la matière organique sont classés en procédés thermochimiques ou biologiques. La gamme thermochimique est composée de la gazéification, de la combustion, de la pyrolyse et de la liquéfaction thermochimique.

La gazéification peut se réaliser en deux modes : la gazéification conventionnelle et la gazéification hydrothermale. La gazéification conventionnelle produit du gaz de synthèse (qui peut être traité pour produire du méthanol) tandis que du méthane est produit à partir de la gazéification hydrothermale. Cette dernière méthode est plus avantageuse puisque la biomasse algale peut être humide et des températures plus faibles sont nécessaires pour la réaction.

Lors de la pyrolyse, la biomasse est transformée en huile, gaz de synthèse et charbon. A ce jour, les résultats montrent que la pyrolyse produit plus d'huile que les matériaux lignocellulosiques, avec un pouvoir calorifique plus élevé.

Actuellement, la liquéfaction thermochimique est la technique de transformation la plus courante, dans le cadre de procédés de conversion thermochimique pour produire une forme d'énergie. L'eau à l'état sous-critique agit comme un solvant qui contribue à la transformation de la matière organique en huile.

En comparant les procédés de transformation thermochimique, la gazéification hydrothermale et la liquéfaction thermochimique sont les procédés les plus intéressants puisqu'ils tolèrent une teneur en eau qui ne nécessite pas de procédés de séchage de la biomasse. Cela permet une diminution de la consommation d'énergie.

Dans la gamme des procédés biologiques, la digestion anaérobie et la fermentation sont les procédés de conversion les plus classiques. La fermentation est réalisée en conditions aérobies en transformant les sucres contenus dans la biomasse en éthanol. La digestion anaérobie utilise les composants des microalgues pour stimuler l'action de bactéries qui dégradent la matière organique en l'absence d'oxygène. Cette dernière est la méthode de conversion biologique la plus utilisée pour transformer la biomasse algale.

Chapitre II: Etude hydrodynamique d'un réacteur airlift à circulation interne pour la culture de microalgues

Les réacteurs du type airlift à circulation interne sont des systèmes utilisés dans des procédés tels que le traitement des eaux usées, la digestion aérobie, les productions d'enzymes, d'antibiotiques et de

protéines. Actuellement, les réacteurs airlifts sont envisagés pour la culture de microalgues. Les réacteurs airlifts occupent moins de surface que les autres réacteurs ; ils présentent un écoulement du liquide et du gaz plus organisé ; l'injection du gaz dans le système favorise les échanges gazeux entre la culture et le milieu ; et les algues sont soumises à un cisaillement inférieur comparativement à d'autres réacteurs où un agitateur mécanique est utilisé.

Parmi toutes les configurations de réacteurs airlifts, le *réacteur airlift à tubes concentriques* a été choisi pour réaliser une étude hydrodynamique. En comparaison avec le réacteur airlift à recirculation externe, ils occupent moins de surface. L'étude comprend la conception d'un modèle hydrodynamique et la construction d'un banc d'essais. Cette étude analyse l'influence de la masse algale sur l'hydrodynamique du réacteur, grâce à l'utilisation de microbilles à différentes concentrations.

L'établissement du modèle hydrodynamique passe par la formulation du bilan entre la force d'entraînement et les pertes de charge dans le réacteur. La force d'entraînement est créée par la pression hydrostatique différentielle entre les compartiments ascendant et descendant, provoquée par l'injection d'air dans le compartiment ascendant. Les pertes de charge sont l'addition des pertes par friction entre le liquide et les parois, des pertes liées au changement de section entre les compartiments descendant et ascendant et des pertes liées au changement de direction du fluide du compartiment ascendant vers le compartiment descendant.

Une phase pseudo-homogène est définie comme une suspension composée de la phase liquide et les microbilles. Cette phase présente des propriétés variables de masse volumique et de viscosité en fonction de la concentration en billes.

Le modèle « Drift flux », qui représente le glissement entre les phases, est employé pour définir une relation entre la rétention du gaz et les vitesses du gaz et de la phase pseudo-homogène. Pour appliquer le modèle « Drift flux », il est nécessaire de déterminer la vitesse terminale des bulles d'air dans le réacteur. Selon Wallis, cette vitesse peut être estimée en réalisant un processus itératif dans lequel il existe quatre régions de vitesses différentes, classées en fonction du diamètre des bulles et du nombre de Reynolds. Le diamètre des bulles est calculé en fonction du diamètre des orifices du distributeur de gaz et des propriétés de la phase pseudo-homogène et du gaz.

Un réacteur airlift à tube concentrique est construit pour valider et compléter le modèle hydrodynamique. Le rapport entre les surfaces des compartiments ascendant et descendant est proche de l'unité. Le volume du travail total est de 21 litres. Un débit d'air, entre 5 et 40 l/min, est injecté dans le cylindre interne à travers un distributeur de gaz composé de 24 orifices de 2 mm de diamètre. Les microbilles, de 10 μm de diamètre, sont ajoutées en concentrations de 0,15 à 5 g/l. Ce banc d'essais permet de mesurer la rétention du gaz dans les compartiments ascendant et descendant, d'observer les régimes de fonctionnement du réacteur et d'étudier l'effet de différentes concentrations de billes sur l'hydrodynamique.

Les premiers résultats expérimentaux montrent qu'à faibles débits d'air, on observe un écoulement homogène de bullage (bubbly flow) dans le compartiment ascendant. A partir d'un débit d'air de 15 l/min, l'écoulement devient turbulent tourbillonnaire (churn turbulent).

D'autre part, on observe trois régimes de fonctionnement du réacteur selon la distribution du gaz.

Dans le régime I, tout le volume du gaz injecté est dégazé vers l'atmosphère tandis que dans le régime II, il existe un petit volume de gaz qui entre vers le compartiment descendant. Dans le régime III, on observe un volume de gaz supérieur dans le compartiment descendant, dont une fraction de gaz circule vers le compartiment ascendant. Le traitement des résultats montre qu'il existe une relation linéaire entre la rétention du gaz et la vitesse superficielle du gaz, validée pour les compartiments ascendant et descendant du réacteur. Cette relation linéaire est maintenue dans les trois régimes du fonctionnement du réacteur.

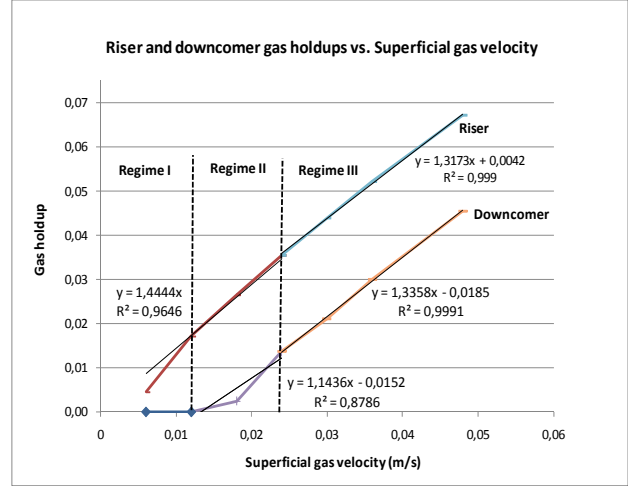


Figure II.1. Rétentions du gaz et régimes de fonctionnement du réacteur

La différence de rétentions de gaz entre les compartiments descendant ($\epsilon_{g,d}$) et ascendant ($\epsilon_{g,r}$) permet d'établir un rapport entre les deux, ce qui est un point discuté dans la littérature scientifique. Actuellement, l'expression la plus utilisée est du type $\epsilon_{g,d} = \alpha \epsilon_{g,r}$ tandis que les résultats expérimentaux montrent qu'il est plus approprié d'utiliser une expression du type $\epsilon_{g,d} = \alpha \epsilon_{g,r} + \beta$. Cette relation démontre qu'il existe une rétention de gaz résiduelle dans le compartiment ascendant même s'il n'existe pas de gaz entraîné vers le compartiment descendant (Equation II.1). Elle est valide pour une vitesse superficielle du gaz supérieure à 0,012 m/s. Cette expression est ensuite incorporée dans le modèle hydrodynamique proposé.

$$\epsilon_{g,d} = 0,817\epsilon_{g,r} - 0,0133 \quad (\text{II.1})$$

La comparaison entre les résultats du modèle et les résultats expérimentaux montre que la déviation la plus importante se produit pour de grands débits d'air. Cet écart peut atteindre 21 % dans le compartiment ascendant.

En étudiant l'influence de solides dans l'hydrodynamique du réacteur, une augmentation de la charge de solides implique une augmentation de la rétention de solides, valide pour tous les débits d'air testés dans cette thèse. D'ailleurs, la rétention de solides dans les deux compartiments du réacteur diminue si la vitesse superficielle du gaz augmente. Cette diminution est plus notable si la concentration de particules est plus élevée.

D'autre part, il est intéressant d'observer la différence de rétentions de solides entre les compartiments ascendant et descendant. En effet, les résultats montrent que, pour toutes les vitesses superficielles (testées) du gaz, la distribution de solides dans le réacteur est homogène puisque la différence de rétentions de solides entre les compartiments est faible.

Par ailleurs, les résultats expérimentaux indiquent que la rétention de gaz varie très peu avec la présence de solides, dans la gamme de concentrations étudiées. En conséquence, une moyenne de la rétention de gaz peut être établie pour chaque débit d'air injecté dans le réacteur. Dans ce cas, il est vérifié que la relation entre la rétention de gaz dans le compartiment ascendant et dans le compartiment descendant est maintenue.

Pour estimer les vitesses de la phase pseudo-homogène, la relation entre la rétention de gaz dans le compartiment ascendant et le compartiment descendant, est introduite dans le modèle hydrodynamique.

Les résultats montrent que les vitesses de la phase pseudo-homogène se situent entre 10 et 30 cm/s. On constate que ces vitesses augmentent avec la vitesse superficielle du gaz. La croissance de vitesse la plus importante a lieu à faibles débits d'air. La raison est l'absence d'air dans le compartiment descendant. Une fois que le débit d'air augmente et que des bulles d'air apparaissent dans le compartiment descendant, la croissance de la vitesse est plus faible. A partir de ces résultats on peut constater qu'il existe une dépendance de type puissance entre la vitesse du liquide et la vitesse superficielle du gaz dans le compartiment ascendant.

En regardant l'effet de la concentration de solides sur les vitesses de la phase pseudo-homogène, on constate que la variation est très faible. En concordance avec les résultats précédents, les vitesses de la phase pseudo-homogène ne sont pas affectées par la présence de solides dans le liquide.

A partir des résultats des vitesses de la phase pseudo-homogène, les temps de séjour de cette phase peuvent être estimés. Ils dépendent également des dimensions du réacteur, notamment de la hauteur du cylindre interne. Dans un réacteur airlift à tubes concentriques et circulation interne, le temps de séjour dans chaque compartiment détermine le temps d'exposition auquel les cellules seront exposées à de plus ou moins fortes intensités lumineuses.

Les valeurs de temps de séjour obtenues sont entre 3 et 8 s dans chaque compartiment. On constate que le temps de séjour dans le compartiment descendant est plus long que celui dans le compartiment ascendant. Le temps de circulation de la phase pseudo-homogène dans le réacteur est estimé entre 6 et 14 s, ce qui est dans la plage des temps de circulation utilisés dans les cultures.

En conclusion, l'injection d'air dans le compartiment ascendant est la force motrice du réacteur. Les rétentions du gaz et les vitesses de la phase pseudo-homogène augmentent si le débit d'air est augmenté dans le compartiment ascendant. D'autre part, on observe que des éventuelles concentrations de cellules entre 0,15 et 5 g/l n'affectent pas les rétentions de gaz, la distribution des solides et les vitesses de la phase pseudo-homogène.

Chapitre III: Modélisation du profil de l'énergie lumineuse dans le réacteur airlift à circulation interne. Estimation de la productivité de la biomasse et du transfert de masse

L'énergie lumineuse est un paramètre essentiel dans la culture de microalgues. Par conséquent, il est nécessaire d'estimer sa disponibilité dans le réacteur, ce qui va dépendre de l'intensité lumineuse, du rayon du PBR et de la concentration de la biomasse. A partir du profil d'énergie, la productivité de la biomasse dans le réacteur peut être estimée, en considérant la lumière comme le seul facteur limitant. Une fois la productivité de la biomasse déterminée, l'intérêt est d'estimer la capacité du réacteur à dégager l'oxygène produit durant la photosynthèse et d'absorber le dioxyde de carbone.

III.1. Estimation du profil de l'énergie lumineuse

Afin d'accroître la disponibilité de l'énergie lumineuse pendant la culture de microalgues, les auteurs parlent de *dilution* de l'énergie dans le réacteur. Le terme *dilution* concerne : 1) la réduction de fortes

intensités lumineuses afin d'éviter l'état de photosaturation ; 2) la dispersion spatiale de l'intensité lumineuse dans tout le réacteur. La dilution de l'intensité lumineuse dans la culture doit éviter la formation de zones obscures où la respiration pourrait avoir lieu. De plus, elle doit garantir une intensité disponible telle que l'efficacité de la photosynthèse soit élevée.

L'intensité lumineuse de compensation (ou l'éclairement de compensation) est définie comme l'énergie minimale disponible dans le réacteur sous laquelle la respiration ne se produit pas. Dans ce cadre, la *fraction éclairée de travail* (γ) est alors définie comme le rapport entre la surface ayant des éclairagements plus élevés que l'intensité lumineuse de compensation et la surface totale. En conséquence, l'intérêt est d'avoir une fraction de travail éclairée égale à 1, dont la disponibilité de la lumière pour la photosynthèse est la plus efficace.

L'énergie lumineuse dans le réacteur airlift à tubes concentriques est estimée grâce au modèle de deux flux (Two Flux method), appliqué par Takache et al. à des photobioréacteurs cylindriques. Ce modèle prend en compte l'atténuation de la lumière grâce à la concentration de la biomasse ainsi que les phénomènes d'absorption et de diffusion (scattering). Dans cette étude, le modèle est appliqué pour la culture de *Chlamydomonas reinhardtii* dans le réacteur airlift à tubes concentriques. Les propriétés optiques de cette algue ont été extraites de l'étude expérimentale réalisée par Takache et al.

Pour appliquer le modèle, l'hypothèse est faite que le rayonnement est isotrope, en négligeant la distribution angulaire de la lumière sur la paroi du réacteur. Le système d'éclairage placé autour du réacteur fournit des intensités lumineuses homogènes sur les parois du réacteur. Les intensités des éclairagements utilisées sont 50, 110, 500 et 1000 $\mu\text{mol}/\text{m}^2\text{s}$.

Les premiers résultats montrent que, pour un éclairage incident, l'intensité lumineuse disponible diminue, d'une manière non linéaire, de la paroi de réacteur jusqu'au centre. Cette intensité diminue ainsi avec l'augmentation de la concentration de la biomasse. On constate que les intensités lumineuses disponibles sont plus élevées dans le compartiment descendant que dans le compartiment ascendant. Le placement d'un cylindre à l'intérieur de la colonne provoque une atténuation importante de la lumière. La transmittance du matériel polyméthacrylate de méthyle est de 49 % ; en conséquence la paroi interne du compartiment ascendant reçoit la moitié de l'intensité qui arrive à la paroi externe.

Dans le compartiment ascendant, pour tous les éclairagements supposés, il existe une zone obscure qui devient plus grande si les concentrations de la biomasse sont plus élevées. L'absorption et la diffusion de la lumière sont plus importantes si la concentration de la biomasse est plus élevée. A une concentration déterminée, les zones obscures sont plus petites si l'éclairage incident est plus élevé. Par conséquent, la fraction éclairée du travail diminue pendant la culture de microalgues en passant d'une valeur supérieure à une valeur inférieure à 1 ($\gamma > 1$ à $\gamma < 1$).

L'atténuation de la lumière dans le compartiment ascendant est plus importante que dans le compartiment descendant. Par ailleurs, l'utilisation d'un cylindre dans la colonne, afin de former le réacteur à tubes concentriques, provoque une forte atténuation de la lumière entrant dans le compartiment ascendant.

Si on regarde le profil de la lumière disponible en fonction de la biomasse, pour un éclairage de 1 000 $\mu\text{mol}/\text{m}^2\text{s}$, elle est complètement atténuée pour une concentration de biomasse de 0,5 g/l.

A partir de ces résultats, on peut conclure qu'il est plus intéressant que le diamètre hydraulique soit plus grand dans le compartiment descendant que dans le compartiment ascendant.

Pour établir un cycle de lumière/obscurité dans le réacteur, le cylindre intérieur peut être construit avec des matériaux opaques. Des études réalisées sur la culture de microalgues montrent qu'il est intéressant d'établir un cycle de lumière/obscurité dans le réacteur pour réparer les dommages apportés aux algues par de fortes intensités de lumière.

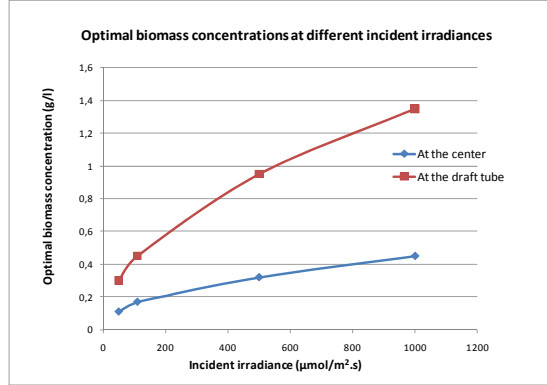


Figure III.1. Concentrations optimales de biomasse

Pour des cultures mises soit sous une exposition continue de lumière, soit sous un cycle de lumière/obscurité, il est pertinent d'estimer les concentrations de biomasse optimales pour éviter l'apparition de zones obscures dans les compartiments éclairés. Les résultats montrent que les concentrations de biomasse optimales sont plus élevées dans le cas où les algues sont soumises à un cycle de lumière/obscurité que dans le cas contraire (Figure III.1).

En garantissant une intensité de lumière locale supérieure à l'intensité lumineuse de compensation, une augmentation de la concentration de la biomasse pourrait conduire à une augmentation de la productivité de la biomasse. Cependant, ce sont des résultats qualitatifs qui ne tiennent pas compte de l'effet que la respiration pourrait produire dans le compartiment ascendant, en réduisant les productivités de biomasse.

III.2. Estimation de la productivité de biomasse

La productivité de la biomasse est définie comme la quantité de biomasse produite par unité de volume et par une unité de temps. Dans cette étude, la productivité de la biomasse est estimée en supposant que la lumière est le seul facteur limitant dans la culture. Cette productivité dépend alors du profil de l'énergie lumineuse dans le réacteur. Deux modèles biologiques sont utilisés : le premier est basé sur la loi de Monod tandis que le deuxième est basé sur le modèle proposé par Cornet et Dussap.

La loi de Monod prévoit le taux de croissance en fonction du taux de croissance maximal (μ_{\max}), la constante de demi-saturation (K_j) et l'intensité lumineuse (G) (Equation II.1).

$$\mu = \mu_{\max} \cdot \frac{G}{G + K_j} \quad (\text{III.1})$$

Cependant, la productivité de la biomasse de *Chlamydomonas reinhardtii* est définie à partir de la loi de Monod en considérant la concentration de la biomasse (Equation III.2).

$$P_x(C_x, r) = C_x \mu_{\max} \frac{G(C_x, r)}{G(C_x, r) + K_j} \quad (\text{III.2})$$

Ainsi, la productivité de la biomasse moyenne est estimée à partir de l'intégration de l'Equation III.2 sur les compartiments descendant et ascendant. L'intensité lumineuse locale disponible est déterminée selon les concentrations de la biomasse et les éclairagements incidents.

Les résultats montrent que les productivités dans le compartiment ascendant ont des valeurs maximales qui sont plus grandes si l'éclairement radiant est augmenté. Ensuite, il existe une forte atténuation de la productivité due à une augmentation de la concentration de la biomasse (Figure III.2).

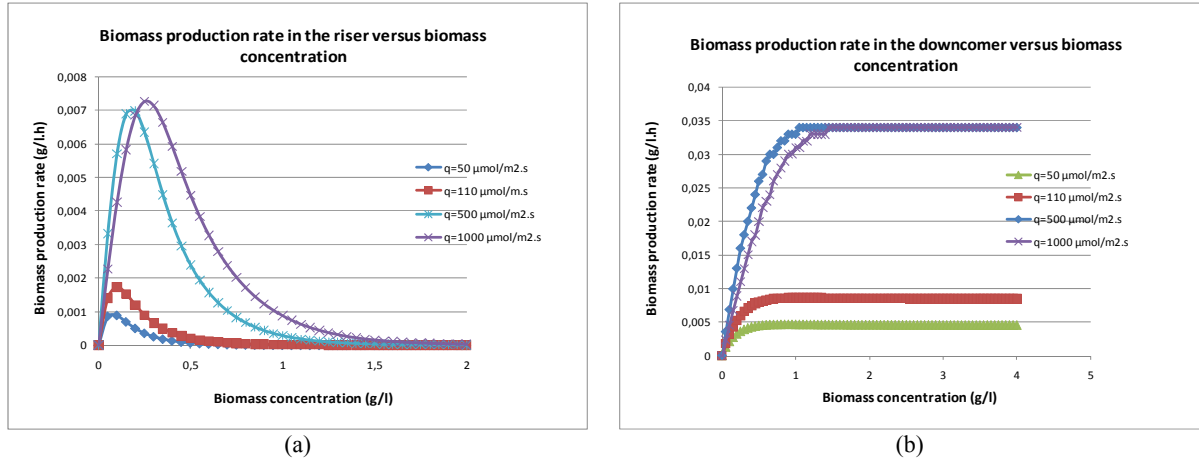


Figure III.2. Productivité de la biomasse en fonction de la concentration a) dans le compartiment ascendant ; b) dans le compartiment descendant

A une concentration de 0,5 g/l, la productivité devient nulle pour des éclairagements incidents de 50 et 110 µmol/m².s tandis que la productivité devient nulle pour une concentration de 1,5 g/l et des éclairagements incidents de 500 et 1000 µmol/m².s. Dans le compartiment descendant, les productivités atteignent des valeurs constantes à des concentrations similaires à partir desquelles les productivités sont complètement atténuées dans le compartiment ascendant.

Si on évalue les productivités pour les concentrations de biomasse optimales obtenues précédemment, pour le cas où la culture est exposée à un éclairage en continu, les productivités totales sont dans la plage entre 3 et 23 mg/l.h. Le temps de culture pour atteindre les concentrations optimales est dans l'intervalle de 28 à 51 heures. Dans le cas où il est assumé un cycle de lumière/obscurité, les productivités totales se situent entre 3,9 et 33 mg/l.h. Le temps de culture pour atteindre les concentrations optimales est entre 50 et 95 heures. Ces temps de culture sont des valeurs basses en comparaison avec les études expérimentales où la culture de microalgues a été réalisée dans une durée moyenne de 15 jours.

D'un autre côté, le modèle de Cornet et Dussap propose une expression de la productivité équivalente à celle de Monod, en conservant une tendance hyperbolique (Equation III.3)

$$P_x(C_x, r) = C_x \rho_m K_j \phi E_a \frac{G(C_x, r)}{G(C_x, r) + K_j} \quad (\text{III.3})$$

Ici, les propriétés optiques des *Chlamydomonas reinhardtii* sont prises en compte, telles que le rendement énergétique maximum pour la conversion des photons (ρ_m), le rendement quantique de masse obtenu en effectuant une analyse stœchiométrique de la photosynthèse (ϕ), le coefficient massique d'absorption (E_a) et la constante de demi-saturation (K_j).

En appliquant le modèle de Cornet et Dussap dans les deux sections du réacteur, on constate que les productivités en fonction de la concentration de la biomasse, ont la même tendance que celle observée en utilisant la loi de Monod. Elles sont aussi complètement atténuées à une concentration de 1,5 g/l. Par contre, les productivités sont plus élevées que celles obtenues avec la loi de Monod.

Si on évalue les productivités pour les concentrations de biomasse optimales obtenues précédemment, pour le cas où la culture est exposée à un éclairage en continu, les productivités totales se situent entre 7,5 et 46 mg/l.h. Dans l'hypothèse d'un cycle de lumière/obscurité, les productivités totales se situent entre 9,5 et 66 mg/l.h. Puisque les productivités sont plus élevées, le temps de culture pour obtenir les concentrations optimales est de l'ordre de 12 heures.

Enfin on constate qu'en appliquant les deux modèles biologiques, les productivités de la biomasse sont du même ordre de grandeur que celles observées dans des cultures réalisées en photobioréacteurs, aujourd'hui.

III.3. Détermination des rendements et productivités du réacteur

Le rendement de la photosynthèse est défini comme l'énergie stockée dans la biomasse produite au cours de la culture par unité d'énergie de la lumière absorbée. L'énergie stockée est le produit entre la productivité de la biomasse et l'enthalpie de la biomasse sèche. La lumière absorbée est la moyenne dans chaque section du réacteur, ce qui est fonction de la concentration de la biomasse, l'intensité lumineuse disponible et le coefficient massique d'absorption.

Les résultats montrent que le rendement photosynthétique diminue lorsque les intensités lumineuses incidentes sont accrues. La productivité de la biomasse n'augmente pas à la même vitesse que l'énergie moyenne absorbée. Le rendement photosynthétique le plus élevé se produit dans le compartiment ascendant (18 %) tandis que la valeur la plus élevée du rendement photosynthétique dans le compartiment descendant est de 14 %. Si on évalue le rendement photosynthétique pour les concentrations de biomasse optimales, on obtient des valeurs entre 11,5 % et 15,4 % dans le compartiment ascendant et entre 2,2 % et 12,2 % dans le compartiment descendant. Ces résultats sont plus élevés que ceux obtenus dans des études expérimentales (les plus courants sont 3, 4 et 6 %).

D'un autre côté, il est également intéressant d'estimer la *productivité surfacique* ainsi que la *productivité en surface éclairée*, qui sont des concepts liés à la géométrie du réacteur et la productivité de la biomasse. Ainsi, la productivité surfacique est définie comme le rapport entre la productivité de la biomasse et la surface occupée par le réacteur. La productivité en surface éclairée est le rapport entre la productivité de la biomasse et la surface éclairée du réacteur. Le tableau III.1 présente les résultats obtenus pour une culture de *Chlamydomonas reinhardtii* soumise à un éclairage en continu (24 heures), en appliquant le modèle de Cornet et Dussap.

Tables III.1. Productivités surfaciques et productivités en surfaces éclairées

Intensité lumineuse ($\mu\text{mol}/\text{m}^2.\text{s}$)	Concentration de biomasse optimale (g/l)	Productivité surfacique ($\text{g}/\text{m}^2.\text{d}$)	Productivité en surface éclairée ($\text{g}/\text{m}^2.\text{d}$)
50	0,11	4,88	7,87
110	0,15	9,29	15
500	0,32	23	37
1000	0,45	29,7	48

Les productivités surfaciques sont du même ordre de grandeur que celles observées dans des photobioréacteurs tubulaires, hélicoïdaux ou bassins ouverts.

Par ailleurs, l'estimation de la *surface spécifique éclairée* est un autre paramètre important dans la caractérisation du réacteur. Elle est définie comme le rapport entre la surface éclairée et le volume de

travail. Dans le cas du réacteur airlift, elle est égale à 20 1/m, ce qui est une valeur basse en comparaison avec les photobioréacteurs tubulaires-horizontaux.

Si toutes ces définitions sont rassemblées pour construire et caractériser un photobioréacteur, le défi est de disposer d'un système avec une grande surface éclairée, une productivité en volume élevée alors que la surface occupée par le système est petite.

III.4. Echange de matière dans un réacteur airlift à circulation interne : étude expérimentale et de modélisation

Dans un réacteur airlift à circulation interne, la circulation du liquide est produite par une injection de gaz au fond du réacteur. Le gaz injecté, principalement de l'air ou de l'air enrichi en CO₂, est en contact direct avec le liquide, donc il existe un échange de matière entre les deux phases. Cet échange est proportionnel à la différence des concentrations de solutés entre les phases, tels que le CO₂ et O₂, et aussi proportionnel au coefficient de transfert global (k) et l'aire d'interface par unité de volume (a)

$$\text{Taux de transfert de matière} = k.a.(\text{différence de concentration}) \quad (\text{III.4})$$

Pour déterminer le flux de matière entre les phases liquide et gazeuse, *la théorie du double film* est appliquée dans cette étude. Cette théorie considère que la résistance au transfert de masse est localisée dans deux films stationnaires situés de chaque côté de l'interface et, qu'à l'intérieur de chacun d'eux, l'échange se produit par diffusion moléculaire.

III.4.1 Détermination du coefficient volumique de transfert

Pour appliquer la théorie du double film, il est nécessaire de recourir à la détermination des coefficients de transfert globaux. On assume que le coefficient de transfert global est égal à celui du côté liquide puisque la résistance au transfert de matière du côté gaz est petite comparativement à celle du côté liquide.

Dans une première approximation, l'aire d'interface par unité de volume est estimée à partir de la rétention du gaz et du diamètre moyen des bulles d'air. Puisque la rétention du gaz est fonction du débit d'air injecté dans le réacteur, l'aire d'interface par unité de volume est plus élevée (entre 18 et 155 1/m environ) dans le compartiment ascendant que dans le compartiment descendant (entre 0 et 100 1/m). Ensuite, le coefficient de transfert du côté liquide est déterminé à partir de trois nombres adimensionnels : le nombre de Sherwood (Sh), de Schmidt (Sc) et de Grashof (Gr), ce qui résulte en coefficients dans la plage entre $6,2 \times 10^{-5}$ to $2,6 \times 10^{-4}$ m/s.

Egalement, le produit du coefficient de transfert global liquide et l'aire d'interface par volume, est appelé le coefficient volumique de transfert ($k_L a$). Dans cette étude, il est déterminé théoriquement en utilisant des expressions proposées dans la littérature. Lamon et Scott expriment le produit $k_L a$ en fonction du nombre de Schmidt, les propriétés du liquide et la vitesse superficielle du gaz. Bello propose d'estimer $k_L a$ à partir de la puissance par unité de volume du liquide et le rapport entre les surfaces des compartiments descendant et ascendant. Van' Riet et Tramper formulent $k_L a$ en fonction de la vitesse superficielle du gaz. Les résultats de $k_L a$, obtenus à partir de ces corrélations et en fonction de la vitesse superficielle du gaz, montrent un écart élevé, entre 49 et 87,5 %.

Par ailleurs, le coefficient de transfert d'oxygène $k_L a$ est déterminé expérimentalement en utilisant la méthode en régime transitoire. Premièrement, l'azote est injecté dans le réacteur pour dégager l'oxygène dissout. Ensuite, l'évolution d'oxygène dissout est mesurée une fois que l'air est injecté à un débit fixe. Les premiers résultats montrent que le taux de dissolution d'oxygène dans l'eau est élevé lorsque le débit d'air est augmenté dans le compartiment ascendant.

A partir de ces résultats, on peut estimer le produit $k_L a$ d'oxygène dans le compartiment ascendant, en réalisant un bilan de matière sur l'oxygène en phase liquide (Equation III.5) et la loi de Henry. Les résultats obtenus sont entre 0,0024 et 0,02 1/s (8,64 et 72 1/h).

$$\frac{dC_{O_2,L}}{dt} = (k_L a)_{O_2} (C_{O_2}^* - C_{O_2,L}) \quad (III.5)$$

Le produit $k_L a$ d'oxygène dans le compartiment descendant est calculé théoriquement en assumant la même valeur du coefficient de transfert global que dans le compartiment ascendant. Alors, le produit $k_L a$ est estimé à partir de l'aire d'interface par volume dans le compartiment descendant. Les résultats sont entre 0 et 0,014 1/s (0 et 50,4 1/h).

A partir des résultats expérimentaux, les corrélations suivantes sont obtenues :

$$k_L a = 0.487 (V_{sg})^{1.035} \quad (III.6)$$

$$(k_L a)_r = 9.10^{-5} (P_g / V_L)^{1.035} \quad (III.7)$$

La figure III.3 montre les valeurs des coefficients volumiques de transfert d'oxygène obtenues à partir des corrélations mentionnées précédemment et les résultats expérimentaux.

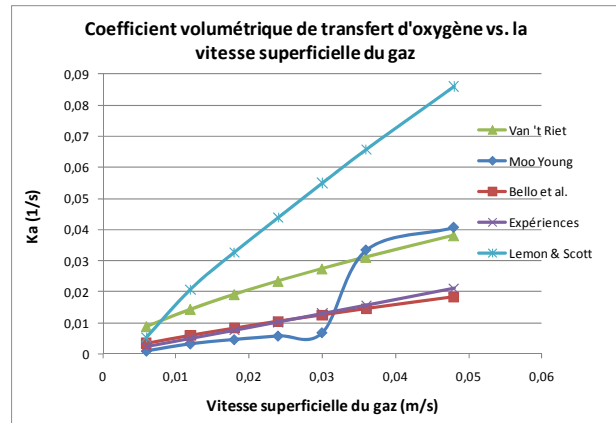


Figure III.3. Coefficients volumiques de transfert d'O₂

En comparant les valeurs des coefficients volumiques de transfert d'oxygène, la corrélation la plus adaptée à des résultats expérimentaux est celle proposée par Bello et al., avec un écart maximal de 37 %.

Par ailleurs, la puissance donnée par l'injection du gaz par unité de volume du liquide (Equation III.7) est estimée à partir de l'expansion isotherme du gaz le long de la hauteur du compartiment ascendant. Les valeurs estimées varient entre 24 et 192 W/m³ pour tous les débits d'air testés (de 5 à 40 l/min).

D'autre part, les valeurs des coefficients volumiques de transfert d'oxygène sont mesurées dans le réacteur en ajoutant deux concentrations de particules (2 et 5 g/l). La déviation maximale est de 10 %. On remarque que les coefficients sont peu affectés par la gamme de concentrations de particules testées. D'autres études montrent qu'il faut ajouter des concentrations plus élevées pour observer une diminution du produit $k_L a$.

L'évolution de l'oxygène dissout dans le réacteur est modélisée en réalisant un bilan de matière et en prenant en compte les coefficients volumiques de transfert d'oxygène obtenus expérimentalement.

$$\frac{dC_{O_2,i}}{dt} = D_z \frac{d^2 C_{O_2,i}}{dz^2} - V_L \frac{dC_{O_2,i}}{dz} + (k_L a)_{O_2} (C_{O_2}^* - C_{O_2,L}) \quad (\text{III.8})$$

(1) (2) (3) (4)

Le bilan de matière prend en compte la diffusion axiale (2) et le transport convectif du soluté (3). Le terme (4) représente le transport d'oxygène entre les phases à partir de l'application de la théorie du double film. L'écoulement de la phase gazeuse est considéré de type *piston*, où la dispersion est négligée, tandis que la phase liquide est caractérisée par le nombre de Peclet. Le nombre de Peclet représente le rapport entre le transfert par convection et le transfert par diffusion, en étant fonction de la vitesse du liquide, la hauteur de la colonne et le coefficient de diffusion axiale.

Le coefficient de diffusion axiale (D_z) dans le compartiment ascendant est calculé à partir de différentes corrélations qui établissent D_z en fonction de la géométrie du réacteur, les propriétés des fluides et la vitesse superficielle du gaz. En appliquant les corrélations avec les conditions du système, les valeurs des coefficients de diffusion axiale sont telles qu'ils ne peuvent pas être négligés. Parmi les cinq corrélations, celle proposée par Sanchez et al. est utilisée dans cette étude pour être la plus récente.

Par ailleurs, l'hypothèse d'un écoulement de type piston dans le compartiment descendant est faite car le nombre de Peclet est élevé. En effet, les vitesses superficielles du gaz sont très faibles dans le régime II, puisque les bulles ne semblent pas se déplacer par rapport à la paroi du réacteur.

En comparant les résultats de la modélisation avec les résultats expérimentaux, la déviation la plus faible (10 %) est observée pour des débits d'air de 5 et 10 l/min. Pour des débits d'air plus élevés, une déviation de 20 % est observée après l'injection d'air tandis qu'elle diminue à 10 % après un certain temps. D'autre part, les résultats de la modélisation illustrent la tendance qu'on retrouve dans les résultats expérimentaux : le flux de matière entre les phases est supérieur une fois que le débit d'air est augmenté.

III.4.2 Modélisation du transfert de matière entre les phases liquide et gazeuse dans le réacteur airlift en réalisant la culture de microalgues

La photosynthèse peut être exprimée quantitativement avec le taux d'absorption de CO_2 et le taux de production d' O_2 . Ces taux sont estimés à partir de la productivité de la biomasse et le rendement de conversion, ce qui est obtenu à partir de la stœchiométrie de la photosynthèse. On suppose que les cellules de microalgues sont complètement immergées dans le liquide et qu'il n'existe pas de résistance au transport de matière dans le film entre le solide et le liquide. En conséquence, les flux de dioxyde de carbone et d'oxygène passent directement dans le liquide.

Le dioxyde de carbone dissout fait partie du carbone inorganique total (CIT) présent dans la culture des algues. Il doit être en équilibre avec l'acide carbonique, le carbonate et le bicarbonate, ce qui est lié aux changements de pH. Dans cette étude, il est assumé que le pH de la culture est maintenu à 7 puisque le pH tend à augmenter pendant la photosynthèse, tandis qu'une injection de CO_2 devient le milieu acide. Les évolutions des concentrations d' O_2 , de CO_2 et de CIT sont alors étudiées en appliquant l'Equation III.8 pour les compartiments ascendant et descendant du réacteur. Le logiciel Dymola est utilisé pour la modélisation.

Les premiers résultats montrent que, plus les intensités lumineuses sont élevées, plus élevés sont les taux d'oxygène produits ; ceci est validé dans les compartiments ascendant et descendant. La production d'oxygène est, en conséquence, plus élevée dans le compartiment descendant. Egalement, le taux d'absorption du CO_2 augmente avec une augmentation des intensités lumineuses ; il est plus élevé dans le compartiment descendant que dans le compartiment ascendant.

Par ailleurs, il est nécessaire d'estimer l'évolution de la concentration d' O_2 le long du réacteur. Au bas du compartiment descendant, l'oxygène dissout dans le liquide atteint sa valeur maximale. A des faibles débits d'air (5 et 10 l/min) il n'existe pas d'air qui entre dans le compartiment descendant qui pourrait dégager l' O_2 dissout. Même si le réacteur travaille dans le régime II, le coefficient volumique de transfert de matière est faible pour éviter l'accumulation de l'oxygène. En haut du compartiment ascendant, la concentration d' O_2 est la plus basse puis que le débit d'air injecté permet de dégager l' O_2 le long de la hauteur du compartiment ascendant.

En comparant les concentrations d' O_2 pour les différentes vitesses superficielles du gaz, la plus faible concentration d' O_2 est observée pour le débit d'air le plus élevé (20 l/min) (Figure III.4). Ce résultat est lié au coefficient de transfert de matière puisqu'il est plus élevé pour ce débit d'air. Ceci provoque un taux de transport de l' O_2 plus élevé du liquide vers le gaz. Il est alors nécessaire d'étudier les concentrations maximales d' O_2 atteignables dans le réacteur pour un débit d'air faible (5 l/min) et sous différentes intensités lumineuses.

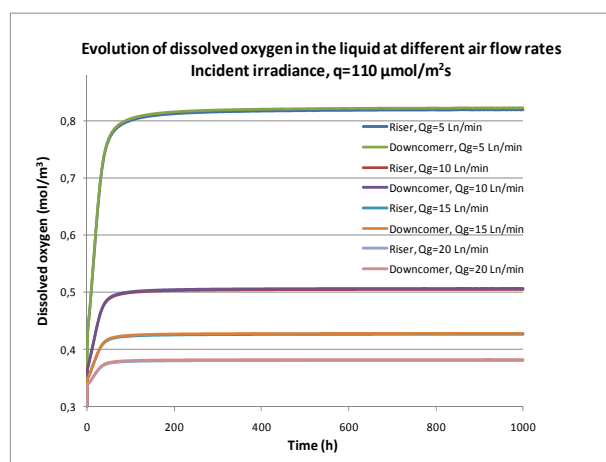


Figure III.4. Evolution d' O_2 dissout en fonction du débit d'air injecté

Selon plusieurs auteurs, si les concentrations d' O_2 dissout sont supérieures à 300 % des concentrations de saturation, on peut observer une inhibition de la photosynthèse. Les résultats de la modélisation montrent que les concentrations d' O_2 atteignent entre 100 % et 294 % des valeurs de saturation, si un éclaircissement de $100 \mu\text{mol/m}^2\text{s}$ est appliqué sur le réacteur. Pour des éclaircissements supérieurs, les concentrations d' O_2 dans le liquide sont très élevées, ce qui probablement occasionnera une inhibition de la photosynthèse. Dans ce cas, il est recommandé d'augmenter le coefficient volumique de transfert de matière dans le compartiment ascendant (e.g. en augmentant la rétention du gaz interfaciale par unité de volume) ou de ne pas réaliser la culture de *Chlamydomonas reinhardtii* sous ces intensités lumineuses.

D'autre part, on constate que les concentrations d' O_2 dissout diminuent si la hauteur du liquide est accrue. La différence entre les concentrations d' O_2 dissout le long de la hauteur du compartiment ascendant est plus élevée pour une hauteur de liquide de 0,78 m que pour une hauteur de 2 m, dans le cas d'un débit d'air fixe. Par contre, on observe une diminution des concentrations d' O_2 dissout plus marquée si on augmente le débit d'air injecté, comparativement à une augmentation de la hauteur de liquide. En conséquence, les concentrations d' O_2 dissout sont plus dépendantes du débit d'air injecté que de la hauteur du liquide.

Quant à l'évolution d'O₂ dans l'air, les résultats montrent que la concentration d'O₂ diminue pendant les premières secondes après l'injection d'air. Ensuite, la concentration d'O₂ augmente jusqu'à atteindre une valeur constante.

En ce qui concerne l'évolution du CO₂ et du CIT, une première étude concerne l'injection d'air ambiant dans le réacteur. Les résultats indiquent que les concentrations de dioxyde de carbone et du carbone total inorganique ne sont pas suffisantes pour satisfaire les besoins de la culture. Pour un éclairage de 110 $\mu\text{mol}/\text{m}^2\text{s}$, les concentrations de CO₂ et de CIT sont limitées en moins d'une heure de culture (Figure III.5). De même, si le coefficient volumique de transfert de matière est augmenté, les concentrations de CO₂ et de CIT ne sont pas suffisantes pour réaliser la photosynthèse.

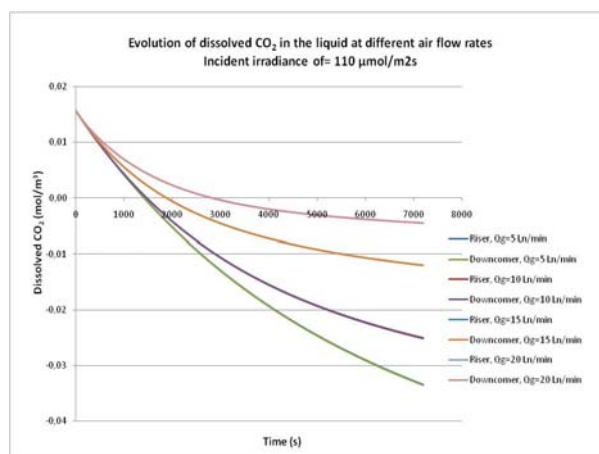


Figure III.5. Evolution de CO₂ dans le liquide en fonction du débit d'air injecté

La modélisation des injections d'air enrichi en CO₂, avec des pourcentages volumique entre 1 et 5 %v/v montre que les concentrations de CO₂ dissout satisfont les besoins des microalgues (Figure III.6). Egalement, le CIT dans le liquide augmente en fonction du pourcentage de CO₂ ajouté à l'air.

Selon les études expérimentales, il existe un niveau de CO₂ dissout sous lequel l'activité photosynthétique peut être inhibée. Les résultats de la modélisation indiquent que cette valeur est dépassée si l'air avec 5 % de CO₂ est injecté dans le réacteur.

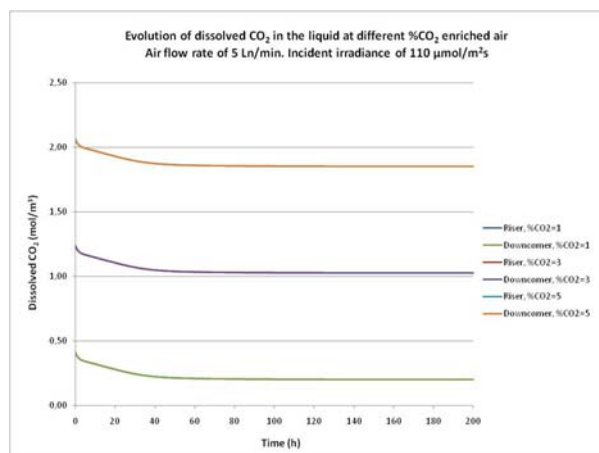


Figure III.6. Evolution de CO₂ dans le liquide en fonction du débit d'air injecté

Quant à l'évolution du CO₂ le long de la hauteur du liquide, les concentrations de CO₂ dissout augmentent dans le compartiment ascendant et diminuent dans le compartiment descendant ; ceci est en cohérence avec le profil de la production de la biomasse dans le réacteur. Par ailleurs, les résultats montrent que le CO₂ dissout est plus uniformément réparti le long du réacteur si la concentration du CO₂ dans l'air est plus élevée. La différence de CO₂ dissout entre la tête et le cuve du réacteur est plus petite.

De plus, il est intéressant d'estimer les pertes de CO₂ dans le réacteur. Ces pertes sont données par ce qui n'est pas absorbé par les algues, aux conditions données. On constate que, si le débit d'air est augmenté dans le compartiment ascendant, les pertes de CO₂ diminuent dans le réacteur. Ceci est en agrément avec l'augmentation des concentrations de CO₂ dans le liquide, le long du réacteur.

Les concentrations de CO₂ dans le gaz à la tête du réacteur donnent des pressions partielles plus élevées que celles recommandées pour éviter l'inhibition de la photosynthèse. Ceci est observé pour les trois pourcentages volumiques de CO₂ modélisés dans le réacteur.

Chapitre IV: Etude hydrodynamique d'un photobioréacteur hélicoïdal

Le photobioréacteur hélicoïdal (HAL) combine le principe de réacteurs airlifts et l'écoulement dans un hélicoïde. Une injection d'air est réalisée dans le compartiment ascendant du réacteur, ce qui provoque la circulation du liquide et le transfert de matière entre les phases liquide et gazeuse. La section hélicoïdale permet de contrôler les vitesses du liquide et d'augmenter le temps de circulation. Dans ce travail, une étude complète hydrodynamique est présentée, en comprenant la formulation d'un modèle et une analyse expérimentale grâce à la construction d'un banc d'essais.

L'étude expérimentale du réacteur est divisée en deux étapes. Tout d'abord, les pertes de charge totales sont mesurées dans la section hélicoïdale à différents débits de liquide, dans le but d'estimer les coefficients de perte de charge. Dans ce cas, un débit de liquide est imposé dans la section hélicoïdale sans réaliser l'injection d'air dans le système.

Les premiers résultats montrent que les coefficients de perte de charge dans la section hélicoïdale sont plus élevés pour des pertes de charge et des débits de liquide faibles. Dans les deux cas, la tendance est du type puissance. Les pertes de charge sont l'addition des pertes par friction et des pertes causées par l'enroulement du tube afin de construire l'hélicoïde.

Par la suite, l'air est injecté dans le compartiment ascendant à différents débits (du 5 à 25 l/min). Les différences de pression dans ce compartiment sont mesurées afin d'évaluer les rétentions dans le compartiment ascendant. Parallèlement, les différences de pression dans la section hélicoïdale sont mesurées pour estimer les vitesses du liquide. Toute cette procédure est réalisée pour des tubes de 25 et 30 mm de diamètre.

Les résultats indiquent que les pressions mesurées dans la section hélicoïdale diminuent en fonction du débit de liquide. Au contraire, les pertes de charge augmentent. En comparant les pertes de charge entre les deux tubes installés dans la section hélicoïdale, celles-ci sont supérieures pour le plus petit diamètre du tube. Le liquide trouve une résistance plus élevée à l'écoulement, compte tenu de la section transversale plus petite.

Une relation du type puissance entre les pertes de charge et le nombre de Reynolds est établie pour chaque tube, dans la section hélicoïdale. Les nombres de Reynolds, calculés pour chaque vitesse du liquide, montrent que l'écoulement est laminaire dans tous les cas. Le nombre de Reynolds critique est calculé en fonction de la géométrie de l'hélicoïde.

A partir des pertes de charge, un coefficient global de frottement peut être estimé en suivant l'équation de Darcy. Une corrélation entre le coefficient global de frottement (f_h), le nombre de Reynolds (Re) et le rapport entre le diamètre du tube et celui de l'enroulement (d/D_c) est établie pour postérieurement estimer les pertes de charge dans la section hélicoïdale (Equation IV.1)

$$\ln(f_h) = -204.6 + 219.6e^{-(d/D_c)} - 1.075 \ln(\text{Re}) \quad (\text{IV.1})$$

Cette relation est validée pour les deux rapports entre le diamètre du tube et celui de l'enroulement, et pour un nombre de Reynolds entre 1100 et 10700.

A partir du débit de liquide estimé dans la section hélicoïdale, les vitesses du liquide correspondant à chaque section sont calculées. Dans tous les cas, les vitesses du liquide augmentent si l'injection d'air dans le compartiment ascendant est augmentée. Comme dans le réacteur étudié précédemment, l'injection d'air crée une différence de pression entre les sections du réacteur qui provoque la circulation du liquide.

Les résultats expérimentaux montrent que, pour les deux tubes testés ici, les vitesses du liquide sont très faibles ou nulles pour un débit d'air de 5 l/min. D'autre part, les vitesses de liquide dans le compartiment ascendant sont très faibles (entre 0 et 0,9 cm/s) comparées à celles estimées dans la section hélicoïdale (entre 0 et 16 cm/s). Des relations du type puissance entre les vitesses du liquide obtenues et les vitesses superficielles du gaz sont établies pour le compartiment ascendant et la section hélicoïdale.

Lorsque le tube de 30 mm de diamètre est installé dans la section hélicoïdale, les vitesses du liquide dans les compartiments ascendant et descendant sont plus élevées. Dans ce cas, les pertes de pression dans la section hélicoïdale sont plus faibles et, en conséquence, l'énergie disponible dans le système est plus élevée. Ces résultats permettent de déterminer le temps de résidence du liquide dans chaque section du réacteur. En comparant les résultats, les temps de résidence du liquide sont très similaires dans le compartiment ascendant et la section hélicoïdale, pour un tube de 30 mm de diamètre.

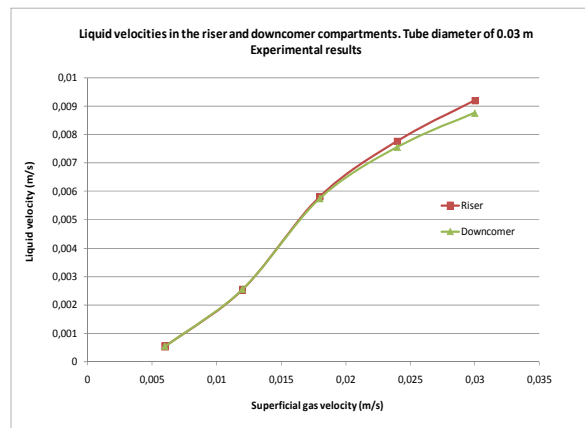


Figure IV.1 Vitesses du liquide dans les compartiments ascendant et descendant. Tube de 30 mm de diamètre

Pour le tube de 30 mm de diamètre, le temps de circulation du liquide est entre 16,2 et 6,6 minutes. D'autre part, pour un tube de 25 mm de diamètre, le temps de résidence du liquide dans le compartiment ascendant est 1,4 fois plus long que ceux trouvés dans la section hélicoïdale. Pour ce tube, le temps de circulation est entre 65,2 et 20,4 minutes.

Les rétentions du gaz, mesurées dans le compartiment ascendant, sont entre 2,5 et 9,6 %v/v. Les valeurs des rétentions de gaz changent légèrement lorsque le diamètre du tube est réduit de 30 mm à 25 mm dans la section hélicoïdale. A partir de ces résultats, les rétentions du gaz et les vitesses du liquide peuvent être liées à la puissance donnée par le gaz. Les relations entre les rétentions du gaz et la puissance sont similaires en comparant les deux tubes installés dans la section hélicoïdale. D'autre part, les résultats des vitesses du liquide indiquent qu'il est nécessaire, pour un tube de 25 mm, d'avoir une puissance du gaz plus élevée pour obtenir les mêmes vitesses que celles observées en utilisant un tube de 30 mm.

Le modèle hydrodynamique est développé à partir d'un bilan établi entre la force d'entraînement et les pertes de charge dans le réacteur. La force d'entraînement est donnée par la différence entre la pression hydrostatique dans le compartiment ascendant et les pressions hydrostatiques dans le compartiment descendant et la section hélicoïdale. Les pertes de charge sont estimées pour chaque section, où l'Equation IV.1 est utilisée pour les estimer dans la section hélicoïdale.

Le modèle « Drift flux » est utilisé pour obtenir une relation entre les phases liquide et gazeuse dans le compartiment ascendant. Les vitesses terminales des bulles d'air sont déterminées en fonction du débit d'air injecté et selon les corrélations proposées par Peebles et Gerber. Ces vitesses se situent entre 20,5 et 23,4 cm/s, et sont inférieures à celles assumées par les auteurs.

Pour appliquer le modèle hydrodynamique aux conditions du réacteur, il est nécessaire de réaliser un calcul itératif. Le coefficient de distribution (Cr) du modèle « Drift Flux » est optimisé afin de minimiser la déviation entre les résultats expérimentaux et les résultats de la modélisation. Pour un tube de 30 mm de diamètre, le coefficient de distribution le plus approprié est 3,8 puisque la déviation est inférieure à 15 % pour les vitesses du liquide et environ 9 % pour les rétentions de gaz. Pour un tube de 25 mm de diamètre le Cr choisi est de 3,5 parce que la déviation moyenne est de 14 % pour les vitesses du liquide et de 5,7 % pour les rétentions du gaz.

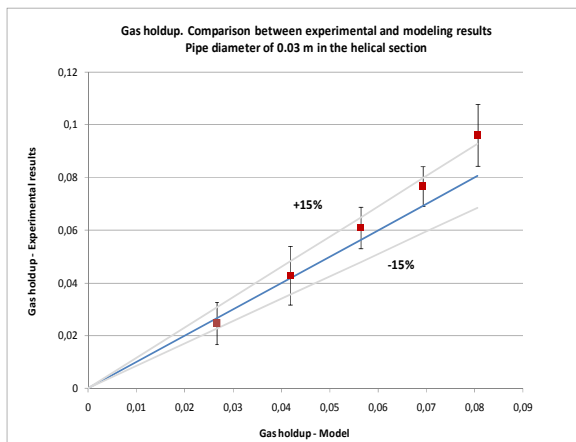


Figure IV.2. Résultats expérimentaux et de modélisation des rétentions du gaz

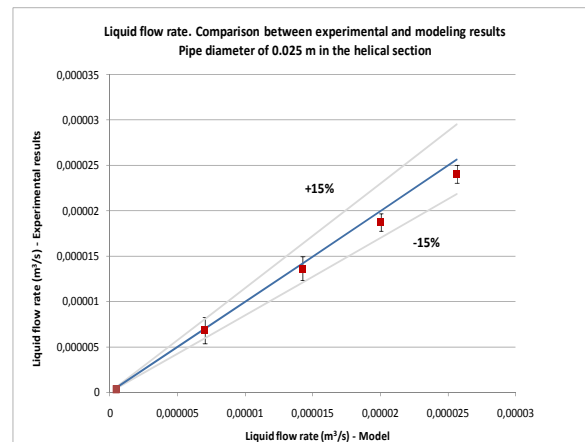


Figure IV.3. Résultats expérimentaux et de modélisation des débits du liquide

Pour des débits d'air de 5 et 10 l/min, les écarts sont très faibles entre les résultats expérimentaux des rétentions du gaz et ceux de la modélisation, pour les deux tubes testés ici (Figure IV.2). Pour des débits d'air plus élevés, le modèle sous-estime les valeurs moyennes de la rétention de gaz, mais ils restent d'un ordre de grandeur de 15 % déviation. Ceci est observé pour les deux tubes installés dans la section hélicoïdale.

En comparant les résultats expérimentaux et ceux de la modélisation pour les débits du liquide, l'écart le plus élevé est observé à des débits d'air élevés et avec un tube de 30 mm installé dans la section hélicoïdale. Le modèle surestime les résultats expérimentaux. Au contraire, pour un tube de 25 mm, la moyenne des valeurs expérimentales est très proche des résultats de la modélisation.

Enfin une comparaison entre le réacteur hélicoïdal et le réacteur airlift à circulation interne peut être établie à partir des résultats hydrodynamiques. D'une part, les rétentions du gaz dans le compartiment ascendant sont plus élevées dans le réacteur hélicoïdal (entre 2,5 et 9,6 %) que celles obtenues dans le réacteur airlift (entre 0,7 et 3,7 %). Les vitesses du liquide dans le compartiment ascendant sont plus élevées dans le réacteur airlift, ce qui implique un volume plus important du gaz dégagé à l'atmosphère, en provoquant une rétention du gaz plus faible.

Puisque le distributeur du gaz est identique dans les deux réacteurs, l'aire d'interface par volume est théoriquement plus élevée dans le réacteur hélicoïdal. En conséquence, les coefficients volumiques de transfert sont supérieurs, en favorisant l'échange de matière entre les phases liquide et gazeuse. En

assumant qu'un système d'éclairage est installé dans la section hélicoïdale, il est nécessaire d'étudier l'accumulation d'O₂ dissout dans cette section. La longueur équivalente de l'hélicoïde est supérieure à la hauteur du compartiment descendant ; en conséquence, des concentrations indésirables d'O₂ peuvent être observées dans cette section.

Les résultats montrent que les débits du liquide sont faibles dans le réacteur hélicoïdal en comparaison avec ceux du réacteur airlift. L'avantage principal du réacteur hélicoïdal est que les débits du liquide peuvent être modifiés en variant les paramètres géométriques tels que le diamètre du tube, le diamètre d'enroulement et le nombre de spires. Dans le réacteur airlift, les vitesses du liquide peuvent être modifiées en changeant le diamètre du cylindre interne, ce qui donne a priori moins de degrés de liberté.

Le tableau IV.1 montre les valeurs des vitesses superficielles du liquide et le temps de circulation pour différents réacteurs airlifts à circulation interne et des réacteurs hélicoïdaux.

Tableau IV.1. Paramètres hydrodynamiques des réacteurs airlifts à circulation interne et des réacteurs hélicoïdaux

<i>Réacteur</i>	<i>Volume du travail (l)</i>	<i>Vitesse superficielle du gaz (m/s)</i>	<i>Vitesse du liquide (m/s)</i>	<i>Temps de circulation du liquide</i>
IALR	21	0,006-0,048	0,11-0,25	6-14 (s)
HALR, d=30 mm	37	0,006-0,048	0,047-0,16	5,2-18 (min)
HALR, d=25 mm	34	0,006-0,048	0,014-0,049	22-79 (min)
IALR	60	0,01-0,497	0,05-0,3	7-23 (s)
IALR	100	0,001-0,01	0,017-0,078	20-90 (s)
IALR	11,3	0,0027-0,22	0,046-0,2	7,5-32,5 (s)
Helical tubular	21	-	0,193	5,2 (min)

Enfin, les deux réacteurs peuvent être comparés en fonction de la surface occupée et le volume de travail. L'objectif est but est d'obtenir un grand volume de travail dans une petite surface.

La section hélicoïdale est un compartiment externe du réacteur hélicoïdal qui occupe une surface plus grande que le réacteur airlift. Pour des tubes de diamètres de 30 et 25 mm, le ratio entre la surface occupée et le volume du travail est de 24,6 et 26,7 l/m, respectivement. Le ratio le plus élevé correspond au réacteur airlift à circulation interne de 37 l/m.

Chapitre V: La culture de microalgues : son intégration et leur impacts environnementaux potentiels

L'exploitation de la biomasse algale est un processus complet qui implique la culture de microalgues et des procédés en amont et en aval. En amont, il est nécessaire d'approvisionner des engrais, de l'énergie sous forme d'électricité, de la chaleur, et du froid ainsi que de l'eau et du CO₂. En aval, le traitement de la biomasse inclut la récolte, la déshydratation, le séchage et la rupture des cellules. La production de biodiesel, la digestion anaérobie, la fermentation sont des procédés aval, réalisés une fois que la biomasse est traitée.

La culture de microalgues commence avec la préservation de souches sous une température et un éclairage adéquat. Dans ce cas, l'électricité est l'énergie principale consommée. Pendant la culture de microalgues, l'agitation du liquide et l'équilibre de la température sont nécessaires. L'électricité est

indispensable pour le transport de liquide (circulation de la culture dans certains photobioréacteurs), le transport du CO₂, la compression de l'air et/ou l'agitation mécanique. En fonction des conditions climatiques, un système de chauffage/refroidissement peut être nécessaire pour maintenir la température. D'autre part, tous les éléments nutritifs et le CO₂ sont fournis dans cette étape.

Les méthodes de récolte actuelles sont basées sur les procédés des usines de traitement des eaux usées. Ces méthodes sont la coagulation-floculation, la sédimentation, la flottation et l'écémage. Généralement, ils sont combinés pour augmenter le rendement de la récolte. Ils nécessitent l'utilisation des produits ainsi que de l'énergie, sous forme d'électricité.

La centrifugation et la filtration sont les techniques utilisées afin de réduire, dans un premier temps, l'humidité de la biomasse, ce qui est appelé la déshydratation. Le séchage est une étape optionnelle qui dépend de la qualité du produit désiré. Le séchage de la biomasse au soleil est la technique la plus conventionnelle cependant, sa faisabilité à grande échelle est à l'étude. Les équipements tels que les séchoirs à tambour tournant, séchoirs à bandes, séchoirs à gaz naturel, etc. sont comparés pour des utilisations à grande échelle.

Jusqu'à présent les études montrent que la culture de microalgues ne peut pas être un procédé isolé. L'énergie utilisée pour produire des engrais et pour l'agitation de la culture ainsi que l'énergie investie dans la récolte, la déshydratation, le séchage sont trop élevées par rapport à l'énergie produite. La culture de microalgues doit être intégrée dans des installations comme les centrales électriques, l'industrie du papier, du ciment et les industries de traitement du cuir. Il est nécessaire de construire un système de production à boucle fermée fondé sur le principe de « technologies propres », à zéro déchet. Dans ce contexte, le concept de bio-raffinerie est pertinent, la biomasse est transformée grâce aux voies biochimiques et thermochimiques, en produits à haute valeur tels que les biocarburants, l'électricité, la chaleur, les biomatériaux, etc. Tout cela doit être réalisé d'une manière la plus efficace possible.

A cet effet, il est indispensable de mener une étude détaillée dans deux directions complémentaires. D'une part, les produits, les coproduits et les déchets du procédé de culture doivent être bien identifiés. D'autre part, les coproduits et déchets du procédé industriel doivent être analysés afin de satisfaire aux exigences de la culture. En ce sens, certains auteurs affirment qu'une option d'intégration appropriée est celle des cultures sur eaux usées afin de récupérer les nutriments nécessaires pour les algues et la réalisation de la fermentation ou de la digestion anaérobie afin de produire de l'énergie.

Les sections suivantes présentent les avantages et les inconvénients de l'utilisation des eaux usées dans la culture de microalgues.

V.1. L'épuration des eaux usées et la culture de microalgues

L'utilisation des eaux usées dans la culture de microalgues est limitée par la composition de l'eau puisque certaines espèces d'algues ne peuvent pas survivre à des concentrations élevées de composants ni à la présence d'autres substances comme des acides organiques ou des phénols. Le concept d'utiliser des eaux usées pour la culture des algues est une idée attrayante pour les usines d'épuration puisque l'usage de produits chimiques peut être réduit ainsi que la consommation d'énergie. De plus, ceci favorise la culture de microalgues à grande échelle.

D'autre part, les microalgues sont capables d'absorber des métaux lourds comme le cuivre, le cadmium, le nickel, l'or et le chrome. Elles sont utilisées comme détecteurs de pollution dans des eaux puisque les ions métalliques s'accumulent dans leurs parois cellulaires ou dans des composants intracellulaires.

Les expériences dans l'épuration des eaux usées montrent qu'une combinaison des bactéries et des algues produit des rendements intéressants. Les algues produisent de l'oxygène nécessaire pour les bactéries afin de dégrader la matière organique. Les bactéries sont capables de mieux dégrader les matériaux tels que les hydrocarbures, les phénols et les solvants organiques.

L'utilisation des eaux usées par les algues présente certaines contraintes. D'une part, le procédé d'épuration généralement demande des temps de séjour longs où il est possible d'observer une limitation de CO₂. D'autre part, il peut être nécessaire de diluer les eaux usées afin d'éviter l'inhibition de la photosynthèse, ce qui implique une quantité plus grande de consommation d'eau.

V.2. La digestion anaérobie et la culture de microalgues

Dans cette section, un exemple d'intégration de la culture de microalgues est présenté. La culture, réalisée en bassins ouverts ou en photobioréacteurs, reçoit les nutriments soit des eaux usées, soit de l'industrie de production des engrais ; le CO₂ provenant des industries telles que les centrales électriques, la production d'ammoniac. Une fois la biomasse récoltée, déshydratée et séchée, les lipides sont extraits ; ensuite, le biodiesel est produit en réalisant la transestérification. La biomasse restante, composée principalement de glucides et de protéines, est soumise à la digestion anaérobie pour produire du biogaz qui peut être utilisé pour produire de l'électricité. Le « gâteau » produit de la digestion anaérobie peut servir de nutriments aux algues. Dans tout ce procédé, il est nécessaire de fournir de l'électricité, de la vapeur, des nutriments, des produits chimiques, de l'eau et du CO₂.

Les productivités de la biomasse, de l'huile algale, du biodiesel, du glycérol, du biogaz et des gâteaux restants après l'extraction de lipides et la digestion anaérobie sont estimées. Les hypothèses sont fondées sur le travail effectué par Stepan et al., Cadoret et Bernard et Campbell et al. Il est assumé que la culture est effectuée dans 200 bassins ouverts avec une surface totale de 100 hectares. Deux types d'algues sont pris en compte : une espèce avec 30 % de lipides en poids (comme les espèces *Phaeodactylum tricornutum*) et 70 % de lipides en poids (comme *Dunaliella tertiolecta*). La productivité de la biomasse se situe entre 10 et 200 tonnes de matière sèche par hectare et par an.

Les résultats montrent que le ratio entre l'huile produite et la biomasse des algues sèche est de 0,24 (en masse), en considérant une espèce contenant 30 % de lipides. Au contraire, pour les espèces contenant 70 % de lipides, le ratio augmente à 0,6. Cela signifie que l'énergie produite à partir de biodiesel varie entre 9,2 et 21 MJ/kg de biomasse d'algues sèches, en fonction des concentrations de lipides. En assumant que le biogaz est utilisé directement par une centrale électrique ou par un générateur d'électricité, l'énergie produite est entre 3,2 et 6,3 MJ/kg, pour une culture de 100 hectares.

Dans ce contexte, les impacts environnementaux potentiels de la culture de microalgues sont présentés, en mettant en évidence l'utilisation des éléments nutritifs, la consommation d'eau et d'autres éléments susceptibles d'altérer la durabilité du procédé.

V.3. Les impacts environnementaux potentiels de la culture de microalgues

Jusqu'à présent la culture de microalgues est l'objet de controverses en ce qui concerne les impacts environnementaux. Analogue à l'agriculture, la culture de microalgues a besoin d'engrais en quantités importantes, ce qui est lié à une consommation d'eau élevée. Ceci pose plusieurs questions sur la viabilité du procédé.

Les nutriments les plus importants sont l'azote et le phosphore. En règle générale, les algues contiennent de l'azote dans une gamme de 5 à 10 % du poids sec et il peut être fourni sous la forme de nitrate d'ammonium, de nitrate de sodium, de chlorure d'ammonium et d'autres éléments. D'autre part, la concentration de phosphore est plus faible, environ 1 %. Il peut être fourni sous forme de phosphate de potassium dihydrogène, phosphate dipotassique et superphosphate. En considérant que la biomasse de microalgues a une composition $\text{CO}_{0.48}\text{H}_{1.83}\text{N}_{0.11}\text{P}_{0.01}$, les quantités requises d'azote et du phosphore peuvent être estimées. Si on suppose une productivité de la biomasse de $25 \text{ g/m}^2 \cdot \text{j}$ (environ 82 t/ha.an), les taux requis sont de $5,4 \text{ t/ha.an}$ pour l'azote et $1,1 \text{ t/ha.an}$ pour le phosphore.

L'utilisation intensive d'engrais affecte le bilan énergétique de la culture de microalgues. La production des engrais est un procédé intensif qui peut atteindre 50 % de l'énergie totale consommée dans les procédés en amont de la culture.

En ce qui concerne les émissions de gaz, la culture intensive de microalgues peut libérer des substances comme l'ammoniac et le protoxyde d'azote. Ces émissions peuvent être observées dans les étangs, car ils sont ouverts à l'atmosphère. La volatilisation de l'ammoniac dépend de facteurs environnementaux comme le pH, la température, les conditions de mélange et les concentrations d'ammonium.

D'ailleurs, si les eaux usées produites ne sont pas manipulées correctement, elles peuvent provoquer des phénomènes de pollution tels que l'eutrophication. Si les eaux sont rejetées dans le sol, elles rentrent en contact direct avec des eaux souterraines, ou en contact indirect avec les lagunes ou la mer, ce qui augmente le risque d'eutrophisation. D'autre part, le risque de filtrations d'eau est plus élevé dans les étangs que dans les photobioréacteurs car les premiers sont en contact direct avec le sol.

Enfin, il est très important d'identifier les éléments nutritifs requis par les algues et ceux qui sont disponibles dans les eaux usées. Tout d'abord, les algues semblent être sensibles à des concentrations élevées d'éléments nutritifs, ce qui définit la productivité de la biomasse et sa composition finale. Une mauvaise manipulation des eaux usées et des engrais peut avoir des répercussions négatives sur l'environnement telles que l'acidification, l'eutrophication et la toxicité.

La consommation d'eau dans la culture de microalgues dépend de plusieurs facteurs, à commencer par le type de système de culture utilisé. Dans les bassins ouverts, les pertes d'eau sont élevées en raison de l'évaporation, alors que ce problème est moins accentué en photobioréacteurs. L'évaporation de l'eau dans des bassins ouverts peut atteindre entre 5 et 6 mm de pertes par jour. Un taux d'évaporation élevé provoque le dépôt de sels, ce qui implique un lavage plus fréquent des bassins et plus de consommation d'eau.

Dans le cas de la culture dans des photobioréacteurs, certains systèmes avec jet d'eau pulvérisent les surfaces du réacteur pour le refroidir. Ceci implique une augmentation de la consommation d'eau totale si elle n'est pas récupérée et réutilisée dans le système. Par ailleurs, d'autres systèmes sont

immergés dans des piscines pour maintenir la température. Les études montrent que la consommation d'eau dans des bassins ouverts se situe entre 32,8 et 685,5 l/kg de biomasse sèche.

Les auteurs suggèrent une réutilisation de l'eau après la récolte des algues (par exemple, l'eau restant dans des bassins de décantation). L'eau de pluie peut aussi être récupérée pour la culture de microalgues et pour les besoins du procédé. Pour la culture, il est nécessaire de préparer l'eau avec les éléments nutritifs les plus appropriés, le pH et la température. Pour le procédé, l'eau de pluie peut être utilisée pour le lavage de bassins.

A part une consommation élevée de nutriments et d'eau, il existe d'autres impacts environnementaux qui sont directement et indirectement liées au procédé de la culture.

Les auteurs proposent actuellement de réaliser la culture de microalgues dans des lacs, des lagunes et des surfaces fermées sur les zones côtières. Ceci pourrait entraîner une modification de la composition de l'eau puisque la culture intensive de microalgues nécessite des concentrations élevées d'éléments nutritifs comme l'azote et le phosphore. De plus, cela pourrait provoquer une prolifération incontrôlée des algues, l'eutrophisation des eaux et l'endommagement de la biodiversité.

S'il la culture de microalgues est réalisée dans des photobioréacteurs, il est important d'étudier la disponibilité de matériaux transparents qui aient une transmission élevée. Ces matériaux doivent être recyclables. De plus, le bilan énergie et d'émissions de gaz à effet de serre doit être effectué.

Les substances telles que le sulfate d'aluminium, le chlorure de fer et le sulfate de fer utilisées dans la floculation, peuvent être absorbées par la biomasse et être toxiques, si un des objectifs est d'alimenter les animaux. D'autre part, une teneur excessive de métaux dans les algues pourraient provoquer des problèmes dans d'autres procédés tels que la pyrolyse. L'huile produite pourrait contenir des concentrations non négligeables de métaux qui peuvent se volatiliser.

Le solvant n-hexane est fortement envisagé pour l'extraction de lipides à partir des algues. Dans ce cas, il est important d'étudier la possibilité des émissions élevées de n-hexane pendant le procédé. De plus, il faut évaluer si la biomasse restante après l'extraction de lipides, contient des quantités résiduelles de n-hexane. Ce solvant a montré des effets négatifs chez les humains, en particulier dans les systèmes respiratoire, optique et nerveux.

L'utilisation de substances telles qu'une solution d'acide peracétique et d'éthanol afin de stériliser les photobioréacteurs demande une manipulation appropriée. Si ces eaux sont rejetées dans le sol ou dans d'autres eaux resserrées, des problèmes liés à la composition et à la biodiversité peuvent se produire.

Pour améliorer l'efficacité de la culture de microalgues, les auteurs proposent l'utilisation d'algues modifiées génétiquement. Dans ce contexte, ces algues doivent être cultivées en photobioréacteurs pour éviter toute leur intromission dans des systèmes naturels, ce qui peut altérer la biodiversité locale.

Enfin, il a été observé que les impacts environnementaux et la consommation d'énergie sont proportionnels. Si un système de culture implique une demande d'énergie élevée, les impacts négatifs sur l'environnement seront plus importants. Pour cette raison, il est indispensable de développer des études parallèles, en évaluant les impacts environnementaux et la consommation d'énergie, afin d'obtenir des bilans sur l'ensemble du système.

Conclusions

Les microalgues sont actuellement envisagées comme des organismes capables de produire de l'énergie ainsi que des substances à très haute valeur pour l'industrie. D'autre part, les microalgues sont considérées comme un moyen de réduction des émissions de gaz à effet de serre. Leur utilisation comme matière première pour la production d'énergie permet de diminuer la dépendance aux énergies fossiles. Pour ces raisons, il est très important de sélectionner un système approprié pour cultiver les microalgues avec un rendement élevé. Actuellement, les systèmes proposés sont les bassins ouverts et les photobioréacteurs ; chacun avec des avantages et des contraintes.

Dans la première partie de ce travail, un photobioréacteur du type airlift à tubes concentriques et circulation interne a été choisi pour réaliser une étude expérimentale et de modélisation hydrodynamique. Afin d'étudier l'effet des concentrations de la biomasse sur l'hydrodynamique, des particules de 10 microns de diamètre ont été ajoutées au système, dans des concentrations allant de 0,15 à 5 g/l.

Les résultats ont montré qu'une injection d'air dans le compartiment ascendant est la force motrice du réacteur. Les rétentions de gaz et les vitesses de la phase pseudo-homogène augmentent si le débit d'air augmente dans le compartiment ascendant. Dans les régimes II et III, une relation linéaire entre les rétentions du gaz des compartiments ascendant et descendant a été obtenue expérimentalement. D'autre part, les rétentions de gaz, les vitesses de liquide et les rétentions de solides n'ont pas été affectées par la présence de particules, dans la gamme de concentrations utilisées.

L'estimation du rendement d'un photobioréacteur implique l'estimation du profil de lumière dans le système, des productivités de la biomasse et de la capacité du réacteur à transférer la matière entre les phases.

Quant au profil de lumière, cette étude a montré que les intensités lumineuses sont plus élevées dans le compartiment descendant que dans le compartiment ascendant. Il est nécessaire d'estimer des concentrations de biomasse optimales pour éviter l'apparition de zones obscures dans le réacteur. Ces concentrations sont plus élevées si l'éclairement du réacteur est accru. Dans le cas où le compartiment ascendant est rendu opaque, les concentrations optimales sont aussi plus élevées.

Les résultats ont démontré qu'il est intéressant d'avoir un compartiment descendant avec une section transversale plus grande que celle du compartiment ascendant. Le but est d'obtenir un volume de culture plus grand exposé à de fortes intensités lumineuses et d'éviter l'atténuation de la lumière causée par le cylindre intérieur. Toutefois, l'hydrodynamique du réacteur doit être bien vérifiée.

Les productivités de la biomasse ont été estimées en fonction du profil de lumière. Celles-ci sont supérieures dans le compartiment descendant pour tous les éclairagements modélisés. En établissant un cycle de lumière/obscurité, les résultats ont montré que les productivités sont plus élevées en comparaison avec une culture soumise à un éclairage continu. Dans ce cas, il est toujours supposé que la photorespiration n'est pas observée dans le compartiment ascendant, donc il n'existe pas une consommation de biomasse.

En comparant les résultats obtenus en utilisant la loi de Monod et le modèle de Cornet et de Dussap, les productivités de biomasse sont plus élevées dans le deuxième cas. Dans tous les cas, la contribution

du compartiment ascendant à produire de la biomasse est faible par rapport à celui du compartiment descendant.

En fonction de l'énergie lumineuse disponible et de la productivité de la biomasse, il y aura une certaine production d'oxygène et une absorption de dioxyde de carbone. En concordance avec l'activité de photosynthèse, les taux de production/absorption augmentent avec une augmentation de l'éclairement du réacteur. En conséquence, le transfert de matière devient crucial, notamment le coefficient volumique de transfert, la rétention de gaz et le débit d'air.

Selon des études expérimentales, les algues ne résistent pas des concentrations d'oxygène ni de CO₂ dissouts très élevées. Les résultats de la modélisation ont montré que pour un éclairement de 110 $\mu\text{mol}/\text{m}^2.\text{s}$ et pour un faible débit, l'O₂ dissout est inférieur à la limite des algues. Cependant, si l'éclairement est augmenté dans le réacteur, la photosynthèse sera probablement inhibée.

Quand l'air ambiant est utilisé dans le réacteur, on a constaté que les taux de consommation de CO₂ et le CIT sont plus élevés que le taux de transfert du gaz au liquide. Pour augmenter le CO₂ dissout dans le liquide, il existe deux options, soit augmenter le coefficient volumique de transfert de matière, soit augmenter la concentration de CO₂ dans le gaz. Dans le premier cas, le CO₂ dissout dans le liquide augmente mais il devient limitant après un certain temps. Dans le second cas, des concentrations de 1, 3, ou 5 %v/v CO₂ dans l'air satisfont les besoins des algues. Néanmoins, une concentration de 5 %v/v CO₂ dans l'air à faible débit inhibera probablement la photosynthèse.

Enfin, la modélisation du réacteur démontre que les productivités de la biomasse sont supérieures à celles des bassins ouverts. La culture de *Chlamydomonas reinhardtii* peut être réalisée si les limites d'éclairements et des débits d'air sont établies dans le système.

Un deuxième photobioréacteur du type hélicoïdal a été étudié. La conception est basée sur l'écoulement provoqué par l'airlift et celui observé dans un tube enroulé en hélice. Deux diamètres ont été testés dans la section hélicoïdale afin d'estimer les vitesses de liquide et des temps de résidence du liquide.

Une relation entre le coefficient de frottement, le nombre de Reynolds et le ratio entre le diamètre du tube et celui de l'enroulement a été établie à partir de résultats expérimentaux. A partir de cette corrélation, les vitesses du liquide ont été obtenues dans l'ensemble du réacteur. Les résultats ont démontré que les vitesses de liquide dans la section hélicoïdale sont plus grandes que celles dans les compartiments ascendant et descendant du PBR concentrique, pour tous les débits d'air testés dans le réacteur.

Une comparaison entre les deux tubes installés dans la section hélicoïdale montre que les pertes de pression sont plus élevées dans le plus petit diamètre du tube. Par conséquent, les vitesses du liquide sont plus faibles et les temps de résidence du liquide plus élevés. Si on compare les vitesses du liquide entre les deux bioréacteurs, les résultats montrent que celles-ci sont inférieures dans la section hélicoïdale à celles observées dans le compartiment ascendant du réacteur airlift. Ainsi, les temps de résidence du liquide sont beaucoup plus faibles dans le réacteur airlift que dans la section hélicoïdale. La géométrie du réacteur hélicoïdal permet de varier l'écoulement du liquide en fonction du diamètre du tube, celui de l'enroulement et le nombre de spires.

En ce qui concerne les rétentions de gaz, leurs valeurs n'ont pas été affectées par les changements du diamètre du tube de 30 à 25 mm. Elles sont plus élevées dans le réacteur hélicoïdal que dans le réacteur airlift. Cela signifie que l'échange de matière entre les phases liquide et gazeuse est supérieur dans le compartiment ascendant du réacteur hélicoïdal que dans le réacteur airlift.

L'exploitation de la biomasse algale implique non seulement le procédé de culture mais aussi les procédés en amont et en aval. Pour extraire des produits et coproduits à haute valeur, il est nécessaire de fournir de l'électricité, de la chaleur, des nutriments, de l'eau, du dioxyde de carbone, et certains produits fossiles. Parmi les nutriments, l'azote et le phosphore sont les principaux et, selon des études expérimentales, ils pourraient être obtenus à partir des eaux usées. Le dioxyde de carbone peut être fourni par certaines fumées de gaz procédés, après réalisation d'un conditionnement approprié.

Certains impacts environnementaux sont associés au procédé de culture. Si les eaux dans les bassins ouverts sont riches en éléments nutritifs, les risques de volatilisation de l'ammoniac et des émissions de N_2O sont plus élevés. Par ailleurs, si les eaux ne sont pas correctement traitées et déposées, elles peuvent provoquer des dommages à l'environnement comme l'eutrophisation. La consommation d'eau est un sujet controversé dans la culture des microalgues. La culture nécessite une plus grande consommation d'eau dans des bassins ouverts que dans des photobioréacteurs à cause de l'évaporation. Dans ce cas, il est intéressant de déterminer si les eaux restantes après la récolte peuvent être recyclées dans la culture. Si les eaux usées et/ou l'eau de pluie sont utilisées dans la culture de microalgues, la consommation d'eau du procédé complet peut devenir acceptable.

La faisabilité de la culture de microalgues nécessite des études approfondies sur la capacité à établir les meilleures conditions de reproduction des algues. En parallèle, les études doivent approfondir la disponibilité des ressources (eau, terres, nutriments...) ainsi que les conditions climatiques. En ce sens, il est important d'établir un bilan d'énergie du système et des impacts environnementaux. Enfin, il est essentiel d'évaluer tous ces paramètres et d'étudier la faisabilité économique du système, afin d'estimer l'investissement nécessaire et les coûts de maintenance.

Perspectives

Dans la première partie de ce travail, l'étude hydrodynamique d'un réacteur airlift à circulation interne est basée sur le modèle « Drift flux », en effectuant un bilan d'énergie du système. Pour appliquer le modèle « Drift flux », il est nécessaire d'estimer le diamètre des bulles d'air et leurs vitesses terminales. Il sera utile de déterminer ces paramètres expérimentalement pour valider les relations proposées par Davidson, Schuler et Wallis. Egalement, il serait intéressant de mesurer ces deux paramètres dans un milieu de croissance des microalgues, afin de vérifier à quel point les propriétés du liquide affectent le diamètre des bulles et leurs vitesses.

Pour évaluer la performance hydrodynamique du réacteur airlift, il est fortement recommandé d'effectuer la culture de microalgues. Il est nécessaire d'évaluer le débit d'air maximal qui ne provoque pas de stress sur les cellules. Certaines cellules de microalgues n'ont pas de paroi rigide, ce qui les rend plus sensibles aux turbulences. Pour cette raison, il serait utile de connaître les caractéristiques physiques de l'espèce. De plus, le débit d'air doit être compatible avec le temps de résidence du liquide, dans chaque section du réacteur, si on veut exposer les algues à un cycle de lumière/obscurité.

En ce qui concerne l'étude de distribution de la lumière dans le réacteur airlift, le modèle pourrait être amélioré en tenant compte de la présence de bulles. D'autre part, il sera intéressant d'évaluer la

faisabilité d'introduire des matériaux réfléchissants à l'intérieur du réacteur, tel que proposé par Richmond. Pour compléter cette étude, il est recommandé d'évaluer la distribution de lumière autour du réacteur.

Quant au modèle de croissance des microalgues, il sera nécessaire de valider les résultats avec la culture de *Chlamydomonas reinhardtii* dans le réacteur airlift. Pour cela, les mêmes conditions d'intensité de la lumière, de la température et du milieu de croissance doivent être établies en fonction de l'étude de Cornet et Dussap. De même, les concentrations d'O₂ et du CO₂ dissout doivent être mesurées afin de valider les résultats de modélisation.

En ce qui concerne le réacteur hélicoïdal, il est souhaitable de revoir la conception de l'arrivée du tube hélicoïdal au compartiment ascendant, afin de récupérer la plus grande quantité d'énergie possible provenant du distributeur de gaz. Comme pour le réacteur airlift, la performance du réacteur devra être validée avec la culture de microalgues. Cultiver *Chlamydomonas reinhardtii* dans les mêmes conditions permettra de comparer les performances des deux réacteurs. Le nombre maximum de spires dans la section hélicoïdale, qui empêchera d'atteindre des niveaux d'oxygène dissout toxiques pour les algues, doit être déterminé. Ceci doit être couplé à la capacité du compartiment ascendant à dégager l'oxygène.

Si le réacteur hélicoïdal est exposé à la lumière artificielle, le profil de la lumière devrait être modélisé lorsque les lampes sont placées à l'intérieur de la section hélicoïdale. Dans ce cas, il est raisonnable d'installer un petit diamètre du tube dans cette section. Toutefois, il sera important d'évaluer la fréquence d'accumulation de biomasse sur les parois du tube.

En ce qui concerne l'hydrodynamique du réacteur hélicoïdal, il serait utile d'étendre l'applicabilité de la corrélation du coefficient de frottement obtenue dans cette étude. Dans ce cas, les ratios entre le diamètre du tube et celui de l'enroulement peuvent être variés et testés. Ceci augmentera la gamme de vitesses du liquide sous laquelle le réacteur pourrait fonctionner.

Enfin, il sera intéressant d'étudier la faisabilité de ces deux réacteurs à plus grande échelle. D'abord, il est nécessaire d'établir le niveau de biomasse souhaité pour la production, le volume de travail, la surface occupée et les conditions environnementales. Dans ce cas, la culture des espèces de microalgues naturelles (algues non génétiquement modifiées capables de se développer dans des eaux usées), devrait être une priorité. Par la suite, le système pourrait être placé dans un procédé de production, en évaluant les synergies potentielles, y compris les entrées et les sorties, notamment gaz, liquides et solides ainsi que les déchets. Cette analyse devrait inclure un bilan d'énergie, l'estimation de la consommation d'eau ainsi que les émissions de gaz à effet de serre, ainsi que les conditions économiques de telles bio-raffineries.

Table of Contents

Introduction	1
I <i>Algae: requirements for growth cultivation systems</i>	7
I.1 The biology of algae	7
I.1.1 Photosynthesis of algae	9
I.1.2 Microalgae growth requirements	10
I.1.2.1 Light energy	10
I.1.2.2 Carbon dioxide	12
I.1.2.3 Water and nutrients	13
I.1.2.4 Mixing	15
I.1.3 Modes of culture - Specific growth rate and doubling time	15
I.2 Microalgae production systems	17
I.2.1 Open ponds	17
I.2.2 Photobioreactors (PBR)	18
I.2.2.1 Tubular photobioreactors	19
I.2.2.2 Flat panel photobioreactors	19
I.2.2.3 Plastic-bag photobioreactors	20
I.2.2.4 Column-photobioreactors	20
I.2.3 Comparison among microalgae culture systems	22
I.2.4 Microalgae harvesting	23
I.2.5 Microalgae oil extraction and production	24
I.2.6 Thermochemical and biological conversion of microalgae	27
I.2.6.1 Thermochemical conversion processes	27
I.2.6.2 Biological conversion processes	28
I.3 Conclusions	31
I.4 References	33
II <i>Hydrodynamic study of an Internal Airlift Reactor for microalgae culture</i>	39
Abstract	39
II.1 Introduction	40
II.2 Theory	41
II.2.1 Holdup	41
II.2.2 Superficial velocity	41

II.2.3 Solids loading and holdup	41
II.2.4 Properties of the pseudo-homogenous phase.....	41
II.3 Model	41
II.4 Materials and methods	44
II.5 Results and discussion	46
II.5.1 Gas holdup	46
II.5.2 Solids holdup	51
II.5.3 Pseudo homogeneous liquid velocities	54
II.5.4 Circulation time	56
II.6 Conclusions.....	58
II.7 References.....	59
III Modeling light energy profile in the IAL reactor. Estimation of biomass productivities and mass transfer	63
III.1 Introduction	65
III.2 Estimation of the light energy profile along the reactor.....	65
III.2.1 One dimension modeling of light energy distribution in IAL reactor: Two flux method.....	67
III.2.2 Light distribution in the IAL reactor: modeling results.....	69
III.2.2.1 Continuous exposition to light	70
III.2.2.2 Microalgae culture under light-dark cycles.....	73
III.2.3 Estimation of the biomass production rate following Monod's law.....	74
III.2.4 Estimation of the biomass production rate following Cornet and Dussap's model.....	81
III.2.5 Determination of reactor efficiencies and productivities	83
III.3 Mass transfer in an Internal Airlift Reactor: experimental and modeling study.....	85
III.3.1 Determination of the overall volumetric mass transfer coefficient $k_L a$	86
III.3.1.1 Theoretical determination of $k_L a$	86
III.3.1.2 Experimental determination of $k_L a$	89
III.3.1.2.1 Materials and methods.....	89
III.3.1.2.2 Results	90
III.3.1.3 Oxygen evolution in the IAL reactor	95
III.3.2 Modeling gas-to-liquid mass transfer in the IAL reactor performing microalgae culture.....	99
III.3.2.1 Results: oxygen evolution	101
III.3.2.2 Results: carbon dioxide evolution	107
II.4 Conclusions.....	114
II.5 References.....	119

IV Hydrodynamical study of a Helical-airlift photobioreactor	125
IV.1 Introduction	127
IV.2 Equipments and methods.....	127
IV.2.1 Equipment	127
IV.2.2 Methods.....	129
IV.3 Experimental results	130
IV.3.1 Estimation of the total loss coefficient in the helical section	130
IV.3.2 Liquid velocities in the reactor.....	132
IV.3.3 Gas holdup and power input.....	136
IV.4 Hydrodynamic model	138
IV.4.1 Macroscopic energy balance in the HALR	140
IV.4.2 Modeling results.....	142
IV.5 Comparison between the IAL and HAL reactors	145
IV.6 Conclusions..	147
IV.7 References.....	149
V Microalgae culture: integration and potential environmental impacts.....	151
V.1 Introduction	153
V.2 Integration of microalgae culture in industrial processes	153
V.2.1 The process of microalgae culture.....	153
V.2.2 Industrial integration	156
V.2.2.1 Wastewater treatment and microalgae culture.....	157
V.2.2.2 Anaerobic digestion and microalgae culture	160
V.3 Potential environmental impacts of microalgae culture	164
V.3.1 Nutrients	164
V.3.2 Water consumption.....	166
V.3.3 Other sources of environmental impacts	168
IV.4 Conclusions..	170
IV.5 References.....	172
Conclusions	177
Perspectives.....	181
Appendix	183

Table of Figures

I	<i>Algae: requirements for growth cultivation systems</i>	5
Figure I.1	Macro and Micro algae	8
Figure I.2	The process of photosynthesis	9
Figure I.3	Theoretical photosynthetic efficiency in microalgae	9
Figure I.4	Requirements for microalgae culture	10
Figure I.5	Photosynthesis vs. Intensity (P/I) curve	11
Figure I.6	Growth phases of <i>Nannochloropsis sp.</i>	16
Figure I.7	Open ponds	17
Figure I.8	Tubular photobioreactors	19
Figure I.9	Flat panel photobioreactor	20
Figure I.10	Sleeves bioreactors	20
Figure I.11	Annular bioreactor	20
Figure I.12	Internal and external airlift reactors	21
Figure I.13	Annual oil productivity of crops and microalgae	25
Figure I.14	Thermochemical, biological, and physico-chemical conversion processes to transform microalgae	27
II	Hydrodynamic study of an Internal Airlift Reactor for microalgae culture	39
Figure II.1	Scheme of an internal airlift reactor	42
Figure II.2	Internal airlift reactor	45
Figure II.3	Sparger for gas injection	45
Figure II.4	Riser and downcomer pressure difference vs. air flow rate	46
Figure II.5	Riser and downcomer gas holdups vs. air flow rate	47
Figure II.6	Riser and downcomer average gas holdups vs. air flow rate	47
Figure II.7	Riser and downcomer gas holdup ratio vs. riser superficial gas velocity	49
Figure II.8	Relationship between riser and downcomer gas holdups	49
Figure II.9	Riser and downcomer average gas holdups. Comparison between experimental modeling results	50
Figure II.10	Driving force in the IAL reactor vs. riser superficial gas velocity	50
Figure II.11	Relationship between solid holdup and solid loading	51
Figure II.12	Riser and downcomer solid holdups vs. superficial gas velocity	52
Figure II.13	Difference between riser and downcomer solid holdups	52
Figure II.14	Gas holdups vs. solid loadings	53
Figure II.15	Average riser and downcomer gas holdups according to solids concentration	54
Figure II.16	Relationship between average riser and downcomer gas holdups	54
Figure II.17	PHL velocity versus riser superficial gas velocity	55
Figure II.18	Riser PHL velocity vs. riser superficial gas velocity at different particle concentrations	56
Figure II.19	PHL circulation time in the reactor vs. superficial gas velocity	57

Figure II.20	PHL circulation time in the reactor vs. riser superficial gas velocity	58
--------------	--	----

III Modeling light energy profile in the IAL reactor. Estimation of biomass productivities and mass transfer 63

Figure III.1	Definition of working illuminated fraction according to Cornet.	66
Figure III.2	Definition of working illuminated fraction in a circular cross sectional area.....	66
Figure III.3	Illustration of the two frames of reference	67
Figure III.4	Illustration of the local irradiance along the reactor	69
Figure III.5	Local light density along the reactor at different biomass concentrations.	70
Figure III.6	Local light intensity along the reactor at different incident irradiances.	71
Figure III.7	Local light intensity in four different radius vs. biomass concentrations...	72
Figure III.8	Optimal biomass concentrations at fourth different irradiances.	73
Figure III.9	Optimal biomass concentrations at the center and the draft tube.....	74
Figure III.10	Local and normalized specific growth rate in the reactor vs. local irradiances.	75
Figure III.11	Normalized specific growth rate integrated over reactor compartments vs. biomass concentration.	76
Figure III.12	Biomass production rate versus biomass concentration following Monod's model	77
Figure III.13	Evolution of biomass concentration in the downcomer.	79
Figure III.14	Evolution of biomass concentration in the riser.....	79
Figure III.15	Time to reach optimal biomass concentration having a light/dark cycle ...	80
Figure III.16	Biomass production rate vs. biomass concentration following Cornet and Dussap's model.	82
Figure III.17	Photosynthetic efficiency vs. biomass concentration.....	84
Figure III.18	Specific interfacial area vs. superficial gas velocities.....	87
Figure III.19	Overall volumetric mass transfer for the riser according to several authors.	89
Figure III.20	Evolution of dissolved oxygen as a function of time vs. air flow rate.	90
Figure III.21	Experimental determination of k_La in the riser for an air flow rate of 10 Ln/min.....	91
Figure III.22	Values of k_La in the riser vs. superficial gas velocity.	91
Figure III.23	Values of k_La in the riser and downcomer compartments.....	92
Figure III.24	Relationship among k_La in the riser, gas holdup, and power input.	93
Figure III.25	Experimental and theoretical results of k_La vs. superficial gas velocity. ...	94
Figure III.26	Values of k_La at different particle concentrations.	95
Figure III.27	Axial dispersion coefficient and Peclet number in the riser.....	97
Figure III.28	Simulation and experimental results of dissolved oxygen in the riser.	98
Figure III.29	Illustration of the film theory applied to microalgae culture.....	99
Figure III.30	Evolution of oxygen production rate.....	102
Figure III.31	Dissolved oxygen in the liquid vs. air flow rate.....	103
Figure III.32	Dissolved oxygen in the liquid vs. incident irradiance.	104
Figure III.33	Percentage of dissolved oxygen with respect to air saturation.....	105
Figure III.34	Percentage of dissolved oxygen with respect to saturation assuming water column height of 2 m.....	105
Figure III.35	Dissolved oxygen in the air vs. air flow rate.....	106
Figure III.36	Evolution of the oxygen transfer driving force vs. air flow rate.	107
Figure III.37	Evolution of carbon dioxide consumption rate	107
Figure III.38	Dissolved CO_2 and TIC in the liquid vs. air flow rate.	109
Figure III.39	Evolution of dissolved CO_2 . Comparison between modeling results and Van't Riet correlation	110
Figure III.40	Evolution of CO_2 and TIC at different % CO_2 -enriched air.....	111
Figure III.41	Dissolved CO_2 in the reactor injecting natural air and 1%, 3%, and 5% CO_2 -enriched air.	112

Figure III.42	Dissolved CO ₂ in the reactor injecting natural air and 1%, 3%, and 5% CO ₂ -enriched air.	113
Figure III.43	CO ₂ concentration in the gas along the riser vs. air flow rate	114
IV	Hydrodynamical study of a Helical-airlift photobioreactor	125
Figure IV.1	Helical airlift reactor.	127
Figure IV.2	Flow circulation in the HAL reactor. Interface designed in CVI.....	129
Figure IV.3	Steps to perform HAL experimental study.	129
Figure IV.4	Total loss coefficients in the helical section for a pipe diameter of 30 mm	131
Figure IV.5	Total loss coefficients in the helical section for a pipe diameter of 25 mm	131
Figure IV.6	Measured pressure and pressure losses in the helical section	132
Figure IV.7	Pressure losses in the helical section as a function of Reynolds number...	133
Figure IV.8	Liquid velocities in all sections of the reactor for a pipe diameter of 30 mm	134
Figure IV.9	Liquid velocities in all sections of the reactor for a pipe diameter of 25 mm	134
Figure IV.10	Liquid residence time in all sections of the reactor for a 30-mm pipe diameter	135
Figure IV.11	Liquid velocities in all sections of the reactor for a 25-mm pipe diameter	136
Figure IV.12	Gas holdup as a function of the superficial gas velocities	137
Figure IV.13	Gas holdups, liquid flow rates and specific power inputs. D _h =30 mm	137
Figure IV.14	Gas holdups, liquid flow rates and specific power inputs. D _h =25 mm	138
Figure IV.15	Bubble diameter and terminal rise velocity of bubbles in the riser.....	140
Figure IV.16	Algorithm to model the hydrodynamics of the helical airlift reactor.....	142
Figure IV.17	Total loss coefficients estimated in steps 1 and 2	143
Figure IV.18	Liquid velocities in all sections of the reactor for a pipe diameter of 25 mm	143
Figure IV.19	Riser gas holdup. Comparison between experimental and modeling results	144
Figure IV.20	Liquid flow rates. Comparison between experimental and modeling results	145
V	Microalgae culture: integration and potential environmental impacts.....	151
Figure V.1.	Microalgae culture and biomass processing. Energy input and materials.....	154
Figure V.2.	Combinations of techniques for harvesting, dewatering and drying algae....	155
Figure V.3.	Synergy among wastewaters, microalgae culture, biodiesel, and anaerobic digestion.	160
Figure V.4	Nitrogen and phosphorus requirements in microalgae culture.....	164

List of tables

I	<i>Algae: requirements for growth cultivation systems</i>	5
	Table I.1 Major algae divisions and classes.	7
	Table I.2 State of microalgae production for 2006.....	8
	Table I.3 Companies producing microalgae.....	18
	Table I.4 Photobioreactors and open ponds productivities nowadays.....	21
	Table I.4 Photobioreactors and open ponds productivities nowadays (cont'd).....	22
	Table I.5 Properties of microalgae biodiesel and fossil diesel.	25
	Table I.6 Lipids contents in microalgae species considered for oil production.	26
	Table I.7 Comparison among conversion processes of microalgae.....	30
II	Hydrodynamic study of an Internal Airlift Reactor for microalgae culture	39
	Table II.1 Terminal velocity of a single gas bubble in liquids	43
	Table II.2 Bubble velocity in a finite vessel	44
	Table II.3 Dimensions of the Internal airlift reactor (IAL).	45
	Table II.4 Particle concentrations. Properties of the pseudo-homogenous phase	46
	Table II.5 Circulation time in previous studies of IAL reactor	58
III	Modeling light energy profile in the IAL reactor. Estimation of biomass productivities and mass transfer	63
	Table III.1 Optical properties of <i>Chlamydomonas reinhardtii</i>	70
	Table III.2 Working illuminated fraction for different irradiances	71
	Table III.3 Biomass productivity under continuous illumination and according to optimal concentrations.	78
	Table III.4 Biomass productivity having the riser opaque and according to optimal concentrations.....	79
	Table III.5 Biomass productivity under continuous illumination and according to optimal concentrations	82
	Table III.6 Biomass productivity having the riser opaque and according to optimal concentrations	82
	Table III.7 Comparison between Monod and Cornet and Dussap models.	83
	Table III.8 Efficiencies and productivities of the designed IAL reactor.	85
	Table III.9 Correlations to estimate the axial dispersion coefficient.....	96
	Table III.10 Equilibrium reactions among CO_2 , HCO_3^- , and CO_3^{2-}	100
	Table III.11 Expressions to estimate O_2 and CO_2 mass transport between phases in the IAL reactor.....	101
	Table III.12 Initial concentrations of CO_2 , HCO_3^- and CO_3^{2-} , and TIC for 0.038, 1, 3, and 5% CO_2 -enriched air.	108

IV	Hydrodynamical study of a Helical-airlift photobioreactor	125
	Table IV.1 Dimensions of the helical-airlift reactor (HALR).	128
	Table IV.2 Relationships between liquid velocities and superficial gas velocities.	135
	Table IV.3 Terminal bubble velocity in an infinite vessel	139
	Table IV.4 Terminal bubble velocity in a finite vessel	140
	Table IV.5 Comparison among IALR, HALR and other experimental reactors	146
V	Microalgae culture: integration and potential environmental impacts	151
	Table V.1 Experimental studies of wastewaters treated by microalgae.	158
	Table V.1 Experimental studies of wastewaters treated by microalgae (cont'd).	159
	Table V.2 Experimental studies of metals absorbed by microalgae	159
	Table V.3 Representative values of products and co-products from a closed system.	162
	Table V.4 Water consumption and losses in microalgae culture	168

Algae are photosynthetic organisms that have been cultivated as a source of valuable products such as proteins, polysaccharides, sterols, enzymes, vitamins and pigments, which can be integrated in food, animal feed as well as in the fabrication of pharmaceuticals and cosmetics products. Currently the most important algae producers in the world are Japan, China, Taiwan, Philippines, India, Australia, United States, Norway, India, Chile and other small country producers.

The interest of microalgae culture started in the 1940s in the United States, Germany, and Japan to produce proteins and to provide food (while exchanging photosynthetic gases) in space missions (Casallo, 2000; BEAM, 2004). In the 60's, Japan started the production of *Chlorella* in commercial scale for nutritional and medical purposes. In the 1970s, *Spirulina* was cultivated in Thailand and Mexico. At this time, the oil crisis occurred and the interest on microalgae increased, as it was considered as a potential source of hydrogen. Larger cultures were then observed in the United States, Australia, India and Israel with the cultivation of *Spirulina*, *Chlorella*, *Dunaliella salina* and *Haematococcus pluvialis* (Richmond, 2007; BEAM, 2004). In the 80's, a reference study was performed by the National Renewable Energy Laboratory (NREL), aiming at identifying the most promising microalgae species for oil production. Three hundred species, mostly green algae and diatoms, were then identified as potential oil producers able to survive under hard environmental conditions (Sheehan et al., 1998; Cadoret et al., 2008).

Nowadays, the interest of algae as energy source has emerged. First and second generation biofuels, as they exist today, are produced from crops including sugarcane, maize, sugar beet, rapeseed oil, sunflower, palm, jatropha, and soybean. Several studies, including Life Cycle Assessments, have discussed the advantages of these biofuels, sometimes reversing the environmental interest of their production, as for palm oil starting with deforestation or crops starting with pasture conversion.

Crops require large cultivation lands, intensifying competition for potentially cultivated lands as well as the destination of collected crops. This demand has increased tropical deforestation, like in Indonesia which cut its surface by 27% from 1990 to 2007. Other examples are countries like Malaysia (8%) and Brazil (9.3%) (FAO, 2010). Ground and water pollutions, due to fertilizers, pesticides and herbicides as well as important emissions of greenhouse gases like CO₂ and N₂O can be added to these environmental impacts.

In this context, microalgae have emerged as a potential and alternative source of energy. Consequently, biological processes such as anaerobic digestion and fermentation, and thermochemical conversion process such as gasification, fast pyrolysis, hydrothermal liquefaction have been under investigated. As previously mentioned, some species are considered as potential sources for biodiesel production: their hydrocarbon and lipids contents can be extracted to produce a type of biofuel. On the other hand, studies have demonstrated that some microalgae species are resistant to high CO₂ concentrations. If energy can be produced from microalgae biomass, they can be considered as a potential tool to reduce greenhouse gas emissions in replacement of fossil fuels.

Microalgae have numerous advantages over terrestrial plants:

- 1) they reproduce with very high productivities compared to terrestrial plants, fixing higher quantities of CO₂ per year;
- 2) they can be grown in fresh, salty and even wastewaters;

- 3) microalgae can be used to treat wastewaters, as they can utilize nitrogen and phosphorus, and to absorb metals (e.g. Cu, Cd);
- 4) flue gases from power plants might be used in algae culture, recovering carbon dioxide;
- 5) microalgae production systems can be installed in the surroundings of industries and in non-cultivable areas, reducing competition for land;
- 6) several studies stress the fact that more oil quantities can be obtained from microalgae compared to oleaginous plants, due to their much higher growth rate;
- 7) microalgae are able to produce hydrogen (Chisti, 2007; Brennan and Owende, 2010).

In this sense, it is of interest to find the most appropriate system to cultivate microalgae with very high productivities. It is essential to provide water, light energy, nutrients, carbon dioxide as well as specific environmental conditions. Open basins, called open ponds, were the first cultivation systems that grew species like *Spirulina*, *Chlorella*, *Dunaliella* and *Haematococcus*.

On the other hand, closed cultivation systems called photobioreactors exist. In these systems, a wider variety of species can be cultivated since the risk of contamination can be strictly controlled and prevented. Environmental conditions are also better controlled and monitored, thus higher biomass productivities can be achieved. Today, universities, enterprises, and governmental research laboratories have studied several configurations of bioreactors, receiving special attention tubular, flat panel, and column photobioreactors. At laboratory scale, these reactors have reached interesting productivities; nevertheless, some limitations referred to their hydrodynamics together with their capacity to distribute light inside the culture.

In this context, *the main purpose* of this work is to perform a hydrodynamic study of two photobioreactors, in order to evaluate the feasibility of microalgae cultivation in these reactors, while identifying advantages and constraints of large-scale microalgae culture.

In *Chapter I*, an overview of algae biology, their needs as well as the influence of the environmental conditions on biomass productivities are presented. This section explains the most promising systems to cultivate microalgae, exposing their advantages and disadvantages. The interest of microalgae will be also explained, indicating the relevance of microalgae as a new source of energy.

Chapter II presents the hydrodynamic characterization of an internal airlift reactor for microalgae culture. Hydrodynamical characterization includes the development of a mathematical model based on energy balance and two-phase flow model. On the other hand, the construction of an internal airlift reactor test bench validate and complete the model.

In *Chapter III*, the distribution of light energy is studied along the reactor as well as the growth rate of the algae species *Chlamydomonas reinhardtii*. A predictive model is applied to a microalgae culture exposed to continuous illumination and to light-dark cycles. According to microalgae growth rates and concentrations, the capacity of the internal airlift reactor to release oxygen and to absorb carbon dioxide is evaluated.

In *Chapter IV*, a second photobioreactor called helical airlift reactor is presented. An experimental and modeling study is performed to characterize the main hydrodynamic parameters. Hydrodynamic results are compared to the hydrodynamics of the internal airlift reactor, identifying limitations and potential of both cultivation systems.

Chapter V presents an overview of advantages and disadvantages of microalgae culture at large scale, including the identification of potential environmental impacts with respect to nutrients utilization, water consumption, and other sources.

Finally, conclusions and perspectives of this work will be presented

Algae: requirements for growth cultivation systems

Nomenclature

I_K	Saturation irradiances	$\mu\text{mol}/\text{m}^2.\text{s}$
K_L	Light saturation constant	$\mu\text{mol}/\text{m}^2.\text{s}$
N	Number of cells	
t	Time	h
t_d	Doubling time	h
X	Biomass weight	kg/m^3
X_o	Initial biomass weight	kg/m^3

Greek letters

α	Slope in the P/I curve	
μ	Specific growth rate	$1/\text{h}$
μ_{max}	Maximum growth rate	$1/\text{h}$

Subscripts

o	Initial
-----	---------

Abbreviations

ADP+Pi	Adenosine Diphosphate
ALR	Airlift reactor
ATP	Adenosine Tri-Phosphate
IAL	Internal airlift
ND	Nitrogen deficiency
NADP	Nicotinamide adenine dinucleotide phosphate
NES	Non-environmental stress
OD	Optical density
PA	Photosynthetic activity
PBR	Photobioreactor
PE	Photosynthetic efficiency
PFD	Photon flux density
VSS	Volatile suspended solids

1. The biology of algae

Algae are aquatic and vegetal organisms that can be found in different climates, from tropical coral reefs to Polar Region, from fresh to marine waters. Their physical appearances reveal the absence of stem, roots, and leaves as they can be identified in terrestrial plants. In an aquatic environment, algae use light energy and water to transform inorganic compounds into biomass and oxygen, in the so-called *photosynthesis* reaction.

Algae are generally differentiated as macroalgae and microalgae, being categorized in divisions and classes according to their pigments, cell wall characteristics, and the type of storage products. Table 1 shows their major divisions and classes.

Table I.1. Major algae divisions and classes.
(Richmond, 2007)

<i>Class</i>	<i>Traditional name</i>
Bacillariophyta	Diatoms
Charophyta	Stoneworts
Chlorophyta	Green algae
Chrysophyta	Golden algae
Dinophyta	Dinoflagellates
Phaeophyta	Brown algae
Rhodophyta	Red algae

Macroalgae are aquatic plants that are attached to the substrate by holdfasts. Seaweeds can be found in marine and fresh waters, achieving large sizes (up to 60 meters). Most of species are green, brown or red, being wracks and kelps the most well known (figure I.1a, I.1b) (Sheehan et al., 1998; Guiry, 2008). In Asian countries, these algae have been introduced and largely cultivated in farms with aim to produce hydrocolloids, food, feed, cosmetics, and pharmaceutical products (Williams et al., 2007). *Laminaria sp.* is the most cultivated species today and largely produced in China and other countries like Japan, Indonesia, Philippines, India, South Korean, North Korean, Chile, Norway, and U.S.A.

Referring to energy production, macroalgae are largely considered for biogas generation, by performing anaerobic digestion, with aim to electricity production. In addition, seaweeds are regarded as potential feedstock for combustion, liquefaction, and pyrolysis processes (Aresta et al., 2005; Ross et al., 2008).

Microalgae are phytoplankton microorganisms that can grow in marine, brackish, fresh waters, and even in soils (Richamond, 2007). Today, it is estimated that between 200,000 and few million of microalgae species are present in the nature and they can be observed as individual cells or forming colonies (Figure I.1c, I.1d) (Pulz and Gross, 2004; Cadoret et al., 2008). According to their size, they are classified as picophytoplankton (0.2-2 μm), nanoplankton (2-20 μm), microplankton (20-200 μm) and mesoplankton (200 μm -5 mm).

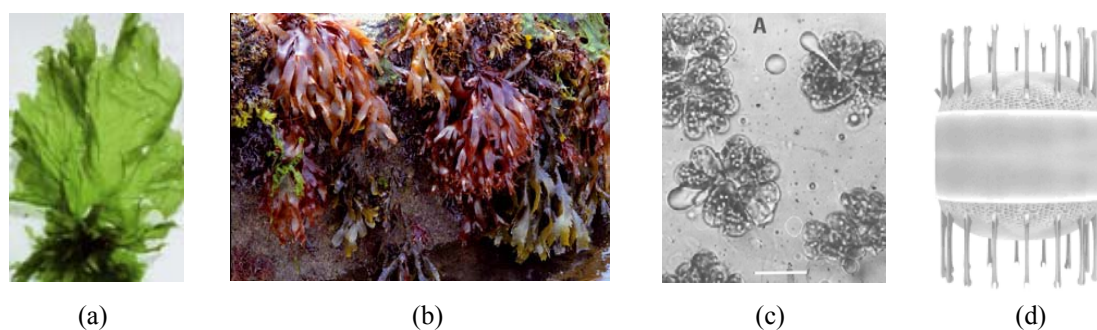


Figure I.1. Macro and Micro algae.

a) Macroalgae *Ulva armoricana* (Chlorophyta) (CNRS, 2008); b) Macroalgae *Palmaria palmate* (Rhodophyta) (CNRS, 2008); c) Microalgae *Botryococcus braunii*. English strain. Scale bar : 10 μ m (Metzger et al., 2005) ; d) Microalgae *Skeletonema costatum* (diatom) (Ifremer, 2010)

According to their physiognomy and environmental growth conditions, microalgae can store important quantities of proteins, carbohydrates, and lipids. For this reason, they have been cultivated for food, nutritional supplements, live feed in aquaculture (e.g. molluscs, crustaceans), additives (e.g. carotenes) as well as for pharmaceutical and cosmetics products (Carlsson et al., 2007). The most cultivated species for these purposes have, *Chlorella*, *Dunaliella salina*, *Haematococcus pluvialis* and the cyanobacteria *Spirulina sp.* (*Arthrospira*) (Becker, 2004; Richmond, 2007). Table I.2 shows the production on large scale of microalgae in 2006 (Spolaore et al. 2006).

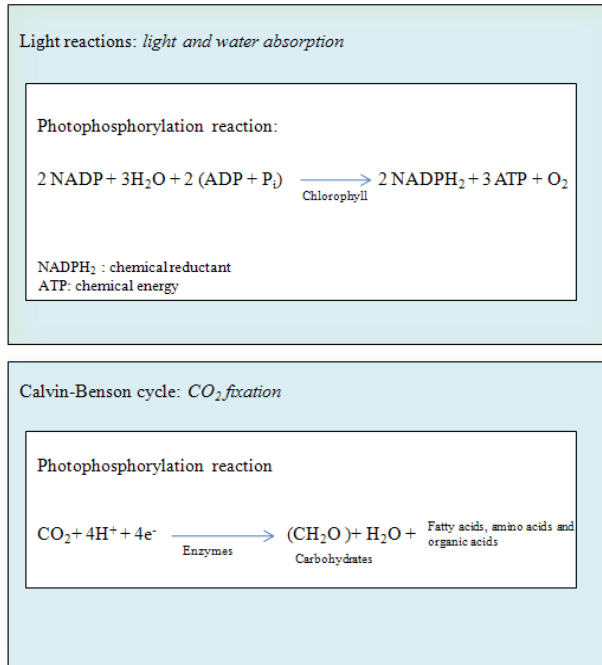
Table I.2. State of microalgae production for 2006.
(Spolaore et al., 2006)

<i>Producer country</i>	<i>Algae species</i>	<i>Annual production (t dry weight)</i>	<i>Products</i>
China, India, USA, Myanmar, Japan	<i>Spirulina</i>	3000	Human & animal nutrition, cosmetics
Taiwan, Germany, Japan	<i>Chlorella</i>	2000	Human nutrition, aquaculture, cosmetics
Australia, Israel, USA, China	<i>Dunaliella salina</i>	1200	Human nutrition, cosmetics, β carotene
USA	<i>Aphanizomenon flos-aquae</i>	500	Human nutrition
USA, India, Israel	<i>Haematococcus pluvialis</i>	300	Aquaculture, astaxanthin
USA	<i>Cryptocodinium cohnii</i>	240 t DHA oil	DHA oil
USA	<i>Shizochytrium</i>	10 t DHA oil	DHA oil

In 1998, the National Research (NREL) identified around 300 species of microalgae as potential oil producers, mostly diatoms and green algae (Sheehan et al., 1998). Nowadays, some of these species have been grown under different environmental conditions and in different culture systems, such as photobioreactors. Results have shown that it is possible to perform microalgae culture with interesting productivities; however, deeper studies have to be performed about the energy efficiency of cultivation, in particular harvesting and oil extraction, as well as the most appropriated environmental conditions for the species to growth.

1.1 Photosynthesis of algae

Photosynthesis is a reduction process divided in two stages: the *photolysis* (light reactions) and the *thermochemical stage* (dark reactions). Light reactions are performed in the thylakoid membranes of the chloroplast, which contain photosynthetic pigments, proteins, and enzymes.



The three major pigments, chlorophylls (green pigments), carotenoids (orange or yellow pigments), and phycobilins, presented in the antennae of photosystems I and II, are in charge of harvesting light while proteins and enzymes help to perform chemical reactions. These chemical reactions create energy by producing a reductant, called NADPH₂ and a high energy compound, called ATP (Figure I.2) (Cascallo, 2000; Richmond, 2007).

The thermochemical stage is also known as the Calvin-Benson cycle. It is performed in four main phases: carboxylation, reduction, regeneration, and production phase. The main objective is to use NADPH₂ and ATP to fix CO₂ by adding it to 5-carbon sugar (called ribulose biphosphate). This sugar will then, be transformed into more simple carbon sugar phosphates (3-carbon) (Figure I.2).

Figure I.2. The process of photosynthesis

Regarding photosynthesis as a chemical process that needs energy to produce storage components, it is of interest to estimate its efficiency in microalgae. Therefore, photosynthetic efficiency (PE) is defined as the ratio between the new biomass produced and the light energy absorbed. This means that the chemical energy produced and, stored as lipids, carbohydrates, and proteins, depends on the light energy available and absorbed in the cultivation system. PE is estimated by coupling efficiencies that are established in each step, from the light absorption to the biomass production (figure I.3).

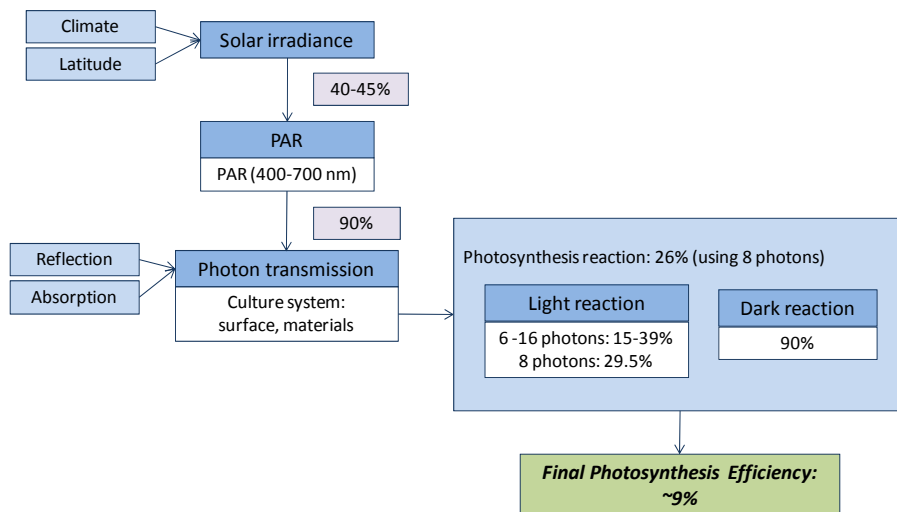


Figure I.3. Theoretical photosynthetic efficiency in microalgae.

Considering the total solar spectrum, algae pigments are capable of harvesting a range of this spectrum (between 40 and 45%), called the *Photosynthetic active radiation* or *PAR*. Since photons are reflected or absorbed by other elements, their transmission to the culture is lower than 100%. Instead, it is considered that 90% are transmitted to the culture. In photosynthesis reaction, the number of absorbed photons are still under discussion (ranging between 6 and 16), but 8 photons are generally agreed. As a consequence, the efficiency of the reaction is between 22% and 26%. Therefore, by coupling all efficiencies, theoretical value of photosynthetic efficiency under solar radiation is estimated around 9% (Janseen et al., 2003; Cadoret et al., 2008; Zemke et al., 2010). According to experimental studies, examples of realistic photosynthetic efficiencies obtained are 2-4% in *Synechococcus*, 6.48%, 6.56%, 7.05% in *Chlorella*, having higher values than the real PE in terrestrial plants, between 1% and 2% (Brennan and Owende, 2010).

1.2 Microalgae growth requirements

As photosynthetic organisms, microalgae require certain elements and environmental conditions to construct their internal components. Figure I.4 shows these elements and their possible sources as well as environmental conditions.

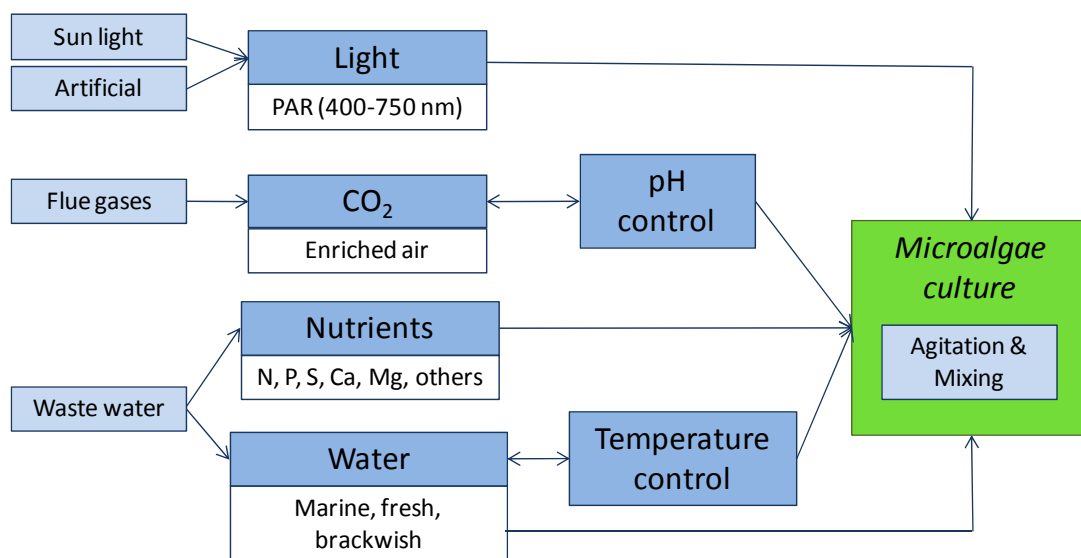


Figure I.4. Requirements for microalgae culture.

Elements and conditions are explained with more details in following sections.

1.2.1 Light energy

As it was explained above, light provides the energy necessary for the first biochemical reactions in photosynthesis. From all electromagnetic radiation spectra, around 40% represent the light spectra under which photosynthesis is performed. This range, from 400 to 700 nm is the so-called *Photosynthetically Active Radiation* (PAR) (Janssen et al., 2002; Richmond, 2007; Zemke et al., 2010).

Light energy is transported to cell pigments in the form of photons. Therefore, whether algal cultures are performed under solar or artificial light, algae growth rate is a function of the *photon flux density*

(PFD, expressed as $\mu\text{mol}/\text{m}^2\cdot\text{s}$) or *irradiance* that reaches the culture system. Moreover, *light flux* is usually expressed as lumens (lm) while the *intensity of illumination* is expressed as lux (lumens/m^2).

Optical properties of microalgae are based on the type and quantity of organic pigments present inside cells. According to the pigments (chlorophylls, carotenoids, and phycobilis), there are maximum peaks or bands of absorption inside the PAR. Chlorophylls are divided into Chl *a*, Chl *b*, Chl *c*, and Chl *d*, which have two major absorption bands: blue or blue-green (450-475 nm) and red (630-675 nm). Carotenoids have an absorption range between 400 and 550 nm while phycobilins absorb blue-green, green, yellow or orange light (500-650 nm) (Richmond, 2007).

Each microalgae species has different quantities and distributions of pigments, so the peaks or the range of energy absorption vary. If it is desired to perform microalgae culture under artificial light, the source can be selected to provide the closest light spectrum corresponding to the absorption of pigments.

Moreover, microalgae species have different photosynthetic responses according to the photon flux density at which they are exposed. This is represented by the *light response curve* (P/I), in which the photosynthetic activity is plotted as a function of photon flux densities. If the photosynthetic activity (PA) is deduced from the specific growth rate, the oxygen produced or the CO_2 absorbed, the P/I curve can result as shown in Figure I.5.

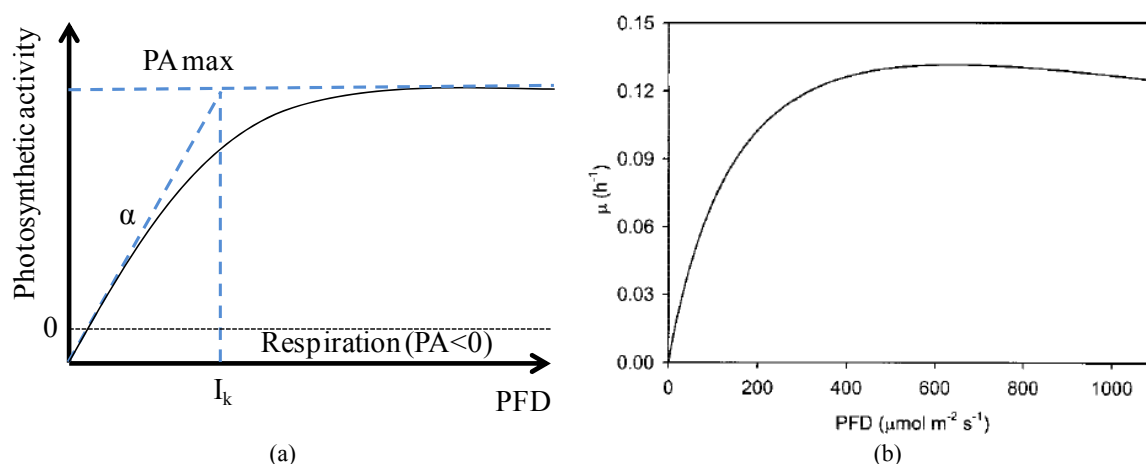


Figure I.5. Photosynthesis vs. Intensity (P/I) curve.

a) Schematic diagram of P/I curve. Based on Richmond, 2007; b) P/I curve: specific growth rate of *Chlamydomonas reinhardtii* as a function of the photon flux density (Janssen et al., 2002)

Curves I.5a and I.5b can be divided into three regions: *light limited region*, *light saturated region*, and *photoinhibited region*. In light limited region, there is an initial slope (α) that establishes a linear relationship between the maximal photosynthetic activity (PA_{max}) and the saturation irradiance (I_k).

At higher irradiances, PA has a lower increase until it reaches a constant value. At this point, the culture is considered light saturated, presenting the maximal photosynthetic activity. If irradiances continue to augment, there is a decline of the PA (Figure I.5b), thus there is photoinhibition of photosynthesis (Wu et al., 2001).

On the other hand, the negative part of the curve represents the respiration state, when microalgae uptake oxygen under the darkness. Here, it is considered that microalgae loss biomass, because some

lipids and carbohydrates fractions are consumed (Converti et al., 2006). However, it is generally agreed that respiration represents less than 10% of the total photosynthetic production, being negligible. Nevertheless, the total photosynthesis activity is the result from carbon uptake (O_2 release) and O_2 uptake (respiration) (Richmond, 2007).

If microalgae are cultivated under artificial light, short light-dark cycles can be established to impose high irradiances, enhancing growth rate and avoiding photoinhibition. According to several studies, results show that at low irradiances, there is no need of exposing cells to darkness because they can repair their physical damages under the light period. Instead, biomass production will diminish if dark periods are imposed (Merchuk et al., 1998). On the contrary, at high irradiances or light saturation conditions, there is the need of having cells under a period of darkness, in order to repair the damages of the photons traps and to promote the formation of new ones. This will compensate losses of biomass production during darkness (Richmond, 2007).

To study the influence of light/dark cycle on the growth rate, experimental studies have cultivated microalgae in photobioreactors, covering a determined surface to manipulate the time of microalgae under light. Generally it appears that, at higher radiations, maximal growth will be obtained by having longer dark periods. There is a balance between the irradiance and the time under lightness that has to be determined in order to reach maximal growth, without damaging photons traps (Wu et al., 2001). In some cases, establishing light/dark cycles has decreased growth rate in comparison to the culture being under continuous illumination (Janssen et al., 2000). Results differ according to microalgae species, type of reactor, circulation time, and irradiances (Janseen et al., 2002).

On the other hand, photon-flux distribution may not be homogeneous over the culture if there is a high-cell concentration, due to shadows originated between the cells (García et al., 1999). In theory, medium-cell densities allow capturing higher photon-flux fraction because there are less or any empty spaces in the culture. This tends to increase algae biomass, first exponentially and then linearly (Richmond, 2007). Nevertheless, authors have observed that biomass growth rates decrease at high cell density due to a shortage of light penetration. This means that, for a constant photon-flux density, there is an optimal cell or biomass concentration (e.g. 0.4 g/L for *Spirulina platensis* in raceway ponds) at which the culture has a high and constant productivity (Radmann et al., 2007). Alternatively, if there is a proper mixing in the system, all cells may be exposed to light, reaching higher productivities at higher biomass concentrations.

Therefore, it is important to notice that the incident irradiation is not the irradiation absorbed by cells in the culture. It varies according to culture concentration and the reactor capacity to promote cell mixing. If the reactor is placed outdoors, each cell receives an average irradiance that depends on reactor location, the season, and the climate (Molina et al., 1999). Consequently, it is necessary to estimate clearly the irradiance available for the culture as well as the capacity of the culture to absorb this energy, according to cell concentrations.

1.2.2 Carbon dioxide

Carbon dioxide is a source of inorganic carbon necessary for phytoplankton to perform photosynthesis. Microalgae, as phytoplankton, are organisms that take the carbon dioxide dissolved in marine, fresh, and brackish waters. Nowadays, oceans are considered as natural sinks in charge of absorbing the so-called “blue carbon”, representing 55% of the carbon taken by photosynthesis in the planet. Apart from phytoplankton, other organisms such as mangroves, salt marshes, and sea grasses

are also responsible of removing the carbon dioxide from the atmosphere (Nellemann et al., 2009). Consequently, microalgae are considered today as organisms capable of taking anthropogenic carbon dioxide from the atmosphere, once it is dissolved into the culture. It is generally agreed that 1 kg of algae absorbs between 1.65 and 1.8 kg of carbon dioxide, since algae biomass is composed of between 45% and 50% of carbon (Becker, 1998; Doucha et al., 2005).

According to several studies, photosynthesis activity increases if CO₂-enriched air is added to the liquid medium. However, CO₂ concentration has to be outside of the range where it becomes intoxicant for the species (Greque and Vieira, 2007).

Carbon dioxide concentrations ranging from 1 to 15 v/v% in air have been employed in experimental studies (Kadam et al., 1998; Doucha et al., 2005; Skjanes et al., 2007). Species like *Chlorella vulgaris*, *Monoruphidium minutum*, *Spirulina platensis*, *Scenedesmus obliquus*, and *Dunaliella tertiolecta* have been grown under these conditions and good productivities have been obtained. From these studies, it has been concluded that there is an optimal CO₂ concentration at which the species reproduce with high rates. This optimal concentration is different among the species (Zeiler et al., 1995; Nagase et al., 2001; Greque and Vieira, 2007).

When carbon dioxide has been injected into open ponds, important CO₂ losses have been observed compared to photobioreactors. As gas injection is better dispersed along the reactor, there is higher capacity to dissolve CO₂ in the culture, thus its availability for microalgae cells is higher. However, losses as high as 51% have been observed (Doucha et al., 2005).

On the other hand, it is important to follow the pH evolution according to the CO₂ injection. As pH tends to increase during photosynthesis, CO₂-enriched air has been employed to control pH since CO₂ dissolved in water tends to decrease it (Zeiler et al., 1995).

Experimental and pilot projects have proposed the use of flue gases, from fossil fuels burning, to feed microalgae cultures. Today, it is considered that flue gases from natural gas power plants can be injected into the microalgae culture due to relatively low CO₂ concentration (up to 15 v/v%) (Vunjak-Novakovic et al., 2005). However, flue gases have to be treated due to their high temperature since solubility of gases in water decreases with temperature. In addition, concentrations of other components such as NO_x and SO_x might damage the culture (Kadam, 1996; Doucha et al., 2005).

Whether flue gases are more or less treated, a determined energy is required to transport the gases to the culture, consequently there is an interest to place the culture as close as possible to the source. In addition, the energy to treat the gas, when needed, and its transport to the culture has to be taken into account when the culture system is installed. Both parameters account in the energy consumption balance and greenhouse gas emissions (Campbell et al., n.d).

1.2.3 Water and nutrients

Water is the liquid medium that contains nutrients required for algae growth. According to the microalgae species, water medium has certain requirements of pH, salinity, nutrients concentrations, and temperature. Salinity refers mainly to sodium and chloride concentrations, followed by other components like magnesium, calcium, and sulfate ions. In response to change in salinity, microalgae may change their composition, for example having more total lipid contents, decreasing unsaturated fatty acids or increasing carotenoids concentrations (Richmond, 2007).

Nutrients like carbon, nitrogen, and phosphorus play an important role in cellular metabolism and biochemical composition of algae. In addition of atmospheric CO₂, algae use carbon in the form of carbonate and bicarbonate. Algal biomass contains between 5 and 10% of nitrogen. The main sources of nitrogen are nitrate, ammonia and urea, being nitrate the most employed in microalgae culture. According to several studies, nitrogen deficiency increases lipid content in some microalgae species while in others, it increases carbohydrates (Becker, 1994; Richmond, 2007). Phosphorus is usually supplied as orthophosphate and it plays an important role in energy transfer and biosynthesis of nucleic acids in microalgae cells. Similarly to nitrogen, phosphorus limitation can induce an increase in β -carotene or astaxanthin (Sheehan et al., 1998; Richmond, 2007). To create a synthetic medium, types and nutrient concentrations to be employed, depend strongly on the species. An example of a synthetic medium is Zarrouck's medium, which is well known to cultivate *Spirulina*.

Temperature is an environmental factor that influences the biochemical composition of microalgae. Each species has an optimal range of temperature and out of this range, characteristics like composition of lipids, enzyme production, and carotenoid contents may change.

Authors have observed that changes in temperature affect the composition of fatty acids in cell membranes, because cells intend to maintain the stability and fluidity of membranes, specifically thylakoids (Richmond, 2007). On the other hand, temperature changes affect the metabolism of fatty acids, modifying the unsaturated to saturated fatty acids ratio. In some species, a decrease in temperature promotes an increase in unsaturated fatty acids and vice versa (e.g. *Spirulina platensis*, *Chlorella vulgaris* and *Botryococcus braunii*) (Sushchik et al., 2002). Changes in algae pigment (astaxanthin, β -carotene and cantaxanthin) quantities have been also observed when temperature was increased.

In culture systems placed outdoors, temperature is a parameter that strongly depends on climate conditions (e.g. temperature decay during the night). In closed systems, even if they are placed outdoors, the temperature is usually regulated by employing a thermobath or heating/cooling heat exchangers (Watanabe et al., 1995). For example, reactors made as tubular serpentine have been introduced in shallow pools filled with water (Sheehan et al., 1998; Huntley et al., 2006; Richmond, 2007).

The pH variation in the medium is mainly due to mineral carbon concentrations presented in the forms of CO₂, carbonic acid (H₂CO₃), bicarbonate (HCO₃⁻), and carbonate (CO₃²⁻). These four elements may vary according to photosynthetic activities, nitrates assimilation, CO₂ concentrations injected into the culture, and CO₂ released during respiration.

Nitrogen absorption also affects the pH of the medium, according to the assimilation of nitrate and ammonia. As it was mentioned, the pH tends to increase due to photosynthesis activity and it is usually controlled by CO₂ injection. Generally, microalgae species can tolerate a range of pH according to the species (e.g. *Spirulina platensis* survives under high pH, around 8.5), being more resistant to progressive variations and less resistant to abrupt pH changes (Becker, 1994; Richmond, 2007).

Dissolved oxygen in liquid medium is related to the oxygen produced and consumed during photosynthesis of microalgae. In the culture, dissolved oxygen is usually measured to quantify the photosynthetic activity, which is directly related to productivity. However, high levels of dissolved oxygen, like 300% of air saturation (depending on the temperature and the barometric pressure),

generally results in photosynthesis inhibition (Vonshak, 1997). To avoid high levels of dissolved oxygen in the medium, it is necessary to have a continuous mixing that provokes the proper turbulence to release it (Sánchez et al., 1999).

1.2.4 Mixing

Mixing microalgae cultures is indispensable to obtain optimal biomass productivities. Mixing magnitudes depend mainly on cell concentrations. As it was mentioned above, creating turbulence in reactors and open ponds help to release dissolved oxygen that might be intoxicant to the culture. Experimental studies have obtained that, at low-cell densities, the variation of mixing rates have not a significant effect on biomass productivities. However, when cell densities start to increase cell self-shading becomes important, thus it is necessary to promote turbulence inside the culture. In this manner, cells can travel from darkness to light and vice versa. On the other hand, dissolved oxygen tends to increase at higher biomass concentrations and, in the same way, mixing becomes necessary (Richmond, 2007; Eriksen, 2008).

In this sense, mixing is frequently performed by injecting gas, usually air or CO₂-enriched air into the reactor. In some cases, diaphragm or peristaltic pumps are used to create a flow circulation in the system (Converti et al., 2006). Conversely, paddle wheels are usually employed in open ponds, at low rotational velocities (Merchuk, 1991).

It is important to mention that stirring and mechanical mixing in microalgae culture has to be well designed in order to avoid shear stress over cells. Impellers may break down cells, especially if these are forming colonies. On the other hand, some studies have observed that high gas injection rate can also result in cells damaging (Eriksen, 2008). If gas injection rate is increased, bubbles tend to coalesce and break, so cells can be dragged to bubbles and finally broken. Even though the gas injection appears as the best method to mix cultures, it is necessary to find the most appropriate flow rate to avoid cell damaging.

1.3 Modes of culture - Specific growth rate and doubling time

Microalgae culture can be performed in batch or in continuous mode. In continuous mode, the volume of culture is relatively constant, because there is a fresh medium rate added to the culture and a removed volume rate. Generally, the feed rate and removal rate are identical (Richmond, 2007).

The dilution rate is a parameter that relates the flow rate at which the culture receives a new medium and the volume of the culture. The dilution rate influences the reactor performance as it determines the biomass productivity of the system (Travieso et al., 2001). The net increase of biomass is the difference between the biomass growth and the biomass removal.

In batch mode operation, an inoculum of microalgae is added to the culture medium already disposed in the cultivation system. Once the desired biomass concentration is reached, the cultivation is completely stopped and biomass is harvested. In a culture working in batch mode, different phases of growth are identified (Richmond, 2007):

Lag phase: once the inoculum is introduced into the culture system, the lag phase is a period of time at which cells adapt to environmental and nutritional conditions. Growth rate is slightly constant

Exponential phase: at the end of the lag phase, an exponential growth starts. Cells multiply very fast, growing exponentially as a function of time. According to cell concentrations, photons pass through the culture, a portion is absorbed or photons are completely absorbed. The growth of cells is exponential until all available photons are completely absorbed.

Linear phase: cells continue a lineal growth until there is a limitation of some nutrient or there is an inhibiting factor (e.g. light energy). When there is a inhibiting factor, growth rate becomes constant and then declines.

Figure I.6 shows a schematic diagram of the growth phases and an example of the evolution of cell numbers of *Nannochloropsis sp.* as a function of time. The culture was performed in a flat panel photobioreactor (Richmond et al., 2003).

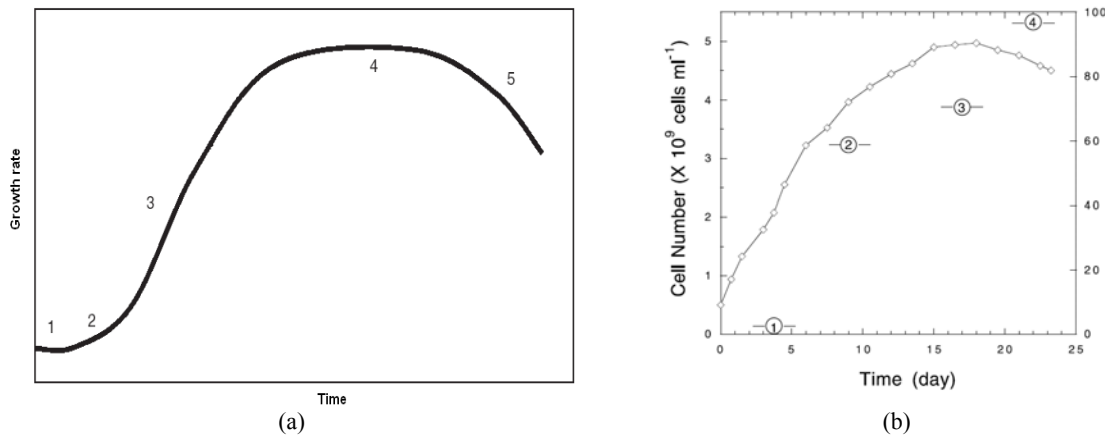


Figure I.6. Growth phases of *Nannochloropsis sp.*

a) Schematic diagram of growth rate phases: 1) lag phase; 2) exponential phase; 3) linear phase; 4) constant phase; 5) inhibition (Richmond, 2007); b) Growth phases of *Nannochloropsis sp.* (Richmond et al., 2003)

The *specific growth rate* is defined as the change of the number of cells (N) or biomass weight (X), in a period of time (t). Most of algae species reproduce by cell division, in which one cell separates into two daughters with identical DNA (Richmond, 2007).

If the cultivation system works in batch-mode, the specific growth rate is determined as follows:

$$\mu = \frac{1}{N} \cdot \frac{dN}{dt} \quad \text{or} \quad \mu = \frac{\ln(N/N_0)}{t - t_0} \quad (\text{I.1})$$

N_0 and N are cell densities at time t_0 and t respectively (Janssen et al., 2002; Kaewpintong et al., 2007). Specific growth rate varies according to the species and the environmental conditions at which the culture is exposed. According to experimental studies, specific growth rates are in the order of 1.82 1/day, varying from 0.2 to 3.8 1/day (Cadoret et al., 2008).

If the nutritional and environmental conditions are constant, the Monod's relation is the most well known to determine the *specific growth rate* according to the irradiance available in the reactor. Then, the specific growth rate is a function of the maximum growth rate (μ_{\max}) attainable at light saturation, the average photon flux density (I), and a light saturation constant (K_1), which is defined as the photon flux density required to achieve half of the maximum specific growth rate (Equation 2)

$$\mu = \mu_{\max} \cdot \frac{I}{I + K_I} \quad (\text{I.2})$$

Several authors have discussed the form of Equation 2, alleging that photoinhibition has not been taken into account. A better approximation of experimental results implies the utilization of Equation 3 but with powers higher than one (Molina et al., 1999).

$$\mu = \mu_{\max} \cdot \frac{I^n}{I^n + K_I^n} \quad (\text{I.3})$$

The *doubling time* (t_d) is defined as the time that takes a number of cells into double. Rearranging Eq. 1 in terms of biomass weight, it is defined as:

$$\ln\left(\frac{X}{X_o}\right) = (\ln 2) \frac{t}{t_d} \quad (\text{I.4})$$

Doubling time depends strongly on microalgae species, environmental, and nutritional conditions as well as the type of culture system. Values can be found as short as 3.5 hours or as long as 10 hours for *Phorphyridium* sp. and 5 days for *Botryococcus Braunii* (Wu et al., 2004; Chisti, 2007).

2. Microalgae production systems

Microalgae production systems refer to a well-controlled system built artificially in order to reach a certain algae productivity. These systems can be mainly divided into two categories: open ponds and photobioreactors.

2.1 Open ponds

Open ponds are referred as shallow open basins that can vary according to size, inclination, construction materials, and type of agitation. They can be found as circular ponds and raceway ponds. Circular ponds are circular basins provided with a rotating arm that creates a circular mixing. Those ponds are still widely used in Japan, Taiwan, and Indonesia (Lee, 2001)

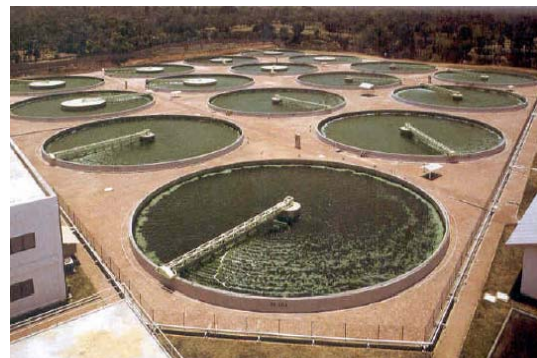
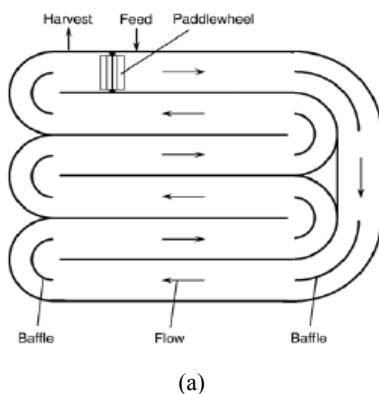


Figure I.7. Open ponds.

a) An scheme of a raceway ponds (Chisti, 2007); b) circular ponds (Ahsan et al., 2008)

Open raceway ponds are the most popular for microalgae culture. They consist in a racetrack that contains the culture, which is in a permanent circulation. This circulation is caused by a mechanical mixer, usually a paddle wheel that allows microalgae increasing the absorption of nutrients and to

release the generated oxygen. The water is kept shallow (usually between 20 and 30 cm deep) in order to give a proper exposition of microalgae to sunlight. Carbon dioxide is injected in form of bubbles and usually in counter-current flow (Sheehan, 1998; Van Harmelen et al., 2006; Chisti, 2007). These ponds can also be enclosed in order to avoid contamination and to better control the temperature. However, they are usually found opened in order to increase sunlight exposure and to reduce costs (Richmond, 2007).

Nowadays, large scale microalgae production is mostly developed in raceway ponds. Producer countries are Israel, United States of America, China, Thailand, Viet Nam, and Taiwan Province. The average dried biomass productivity is 10 to 25 g/m².d, having biomass concentrations in the order of 0.5 g/L (Becker, 1998; Lee, 2001). As an example, more than 80 companies produced *Spirulina* in China in 1997. In 2004, the worldwide production of *Spirulina* was 41,570 tons, representing 33% of world production of aquatic plants (FAO, 2007). The most well-known companies producing *Spirulina* today are Cyanotech, with a surface of 32 ha and biomass production of 350 t/year, and Earthwise with 43 hectares and a production of 450 t/year (Cyanotech, n.d.). Table I.3 shows a list of some companies producing microalgae at the present.

Table I.3. Companies producing microalgae.
(Carlsson et al., 2007, Edwards, 2008)

Company	Country	Product
AlgaTechnologies	Israel	Astaxanthin
Alpha Biotech	France	Phycocyanin
AquaCarotene	Australia	β-carotene & astaxanthin
BioEarth Spirulina	Italy (ponds in Mexico)	Spirulina
Cyanotech	Hawaii, USA	Phycocyanin & astaxanthin
Green Valley	Germany (ponds in Mexico)	Spirulina
Mera Pharmaceuticals	Hawaii, USA	Astaxanthin
Nature Beta Technologies	Japan	β-carotene
Parry Neutraceuticals	India	Astaxanthin, carotenoids
SeamBiotic	Germany	Omega 3
Western Biotechnology	Australia	β-carotene

2.2 Photobioreactors (PBR)

Photobioreactors are closed systems where the culture is not in direct contact with the environment. They are made of transparent materials, thus the light can pass through the walls to reach the culture. Today, they can be found in many types with many shapes. Their design is based on light surface exposure, culture mix efficiencies, and temperature and oxygen control as well as biomass productivities. One of the most important parameters for reactor design is the surface-to-volume ratio (s/v), which represents the reactor surface exposed to light per volume of reactor. Generally, biomass concentrations and volumetric productivities are higher as s/v ratio increases.

As open ponds, photobioreactor performance is evaluated according to its biomass productivity. Three parameters are commonly used to determine it: volumetric productivity, referred to biomass weight per reactor volume (g/L.d); areal productivity, referred to the biomass weight per unit of ground area occupied by the reactor (e.g. g/m².d); and illuminated surface productivity, referred to the biomass weight per unit of reactor illuminated surface area (e.g. g/m².d). A fourth parameter called

“overall areal productivity” can be included to the list in order to measure the productivity of the total area occupied by a group of reactors, including empty spaces (Richmond, 2007).

Next sections present a general description of different photobioreactor configurations.

2.2.1 Tubular photobioreactors

Tubular photobioreactors consist in a set of transparent tubes or pipes made of glass, acrylic or plexiglass installed in array. Generally, the system works in a close-loop where the microalgae culture flows continuously. Nutrients, CO₂, and water are fed to a vessel, from which they are pumped to the tubes. At the end of the circuit, algal biomass is collected according to microalgae maturity (Richmond, 2007; Molina et al. 1999).

Tubular photobioreactors can be found with many configurations. They can form a vertical or horizontal serpentine structure where tube ends are connected with U-bends (Figure I.8a). More recently, a tubular and triangular structure has been proposed in order to obtain a specific light-dark cycle. The hypotenuse is exposed to sunlight and the other two sides to the shadow (Figure I.8b). (Vunjak-Novakovic et al., 2005).

The most important geometrical parameters for tubular reactor design are tube diameter and wall thickness as well as mixing design. Previously, these types of photobioreactors have presented some problems referring to temperature control and oxygen release. Nowadays, an airlift compartment has been incorporated at the end of the circuit to release the accumulated oxygen (Richmond, 2007).



Figure I.8. Tubular photobioreactors.

a) Horizontal serpentine photobioreactor (Molina et al., 1999); b) Triangular tubular photobioreactor: pilot project (Vunjak-Novakovic et al., 2005).

2.2.2 Flat panel photobioreactors

A flat panel photobioreactor can be defined as a flat and thin reactor made of transparent panels that can be disposed horizontally, vertically or with a defined angle (figure I.9). Outdoors they can be exposed to solar energy and indoors to artificial light, illuminating both sides of the panels (Richmond and Wu, 2001). Generally, liquid circulates by using a mechanical pump or by gas injection. They have been largely employed at laboratory scale due to its easy operation and light measurement.

Flat panel photobioreactors are characterized geometrically by the light path. Several thicknesses have been tested and it has been found that there is an optimal light pass at which productivity is maximal (Richmond, 2007).

According to some experimental studies, these types of reactors can accumulate high level of dissolved oxygen, which can result into inhibition of photosynthesis activity. In addition, microalgae cells can attach to the corners due to the squared shape of the reactor (Sato et al., 2005)



Figure I.9. Flat panel photobioreactor. (Wageningen University, 2008)

2.2.3 Plastic-bag photobioreactors

These photobioreactors consist of a set of plastic, polyethylene bags hanging along a metallic support or frame. They can be found as sleeves (figure I.10) or panels, working in batch or continuous mode. Plastic bags have been operated indoors under artificial light, having a better temperature control.

Sleeves have relative low s/v ratio and they may present problems of biofouling. However, they can be considered as practical culture systems because they are easy to install and to replace sleeves. Sleeves have been tested in a pilot plant placed outdoors, forming a matrix and receiving CO₂ from flue gases of a power plant (Pulz, 2007).



Figure I.10. Sleeves bioreactors. GreenFuel Technologies (Pulz, 2007)

2.2.4 Column-photobioreactors

Column-bioreactors are the most employed in small microalgae production like in hatcheries (Richmond, 2007). Compared to horizontal serpentine PBR and open ponds, they occupy smaller surface. The culture is continuously mixed by a mechanical agitator or by gas injection. These reactors can be found with many configurations such as bubble and annular columns as well as airlift bioreactors.

Bubble columns consist in a simple cylinder in which a gas is injected at the bottom, creating bubbles that promote a random-cell agitation, culture mixing as well as exposition of cells to light and nutrients.

Annular bioreactors consist in two concentric cylinders forming an annular culture chamber. Placed indoors, artificial light is installed in the internal cylinder to illuminate the internal surface. Placed outdoors, the external surface receives the sunlight. In each case, the illuminated surface change being smaller in the first case than in the second case (Figure I.11).



Figure I.11. Annular bioreactor. (Fotosintetica Microbiologica s.r.l., 2008)

Airlift reactors (ALR) are composed of two cylinders that, according to their disposition, classify the reactor as internal or external. The riser corresponds to the cylinder where the gas is injected, to promote liquid circulation. In the downcomer, the liquid flows downward and it comes back to the riser. The gas is released through a degassing zone.

In internal airlift reactors, the two cylinders are placed concentrically forming an annular space. The internal cylinder is the riser compartment while the downcomer is the annular space. On the contrary, in external airlift reactor, the riser is placed next to the downcomer and they are connected on the top and at the bottom (Figure I.12).

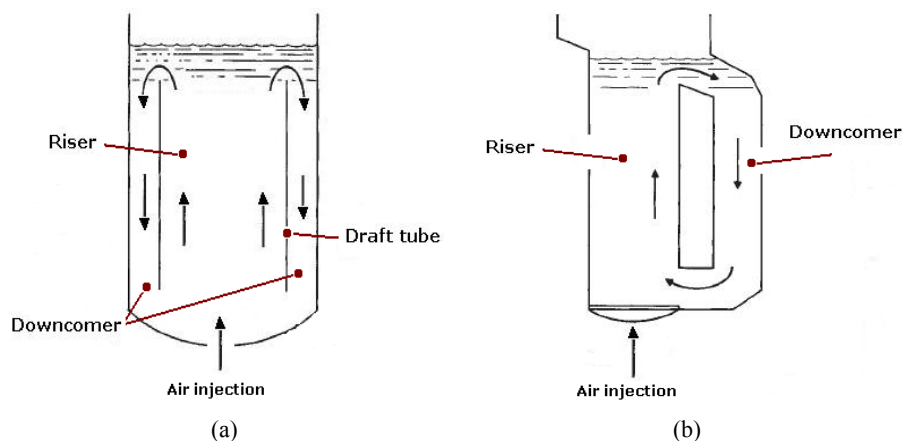


Figure I.12. Internal and external airlift reactors.

a) Internal airlift reactor; b) external airlift reactor (Perry et al., 1999)

Comparing airlift reactors with other configurations, they present the following advantages:

- Compared to bubble columns, liquid and cells have a more organized flow pattern since there are an upward and downward flows in relatively small cross sectional areas. In bubble columns, liquid and solid flows are random in a bigger cross sectional area, having less control over solids trajectory.
- Because ALR are vertical columns, they occupy less land surface compared to horizontal tubular photobioreactors or with inclined flat panels. This may lead to higher biomass productivities per land occupied.
- Compared to systems where an impeller is employed, airlift reactors are more cautious with microalgae cells because gas injection can be regulated in order to avoid cell damages. Mechanical mixed systems can provoke high shear rate over algae cells. On the other hand, air injection promotes gas exchange between the culture and the medium (Molina et al., 1999).
- Airlift reactors can be combined with tubular PBR to promote aeration in the culture, which is a major problem in tubular photobioreactors (Richmond, 2007).

Table I.4 shows a comparison among some photobioreactors and open productivities obtained until nowadays.

Table I.4. Photobioreactors and open ponds productivities nowadays.

Cultivation system	Species	P (g/m ² .d)	P (g/L.d)	References
Open pond	<i>Spirulina Platensis</i>	27	0.18	Lee, 2001
Open pond	<i>Spirulina Platensis</i>	14	0.05	Brennan & Owen, 2010
Open pond	<i>Chlorella sp.</i>	25	2.50	Lee, 2001
Flat plate	<i>Chlorella</i>	24	---	Richmond, 2007
Flat plate	<i>Nannochloropsis sp.</i>	---	0.27	Wu et al., 2001
Flat plate	<i>Haematococcus pluvialis</i>	10.2	---	Huntley & Redalje, 2007
Bubble column	<i>Haematococcus pluvialis</i>	---	0.06	García et al., 2006
Internal airlift reactor	<i>Chlorella sp.</i>	---	0.21	Xu et al., 2002

Table I.4. Photobioreactors and open ponds productivities nowadays (cont'd).

<i>Cultivation system</i>	<i>Species</i>	<i>P (g/m².d)</i>	<i>P (g/L.d)</i>	<i>References</i>
Internal airlift reactor	<i>Phaeodactylum tricornutum</i>	---	0.75	García et al., 1999
Outdoor tubular horizontal	<i>Phaeodactylum tricornutum</i>	---	0.017	Sánchez et al., 2002
Tubular	<i>Spirulina Platensis</i>	25.4	1.15	Carlozzi, 2002
Tubular manifold	<i>Spirulina Platensis</i>	28	1.13	Richmond, 2007
Helical bioreactor	<i>Spirulina Platensis</i>	6.45	0.4	Travieso et al., 2001
Outdoor helical bioreactor	<i>Phaeodactylum tricornutum</i>	---	1.4	Hall et al., 2003

2.3 Comparison among microalgae culture systems

When comparing microalgae culture systems, it is important to consider how it is desired to evaluate their performance, as not all photobioreactors fulfill all requirements. Moreover, cultivated species plays an important role in this evaluation, as one photobioreactor can be more adapted to some species than others. Compared with open ponds, nowadays photobioreactors are considered as the highest productive systems because:

- Parameters such as gas rate of injection, nutrients concentrations, temperature and pH of the liquid medium, and microalgae cell sizes are better monitored and controlled.
- Microalgae can be maintained isolated of other microorganisms that are considered as undesirable contaminants.
- The s/v ratio is higher (usually from 20 to 200 m⁻¹) compared to open ponds (from 5 to 10 m⁻¹), which means higher algal biomass productivity.
- Water losses due to evaporation are less important than in open ponds. In open ponds, this leads to important temperature fluctuations as well as changes in ionic composition of the liquid medium (Brennan and Owende, 2010).
- When photobioreactors are placed indoors and artificial light is employed, light-dark cycles can be manipulated in order to increase algal productivities. In open ponds, the light energy depends on the sun availability. If photobioreactors are placed outdoors, they can be inclined according to angles of sun rays, as it occurs with flat plate reactors (Borowitzka, 1999).

However, photobioreactors are more expensive than open ponds, with respect to construction, installation, and maintenance. Their productivity might decrease if constraints like biofouling, materials deterioration, artificial light depletion, oxygen accumulation or high cell shear stress are occurring. Photobioreactor design is strongly influenced by the growing characteristics of microalgae species. However, photobioreactors allow cultivating species that are not easily cultivable in ponds (Richmond, 2007).

On the other hand, photobioreactors have to include a degassing zone carefully designed in order to release the oxygen produced during photosynthesis. In raceway ponds, there is no need of a degassing zone because the constant mixing and open surfaces allow releasing oxygen easily (Chisti, 2007). Open raceway ponds systems deal with important water losses due to evaporation compared to photobioreactors, which means that the level of water has to be established in order to satisfy water volume required for the culture, light penetration, and mixing.

Different configurations of vertical bioreactors have been compared and in general, airlift reactors present higher productivity compared to bubble columns. In airlift reactors, the light-dark cycles can be better controlled and the culture is more exposed to light. In bubble columns, algae cells might have stress problems due to bubble blasts while in airlift reactors, bubbles are more uniformly distributed and controlled in the riser (Oncel et al., 2007). Column-bioreactors release more efficiently the oxygen produced by photosynthesis compared to tubular photobioreactors. Incorporation of airlift systems into tubular photobioreactors has diminished oxygen intoxication in cultures as well as reduction of cell breakages (Molina et al., 1999).

Culture systems made with plastic bags are relatively simple to construct compared to tubular and vertical reactors, having also higher productivities compared to open ponds. These systems might have problems of biofouling, but they can be easily replaced and do not imply high costs. In addition, they may present mixing deficiencies (Borowitzka, 1999; Richmond, 2007)

Finally, it can be observed that the design of open ponds and photobioreactors implies compromises between several factors that will affect their performance. The main objective is to create a culture system that guarantees a good control of the growth medium conditions: temperature, pH, oxygen and nutrient concentrations as well as an efficient mixing and light distribution over algae cells. As a consequence, a number of challenges have to be overcome for the development of photobioreactors. Several scaling up attempts have demonstrated that controlling growth conditions is more difficult than expected. Nowadays, scaling-up requires higher expenses compared to open ponds, which affects the final balance between costs and returns. The big challenge consists in finding a culture system with good control of growth conditions, reaching important biomass productivities and being cost effective.

2.4 Microalgae harvesting

Several methods are proposed to collect microalgae biomass once the cells have reached an appropriate size. The most common methods are flocculation, filtration, sedimentation, and centrifugation, which can be combined according to the desired quality of the final products (Molina et al., 2003).

Bioflocculation, chemical flocculation, and coagulation have been employed in wastewater treatment to create a dense mass of microalgae easier to remove. In bioflocculation, microalgae start to attach themselves forming flocks by using a non-algal microbial flocculant. In chemical flocculation, polymers are added to the system in order to decrease the electrostatic repulsive force between algae cells. In coagulation, the pH of the culture is manipulated to stimulate the formation of a denser mass, usually increasing pH according to the composition of the culture (Richmond, 2007).

In both chemical flocculation and coagulation, chemicals like ferric chloride, aluminum sulfate, ferric sulfate, and chitosan are used to promote the formation of flocks. Main disadvantages of both methods are the chemical toxicity, if they are not properly handled, as well as the costs to acquire them (Sheehan et al., 1998; Molina et al., 2003; Richmond, 2007). The slurry obtained after following one of these options, usually contains 3 to 5% of solids (Van Harmelen and Oonk, 2006).

These three techniques are usually followed by sedimentation, filtration or centrifugation. In sedimentation, suspended microalgae are deposited by the action of the gravity, creating a mass

concentration easier to remove. Centrifugation is a very common method used to recover high value metabolites. It promotes biomass sedimentation by the action of gravitational forces. According to the type of centrifuges and centrifugation forces, we can find harvesting efficiencies of 40%, 60%, and 95%. However, centrifugation is highly energy consuming (Molina et al., 2003; Brennan and Owende, 2010).

Filtration is a technique suitable for certain sizes of microalgae, while it is not successful for microalgae having very small sizes, close to bacterial sizes (<30 µm). The most common type of filters used at large scale, are rotary filters (that can work in vacuum or pressure mode) and chamber filter press. At laboratory scale, it is common to use micro strainers (typically 25 to 50 µm openings) to harvest microalgae. Other techniques such as microfiltration and ultrafiltration have been also considered for species that are more fragile, but their application has been scarce. It is important to highlight that if filtration is performed before centrifugation, higher concentration efficiencies and energy savings can be reached (Sheehan et al., 1998; Molina et al., 2003)

The next step after harvesting is to remove the remaining water in biomass. Typically, harvested biomass contains 5 to 15% of solids content (Brennan and Owende, 2010). The most common method to dry microalgae biomass in large scale is spray-drying. Spray-drying consists in creating small droplets of the harvested paste by using atomizers. Hot air is used to transform these droplets into powder. This method has been widely used for microalgae dehydrating and it has been applied to species like *Spirulina*, *Chlorella*, and *Dunaliella* (Richmond, 2007). Other methods are sun drying, low-pressure shelf drying, drum drying, fluidized-bed drying, and freeze drying, being more or less adequate to the process according to the desired final product (e.g oils, pigments, proteins, etc) (Brennan and Owende, 2010). At lower or experimental scale, the biomass is usually dried with hot air or by using a small oven.

2.5 Microalgae oil extraction and production

Lipids in microalgae are fatty acids presented in some of their components. Nowadays, the interest of microalgae oil resides in polyunsaturated fatty acids (PUFA) like arachidonic acid and eicosapentaenoic acid, important for human and animal nutrition, as well as neutral fatty acids like triacylglycerol and hydrocarbons. Lipids are in charge of providing energy in the form of ATP as well as the formation of cells and membranes (Volkman et al., 1998).

Today, one interest of microalgae lipids resides in the production of biodiesel. As oil is extracted from oleaginous plants, lipids are extracted from microalgae to perform transesterification reaction and produce biodiesel. In transesterification reaction, triglycerides react with methanol or ethanol to produce (m)ethyl esters and glycerol. Here, one ton of oil produces one ton of biodiesel. The main idea of transesterification is to reduce viscosity, reducing the large molecular structures of the algal oil (Chisti, 2007). Table I.5 shows an example of biodiesel properties from growing heterotrophically *Chlorella protothecoides*, compared to fossil diesel properties (Mia and Wu, 2006).

Table I.5. Properties of microalgae biodiesel and fossil diesel.
(Mia and Wu, 2006)

<i>Properties</i>	<i>Microalgae diesel</i>	<i>Fossil diesel (ASTM standards)</i>
Density (kg/L)	0.864	0.838
Viscosity (mm ² /s, cSt at 40°C)	5.2	1.9-4.1
Flash point (°C)	115	75
Solidifying point (°C)	-12	-50 to -10
Cold filter plugging point (°C)	-11	-3 (max. -6.7)
Heating value (MJ/kg)	37.2-41	40-45
H/C ratio	1.81	1.81

However, microalgae biodiesel characteristics depend, in a certain range, on species and growing conditions (Tran et al., 2010). In the case showed above, the biodiesel heating value is in the range of that of fossil diesel. In addition, it has an interesting value of cold filter plugging point, which means this biodiesel can be employed in cold winters.

According to several studies, it is estimated that some microalgae species have the potential to produce 30 times more oil than palm, the highest oil producer plant. Figure I.13 presents the current minimum and maximum oil production from oleaginous plants (t/ha.y) (Sazdanoff, 2006; Chisti, 2007; Tan et al., 2007). As it was mentioned above, by changing environmental conditions or nutrient concentrations, lipid concentrations can be altered. However, in most cases, this results in reducing biomass productivity (Cadoret et al., 2008).

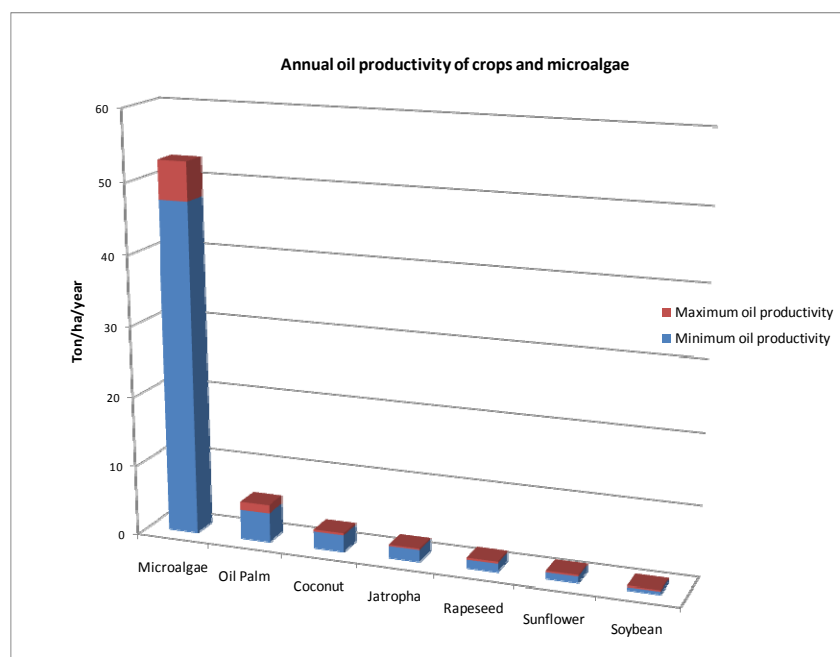


Figure I.13. Annual oil productivity of crops and microalgae.
(Sazdanoff, 2006; Chisti, 2007; Tan, 2007)

Examples of promising species for oil production are listed in Table I.6. This table shows the range of oil contained in species, both under environmental stress and non-environmental stress, expressed as percentage of dry weight.

Table I.6. Lipids contents in microalgae species considered for oil production.
ND: Nitrogen deficiency, NES: Non-environmental stress.

<i>Species</i>	<i>Stress</i>	<i>Lipids (%wt)</i>	<i>References</i>
<i>Cyclotella Cryptica</i>	ND	18	Feinberg, 1984
<i>Dunaliella salina</i>	ND	14.4-18.5	Feinberg, 1984
	NES	6	Spolaore et al., 2006
<i>Dunaliella tertiolecta</i>			
<i>Nitzschia sp.</i>	NES	45-47	Chisti, 2007
<i>Phaeodactylum tricornutum</i>	NES	20-30	Molina et al., 2001; Acién et al., 2003; Chisti, 2007
<i>Botryococcus Braunii</i>	ND	54.2	Feinberg, 1984; Sawayama et al., 1995.
	NES	25-75	Chisti, 2007
<i>Chlamydomonas sp.</i>	NES	23	Feinberg, 1984
<i>Chlorella sp.</i>	NES	20.7	Feinberg, 1984
	NES	28-32	Chisti, 2007
<i>Chlorella vulgaris</i>	ND	18	Illman et al., 2000; Huntley et al., 2006
	NES	14-22	Spolaore et al., 2006
<i>Nannochloris sp.</i>	NES	20-35	Chisti, 2007
<i>Nannochloropsis sp.</i>	ND	33.3-37.8	Huntley et al., 2006
	NES	31-68	Chisti, 2007
<i>Nannochloropsis salina</i>	ND	54	Feinberg, 1984
	NES	28.6	Feinberg, 1984
<i>Spirulina platensis</i>	NES	16.6	Feinberg, 1984
<i>Tetraselmis sueica</i>	ND	20-30	Huntley et al., 2006
	NES	15-23	Chisti, 2007
<i>Isochrysis sp.</i>	ND	26-45	Feinberg, 1984
	NES	25-33	Chisti, 2007

In order to extract the oil contained in microalgae biomass, two techniques are commonly found: mechanical pressing and solvents. Using mechanical pressing, algal oil can be extracted in a range varying from 70 to 75%.

Chemicals like n-hexane, benzene, methanol, ethanol, chloroform, and diethyl-ether can be used as solvents to extract fatty acids and other components such as β -carotene and astaxanthin from algae biomass (Molina et al., 2003; Brennan and Owende, 2010). The most common solvent to extract triglycerides is n-hexane, which is first added to the algae paste and then removed (e.g by adding a potassium bicarbonate solution or by using a rotary evaporator) (Rocheleau et al., 2000). Around 90% of lipids can be extracted from algae by using n-hexane (Richmond, 2007). The type of solvent to be used is carefully chosen according to its volatility and its capability to react with other biomass components.

According to Van Harmelen and Oonk, a target of 100 t/ha.y (around 27.4 g/m².d) of dried biomass can be produced (Van Harmelen and Oonk , 2006). Assuming that microalgae contain 50% of oil in weight and 90% can be extracted, the oil production will be around 45 t/ha.y. Comparing this value to results showed in Figure I.13, it seems this production should be possible in relatively short-term.

2.6 Thermochemical and biological conversion of microalgae

As it was mentioned above, the additional interest of microalgae is their potential to produce a form of energy like oil, biogas (methane), ethanol or char by performing thermochemical or biochemical conversion processes. Conventional conversion processes used to transform every type of biomass (e.g. wood in all its forms, organic waste, etc.) can be also employed, under certain conditions, to convert microalgae into energy. The final physico-chemical characteristics of the products will depend on the microalgae species, their growth environment and clearly, conditions of the process. Figure I.14 shows thermochemical and biochemical conversion processes proposed nowadays as well as their final products.

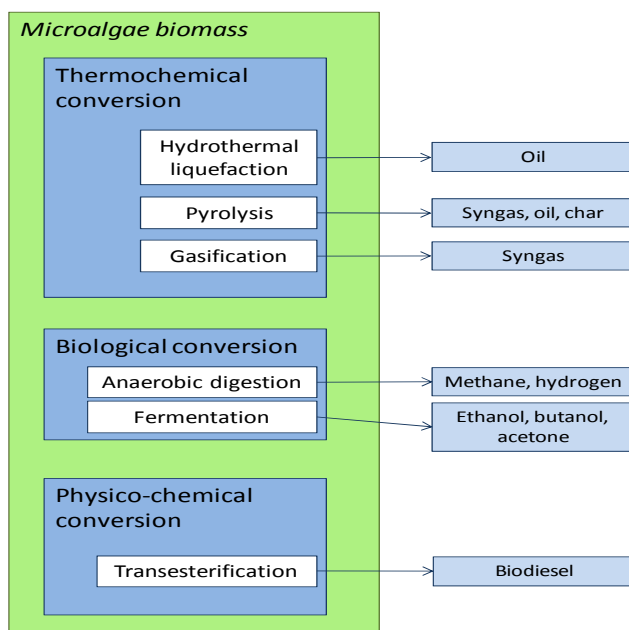


Figure I.14. Thermochemical, biological, and physico-chemical conversion processes to transform microalgae. Based on Brennan and Owende, 2010

2.6.1. Thermochemical conversion processes

Thermochemical conversion consists in transforming organic components of the biomass into a type of energy, by thermal decomposition. Inside this category processes like gasification, pyrolysis, combustion, and thermochemical liquefaction are included (Goswami and Kreith, 2008).

In gasification, biomass is oxidized at high temperatures to produce combustible gas called syngas, containing CO, CO₂, N, CH₄. Two types of gasification can be found today: *conventional gasification* and *supercritical water (or hydrothermal) gasification*. In the first case, biomass is decomposed without oxygen at high temperatures (800 to 1000°C) and pressures (Brennan and Owende, 2010). In the second case, biomass is brought to less high temperatures (250 to 600°C) and pressures (100-400 bar), reaching supercritical water state. In this state, water acts as a catalyst to transform biomass into valuable products, especially methane. Advantages of hydrothermal gasification over conventional gasification are that algae biomass can be wet and lower temperatures are required to perform the reaction (Wang et al., 2008). Microalgae species such as *Phaeodactylum tricornutum*, *Dunaliella bioculata*, and *Chlorella vulgaris* have been treated under hydrothermal gasification for full conversion of organic matter to a methane-rich gas (Haiduc et al., 2009).

In *pyrolysis*, the transformation of biomass is carried out under temperatures ranging from 200 to 700°C without air, producing oil, syngas (containing CO, CO₂, and CH₄) and charcoal. Studies with *Chlorella protothecoides* have shown that high oil yields above 50%, being higher than lignocellulosic materials (Peng et al., 2000). According to authors, the resulted oil from pyrolysis of *Chlorella protothecoides* has a heating value in the range of 30 to 41 MJ/kg while the heating value of wood pyrolysis is estimated between 17 and 21 MJ/kg (Bridgwater and Peacocke, 2000; Mia and Wu, 2004).

In *thermochemical liquefaction*, wet biomass is exposed to high pressures and temperatures (300 to 350°C) in order to reach sub-critical water state, on the contrary of hydrothermal gasification. In the presence of catalysts (e.g. potassium hydroxide, sodium carbonate) the biomass solves into the water, resulting in a type of bio-crude. Species like *Botryococcus braunii*, *Dunaliella tertiolecta*, *Spirulina platensis*, and *Chlorella* have been employed in hydrothermal liquefaction. According to FAO, oil yields are in the range of 31 to 44% with a heating value of 34.7 MJ/kg, which is lower than that estimated for microalgae biodiesel (Mia and Wu, 2006; Amin, 2009).

By comparing mentioned thermochemical conversion processes, the main difference resides in whether biomass can be wet or has to be previously dried. Once microalgae are harvested from the culture, they have high water content and, according to the conversion process to be performed, the biomass would have to be just thickened or both thickened and dried. In this sense, hydrothermal gasification and thermochemical liquefaction are more interesting processes, in terms of energy savings and costs, since algae biomass can be wet in a certain range (FAO bioenergy, 2009).

2.6.2. Biological conversion processes

Biological conversion processes refer to the biological degradation of polymers formed in algae due to photosynthesis. Nowadays, anaerobic digestion and fermentation are conversion processes employed in large scale to transform raw materials like organic wastes from landfill and farms, sewage sludge from wastewater treatment, food industry waste, manure, and others.

In *anaerobic digestion*, the organic material is degraded by some bacteria in the absence of oxygen. The final products are methane and carbon dioxide in larger proportion and, in smaller proportion, methane, water, and hydrogen sulfide. Microalgae contain minerals that serve as nutrients for anaerobic microflora and other nutrients- like zinc, iron, cobalt- that stimulate methanogenesis (Sialve et al., 2009). The utilization of microalgae as a raw material for anaerobic digestion can be considered by taking the entire biomass or after extracting some of their components. In the first case, algae biomass can be collected from open ponds and perform anaerobic digestion in covered lagoons (Campbell et al., 2010.). Nevertheless, there are limitations due to the characteristics of cell walls, which hinder the access to algae components if not disrupted. Some techniques (e.g. ultrasonic lysis, ozonation, acids and bases addition, thermal treatment, etc.) are used to reduce the resistance of cell walls to bacteria degradation (Sialve et al., 2009). However, these processes might be high energy intensive.

In the second case, oil can be extracted from microalgae for biofuel production. The remaining biomass, containing proteins and carbohydrates, can be used for anaerobic digestion to take advantage of the residual carbon. According to several studies, the higher the quantity of lipids, higher is the quantity of methane presented in the biogas. Therefore, it is necessary to determine whether it is more interesting, from the point of view of energy consumption and greenhouse gas emissions, to first

extract the lipids for biodiesel production before performing anaerobic digestion or to perform anaerobic digestion with the entire algae biomass. Microalgae species such as *Chlorella vulgaris*, *Spirulina*, *Dunaliella*, *Tetraselmis*, and *Microcystis* have been considered for anaerobic digestion (Sialve et al., 2009).

Fermentation consists in the transformation of sugars into ethanol by the action of bacteria. On the contrary of anaerobic digestion, here the reaction is performed under oxygen. In microalgae fermentation, there are two paths to profit from the starch accumulated in microalgae. The first is to add microalgae with high amounts of starch directly into the digester, letting them to metabolize the starch into ethanol. This path requires algae being capable of producing ethanol at high rate. The second path consists in extracting starch from microalgae and then, employing yeasts to transform the starch into ethanol, as it is practiced nowadays with sugar or corn starch (Benemann, 2008; Xu et al., 2010).

Finally, Table I.7 presents a short comparison among thermochemical and biological conversion processes for the transformation of algae biomass

Table I.7. Comparison among conversion processes of microalgae

		<i>Temp (°C)</i>	<i>Pressure (bar)</i>	<i>Microalgae specie</i>	<i>Yields</i>	<i>Heating value (MJ/kg)</i>	<i>Constraints</i>	<i>References</i>
Thermochemical conversion processes	<i>Conventional gasification</i>	800-1000		<i>Spirulina</i>	0.4-0.64 g methanol / g biomass	20.4	Biomass dehydrating is required	Hirano et al., 1998; Brennan and Owende, 2010
	<i>Supercritical gasification</i>	200-600	100-400	<i>Phaeodactylum tricornutum</i> , <i>Dunaliella bioculata</i> , <i>Chlorella vulgaris</i>	Efficiency 68-74%			Haiduc et al., 2009
	<i>Pyrolysis</i>	200-700		<i>Chlorella protothecoides</i> , <i>Emiliana huxleyi</i> , <i>Gephyrocopsa oceanica</i>	50-87 %wt oil	32.5-39.7	Biomass drying is required	Peng et al., 2000; Demirbas, 2010
	<i>Thermochemical liquefaction</i>	300-350	100-200	<i>Botryococcus braunii</i> , <i>Dunaliella tertiolecta</i> , <i>Spirulina platensis</i> , <i>Chlorella vulgaris</i> , <i>Nannochloropsis oculata</i> , <i>Porphyridium cruentum</i>	31-64 %wt oil	33- 39.9		Mia and Wu, 2006; Amin, 2009; Demirbas, 2010; Ross et al., 2010
Biological conversion processes	<i>Anaerobic digestion</i>	35-50	Atmospheric pressure	<i>Chlorella vulgaris</i> , <i>Spirulina</i> , <i>Dunaliella</i> , <i>Tetraselmis</i> , <i>Microcystis</i>	Methane: 147-240 mL/g vss; 530-790 mL/g vss	Methane 36.8 MJ/t	Inhibiting factors: high N and Na contents in biomass. Cell walls characteristics	Sialve et al., 2009; Ras et al., 2010
	<i>Fermentation</i>	15-40	Atmospheric pressure	<i>Chlamydomonas</i> , <i>Haematococcus</i> , <i>Chlorococcum littorale</i>	Ethanol: 4.67-14 L/m ² .y	Ethanol: 26.7 MJ/kg	Inhibiting factors: high N contents in biomass. Cell walls characteristics	Ueno et al., 1998; Beng, 2006; Xu et al., 2010

3. Conclusions

Microalgae are considered as organisms capable of producing very high valuable products for nutritional and industrial purposes, and nowadays as a source for energy generation. On the other hand, microalgae are considered as a potential tool to reduce greenhouse gas emissions, as their utilization as energy feedstock would demand less use of fossil fuels.

Microalgae are photosynthetic organisms; they require certain elements and conditions to live according to the species. Generally they need light energy, carbon dioxide, nutrients, water as well as specific conditions of temperature, and pH. Therefore, it is of interest to study how to obtain the mentioned elements as well as the appropriated cultivation system that will provide the required environmental conditions.

Several experimental studies employed flue gases to obtain the carbon dioxide demanded for photosynthesis. Results have shown that concentrations of CO₂ are limited because some species are more resistant than others. In addition, the ability to absorb CO₂ is linked to the nutrients contained in the growth medium as well as gases temperatures and pH. Therefore, the challenge is to find species that could resist high CO₂ concentrations while producing valuable products.

Moreover, the absorption of CO₂ by algae is interesting in other industrial processes. As some industrial processes produce important quantities of CO₂, the cultivation of algae might produce valuable products or can be employed to feed other energy production processes such as anaerobic fermentation, hydrothermal liquefaction and others.

In this sense, it is very important to select the most appropriated system to cultivate microalgae with high productivities. Cultivation systems as open ponds and photobioreactors have been proposed. At a large scale, working with open ponds has been frequently experimented, however there are disadvantages linked to the low biomass productivity and limitations to some microalgae species. Photobioreactors imply high investment and maintenance costs, but these constraints can be offset by higher algal biomass productivities as a result of better control of the process and environmental conditions.

Microalgae species have to be well selected to produce biodiesel. Microalgae produce higher quantities of oil compared with terrestrial oleaginous plants and, in certain species, oil productivities might be enhanced under environmental stress. This makes microalgae more interesting than palm plant for example, which is considered the highest oleaginous producer today, but with heavy environmental impacts like deforestation, resulting in carbon and biodiversity losses. However, all species are not expected to produce lipids in quantities which could be attractive enough to invest in microalgae culture. The compromise consists in selecting a cultivation system able to attain high photosynthetic efficiency and establish the best growth conditions.

Microalgal biomass can also be used in other energy generation processes, once the oil has been extracted. Depending on the residual biomass composition, it might be valuable to produce biogas by anaerobic digestion, ethanol by fermentation or syngas by pyrolysis. These conversion processes will produce co-products that might be valuable for other purposes. For example, after anaerobic digestion, residues can contain nitrogen and phosphorus potentially usable as fertilizers.

The feasibility of microalgae cultures requires deep studies about climate conditions, land availability,

available resources as well as positive and negative environmental impacts of the system. In this sense, it is important to evaluate the energy consumption needed by the system and the nutrients required, as well as the treatments needed for the effluents.

Finally, it is essential to evaluate all these parameters and to study the economical feasibility in order to estimate required investment and maintenance costs, as well as an economical, energetical and environmental balance of the process performed in a sustainable manner.

4. References

- Ahsan, M., Habib, B., Parvin, M., Huntington, T., Hasan, M. (2008) FAO: A review on culture, production and use of Spirulina as food for humans and feeds for domestical animals and fish [online] Available from: <ftp://ftp.fao.org/docrep/fao/011/i0424e/i0424e00.pdf> [Accessed 24 mars 2010]
- Amin, S. (2009) Review on biofuel oil and gas production process from microalgae. *Energy Conversion Management* 50, 1834-1840.
- Aresta, M., Dibenedetto, A., Barberio, G. (2005) Utilization of macro-algae for enhanced CO₂ fixation and biofuels production: Development of a computing software for an LCA study. *Fuel Processing Technology* 86, 1679-1693.
- BEAM. (2004). *Biotechnological and Environmental Applications of Microalgae*. [Online] Available from: Culture systems <http://www.bsb.murdoch.edu.au/groups/beam/BEAM-Appl4.html> [Accessed April, 2010]
- Becker, E. (1994) *Microalgae: Biotechnology and microbiology*. New York: Cambridge University Press.
- Benemann, J. (2008) Opportunities and challenges in algae biofuel production. [online] Available from: http://www.fao.org/uploads/media/algae_positionpaper.pdf [Accessed 10 december 2008]
- Berg, J. (2006) *Production of Micro algae-based Products. A map of available production methods for micro algae and market opportunities for algae-based products as a basis for establishing commercial operations*. Nordic Innovation Centre.
- Borowitzka, M., (1999) Commercial production of microalgae: ponds, tanks, tubes and fermenters. *Journal of Biotechnology* 70, 313-321
- Brennan, L., Owende, P. (2010) Biofuels from microalgae-A review of technologies for production, processing, and extractions of biofuels and co-products. *Renewable and Sustainable Energy Reviews* 14, 557-577.
- Bridgwater, A., Peacocke, G. (2000) Fast pyrolysis processes for biomass. *Renewable and Sustainable Energy Reviews* 4, 1-73.
- Cadoret, J., Bernard, O. (2008) La production de biocarburant lipidique avec des microalgues: promesses et défis. *Société de Biologie* 202, 201-211.
- Campbell, P., Beer, T., Batten, D. (n.d.) Greenhouse gas sequestration by algae – Energy and greenhouse gas life cycles studies. Transport Biofuels Stream, CSIRO Energy Transformed Flagship [online]. Available from: <http://www.csiro.au/resources/Greenhouse-Sequestration-Algae.html> [Accessed 27 january 2010]
- Carlozzi, P. (2000) Hydrodynamic aspects and *Arthrospira* growth in two outdoor tubular undulating row photobioreactors. *Applied Microbiology and Biotechnology* 54, 14-22.
- Carlsson, A., van Beilen, Möller, R., Clayton, D. (2007) Micro- and Macro algae: utility for industrial applications. Available from: <http://epobio.net/pdfs/0709AquaticReport.pdf> [Accessed 28 may 2008]

Cascallo, Anna. (2000) *Conception, contrôle et fonctionnement d'un photobioréacteur pour la culture en mode continu de la cyanobactérie Spirulina Platensis*. Ph. D thesis. Université de Technologie de Compiègne. Universitat Autònoma de Barcelona.

Chisti, Y., (2007) Biodiesel from microalgae. *Biotechnology Advances* 25, 294–306.

CNRS. Le journal du CNRS : Ces algues aux mille vertus. Laurianne Geffroy. (2008) [online] Available from: <http://www2.cnrs.fr/presse/journal/4238.html> [Accessed 18 mars 2010]

Converti, A., Lodi, A., Del Borghi, A., Solisio, C. (2006) Cultivation of *Spirulina platensis* in a combined airlift-tubular reactor system. *Biochemical Engineering Journal* 32, 13–18

Cyanotech (n.d.) *Spirulina*. [online] Available from: <http://www.cyanotech.com/spirulina.html> [Accessed 22 Mars 2010]

Demirbas, A. (2010). Use of algae as biofuel sources. *Energy Conversion and Management* 51, 2738–2749

Doucha, J., Straka, F., Livansky, K (2005) Utilization of flue gas for cultivation of microalgae (*Chlorella sp.*) in an outdoor open thin layer photobioreactor. *Journal of Applied Phycology* 17, 403–412.

Edwards, M. (2008) Green Algae Strategy End Oil Imports and Engineer Sustainable Food and Fuel [online] Available from: http://alextiler.com/agribusiness_resource/green_algae_strategy_paper.pdf [Accessed 22 July 2009]

Eriksen, N. (2008) The technology of microalgae culturing. *Biotechnology Letter* 30, 1525–1536.

FAO (2007) FAO yearbook. Fishery and Aquaculture Statistics. [online]. Available from : <http://www.fao.org/fishery/publications/yearbooks/en> [Accessed 24 mars 2010]

FAO Bioenergy (2009) Algae-based biofuels: a review of challenges and opportunities for developing countries. [Online]. Available from: http://www.fao.org/fileadmin/templates/aquaticbiofuels/docs/0905_FAO_Review_Paper_on_Algae-based_Biofuels.pdf [Accessed 24 January, 2010]

FAO. (2010). *ResourceSTAT-Land*. [Online] Available from: FAOSTAT <http://faostat.fao.org/site/377/default.aspx#ancor> [Accessed April 2010]

García, F., Contreras, A., Acien, F., Fernández, J., Molina, E. (1999) Use of concentric-tube airlift photobioreactors for microalgal outdoor mass cultures. *Enzyme and Microbial Technology* 24, 164–172.

García, M., Del Río Sánchez, E., Casas Lopez J, Acien, F., Fernandez, J., Rivas J, (2006) Comparative analysis of the outdoor culture of *Haematococcus pluvialis* in tubular and bubble column photobioreactors. *Journal of Biotechnology* 123, 329–342.

Goswami, Y., Kreith, F. (2008) *Energy Conversion*. Taylor & Francis Group. Boca Raton.

Grecque, M., Vieyra, J. (2007) Carbon dioxide fixation by *Chlorella kessleri*, *Chlorella vulgaris*, *Scenedesmus obliquus* and *Spirulina sp.* Cultivated in flasks and vertical tubular photobioreactors. *Biotechnology Letter* 29, 1349–1352

Guiry, M. (2008) Seaweed Site [Online]. Available from : <http://www.seaweed.ie/default.lasso> [Accessed 15 mars 2010]

Haiduc, A., Brandenberger, M., Suquet, S., Vogel, F., Latmani, R., Ludwig, C. (2009) SunCHem: an integrated process for the hydrothermal production of methane from microalgae and CO₂ mitigation. *Journal of Applied Phycology* 21, 529–541

Hall D., Acien F., Canizares, E., Krishna, K., Molina, E. (2003) Outdoor helical tubular photobioreactors for microalgal production: modeling of fluid-dynamics and mass transfer and assessment of biomass productivity. *Biotechnology and Bioengineering* 82, 62–73.

Hirano, A., Hon-Nami, K., Kunito, S., Hada, M., Ogushi, Y. (1998) Temperature effect on continuous gasification of microalgal biomass: theoretical yield of methanol production and its energy balance. *Catalysis Today* 45, 399-404.

Huntley M., Redalje, D. (2007) CO₂ mitigation and renewable oil from photosynthetic microbes: a new appraisal. *Mitigation and Adaptation Strategies for Global Change* 12, 573–608.

Ifremer. Le phytoplancton : *Skeletonema costatum*. [Online]. Available from : http://wwwz.ifremer.fr/var/envlit/storage/documents/documents_pedagogiques/phyto3d/almphyto3d.html [Accessed 18 mars 2010]

Janssen, M., Bresser, L., Baijens, T., Mur, L., Snel, J., Wijffels, R., (2000) Scale-up aspects of photobioreactors: effects of mixing induced light/dark cycles. *Journal of Applied Phycology* 12, 225–237.

Janssen, M., Slenders, P., Tramper, J., Mur, L., Wijffels, R. (2001) Photosynthetic efficiency of *Dunaliella tertiolecta* under short light/dark cycles. *Enzyme Microbiology Technology* 29, 298–305.

Janssen, M., Tramper, J., Mur, L., Wijffels, R. (2002) Enclosed Outdoor Photobioreactors: Light Regime, Photosynthetic Efficiency, Scale-Up, and Future Prospects. *Biotechnology and Bioengineering* 81, 193-210.

Kadam, K (1996) Power plant flue gas a source of CO₂ for microalgae cultivation: economic impact of different process options. *Energy Conversion Management* 38, S505-S510.

Kaewpintong, K., Shotipruk, A., Powtongsook, S., Pavasant, P. (2007). Photoautotrophic high-density cultivation of vegetative cells of *Haematococcus pluvialis* in airlift bioreactor. *Bioresource Technology* 98, 288–295.

Lee, Y. (2001) Microalgal mass culture systems and methods: Their limitation and potential. *Journal of Applied Phycology* 13, 307–315

Merchuk, J. (1991) Shear effects on suspended cells. *Advanced Biochemical Engineering* 44, 65–95.

Merchuk, J., Ronen, M., Giris, S., Arad, S. (1998) Light/Dark Cycles in the Growth of the Red Microalga *Porphyridium Sp.* *Biotechnology and Bioengineering* 59, No. 6.

Metzger, P., Largeau, C. (2005) *Botryococcus braunii*: a rich source for hydrocarbons and related ether lipids. *Applied Microbiology Biotechnology* 66, 486–496

Miao, X., Wu, Q., (2004) High yield bio-oil production from fast pyrolysis by metabolic controlling of *Chlorella protothecoides*. *Journal of Biotechnology* 110, 85–93

- Miao, X., Wu, Q., (2006) Biodiesel production from heterotrophic microalgal oil. *Bioresource Technology* 97, 841–846.
- Molina, E., Ación, F., Camacho, F., Chisti, F. (1999) Photobioreactors: light regime, mass transfer, and scaleup. *Journal of Biotechnology* 70, 231–247.
- Molina, E., Belarbi, E.H., Ación Fernández, F.G., Robles Medina, A., Chisti, Y. (2003) Recovery of microalgal biomass and metabolites: process options and economics. *Biotechnology Advances* 20, 7–8, 491–515.
- Nagase, H., Yoshihara, K., Eguchi, K., Okamoto, Y., Murasaki, R., Yamashita, R., Hirata, K., Miyamoto, K. (2001) Uptake pathway and continuous removal of nitric oxide from flue gas using microalgae. *Biochemical Engineering Journal* 7, 241–246
- Nellemann, C., Corcoran, E., Duarte, C. M., Valdés, L., De Young, C., Fonseca, L., Grimsditch, G. (2009) Blue Carbon. A Rapid Response Assessment. United Nations Environment Programme, GRID-Arendal [online] Available from: <http://www.grida.no/publications/rr/blue-carbon/> [Accessed 30 mars 2010]
- Oncel, S., Sukan, V. (2007) Comparison of two different pneumatically mixed column photobioreactors for the cultivation of *Artrospira Platensis* (*Spirulina Platensis*). *Bioresource Technology* 99, 4755–4760.
- Peng, W., Wu, Q., Tu, P. (2000) Effects of temperature and holding time on production of renewable fuels from pyrolysis of *Chlorella protothecoides*. *Journal of Applied Phycology* 12, 147–152.
- Perry, R., D. Green, et J. Maloney (1999) *Perry's Chemical Engineers's handbook*. United States of America: McGraw-Hill.
- Pulz, O. (2007) Performance Summary Report. Evaluation of GreenFuel's 3D Matrix Algae Growth. Engineering Scale Unit. APS Red Hawk Power Plant. [online] Available from: http://moritz.botany.ut.ee/~olli/b/Performance_Summary_Report.pdf [Accessed 26 September 2007]
- Pulz, O., Gross, W. (2004) Values products from biotechnology of microalgae. *Applied Microbiology Biotechnology* 65, 635–648.
- Radmann, E., Reinehr, C., Costa, J. (2007) Optimization of the repeated batch cultivation of microalga *Spirulina platensis* in open raceway ponds. *Aquaculture* 265, 118–126.
- Ras, M., Lardon, L., Sialve, B., Bernet, N., Steyer, J.P. (2010) Experimental study on a coupled process of production and anaerobic digestion of *Chlorella vulgaris*. *Bioresource Technology* 102, 200–206.
- ResourceSTAT-Land (2009) Land Use Database. [online] Available from: <http://faostat.fao.org/site/377/default.aspx#ancor> [Accessed 1 April, 2010]
- Richmond, A. (2007) *Handbook of Microalgal Culture*. Biotechnology and Applied Phycology. Blackwell Science.
- Richmond, A., Wu, Z. (2001) Optimization of a flat plate glass reactor for mass production of *Nannochloropsis* sp. outdoors. *Journal of Biotechnology* 85, 259–269
- Richmond, A., Wu, Z., Zarmi, Y. (2003) Efficient use of strong light for high photosynthetic productivity: interrelationships between the optical path, the optimal population density and cell-growth inhibition. *Biomolecular Engineering* 20, 229–36.

Rocheleau R., Benemann, J. (2000) Biohydrogen Production. Report to the U.S Department of Energy Hydrogen Program. Hawaii Natural Energy Institute, University of Hawaii. [online] Available from: <http://www.hnei.hawaii.edu/docs/seminars/2002/HNEI2001H2Rptfinal.pdf> [Accessed 2 February 2010]

Ross, A., Jones, J., Kubacki, M., Bridgeman, T. (2008) Classification of macroalgae as fuel and its thermochemical behavior. *Bioresource Technology* 99, 6494–6504

Ross, A., Jones, J., Kubacki, M., Bridgeman, T. (2010) Hydrothermal processing of microalgae using alkali and organic acids. *Fuel* 89, 2234–2243.

Sánchez, A, Ceron, M., García, F., Molina, E, Chisti, Y. (2002) Growth and biochemical characterization of microalgal biomass produced in bubble column and airlift photobioreactors: studies in fed-batch culture. *Enzyme and Microbial Technology* 31, 1015–1023.

Sato, T., Usui, S., Tsuchiya, Y., Kondo, Y. (2006) Invention of outdoor closed type photobioreactor for microalgae. *Energy Conversion and Management* 47, 791–799.

Sazdanoff, N. (2006) Modeling and Simulation of the Algae to Biodiesel Fuel Cycle. Report, Department of Mechanical Engineering, The Ohio State University, United States. [online] Available from: https://kb.osu.edu/dspace/bitstream/1811/5981/1/Modeling_and_Simulation_of_the_Algae_to_Biodiesel_Fuel_Cycle-Sazdanoff_undergrad_thesis.pdf [Accessed 11 December 2007]

Sheehan, J., Dunahay, T., Benemann, J., Roessler, P., (1998) A Look Back at the U.S. Department of Energy's Aquatic Species Program—Biodiesel from Algae. Report, U.S. Department of Energy's Office of Fuels Development. [online] Available from: <http://www.nrel.gov/docs/legosti/fy98/24190.pdf> [Accessed 18 April 2008]

Sialve, Bruno, Bernet, N., Bernard, O. (2009) Anaerobic digestion of microalgae as a necessary step to make microalgal biodiesel sustainable. *Biotechnology Advanced* 27, 409–416.

Skjanes, K., Lindblad, P., Muller, J., (2007). BioCO₂ – A multidisciplinary, biological approach using solar energy to capture CO₂ while producing H₂ and high value products. *Biomolecular Engineering* 24, 405–413

Spolaore, P., Joannis-Cassan, C., Duran, E., Isambert, A., (2006) Commercial Applications of Microalgae. *Journal of Bioscience and Bioengineering* 101, 2, 87–96

Stepan, D., Shockey, T., Moe, T., Dorn, R. Subtask 2.3 – Carbon dioxide sequestering using microalgal systems. [online] Available from: <http://www.osti.gov/bridge/purl.cover.jsp?jsessionid=83B7F08746133055D05D2D1C8ECF8086?purl=/882000-St23VC/> [Accessed 7 July 2009]

Sushchik N., Kalacheva G., Zhila N., Gladyshev M., Volova, T. (2003) A temperature dependence of the intra- and extracellular fatty acid composition of green algae and cyanobacterium. *Russian Journal Plant Physiology* 50, 374–80.

Ueno, Y., Kurano, N., Miyachi, S. (1998). Ethanol Production by Dark Fermentation in the Marine Green Algae, *Chlorococcum littorale*. *Journal of Fermentation and Bioengineering* 86, 38–43

Tan, K., Lee, K., Mohamed, A., Bhatia, S. (2007) Palm Oil: Addressing issues and towards sustainable development. *Renewable and Sustainable Energy Reviews* 13, 420–427

- Tran, N., Bartlett, J., Kannangara, G., Milev, A., Volk, H., Wilson, M. (2010) Catalytic upgrading of biorefinery oil from micro-algae. *Fuel* 89, 265–274.
- Travieso L, Hall DO, Rao KK, Benitez F, Sánchez E, Borja R (2001) A helical tubular photobioreactor producing *Spirulina* in a semicontinuous mode. *International Biodeterioration Biodegradation* 47,151–155.
- Van Harmelen, T., Oonk, H. (2006) MICROALGAE BIOFIXATION PROCESSES: Applications and Potential Contributions to Greenhouse Gas Mitigation Options. Report, International Network on Biofixation of CO₂ and Greenhouse Gas Abatement [online] Available from: <http://www.fluxfarm.com/files/Biofixation.pdf> [Accessed 19 november 2007]
- Vilchez, C., Garhayo, I., Lobato, M., Vega, J. (1997) Microalgae-mediated chemicals production and wastes removal. *Enzyme and Microbial Technology* 20, 562-572.
- Volkman, J., Barrett, S., Blackburn, S., Mansour, M., Sikes, E., Gelin, F. (1998) Microalgal biomarkers: A review of recent research developments. *Organic Geochemistry* 29, 1163-1179
- Vonshak, A. (1997). *Spirulina Platensis (Arthrospira): Physiology, Cell-biology and Biotechnology*. London: Taylor & Francis.
- Vunjak-Novakovic, G., Kim, y., Wu, X., Berzin, I., Merchuk, J. (2005) Air-Lift Bioreactors for Algal Growth on Flue Gas: Mathematical Modeling and Pilot-Plant Studies. *Industrial Engineering Chemical Resources* 44, 6154-6163.
- Wang, B., Li, Y., Wu, N., Lan, C. (2008) CO₂ bio-mitigation using microalgae. *Applied Microbiology Biotechnology* 79, 707–718.
- Watanabe, Y., Hall, D. (1995) Photosynthethic CO₂ fixation technologies using a helical tubular bioreactor incorporating the filamentous cyanobacterium *Spirulina platensis*. *Energy Conversion Management* 36, 721-724.
- Wiliams, S., Smith, J. (2007). A global review of the distribution, taxonomy and impacts of introduced seaweeds. *Annual Review of Ecology, Evolution Systematics* 38, 327–59.
- Wu, X., Merchuk, J. (2001) A model integrating fluid dynamics in photosynthesis and photoinhibition processes. *Chemical Engineering Science* 56, 3527 – 3538.
- Xu, Y., Isom, L., Hanna, M. (2010) Adding value to carbon dioxide from ethanol fermentations. *Bioresource Technology* 101, 3311-3319.
- Xu, Z., Baicheng, Z., Yiping, Z., Zhaoling, C., Weil, C., Fan, O. (2002) A simple and low-cost airlift photobioreactor for microalgal mass culture. *Biotechnology Letters* 24, 1767–1771.
- Zeiler, K., Heacox, D., A., Toon, S., Kadam, K., Brown, L. (1995) The use of microalgae for assimilation and utilization of carbon dioxide from fossil fuel-fired power plant flue gas. *Energy Conversion Management* 36, 707-712.
- Zemke, P, Wood, B., Dye, D. (2010). Considerations for the maximum production rates of triacylglycerol from microalgae. *Biomass and Bioenergy* 34, 145-151.

Hydrodynamic study of an Internal Airlift Reactor for microalgae culture

(Article submitted in Applied Microbiology and Biotechnology)

Hydrodynamic study of an internal airlift reactor for microalgae culture

A. Rengel, A. Zoughaib, D. Dron, D. Clodic

Centre Energétique et Procédés (CEP). MINES ParisTech
5 rue Léon Blum. Palaiseau. 91120. France

Abstract

Internal airlift reactors are closed systems considered today for microalgae cultivation. Several works have studied their hydrodynamics but based on important solid concentrations, not with biomass concentrations usually found in microalgae cultures.

In this study, an internal airlift reactor has been built and tested in order to clarify the hydrodynamics of this system, based on microalgae typical concentrations. A model is proposed taking into account the variation of air bubble velocity according to air flow rate injected into the system. A relationship between riser and downcomer gas holdups is established, which varied slightly with solids concentrations. The repartition of solids along the reactor resulted to be homogenous for the range of concentrations and air flow rate studied here. Liquid velocities increases with air flow rate are observed when solids are added to the system. Finally, liquid circulation time found in each section of the reactor is in concordance with those employed in microalgae culture.

Keywords: internal airlift reactor; hydrodynamic; microalgae

Nomenclature

A	Cross sectional area	m ²
C _r	Distribution parameter – Drift flux model	
D	Diameter	m
G	Gravitational acceleration	m/s ²
J	Volumetric flux	m ³ /m ² .s
P	Pressure	Pa
Q	Volumetric flow rate	m ³ /s
Re	Reynolds number	
U _{bt}	Terminal bubble velocity	
V	Volume	m ³
V _∞	Terminal bubble velocity in an infinite vessel	m/s
V _b	Bubble slip velocity	m/s
X	Solids loadings	
PHL	Pseudo-homogenous liquid	

Greek symbols

ε	Holdup
α	Parameter - relationship between gas holdups

β	Parameter - relationship between gas holdups	
μ	Viscosity	Pa.s
ρ	Density	kg/m ³
σ	Surface tension	N/m

Subscripts

b	Bubble
d	Downcomer
g	Gas
h	Pseudo-homogenous phase
i	Phase
j	Reactor section
l	Liquid
r	Riser
s	Solids
Sp	Superficial

1. Introduction

Bioreactors are closed systems that have been extensively used in the field of biotechnology, involving microorganism production. Nowadays, they can be found with many configurations at laboratory scale and in the industry. However, few bioreactors operate according to the conditions required for the process.

In this sense, airlift reactors (AL) have been employed in processes such as aerobic digestion in wastewater treatment, animal cell culture, the production of enzymes, antibiotics, and proteins (Heijnen et al., 1997). Their advantages over other closed systems lay in the utilization of compressed gas to promote liquid circulation as well as mass exchange between the gas and the liquid medium. Compared to systems where an impeller is employed, airlift reactors are more cautious with microalgae cells because gas flow rate can be regulated in order to avoid cell damages. They do not stress the cells as it occurs in mechanical mixing.

Nowadays, there is a special interest in performing microalgae culture due to their potential for energy production. Microalgae are considered as a promising biomass source that can be employed as raw material in processes, such as anaerobic digestion, hydrothermal conversion, production of lipids, to produce fuels. Their cultivation is highly demanding of well-controlled environmental conditions, which vary according to the specie. In this context, internal airlift reactors (IAL) appear as a potential bioreactor that provide required conditions for algae cells to reproduce: proper exposition to light energy, good mass exchange between the gas and the liquid, flow mixing and low shear stress over the cells. Microalgae species like *Phaeodactylum tricornutum*, *Haematococcus pluvialis*, *Spirulina Platensis*, *Chlorella sp.* and *Botryococcus Braunii* have been cultivated in this type of reactor and studies have demonstrated that important productivities are reachable (Merchuk et al., 1998; Sanchez Miron et al., 2002; Zhang et al., 2002; Oncel and Sukan, 2007).

In order to provide the best conditions for microalgae in IAL reactors, it is of interest to determine all the parameters that characterize their hydrodynamics. IAL reactors have been largely studied, obtaining gas holdups, liquid velocities as well as the influence of solids on their operation (Chisti, 1989; Freitas et al., Livingston et al., 1993). However, few studies have determined the relationship between gas holdups as well as the influence of real concentrations of algae biomass obtained during cultivation.

The aim of this work is to study an internal airlift reactor for microalgae culture. The objective is to perform an experimental and modeling study in order to examine the influence of typical microalgae concentrations on gas distribution and liquid velocities along the reactor. In addition, a relationship between riser and downcomer gas holdup is proposed, as a result of the experimental work. Final results show the residence time of cells in each section, which is an important design parameter influencing the light energy distribution inside the reactor.

2. Theory

2.1 Holdup

Gas (ε_g), liquid (ε_l), and solid holdups (ε_s) are defined as the volume of each phase related to the total volume of the mix, encompassing liquid, solids, and gas phases

$$\varepsilon_i = \frac{V_{\text{volume},i}}{V_{\text{volume},s} + V_{\text{volume},g} + V_{\text{volume},l}} \quad \text{With } i = g, l, s \quad (\text{II.1})$$

When microalgae culture is performed in an airlift reactor the system works with three-phase flow. The liquid is a solution composed of minerals and vitamins, the gas is a combination of air and CO₂ while solids are represented by microalgae biomass.

2.2 Superficial velocity

Superficial velocity ($V_{\text{sp},i}$) of a phase i is the velocity at which one phase would flow alone through the cross-sectional section.

$$V_{\text{sp},i} = \frac{Q_i}{A} \quad \text{With } i = g, l, s \quad (\text{II.2})$$

The actual velocities are related to superficial velocities in the form given by Equations II.3 and II.4.

$$V_{\text{sp},i} = \varepsilon_i \cdot V_i \quad (\text{II.3})$$

$$V_{sl} = \varepsilon_l \cdot V_l = (1 - \varepsilon_g) \cdot V_l \quad (\text{II.4})$$

2.3 Solids loading and holdup

Solids loading (X_s) refers to the solid volume presented in the liquid. In this study, it is considered that solids loading is homogeneous in each compartment of the reactor.

$$X_s = \frac{V_{\text{volume},s}}{V_{\text{volume},s} + V_{\text{volume},l}} \quad (\text{II.5})$$

From solids loading and holdup definitions, the following relationship can be established:

$$\varepsilon_s = X_s (1 - \varepsilon_g) \quad (\text{II.6})$$

2.4 Properties of the pseudo-homogenous phase

In this study, liquid and solids are considered a pseudo-homogenous liquid phase that follows average physical properties such as density and viscosity. These properties are estimated following the correlations proposed by Wallis (Wallis, 1969):

$$\rho_h = \rho_l (1 - X_s) + \rho_s X_s \quad (\text{II.7})$$

$$\mu_h = (1 + 2.5X_s + 7.25X_s^2) \mu_l \quad (\text{II.8})$$

3. Model

Several models have been proposed to estimate gas holdups and liquid circulation velocities according to the gas flow rate injected into the system. Two types of mathematical models are generally found in the literature. A first proposition is based on the two-phase *Drift-flux model* and performing a balance between the hydrostatic pressure difference and the losses in the entire system (Lu et al. 1994; Freitas et al., 1999; Livingston et al., 1993). A second proposition consists in a macroscopic energy balance in the system, taking into account the energy given by the gas to the liquid and energy dissipations in the reactor (Merchuk et al., 1995; Wongsuchoto

et al., 2004). A certain number of these models are not applicable when there is recirculation of the gas to the riser, limiting their applicability (Chisti et al., 1988).

In this work, a mathematical model, based on a macroscopic balance, is developed. Figure 1 shows a scheme of an internal airlift reactor and the variables considered for the model.

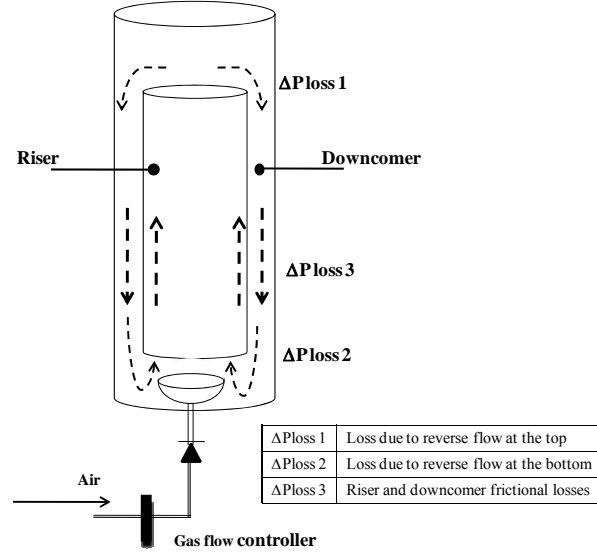


Figure II.1. Scheme of an internal airlift reactor.
Parameters taken into account to model reactor hydrodynamics.

The pressure difference between the riser and the downcomer (ΔP_h) and losses in the system (ΔP_{loss}) are considered equal, as a result of applying the momentum equation (Lu et al. 1994; Freitas et al., 1999; Livingston et al., 1993).

$$\Delta P_h = -\Delta P_{loss} \quad (II.9)$$

The hydrostatic pressure difference between the two compartments is a consequence of the gas injection in the riser. In the riser, the pressure head diminishes while the gas is injected into the system. In the downcomer, pressure head is always higher than in the riser, due to the absence or very low gas volume. The result is a liquid circulation from the riser to the downcomer. Consequently, ΔP_h is defined as follows:

$$\Delta P_h = gH \left((\rho_{h,d}(1-\epsilon_{g,d}) + \rho_{g,d}\epsilon_{g,d}) - (\rho_{h,r}(1-\epsilon_{g,r}) + \rho_{g,r}\epsilon_{g,r}) \right) \quad (II.10)$$

$$\Delta P_h = gH (\epsilon_{g,r} - \epsilon_{g,d}) (\rho_h - \rho_g) \quad (II.11)$$

While ΔP_{loss} is the sum of all pressure losses in the system,

$$-\Delta P_{loss} = \sum (-\Delta P_f)_j \quad (II.12)$$

$(\Delta P_f)_j$ are the losses in each section j of the reactor. These losses are due to the friction in the riser and downcomer tube, the change of section at the bottom of the reactor as well as the reversed flow at the top of the draft tube (Lu et al., 1994; Freitas et al., 1999).

$$(-\Delta P_f)_j = \sum \frac{1}{2} \rho_h \cdot k_j \cdot V_{l,j}^2 \quad (II.13)$$

Where V_{lj} is the velocity of the pseudo-homogenous phase in each part of the reactor while k_j is the coefficient that represents the correspondent loss.

In this study, solids and liquid phases are taken as a pseudo-homogenous liquid (PHL) phase with average physical properties such as density and viscosity, according to the solids concentrations (Wallis, 1969). Since, the solids are represented by micro-particles with densities close to that of water, the flow of a single pseudo-homogenous liquid phase can be assumed. Consequently, the same hydrodynamic correlations for one-phase flow can be applied to the PHL phase, including Reynolds number as well as the frictional factors (Livingston et al., 1993; Heijnen et al., 1997; Freitas et al., 1999).

The *Drift-Flux Model* is employed in this work to determine the relationship between the gas holdup and the velocity of the pseudo-homogenous phase, taking into account the relative motion between these two phases (Wallis, 1969). In the case of airlift reactors, this relationship is applicable for the riser and the downcomer compartments. Following Zuber and Findlay's correlation, the gas velocity in the riser is:

$$V_{g,r} = \frac{V_{sg,r}}{\epsilon_{g,r}} = (C_r \cdot J_r) + U_{bt} \quad (\text{II.14})$$

C_r is a distribution parameter that ranges between 1.02 and 1.17 depending on the upward (riser) or downward (downcomer) directions of the flow (Lu et al., 1995; Contreras et al., 1999).

J_r is considered as the superficial velocity of the mixture, covering velocities of each phase presented in the system. Therefore, the gas velocity in the riser, as expressed in Equation 14, is now written as:

$$V_{g,r} = \frac{V_{sg,r}}{\epsilon_{g,r}} = C_r (V_{sp,h,r} + V_{sp,g,r}) + U_{bt} \quad (\text{II.15})$$

In Equations (14) and (15), V_b is the bubble velocity and, contrary to the previous work it is not considered constant here (usually ranging between 0.25 and 0.40 m/s) (Livingston et al., 1993; Heijnen et al., 1997). Instead, the bubble velocity depends on the volumetric flow that passes through an orifice of the sparger, the orifice diameter, and the physical properties of the liquid.

According to Davidson and Schüller, the volume (V_b) of a bubble formed in a viscous liquid is in the form of:

$$V_b = \left(\frac{4\pi}{3} \right)^{0.25} \left(\frac{15\mu_l Q_{g,orifice}}{2g(\rho_l - \rho_g)} \right)^{3/4} \quad (\text{II.16})$$

Assuming that bubbles are spherical, the equivalent radius is obtained from their volume, which is calculated from Equation II.16.

The terminal bubble velocity, referred as the velocity of a single bubble that rises in an infinite and static medium, is classified in four regions depending on its diameter and its Reynolds number (Table II.1) (Wallis, 1969).

Table II.1. Terminal velocity of a single gas bubble in liquids.

Regions	Terminal velocity	Range of applicability
Region 1	$V_\infty = \frac{2R_b^2(\rho_l - \rho_g)g}{9\mu_l}$	$Re_b < 2$
Region 2	$V_\infty = 0.33g^{0.76} \left(\frac{\rho_l}{\mu_l} \right)^{0.52} R_b^{1.28}$	$2 < Re < 4.02G_1^{-2.214}$
Region 3	$V_\infty = 1.35 \left(\frac{\sigma}{\rho_l R_b} \right)^{0.5}$	$4.02G_1^{-2.214} < Re_b < 3.1G_1^{-0.25}$ or $16.32G_1^{0.144} < G_2 < 5.75$
Region 4	$V_\infty = 1.18 \left(\frac{g\sigma}{\rho_l} \right)^{0.25}$	$3.1G_1^{-0.25} < Re_b$ $5.75 < G_2$

$$\text{Re}_b = \frac{2\rho_l \cdot V_\infty \cdot R_b}{\mu_l} \quad G_1 = \frac{g \cdot \mu_f^4}{\rho_l \cdot \sigma^3} \quad G_2 = \frac{g \cdot R_b^4 \cdot V_\infty^4 \cdot \rho_l^3}{\sigma^3} \quad (\text{II.17})$$

From this terminal velocity, bubble velocity in a cylinder can be determined according to the vessel internal diameter, D (Table II.2).

Table II.2. Bubble velocity in a finite vessel.

Terminal velocity	Range of applicability
$U_{bt} = V_\infty$	$\frac{d_b}{D} < 0.125$
$\frac{U_{bt}}{V_\infty} = 1.13e^{-\frac{d_b}{D}}$	$0.125 < \frac{d_b}{D} < 0.6$
$\frac{U_{bt}}{V_\infty} = 0.46 \left(\frac{d_b}{D} \right)^{-1/2}$	$0.6 < \frac{d_b}{D}$

Once the bubble terminal velocity is calculated, the gas holdup in the riser can be determined by applying Equation II.14 of the *Drift Flux Model*. However, it is necessary to perform an iterative process by assuming a first value of the pseudo-homogenous phase velocity in the riser. The final riser velocity is obtained from Equation II.13. The pseudo-homogenous phase velocity in the downcomer is determined by using liquid continuity between the sections. In this case, it is necessary to know previously the downcomer gas holdup and therefore, the regime of operation.

In internal airlift reactors, three regimes of flow operation exist according to the gas distribution along the compartments. In regime I, the whole gas injected into the system is released to the atmosphere, thus no bubbles enter the downcomer. In regime II, some gas bubbles are present in the downcomer. Bubbles seem stationary because their slip velocity is close to the liquid velocity. Only very small bubbles move up and down along the downcomer. If the gas flow rate is further increased, there is a recirculation of the gas into the riser, observing the so-called regime III (Livingston et al., 1993; van Benthum et al., 1999).

In regimes II and III the relationship between riser and downcomer gas holdups depends on the reactor geometry (Ar/Ad ratio), the design of the degassing zone as well as the physical properties of working phases. Contreras et al. showed in their study a set of empirical correlations between riser and downcomer gas holdups, obtained by performing experimental studies with different reactors (e.g. internal airlift reactor, external airlift reactor, etc). Results show that these relationships can be determined only experimentally (Contreras et al., 1998).

Consequently, an empirical relationship between riser and downcomer gas holdup is obtained in this study to further determine downcomer PHL velocity.

4. Materials and methods

An internal airlift (IAL) reactor has been built by placing two cylinders concentrically. The cylinders are made of polymethyl methacrylate (PMMA), a transparent material that allows visualizing the flow. The internal cylinder is the “riser” compartment while the annular section forms the “downcomer” (Figure II.1). In order to have riser and downcomer compartments communicate, the internal cylinder was placed 10 cm over the reactor base, forming the so-called “bottom section”. A picture of the constructed reactor is shown in Figure II.2.



Figure II.2. Internal airlift reactor.

The corresponding dimensions are shown in Table II.3.

Table II.3. Dimensions of the Internal airlift reactor (IAL).

	Draft tube	External cylinder
Internal diameter (m)	0.133	0.19
External diameter (m)	0.139	0.2
Height (m)	0.65	1.2
Ar/Ad	1.053	
Bottom clearance (m)	0.1	
Total working volume (L)	21.3	

The gas injection system is designed in the form of a shower sprinkler with 24 holes of 2-mm diameter (Figure II.3).



Figure II.3. Sparger for gas injection.

Compressed air is injected into the system and air flow rate is set by using a “gas flow controller” with integrated regulator. In the line, air pressure is maintained at 2 bars, which is much higher than the water column weight. Air working flow rates were chosen as 5, 10, 15, 20, 25, 30 and 40 L_n/min. Two pressure sensors are installed in each compartment of the reactor, in order to measure the correspondent pressure difference and therefore, the corresponding gas holdup.

Demineralized water at ambient temperature is employed as liquid phase.

To study the influence of solids on the reactor hydrodynamics, glass beads particles with nano-plancton sizes of 10 μm and a density of 1100 kg/m^3 are employed. Particle concentrations are chosen according to biomass concentrations found nowadays in microalgae culture. Usually, initial biomass concentration is around 0.15 g/L and it can reach values of 5 g/L at laboratory and larger scales (Contreras et al., 1998; Sánchez Mirón et al., 2002; Radmann et al., 2007). Table II.4 shows densities and viscosities of the PHL phase according to particle concentrations (Equation II.7 & II.8), ranging from 0.15 to 5 g/L:

Table II.4. Particle concentrations. Properties of the pseudo-homogenous phase.

Concentrations (g/l)	Solid loadings (%v/v)	Density (kg/m^3)	Viscosity (Pa.s)
0.15	0.013635	1000.014	0.000890
0.5	0.045434	1000.045	0.000891
1	0.090827	1000.091	0.000892
1.5	0.136178	1000.136	0.000893
2	0.181488	1000.181	0.000894
5	0.452489	1000.452	0.000900

In each set of experiments, the reactor is filled with demineralized water to a level of 3 cm over the draft tube. Subsequently, compressed air is injected into the system and set to a specific flow rate. Once steady state is reached, pressure differences are measured in each compartment during 10 minutes.

5. Results and discussion

5.1 Gas holdup

The pressure difference measured between two ports in each section of the reactor provides an average value of the gas holdup in the corresponding section. In this sense, it is of interest to observe the evolution of this pressure difference according to the air flow rate.

Figure II.4 shows that pressure difference in both compartments decreases as air flow rate is increased in the riser. The tendency is linear, always observing a higher pressure difference in the downcomer than in the riser. The lower pressure difference in the riser is due to the air volume that generates a decrease of the column density.

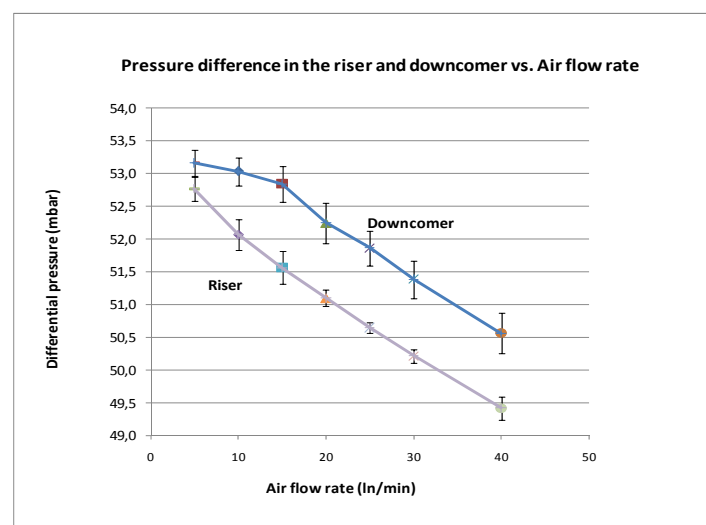


Figure II.4. Riser and downcomer pressure difference vs. air flow rate
Vertical bars represent standard deviation

Observing both curves, the slopes change once the air flow rate is higher than 15 L_n/min (corresponding to a superficial velocity of 0.018 m/s). In the riser, this difference reflects a change in the flow regime, passing from

homogeneous to heterogeneous churn flow. In homogenous flow, gas bubbles have spherical shape while in heterogeneous flow, larger bubbles are formed and they tend to flow in the center of the riser. Blazej et al. observed this change in flow pattern at gas superficial velocity around 0.015 m/s, which is close to the velocity at which the flow pattern change is observed in this study (Levy, 1999; Blazej et al., 2004; Cerry et al., 2008). In the downcomer, the change of slope is because bubbles start to flow from the riser to the downcomer, decreasing the downcomer column density.

At low air flow rates, reactor operates in regime I. The whole gas flows directly to the atmosphere, thus the pressure difference in the downcomer decreases slowly at low air flow rates due to the absence of air bubbles in this compartment (Figure II.4).

By increasing the air flow rate, a higher volume of gas is present in the reactor, reflected as an increase of riser and downcomer gas holdups (Figure II.5). According to these experimental results and those obtained by several authors, riser and downcomer gas holdups increase linearly with air flow rates (or corresponding superficial gas velocities) (Chisti, 1998; Van Benthum et al., 1999, Blazej et al., 2004).

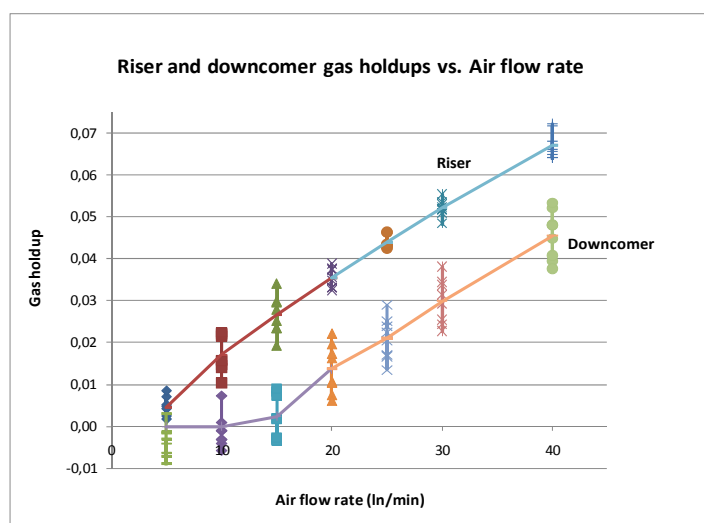


Figure II.5. Riser and downcomer gas holdups vs. air flow rate

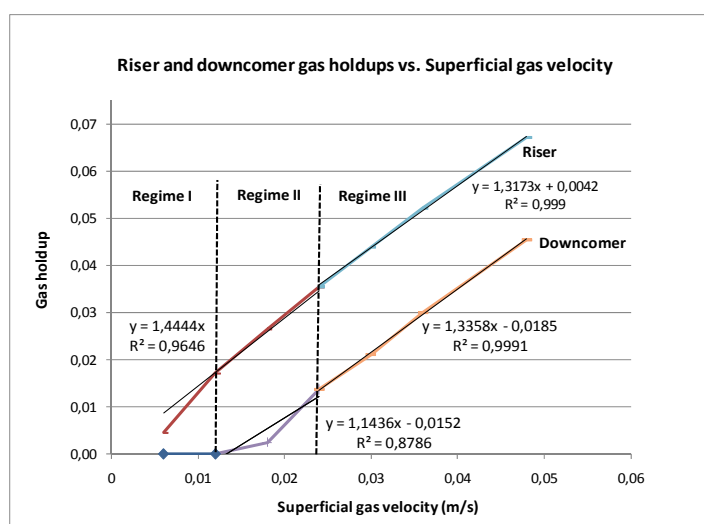


Figure II.6. Riser and downcomer average gas holdups vs. air flow rate
Regression applied to experimental results

Once some bubbles enter the downcomer, regime II starts. Figure II.6 shows that this occurs when the air flow rate is around 10 L_n/min (superficial gas velocity of 0.012 m/s). Bubbles in the downcomer have spherical shape and they are uniformly distributed around the walls. Some of these bubbles move up and down, along the upper section of the downcomer, while others flow to the top leaving to the atmosphere.

As the air flow rate is increased, bubbles tend to descend progressively to the downcomer bottom. Bubbles do not agglomerate; instead they keep their spherical shape. Their up and down flows are smooth.

At flow rates higher than 20 L_n/min (0.024 m/s), small bubbles start to flow back from the downcomer to the riser, and regime III is observed. At the bottom, the bubbles are drawn to the riser with high acceleration due to the change in the cross sectional area. Larger bubbles stay in the downcomer, maintaining their spherical shape and flowing up and down.

In the riser, regimes I and II are represented by a linear regression that intercepts the origin, representing a null gas holdup when there is no gas injection into the system. A second linear function represents regime III.

In the downcomer, regime II starts at a superficial gas velocity of 0.012 m/s. At lower superficial gas velocities, the downcomer gas holdup is nil, representing regime I.

Observing the evolution from regime II to regime III, very small bubbles are beginning to re-circulate to the riser while larger bubbles stay in the downcomer. As in the riser, a second linear function represents regime III in the downcomer.

Considering linear regressions of regime III in Figure 6, slopes corresponding to the riser and the downcomer gas holdups change compared with regime II. Variations of gas holdups in regime III are very close for both compartments, meaning that gas holdups increase slightly when air injection is increased.

Observing these experimental results, it is demonstrated that gas holdups increases linearly when the superficial gas velocity is increased. Similar values of gas holdups corresponding to these superficial gas velocities were found by Contreras et al. in their study of an IAL reactor with the ratio Ar/Ad=1 and having a sparger with pore sizes of 1 mm (Contreras et al., 1999). On the other hand, Van Benthum et al. found that riser and downcomer gas holdups increase faster in regime II than in regime III, which is also observed in this study for the riser compartment (Van Benthum et al., 1999). Blazej et al. worked with three dimensions of IAL reactors. In all cases, authors found a linear relationship between gas holdups and riser superficial gas velocity (Blazej et al., 2004).

One parameter that characterizes the IAL reactor hydrodynamic is the relationship between the riser and downcomer gas holdup, once the reactor works in regimes II and III. If there is an association between the gas flow injected into the system and the riser gas holdup then, a relationship between gas holdups in both compartments allows determining flow velocities along the reactor as well as residence time of the pseudo-homogenous phase.

Chisti et al. proposed a simple relationship in the form of $\epsilon_{g,d} = \alpha \epsilon_{g,r}$ to be applied in regimes I and II (with $\alpha = 0.89$) (Bello, 1981; Chisti et al., 1995). This relationship has been largely employed in IAL reactors studies due to its simplicity (Bakker et al., 1933; Janssen et al., 2002). However, as it was explained lately by Chisti, this relationship is incongruent when the downcomer gas holdup is zero, because it means that the riser gas holdup is zero, neglecting regime I (Contreras et al., 1998).

On the other hand, the value of α vary according to air superficial gas velocities, as it was demonstrated by Blazej et al. If α is calculated as $\alpha = \epsilon_{g,d} / \epsilon_{g,r}$ and plotted versus the superficial gas velocity, its variation is very important at low superficial gas velocities, searching for a constant value at higher superficial gas velocities, in regime III (Figure II.7) (Blazej et al., 2004).

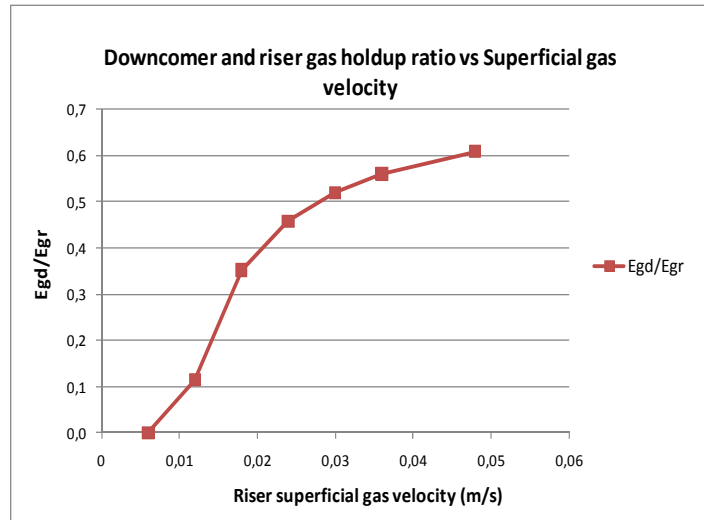


Figure II.7. Riser and downcomer gas holdup ratio vs. riser superficial gas velocity

As the riser gas holdup is linked to the superficial gas velocity, a relationship in the form of $\varepsilon_{g,d} = \alpha \varepsilon_{g,r} + \beta$ is applicable to experimental results obtained in regimes II and III (Contreras et al., 1998).

If a linear relationship is applied to the plot of riser versus downcomer gas holdup for regimes II and III (Figure 8), α is equal to 0.817, being in the range of values found by Chisti (between 0.8 and 0.9) and also observed in other studies (Contreras, 1996; Freitas et al., 1999). The relationship is valid once air bubbles start to flow to the downcomer, which means at superficial gas velocities higher than 0.012 m/s and riser gas holdup higher than 0.017.

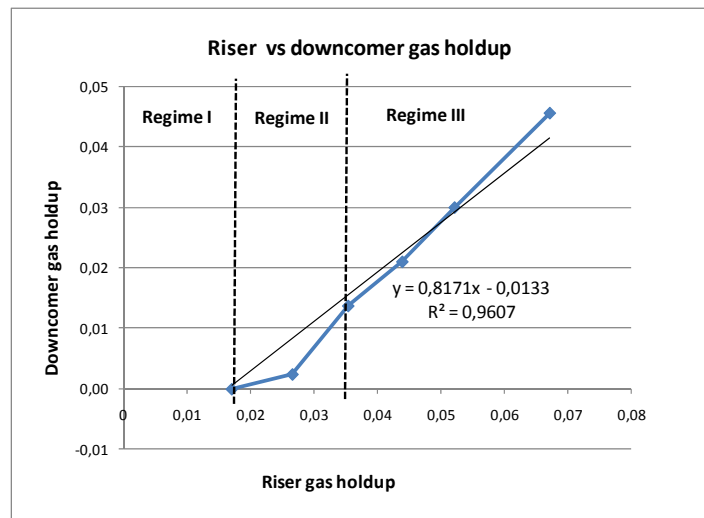


Figure II.8. Relationship between riser and downcomer gas holdups.

According to several studies, it appears that α value depends on the reactor geometry (riser to downcomer cross sectional ratios, reactor height, sparger type, and holes diameter) as well as the type of liquid or solution employed in the reactor. For example, Contreras observed that, for the same riser-to-downcomer cross sectional ratio used in this study ($A_D/A_R=1.054$), α had values between $0.77 < \alpha < 0.798$ according to the sparger hole diameter. They used a perforated pipe sparger and sea water as a working fluid (Contreras, 1996).

Bello found that, for three different downcomer to riser cross sectional areas, α had the same value of 0.89 using air-water in the system. Bakker et al. found a value of 0.875 using an air-salt solution (Bakker et al., 1993).

As the ratio A_D/A_R changes, the number of bubbles in the downcomer changes for the same air flow rate. If the downcomer is smaller than the riser, the liquid velocity is higher in this section and it might be higher than the

bubbles slip velocity. As a consequence, there are more bubbles entering to the downcomer compared to a reactor where the downcomer is larger than the riser, affecting values of α (Lu et al., 1995).

Figure II.9 shows riser and downcomer gas holdups obtained once the experimental relationship is incorporated into the model proposed here. Modeling results are compared with experimental results.

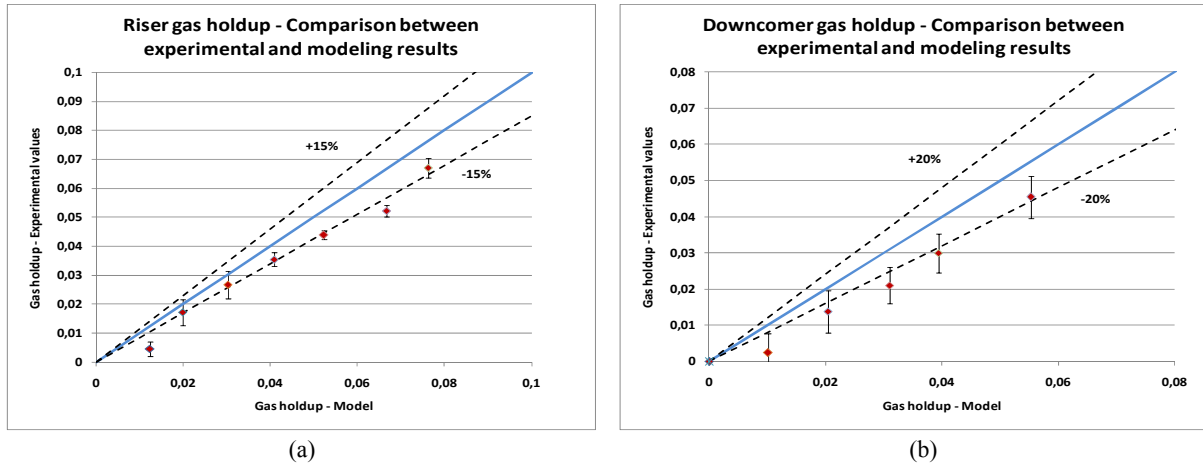


Figure II.9. Riser and downcomer average gas holdups. Comparison between experimental and modeling results. Vertical bars represent standard deviation

Results show that calculated riser gas holdups are higher than those found in experiments, particularly at high flow rates. In general, the difference between experimental and modeling results is around 15% for riser gas holdups (Figure II.9a). In the downcomer, the deviation is higher, around 25% (Figure II.9b). Modeling results overestimate averaged values of experimental gas holdups.

Alternatively, it is important to observe the evolution of the driving force in the reactor when air injection is increased. As it is explained above, the difference between riser and downcomer gas holdups is the driving force that promotes the PHL circulation in the reactor.

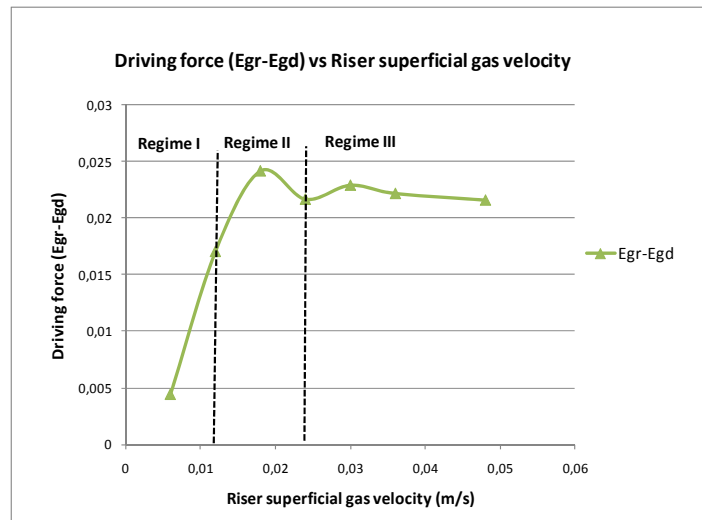


Figure II.10. Driving force in the IAL reactor vs. riser superficial gas velocity

Figure II.10 illustrates that driving force increases faster when the reactor works in regimes I and II. The reason is the low gas volume presented in the downcomer. Once regime III starts, it appears that the driving force increases no longer; instead it reaches an asymptotic value. The same behavior was observed by Blazej et al. (Blazej et al., 2004).

5.2 Solids holdup

Since the aim is to perform microalgae culture in an IAL reactor, solid holdups represent the volume of cells that circulate in each compartment. This is of interest because, once the culture is exposed to high light intensities, there will be a fraction of biomass receiving the highest intensity, in this case in the downcomer, diminishing gradually to the riser.

In previous studies performed with IAL reactors, gas holdups were affected when solids concentrations were more important (e.g. between 24 to 120 g/L), causing a decrease in gas holdups and, as a consequence, in PHL velocities (Livingston et al., 1993). This study focuses on very low solid holdups due to the low biomass concentrations observed in microalgae culture nowadays.

As it was mentioned above, solid loadings are directly related to the particle concentrations and weight, while solid holdups depend on the gas holdup distribution along the reactor (Equation II.6). Therefore, it is important to study the relationship between solid loadings and solid holdups, as well as the influence of air flow rate on the solids distribution.

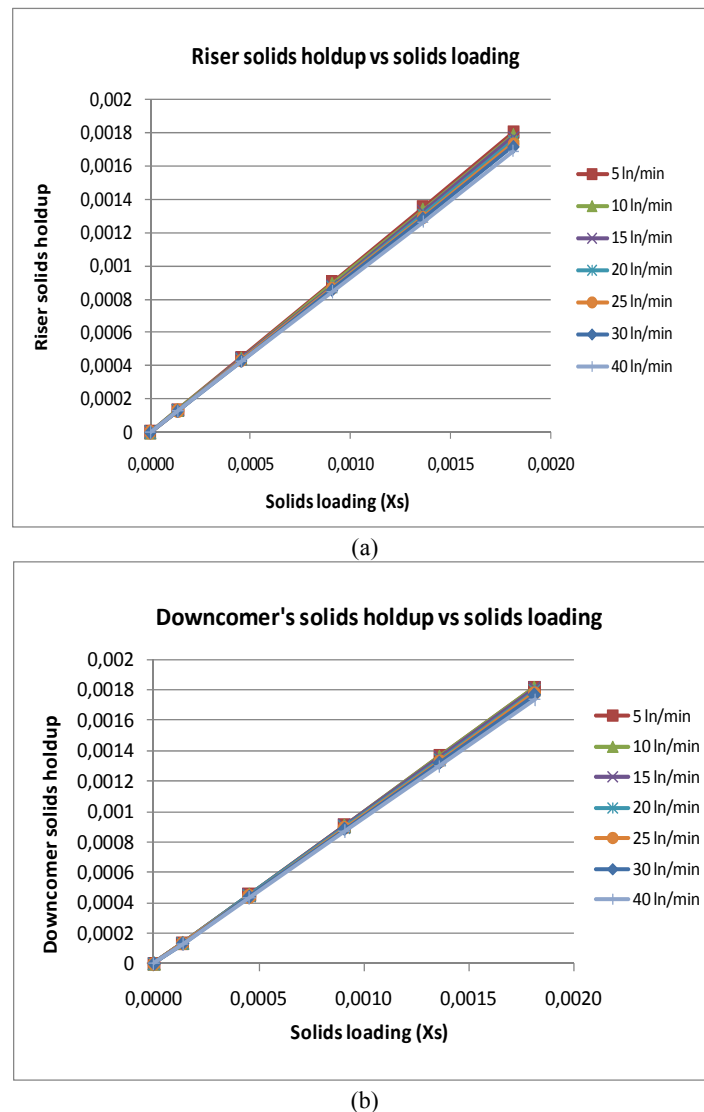


Figure II.11. Relationship between solid holdup and solid loading, (a) in the riser, (b) in the downcomer.

As it is expected, an increase in solid loadings promotes an increase in solid holdups in the riser and downcomer (Figure II.11). At low particle concentrations (C_x values of 0.15, 0.5 and 1 g/L), the superficial gas velocity does not have an effect on the solid holdups. On the contrary, at higher particle loadings, solid holdups diminish

slightly when air flow rate increases. The PHL phase is redistributed because a higher volume is filled by the gas.

Since the gas volume in the downcomer is lower, the difference among solid holdups according to the air flow rate is lower. The same tendency was observed by Freitas et al., even though glass beads with different densities were used (1016 and 1038 kg/m³) (Freitas et al., 1998).

Regarding the effect of superficial gas velocity on riser and downcomer solid holdups, solid holdups decrease slightly as long as the superficial gas velocity is increased. The difference between solid holdups at 0.006 m/s (or 5 L_n/min) and 0.048 m/s (40 L_n/min) is around 6,6% for the riser and 5% for the downcomer (Figure II.12).

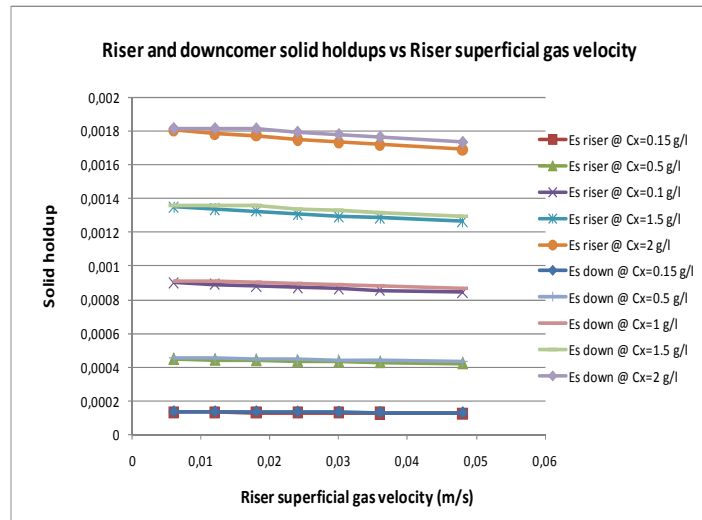


Figure II.12. Riser and downcomer solid holdups vs. superficial gas velocity

Comparing riser and downcomer solids holdups (Figure II.12), the highest difference is around 3%. Highest differences are observed at high superficial gas velocities and especially at 5 g/L of particles concentration. At low superficial gas velocities, the gas presented in the downcomer is nil or very low, thus the solids holdup is higher. Once the air flow rate is increased, the difference reaches a constant value, which means that the solid holdup is independent of the air flow rate (Figure II.13). This behavior is influenced by the reactor geometry because the cross sectional areas of riser and downcomer compartments are identical ($A_r/A_d \sim 1$). The solid repartition is slightly affected by the quantity of gas injected, resulting in a homogenous distribution along the reactor. Freitas et al. affirmed that, for particle densities higher than the liquid phase, at low solid concentrations and low air flow rate, higher solid volumes were observed in the riser than in the downcomer. Once the air flow rate was increased, a uniform distribution of solids holdup between the riser and downcomer was observed (Freitas et al., 1998).

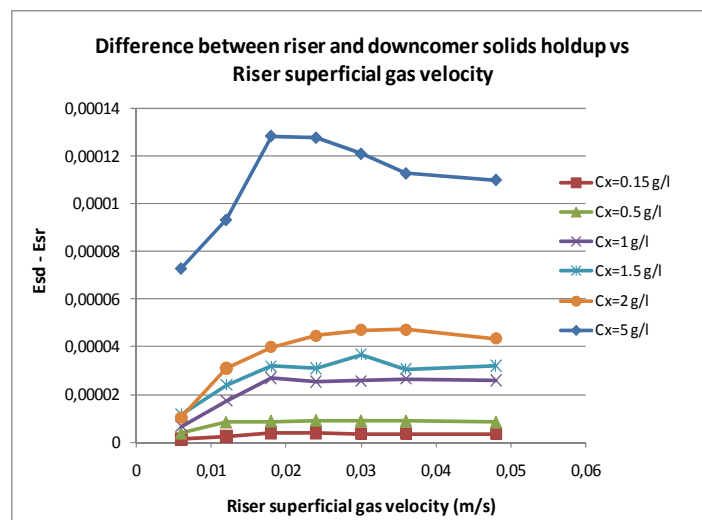
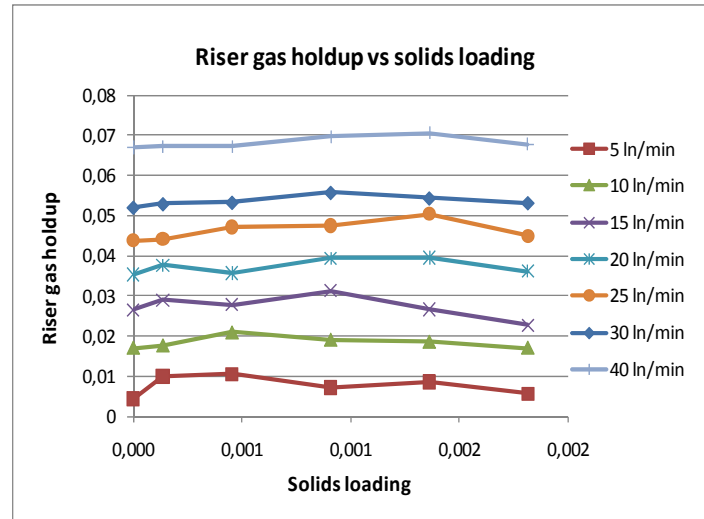
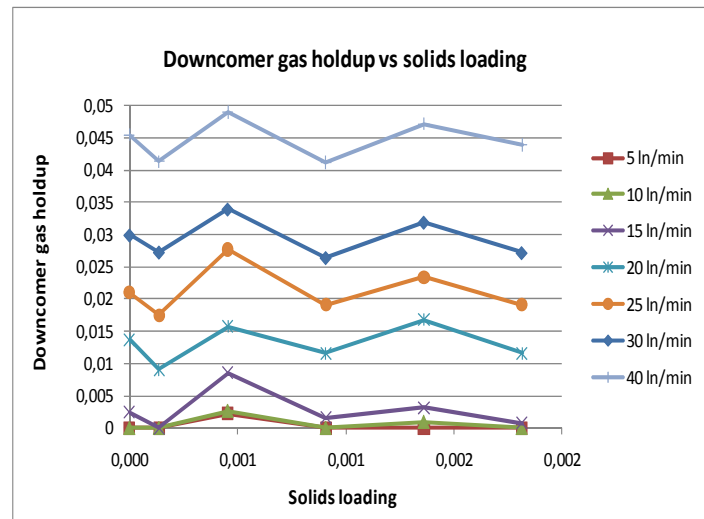


Figure II.13. Difference between riser and downcomer solid holdups

Figures II.14a and II.14b show that there is not a significant effect of the solid loadings on the riser and downcomer gas holdups for all tested air flow rates. The solid concentrations added into the system are very low to cause any effect on the gas distribution, especially coalescence of bubbles that reduce gas holdups (Lu et al., 1995; Jin et al., 2004). In the downcomer, bubbles keep the same size and shape as when there are no particles in the reactor.



(a)



(b)

Figure II.14. Gas holdups vs. solid loadings, a) in the riser, b) in the downcomer.

Observing these results, an average gas holdup can be determined for the range of solid concentrations and each air flow rate studied here. Figure II.15 shows this average value as well as the standard deviation. As it is expected, higher deviations are observed in downcomer gas holdups.

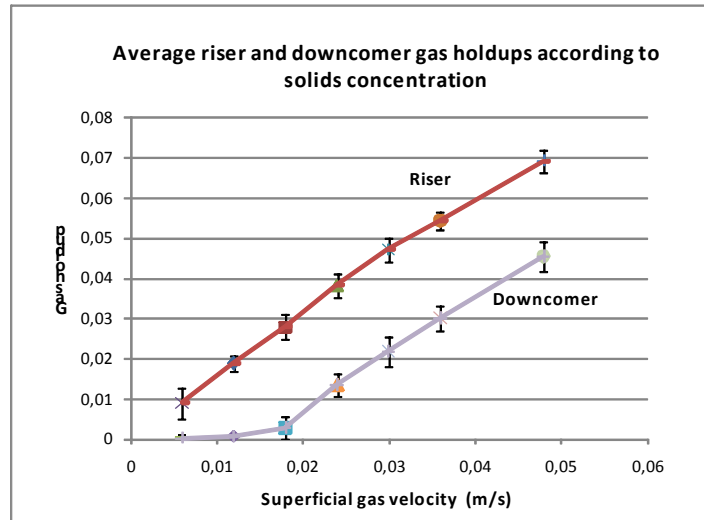


Figure II.15. Average riser and downcomer gas holdups according to solids concentration. Bars represent standard deviation.

On the other hand, it is interesting to verify whether the relationship between riser and downcomer gas holdups is affected when the gas holdups are averaged with respect to solid concentrations. Figure II.16 shows that the linear relationship between both gas holdups is not affected by the presence of particles. The values of α and β are very close to those obtained when there were no particles in the reactor, indicating that the proportionality between riser and downcomer gas holdups remains constant.

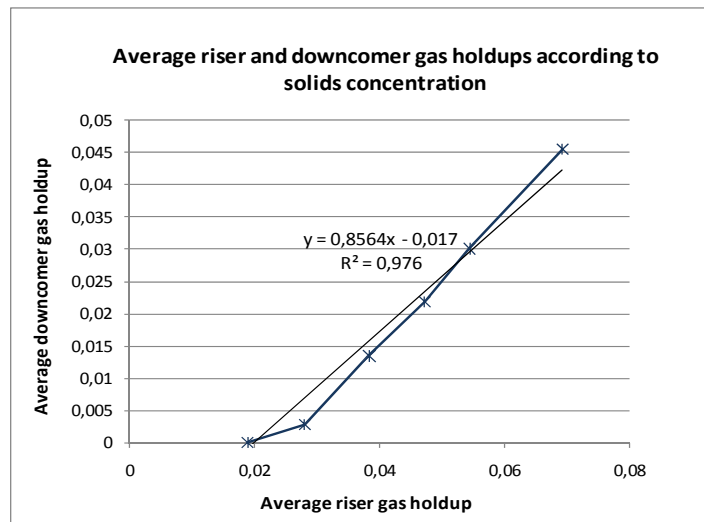
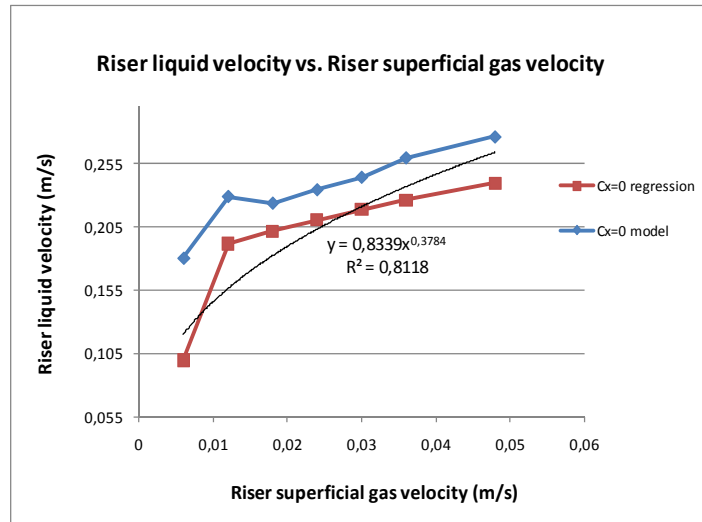


Figure II.16. Relationship between average riser and downcomer gas holdups.

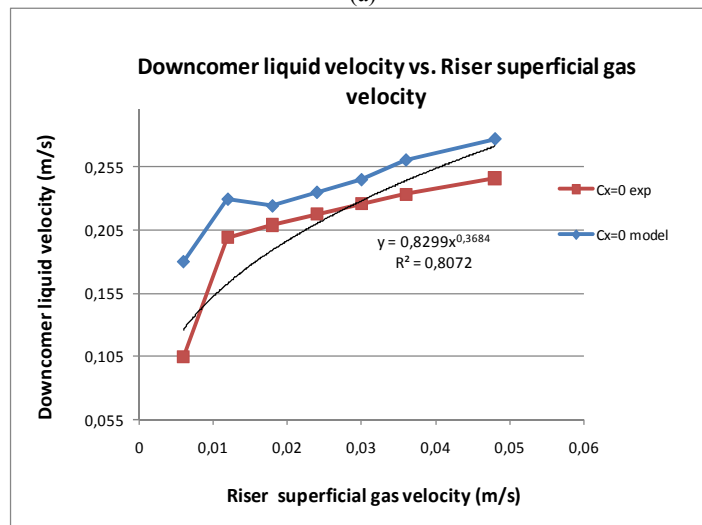
5.3 Pseudo homogeneous liquid velocities

As it is mentioned above, liquid and particles are considered together as a pseudo-homogenous liquid phase that flows along the reactor according to the air flow rate injected into the system. Because an increase in the air flow rate generates an increase in the driving force in the system, it is expected that the PHL velocity will increase in both sections of the reactor.

In Figure II.17, PHL velocities corresponding to experimental and modeling results are shown. To obtain theoretical PHL velocities, it is necessary to use the relationship between riser and downcomer gas holdups found from experiments. As this relationship is very similar for all solid concentrations (Figures II.8 and II.16), the correlation found at zero solids concentrations is used here.



(a)



(b)

Figure II.17. PHL velocity versus riser superficial gas velocity, (a) in the riser, (b) in the downcomer.

In the riser and downcomer compartments, there is a sharp increase in PHL velocities at low air flow rate. As illustrated in Figure II.8, there is an abrupt increase of the driving force in the reactor when the riser superficial gas velocity reaches 0.019 m/s, which occurs in regimes I and II (Blazej et al., 2004). These results indicate that the system is sensitive at low air flow rates, having the highest variations in driving forces and PHL velocities.

At higher air flow rates, the driving force becomes stable thus PHL velocities increase slightly. As it was also observed experimentally by Livingston et al., it appears that riser and downcomer PHL velocities are stabilized or they increase slightly when there is a further increase in the air flow rate (Livingston et al., 1993).

Regarding modeling and experimental results, the highest deviation is observed for the riser at the lowest superficial gas velocity while this difference is stabilized at higher superficial gas velocities (around 10%). For the downcomer, the deviation is always around 10%.

While PHL velocities in the riser and downcomer increase with air flow rates, the downcomer PHL velocity is slightly higher than in the riser, due to the small difference between both cross sectional areas ($A_r/A_d = 1.054$).

Regarding these experimental results, the best regressions found for both compartments are in the form of:

$$V_L = aV_{sg,r}^b \quad (\text{II.18})$$

The same tendency is observed by several authors at laboratory (García et al., 2000) and pilot scales (Heijnen et al., 1997). Values of “a” and “b” are very similar for the riser and downcomer: b is close to 0.4 as it is found by

other authors (Bello et al., 1984; Siegel et al., 1986; Chisti et al., 1989). According to Chisti, “a” depends on the reactor geometry and liquid properties while “b” is a function of the flow regime (Chisti, 1989).

On the other hand, it is necessary to identify PHL velocities at the bottom and degassing zones in order to estimate cell residence times in both sections. At the bottom, the PHL velocity is influenced by the change of section, from the riser to the downcomer as well as the bottom clearance. At the top, the PHL phase reaches a free surface where velocity diminishes. Then, the PHL phase is dragged to the downcomer due to the pressure difference between sections.

In this study, it is assumed that in the degassing zone, the flow entering to the downcomer has the same PHL velocity as in the riser. At the bottom, the PHL velocity is calculated according to the change of section.

In Figure II.18, PHL velocities are shown for different particle concentrations. Two types of relationship between riser and downcomer gas holdups are used. The first is the relationship employed between riser and downcomer gas holdups is the one obtained when no solids were added into the reactor.

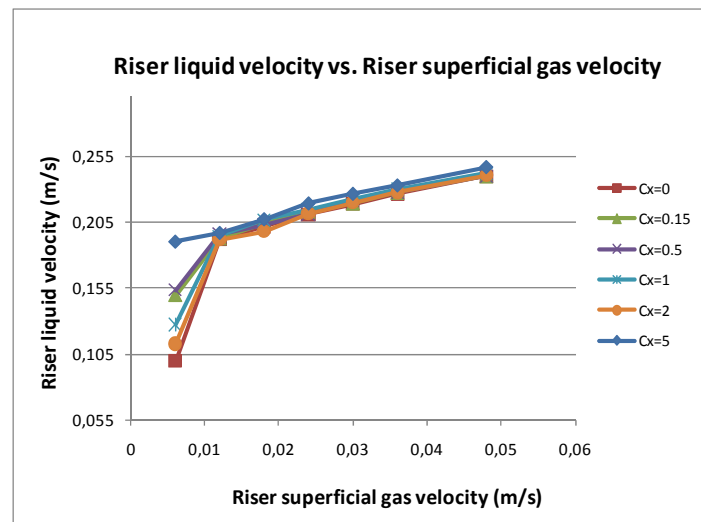


Figure II.18. Riser PHL velocity vs. riser superficial gas velocity at different particle concentrations.

Comparing PHL velocity values given for each solid concentration and regressions proposed above, the largest difference among values is around 10%. For an air flow rate higher than 10 Ln/min, the highest difference among PHL velocities is around 10%. Therefore, it can be concluded that solid concentrations used in this study are too low to generate a decrease in PHL velocities when loading of particles is increased, as it is also found for the gas holdups. PHL velocities are not affected by the increase in particle concentrations, despite the fact that density and viscosity properties are modified.

From results shown above, PHL velocities vary between 10 and 30 cm/s, being in the range of those employed in microalgae cultures when they were performed in photobioreactors and open ponds (Van Harmelen et al., 2006; Luo et al., 2008).

In theory, increasing PHL velocities increases biomass productivity because the oxygen dissolved in the culture is released. An increase in the PHL velocity may lead to better mixing, thus better exposition of cells to light energy (Sánchez Mirón et al., 1999). However, there are limited velocities at which the culture can flow in the system; a minimal velocity should guarantee a proper oxygen release and CO₂ absorption, while a maximal velocity should be established to avoid stress in the fluid and further cell damage (Contreras et al., 1998; Brindley et al., 2004).

5.4 Circulation time

Once circulation velocity is established, the next step is to estimate the residence time of cells in each section of the reactor. This is linked to the exposition time of cells to light and darkness, which might affect biomass productivity.

Because the reactor is composed of two sections, light intensities are not equally distributed along the reactor. Instead, the downcomer receives the highest light intensity while the riser receives less or any light energy. When microalgae cultures were performed in IAL reactors, authors made the riser opaque so the cells received the light energy during their residence time in the downcomer and darkness in the riser. In this case, a type of light/dark cycle is established during the entire culture (Merchuk et al., 1998; Jansen et al., 2000). In other studies, the riser is built with transparent material as the downcomer (Sánchez Mirón et al., 2002; Zhang et al., 2002).

In consequence, it is necessary to estimate the residence time of the pseudo-homogeneous liquid phase in each section. The residence time is estimated from velocities and compartment heights. Riser height is taken as the length of the draft tube, which establishes the time that cells spend in darkness when the riser is opaque. Similarly, the PHL residence time in the downcomer is estimated by taking the length of the draft tube (Livingston et al., 1993; Lu et al., 1994). However, when it comes to calculate cell- residence times under light, the bottom and the upper sections have to be considered. At the bottom, the circulation time is short and its change is very small according to superficial gas velocities. At the degassing zone, there is an open surface at which the PHL velocity is zero. However, close to the draft tube there is a reversed flow, so the PHL velocity can be considered close to that of the downcomer. Results are shown in Figure II.19.

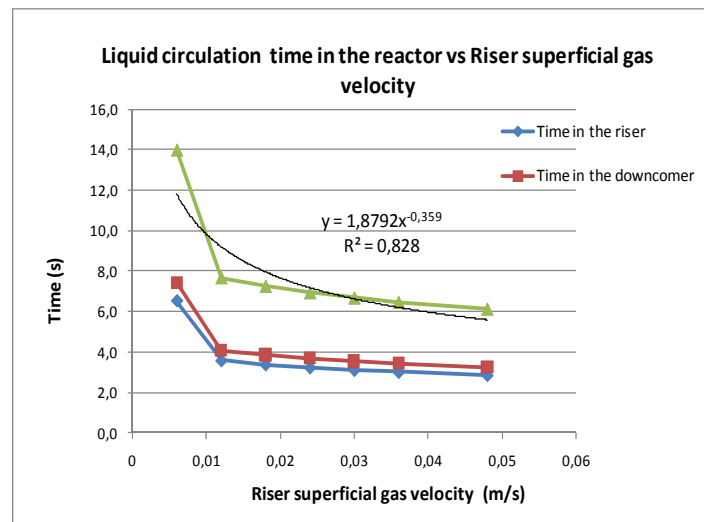


Figure II.19. PHL circulation time in the reactor vs. superficial gas velocity.

As expected, circulation times in the riser and downcomer are very similar. At low air flow rates, the circulation time depends more on the riser superficial gas velocity while this dependency is reduced at higher air flow rates. Similar results were reported by Freitas et al., which means that gas injection at high flow rates might not be interesting if the desired PHL velocity already attained with a lower flow rate.

As PHL velocities are not affected by solid concentrations, neither is the circulation time. Freitas et al. concluded in their study that the circulation time is almost constant for solids loading lower than 30%, as it is found in this study (Figure II.20) (Freitas et al. 1999).

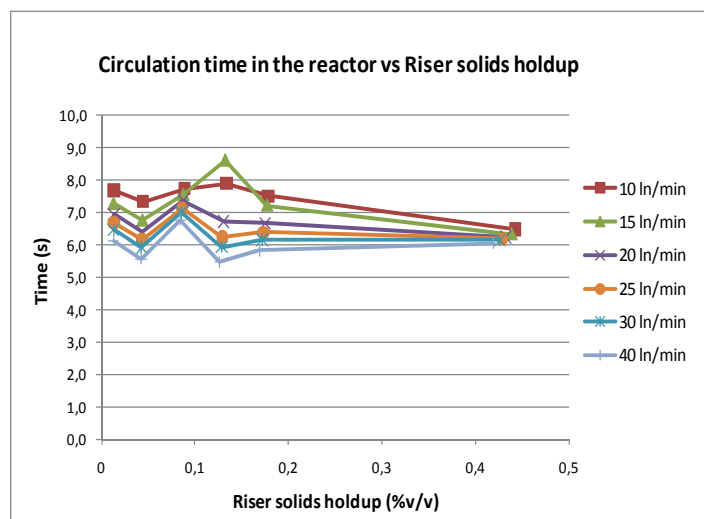


Figure II.20. PHL circulation time in the reactor vs. riser superficial gas velocity.

In Table II.5, some examples of circulation time found in the literature in airlift reactors are shown.

Table II.5. Circulation time in previous studies of IAL reactors.

Working volume (L)	Superficial gas velocity (m/s)	Circulation time (s)	Reference
21.3	0.006-0.048	6-14	This study
100	0.001-0.01	20-90	Xu et al., 2002
0.6		12.9	Janssen et al., 1999
60	0.01-0.497	7-23	Freitas et al., 1998
35	0.001-0.006	15.6-80	Merchuk et al., 1998
11.3	0.0027-0.22	7.5-32.5	Contreras et al., 1999

Experimental results show that circulation time of the pseudo-homogenous liquid phase is in the range of those times employed in microalgae culture (Merchuk et al., 1998; Janssen et al., 1999).

6. Conclusions

The hydrodynamics of an internal airlift reactor have been studied to perform microalgae culture. Previous studies and this work show that a macroscopic balance using only the momentum equation is not sufficient to estimate gas holdups as well as PHL velocities. It is necessary to know the relationship between PHL and gas velocities since these two phases do not flow at the same velocity. To include the effect of microalgae cells in the system, they are considered as micro-solids whose densities are close to the water density. Because the microalgae concentration varies along the culture period, physical properties of the flow vary according to these concentrations.

Today, biomass concentrations in the microalgae culture are relatively low. However, it is of interest to study whether these concentrations influence the reactor hydrodynamics. This work has demonstrated that typical concentrations ranging from 0.15 to 5 g/L do not affect gas holdups as well as solids distribution along the reactor.

As observed in previous works, the gas volume injected in the riser to generate the circulation is the essential parameter to characterize the hydrodynamics. Gas holdups, which define the driving force in the system, as well as PHL velocity increase with the increase of the superficial gas velocity. However, even though gas holdups continue to increase with superficial gas velocity, the driving force stabilizes and, as a consequence, PHL velocities increase slightly in comparison with low air flow rates.

On the other hand, a relationship between riser and downcomer gas holdups has been established when superficial gas velocity is high enough to observe bubbles entering to the downcomer and even circulating to the riser (regimes II and III). For instance, this relationship can be determined only experimentally and it is indispensable if a further aeration in the downcomer is needed. Results show that a lineal relationship can be established and it does not vary if particles are added to the system, under the concentrations employed in this study.

As it is observed, in regimes II and III air flow rates are high. Therefore, it is important to consider that, increasing gas flow rate in IAL reactors may damage microalgae cells, due to higher bubble breaking and coalescence. On the other hand, at higher gas flow rates, cell residence times in each section is reduced, so shorter light/dark cycles can be established and cells could be exposed to a higher radiation. In addition, higher gas flow rate implies higher gas holdup and thus higher volumetric mass transfer, implying higher mass exchange between the gas and the pseudo-homogenous phase.

In this sense, it is necessary to determine at which regime of operation the reactor should work. In regime I, a type of degasser section could be adjusted to the reactor in order to release all the gas injected into the riser. The reactor will work as a bubble column but with a downcomer section in which the PHL phase flows with a more organized flow pattern. In regimes II and III, downcomer is also aerated since small bubbles are present, thus there is higher mass exchange between the pseudo-homogenous liquid phase and the gas. However, there is a risk of damaging microalgae cells due to high flow rate in the riser.

Internal airlift reactors have a great potential for microalgae cultivation. They do not occupy large surfaces as other photobioreactors and, as observed in this study, their hydrodynamics can be adapted to satisfy microalgae culture requirements. Some authors have claimed that their scalability is not straight from laboratory however, further tests with the same logistic as in laboratory scale, can be performed in order to confirm their hydrodynamics.

7. References

- Bakker, W., van Can, H., Tramper, J., de Gooijer, C. (1993) Hydrodynamics and mixing in a multiple air-lift loop reactor. *Biotechnology Bioengineering* 42, 994-1001.
- Bello, R. A. (1981) A characterization study of airlift contactors for application to fermentations. Ph.D. Thesis, University of Waterloo, Ontario, Canada.
- Blazej, M., Kisa, M., Markos, J. (2004). Scale influence on the hydrodynamics of an internal airlift loop airlift reactor. *Chemical Engineering and Processing* 43, 1519-1527.
- Brindley, C., García, M., Acién, F., Fernández, J., García, J., Molina, E. (2004) Influence of Power Supply in the Feasibility of *Phaeodactylum tricornutum* Cultures. *Biotechnology and Bioengineering*. Vol 87. No. 6, 723-733.
- Chisti, M. (1989). *Airlift bioreactors*. Elsevier Science Publishers Ltd, London.
- Chisti, Y., Wenge, F, Moo-Young, M. (1995). Relationship between riser and downcomer gas holdup in internal airlift reactors without gas-liquid separators. *The Chemical Engineering Journal*. 57: B7-B13.
- Contreras, A., García, F., Molina, E., Merchuk, J. (1998). Interaction between CO₂-mass transfer, light availability, and hydrodynamic stress in the growth of *Phaeodactylum tricornutum* in a concentric tube airlift photobioreactor. *Biotechnology and Bioengineering*, 60, 317-325.
- Contreras, A., Chisti, Y., Molina, E. (1998). A reassessment of relationship between riser and downcomer gas holdups in airlift reactors. *Chemical Engineering Science*. 53: 4151-4158.

- Contreras, A., García, F., Molina, E. Merchuk, J. (1999). Influence of sparger on energy dissipation, shear rate, and mass transfer to sea water in a concentric-tube airlift bioreactor. *Enzyme and Microbial Technology* 25, 820–830.
- Converti, A., Lodi, A., Del Borghi, A., Solisio, C. (2006) Cultivation of *Spirulina platensis* in a combined airlift-tubular reactor system. *Biochemical Engineering Journal* 32, 13–18
- Freitas, C., J., Teixeira, J. (1998) Hydrodynamic studies in an airlift reactor with an enlarged degassing zone, *Bioprocess Engineering*. 18, 267–279.
- Freitas, C., J., Teixeira, J. (1998). Solid-phase distribution in an airlift reactor with an enlarged degassing zone. *Biotechnology Techniques* 12, 219–224
- Freitas, C., Fialova, M., Zahradnik, J., Teixeira, J. (1999) Hydrodynamic model for three-phase internal- and external-loop airlift reactors. *Chemical Engineering Science* 54, 5253-5258
- García, J., Lavin, A., Diaz, M. (2000) High liquid holdup airlift tower loop reactor. I. Riser hydrodynamic characteristics. *Journal of Chemical Technology*, 75, 369-377.
- Hall, D., Acien, F., Canizares, G., Rao, K., Molina, E. (2002). Outdoor helical tubular photobioreactors for microalgal production: Modeling of fluids-dynamics and mass transfer and assessment of biomass productivity. *Biotechnology Bioengineering*, Vol. 82, No. 1, 63-73.
- Heijnen, J., Hols, J., Van der Lans, R., Van Leeuwen, H., Mulder, A., Weltevrede, R. 1997. A simple hydrodynamic model for the liquid circulation velocity in a full-scale two- and three-phase internal airlift reactoroperating in the gas recirculation regime. *Chemical Engineering Science*. 52, 2527-2540
- Janssen et al. (1999) Specific growth rate of *Chlamydomonas reinhardtii* and *Chlorella sorokiniana* under medium duration light:dark cycles: 13–87 s. *Journal of Biotechnology* 70, 323–333
- Jin, B., Lant, P. (2004). Flow regime, hydrodynamics, floc size distribution and sludge properties in activated sludge bubble column, air-lift and aerated stirred reactors. *Chemical Engineering Science* 59, 2379 – 2388
- Jin, B., Yin, P., Lant, P. (2006). Hydrodynamics and mass transfer coefficient in three-phase air-lift reactors containing activated sludge. *Chemical Engineering and Processing* 45, 608–617.
- Levy, S. (1999). Two phase flow in complex systems. Wiley-Interscience Publication. John Wiley & Sons. United States of America.
- Livingston, A., Zhang, S. (1993). Hydrodynamic behaviour of three-phase (gas-liquid-solid) airlift reactors. *Chemical Engineering Science*, 48, 1641-1654.
- Lu, W., Hwang, S., Chang, C. (1995) Liquid velocity and gas holdup in three-phase internal loop airlift reactors with low-density particles. *Chemical Engineering Science*, 50, 1301-1310.
- Luo, H., Muthanna H. (2008). Local characteristics of hydrodynamics in draft tube airlift bioreactor. *Chemical Engineering Science* 63 (2008) 3057-3068
- Merchuk, J., Ronen, M., Giris, S., Shoshana (Malis), A. (1998). Light/Dark Cycles in the Growth of the Red Microalga *Porphyridium Sp.* *Biotechnology and Bioengineering*, Vol. 59, No. 6, 705-713
- Oncel, S., Sukan, V. (2007). Comparison of two different pneumatically mixed column photobioreactors for the cultivation of *Artrospira Platensis* (*Spirulina Platensis*). *Bioresource Technology*. Article in Press.

Radmann, E., Radmann, C., Reinehr, Costa, J. (2007). Optimization of the repeated batch cultivation of microalgae *Spirulina platensis* in open raceway ponds. *Aquaculture* 265, 118–126.

Sánchez Mirón A, Contreras Gómez A, García Camacho F, Molina Grima E, Chisti Y (1999) Comparative evaluation of compact photobioreactors for large-scale monoculture of microalgae. *Journal of Biotechnology*. 70, 249–270.

Sánchez Mirón A, Cerón M., García Camacho F, Molina E, Chisti Y. (2002). Growth and biochemical characterization of microalgal biomass produced in bubble column and airlift photobioreactors: studies in fed-batch studies. *Enzyme and Microbial Technology* 31, 1015-1023.

Van Benthum W., van der Lans R., van Loosdrecht M., Heijnen J. (1999) Bubble recirculation regimes in an internal airlift loop reactor. *Chemical Engineering Science* 54, 3995–4006.

Van Harmelen, T., Oonk, H., (2006). *MICROALGAE BIOFIXATION PROCESSES: Applications and Potential Contributions to Greenhouse Gas Mitigation Options*. Report, International Network on Biofixation of CO₂ and Greenhouse Gas Abatement, The Netherlands.

Wallis, G. (1969). *One-Dimensional Two Phase Flow*. New York: McGraw-Hill.

Xu, Z., Baicheng, Z., Yiping, Z., Zhaoling, C., Wei, C., Fan, O. (2002). A simple and low-cost airlift photobioreactor for microalgal mass culture. *Biotechnology Letters* 24: 1767–1771.

Modeling light energy profile in the IAL reactor
Estimation of biomass productivities and mass transfer

Nomenclature

a	Specific interfacial area	$1/m$
A	Local volumetric radiant power density absorbed	$\mu\text{mol E/m}^3.\text{s}$
A	Cross sectional area	m^2
b	Back-scattered fraction	
C_x	Concentration	mol/ m^3
C^0	Initial concentration	mol/ m^3
C^*	Equilibrium concentration	mol/ m^3
d_B	Bubble diameter	m
d	Diameter	m
d_c	Critical diameter	m
D_{equiv}	Equivalent reactor diameter	m
D_L	Diffusion of the species in the liquid	m^2/s
D_Z	Axial dispersion coefficient	m^2/s
E_a	Mass absorption coefficient	m^2/kg
E_s	Mass scattering coefficient	m^2/kg
G	Local light flux density or irradiance	$\mu\text{mol E/m}^2.\text{s}$
G_c	Compensation irradiance	$\mu\text{mol E/m}^2.\text{s}$
H	Height	m
H_e	Henry's constant	
H_g	Enthalpy of the dried algal biomass	kJ/g
I	Radiant flux	$\mu\text{mol E/m}^2.\text{s}$
I_0	Zero Bessel function	
I_1	One order modified Bessel function	
k_g	Gas mass transfer coefficient	m/s
K_j	Light saturation constant	$\mu\text{mol E/m}^2.\text{s}$
k_L	Liquid mass transfer coefficient	m/s
K_{tic}	Equilibrium constant between total inorganic carbon and CO_2	
m	Number of angles for the considered frame of reference	
P_a	Atmospheric pressure	Pa
P_b	Biomass productivity	g/L.h
P_g	Power input giving by the gas	W
Q_g	Air flow rate	Ln/min
q	Incident light flux density or irradiance	$\mu\text{mol E/m}^2.\text{s}$
r	Radius	
R	Universal gas constant	J/K.mol
R_{O_2}	Oxygen production rate	mol/m^3
R_{CO_2}	Carbon dioxide production rate	mol/m^3

T	Temperature	K
t	Time	s
V_L	Liquid volume in the IAL reactor	m^3
V_{SG}	Superficial gas velocity	m/s
V_{SL}	Superficial liquid velocity	m/s
$Y_{O_2/X}$	Oxygen to algae biomass conversion coefficient	mol O_2 /kg biomass
$Y_{CO_2/X}$	Carbon dioxide to algae biomass conversion coefficient	mol CO_2 /kg biomass
Z	Normalized radio ($Z = r/R$)	
z	Vertical reference coordinate (axial direction)	m

Dimensionless numbers

Re	Reynolds number
Sc	Schmidt number
Sh	Sherwood number
Gr	Grashof number

Greek letters

α	Slope in the P/I curve	
α	Linear scattering modulus	
β	Term grouping optical properties of algae	1/s
γ	Fraction for working illuminated volume in the photobioreactor	
δ	Extinction coefficient	1/m
ε	Holdup	
θ	Polar angle	
μ	Specific growth rate	1/h
ρ	Liquid density	kg/m^3
ρ_m	Maximum energetic yield for photon conversion at the antenna level	
ϕ	Mean mass quantum yield for the Z-scheme of photosynthesis	kg/ μ mol E
Ω	Euclidean operator	

Subscripts

d	Downcomer
g	Gas
i	Phase
l	Liquid
max	Maximum
r	Riser

Abbreviations

IAL	Internal airlift
LFD	Light flux density
PBR	Photobioreactor
PE	Photosynthetic efficiency
PFD	Photon flux density
PMMA	Polymethyl methacrylate
TIC	Total inorganic carbon in the liquid phase

1. Introduction

Phototrophic microalgae require a minimum of light energy in order to activate the first biochemical reactions of photosynthesis. When microalgae culture is performed in closed systems, it is indispensable to determinate the light energy available inside the reactor if it is desired to estimate its capacity to produce algal biomass. The light energy available inside a photobioreactor is not constant during the culture. Instead, it is attenuated according to biomass concentration, incident irradiance as well as reactor geometry. In this study, it is considered that the incident light comes from an artificial source that provides a constant flux. One dimension light energy transfer model is applied along the internal airlift reactor, taking into account reactor geometry, the optical properties of a microalgae species and biomass concentrations. The model is applied in two different situations: 1) when the reactor is completely illuminated and 2) when the riser is opaque, thus there is a light-dark cycle established along the culture. Results from the model determine an optimal biomass concentration, for each incident light flux density, that leads photons to reach the rear of the reactor guaranteeing the minimal energy necessary for photosynthesis.

The following step is to estimate the biomass production rate in each compartment of the reactor and according to the light energy profile. It is considered that light is the only limiting factor thus all nutrients are accessible and all environmental conditions (e.g. pH, temperature, and salinity) are respected according to the species. Therefore, the optimal biomass production rate is limited to the optimal biomass concentration.

Since the biomass productivity is associated to an oxygen production rate and carbon dioxide absorption, it is necessary to estimate reactor capacity to release the oxygen dissolved in the medium and to absorb the carbon dioxide according to reactor hydrodynamics. The resistance to transfer the oxygen and carbon dioxide from and to the culture might be a reason of photosynthesis inhibition.

Finally, all results will provide an overview of reactor limitations as well as its capacity to perform microalgae culture.

2. Estimation of the light energy profile along the reactor

Light provides the energy necessary for the first biochemical reactions in photosynthesis. When the culture is exposed to sunlight, there is a change of the irradiance according to the hour and the day of the year as well as with the geographic latitude (Ación et al., 1997). When microalgae culture has been placed outdoors, photosynthesis inhibition has been observed in mid-day due to the strong light flux density. In this sense, there is an interest of reducing this high intensity into a lower photon flux density, avoiding photoinhibition and providing the energy necessary to perform photosynthesis with high efficiency. Similarly, when microalgae are exposed to artificial light, the interest is to expose microalgae culture to the highest light intensity without having photoinhibition in order to produce high biomass production rates.

Whether microalgae culture is performed under sunlight or artificial light, it is necessary to estimate the light energy profile along the culture. Under sunlight, it is necessary to calculate the solar irradiance according to the position of the sun during the day (e.g. angle of incidence of direct radiation) (Ación et al., 1997) while under artificial light, it is essential to place the light sources around the culture in order to guarantee homogenous incident light at the culture surface. In photobioreactors, this is a challenge since light energy availability depends on the geometry and the evolution of biomass concentration.

According to several experimental studies, it has been observed that light is the first limiting parameter in microalgae culture (Richmond, 2004).

In order to increase light energy availability in microalgae culture, authors talk about *diluting* the light energy in the reactor. The term dilution involves: 1) the reduction of strong incident light intensities into a low light flux in order to avoid saturation state and 2) the spatial dispersion of light flux density into the entire culture volume (Tredici and Chini Zittelli, 1997; Richmond, 2004). The diluted light flux density has to be high enough compared to the irradiance at which respiration occurs (irradiance of compensation) and low enough to maintain a high value of thermodynamic efficiency (Cornet, 2010). The aim is to dilute the light into the culture to reach the maximal energy absorption and therefore, to achieve the highest biomass production rate.

In this sense, it is crucial to optimize two main parameters referring to photobioreactor geometry: the specific illuminated area and the working illuminated fraction. The specific illuminated area refers to the ratio between the illuminated surface and the culture volume. Conversely, the working illuminated fraction is defined as the ratio between the surface having irradiances higher than the compensation irradiance and the total surface. According to Cornet, there are three main states of light distribution for microalgae culture (Figure III.1) (Cornet, 2010):

- 1) A fraction of the incident light flux density is lost at the back of the reactor since the biomass concentration is too low ($\gamma > 1$).
- 2) All the light flux density is attenuated inside the system, in such a manner that the irradiance at the rear of the reactor is equal to the irradiance of compensation ($\gamma = 1$).
- 3) The biomass concentration is too high, therefore there are dark zones or zones with irradiances lower than the compensation irradiance ($\gamma < 1$).

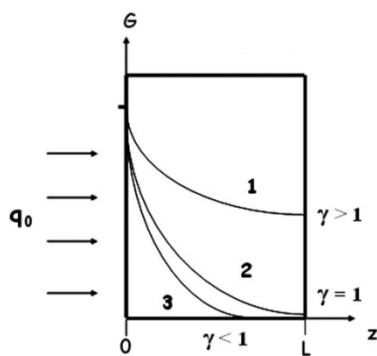


Figure III.1. Definition of working illuminated fraction according to Cornet (Cornet, 2010)

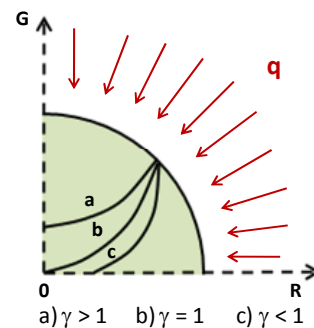


Figure III.2. Definition of working illuminated fraction in a circular cross-sectional area

Relating these two parameters, the interest is to obtain a high specific illuminated area providing a light distribution along the reactor that, at high biomass concentrations, the working illuminated fraction is close to one (Tredici and Chini Zittelli, 1997; Takache et al., 2010). In consequence, it is crucial to have a well approximated model to estimate the irradiance profile along the reactor.

Several authors have studied light attenuation in photobioreactors by applying the Lambert-Beer's law, considering the exponential light reduction along the culture due to its absorption by the cells (Ogbonna et al., 1995; Wu and Merchuk, 2004). Cornet et al. found that this approach was acceptable to estimate the available light flux density when the biomass concentration of *Spirulina platensis* was lower than 0.1 g/L (Cornet et al., 1998). However, experimental studies have considered the Lambert-

Beer's law simple since it does not take into account the scattering effect by the cells, which becomes important if biomass concentrations are important. The scattering effect is highly dependent on the microalgae species, their size as well as their optical properties (Acién et al., 1997; Pruvost et al., 2002).

In this study, the irradiance profile along the reactor is estimated from applying the two flux model proposed by Takache et al. and Cornet to the internal airlift reactor (Takache et al., 2010; Cornet, 2010). The aim is to predict the evolution of light energy available inside the reactor according to biomass concentrations as well as to determine the optimal biomass concentration to avoid the appearance of zones with irradiances lower than the compensation irradiance.

2.1 One-dimension modeling of light energy distribution in IAL reactor: Two flux method

The two flux method is a mathematical and physical approach originally proposed by Schuster and Schwarzschild in order to estimate the light energy transfer in a precise geometry. It considers that the system to be studied is divided in two hemispheres and *“it is presumed that the energy transfer is monodimensional and the intensity is isotropic for all radiations with components in the positive coordinate direction, and is also isotropic in the negative direction with different values”* (Siegel and Howell, 2002; Cornet, 2010).

Takache et al. have demonstrated that this method is applicable to rectangular and cylindrical photobioreactors cultivating microalgae species such as *Chlamydomonas* and *Spirulina platensis* (Cornet and Dussap, 2009; Takache et al., 2010). The solution proposed by Takache et al. for cylindrical photobioreactors is employed in this study to estimate the local irradiance available for microalgae culture in an IAL reactor.

Considering that the radiant intensity is averaged in all the spectrum of the photosynthetically active radiation (PAR) at which photosynthesis takes place, the spatial variation of the radiant flux in cylindrical coordinates is

$$\nabla(\Omega I) = \frac{dI}{dr} \cos \theta \quad (\text{III.1})$$

The left side of the equation is a five Euclidean operator that relies on two frames of reference: a fixed frame with three parameters depending on the geometry of the problem and a moving frame with two parameters independent of the geometry. The angle θ is the zenithal angle (Figure III.3) (Siegel and Howell, 2002; Cornet, 2010; Takache et al., 2010)

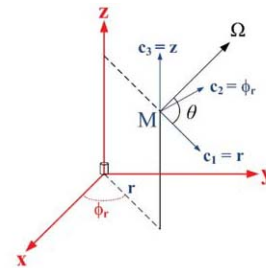


Figure III.3. Illustration of the two frames of reference (Takache et al., 2010)

Considering an angular distribution of the radiant intensities I^+ and I^- in two hemispheres of the system and assuming a quasi-collimated field of radiation, Equation III.1 results in two equations (Takache et al., 2010)

$$\begin{aligned} I^+(\theta) &= I^+ \delta(\theta - \theta_c) \\ I^-(\theta) &= I^- \delta(\theta - \theta_c) \end{aligned} \quad (\text{III.2})$$

The term $\delta(\theta - \theta_c)$ is the Dirac function. These two expressions lead to the formulation of two equations that, after being averaged in each hemisphere, results in the form of:

$$\begin{aligned} \frac{dI^+}{dr} &= -E_a C_x I^+ - b E_s C_x (I^+ - I^-) \\ \text{and} \\ \frac{dI^-}{dr} &= E_a C_x I^- - b E_s C_x (I^+ - I^-) \end{aligned} \quad (\text{III.3})$$

Where E_a is the mass absorption coefficient, E_s is the mass scattering coefficient while b is the back scattered fraction. Microalgae optical properties are parameters that affect the flux of radiant intensities and they are typical of species. Here, it is assumed that microalgae culture is a non-emitting medium. These two equations are combined to give:

$$\frac{d(I^+ + I^-)}{dr} = (-E_a + 2b) E_s C_x (I^+ - I^-) \quad (\text{III.4})$$

On the other hand, if a local balance of the radiant energy is performed on the photonic phase gives:

$$\frac{d(I^+ - I^-)}{dr} + \frac{m}{r} (I^+ - I^-) = -E_a (I^+ + I^-) \quad (\text{III.5})$$

Where m is the number of angles for the considered frame of reference ($m = 1$ for the case of cylindrical reactor). Combining Equations III.4 and III.5 provides a general equation of the radiant energy transfer for any geometry in the form of:

$$\frac{d^2(I^+ + I^-)}{dr^2} + \frac{m}{r} \frac{d(I^+ + I^-)}{dr} - E_a C_x (E_a + 2b E_s) C_x (I^+ + I^-) = 0 \quad (\text{III.6})$$

Defining the local irradiance G as the flux $(I^+ + I^-)$ and the radiant flux energy q as $(I^+ - I^-)$, the solution of Equation III.6 for a cylindrical reactor with an incident homogenous hemispherical and quasi-collimated light flux density results in:

$$\frac{G}{q} = 2 \frac{I_0(\delta r)}{I_0(\delta R) + \alpha I_1(\delta R)} \quad (\text{III.7})$$

where I_0 and I_1 are the zero and one order modified Bessel functions of the first kind, respectively. The factors δ and α group the scattering and absorption coefficients as well as the biomass concentration C_x , in the form of:

$$\delta = C_x \sqrt{E_a (E_a + 2b E_s)} \quad (\text{III.8})$$

$$\alpha = \sqrt{\frac{E_a}{(E_a + 2bE_s)}} \quad (\text{III.9})$$

Assuming an isotropic field of radiation and neglecting the angular distribution of light over the reactor wall, the local irradiance G in each radius r , is determined by applying Equation III.7, from the downcomer to the riser section. The incident irradiance is represented by a homogenous flux, q (Figure III.4). The local irradiance is then affected by the biomass concentration, characterized by the extinction coefficient δ .

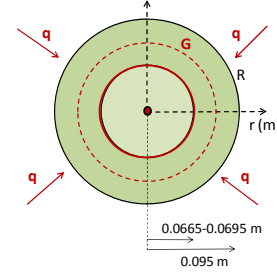


Figure III.4. Illustration of the local irradiance along the reactor

In a reactor operating in batch conditions, the biomass concentration will evolve in time with certain rate according to microalgae species and environmental conditions. In consequence, the light flux energy available for algae will also evolve in time. Thus, it is crucial to find maximal and optimal biomass concentrations according to the incident irradiance, to avoid the appearance of dark zones inside the reactor with irradiances lower than the compensation irradiance, guaranteeing the light flux energy necessary for photosynthesis.

Similarly, if the reactor operates in turbidostat mode, an optimal biomass concentration has to be determined according to the geometry and the incident irradiance. Once the culture reaches the optimal concentration, the working volume has to be adjusted, by controlling the liquid flow upstream and downstream, in order to preserve the optimal concentration. This might lead to higher biomass production rate, if all nutrients are maintained in the optimal concentrations (Richmond, 2007).

Following section show results from applying the two-flux method to the internal airlift reactor proposed in this study, working in batch mode.

2.2 Light distribution in the IAL reactor: modeling results

In order to estimate the light distribution along the reactor compartments, one microalgae species has been selected. *Chlamydomonas reinhardtii* is an eukaryotic microalga that has been considered as a potential organism capable of producing hydrogen under sulfur deprivation (Skjanes et al., 2007, Oncel and Vardar-Sukan, 2009). As eukaryotic microalgae, *Chlamydomonas reinhardtii* performs respiration when the available irradiance is lower than the compensation irradiance.

The optical properties of *Chlamydomonas reinhardtii* and its affinity for light have been taken from the study performed by Takache et al. In their study, optical properties were determined according to concentrations and the type of pigments. The characteristics of the light harvesting system depend on the pigments; varying according to the irradiances at which they algae are exposed (Richmond, 2004). Table III.1 presents optical properties of *Chlamydomonas reinhardtii* for four incident irradiances.

Table III.1. Optical properties of *Chlamydomonas reinhardtii* (Takache et al., 2010).

Light flux density ($\mu\text{mol E E/m}^2.\text{s}$)	50	110	500	1000
E_a (m^2/kg)	220 ± 10	200 ± 10	160 ± 10	130 ± 10
E_s (m^2/kg)	830 ± 50	850 ± 80	850 ± 70	910 ± 80
b	0.0081 ± 1.10^{-4}	0.0080 ± 1.10^{-4}	0.0077 ± 1.10^{-4}	0.0080 ± 1.10^{-4}
G_c ($\mu\text{mol E E/m}^2.\text{s}$)			10 ± 3	
K_j ($\mu\text{mol E E/m}^2.\text{s}$)			110 ± 20	

Next sections present light energy profiles obtained along the reactor in two different situations: 1) when the reactor is completely illuminated and 2) when the riser is opaque, thus there is a light-dark cycle established along the culture. The computational language *Mathcad* has been employed as a tool to develop the light energy distribution model.

2.2.1 Continuous exposition to light

In this first case, it is assumed there is a local light flux density attenuated from the riser to the downcomer. This attenuation is estimated by applying Equation III.7.

Considering that an incident irradiance of $110 \mu\text{mol E E/m}^2.\text{s}$ is homogenously distributed around the internal walls of the downcomer, the light flux density along the radius of the reactor, from the downcomer to the riser presents the profile shown in Figure III.5.

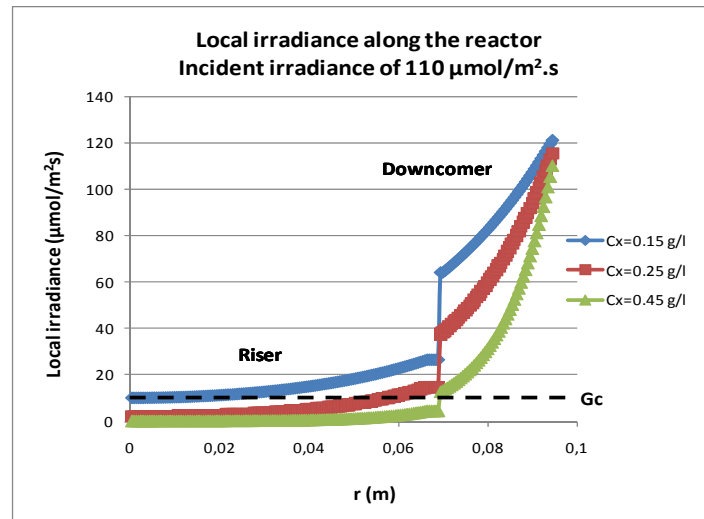


Figure III.5. Local flux density along the reactor at different biomass concentrations
Incident irradiance of $110 \mu\text{mol E E/m}^2.\text{s}$

Figure III.5 shows that highest light flux intensities are found in the downcomer section. The internal cylinder or the draft tube has a certain transmissivity, which means that not all the photons reaching the external radius of the draft tube are transported to the riser section. In this study, polymethyl methacrylate (PMMA), a transparent material used to build the reactor, has a transmissivity equal to 0.49. This means that the light flux density reaching the draft tube is reduced to almost the half in the riser section.

On the other hand, Figure III.5 demonstrates that the local irradiant energy available diminishes with biomass concentration. At biomass concentrations of 0.25 and 0.45 g/L the local irradiance is lower

than the irradiance of compensation at the center of the reactor. This means that, if an incident light energy of $110 \mu\text{mol E E/m}^2.\text{s}$ is applied to a culture of *Chlamydomonas reinhardtii*, photorespiration probably will be observed at the center of the reactor and close to it, if the above concentrations are reached in the culture. In this case, it is perceivable that the working illuminated fraction is lower than one. On the contrary, a biomass concentration of 0.15 g/L , the local irradiance is higher than the irradiance of compensation.

Similarly to Figure III.5, the light flux density profile along the reactor is presented in Figure III.6 at biomass concentration of 0.15 g/L and different incident irradiances. In experimental studies, 0.15 g/L is usually the concentration to start microalgae culture (inoculum) in a photobioreactor (Converti et al., 2006; Radmann et al., 2007).

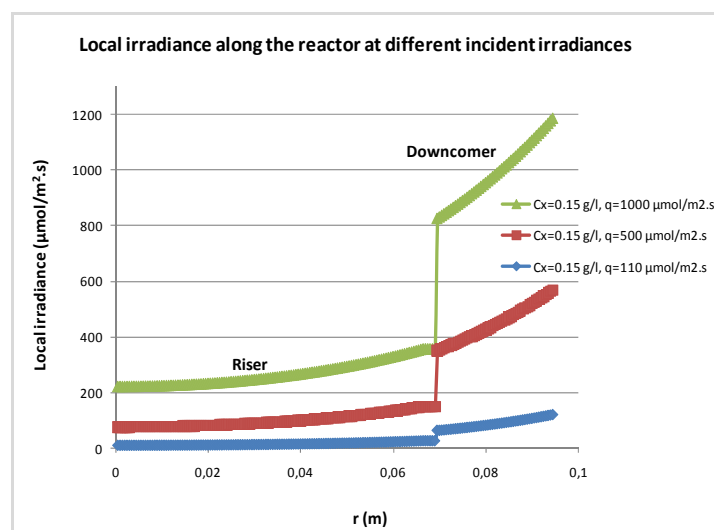


Figure III.6. Local light intensity along the reactor at different incident irradiances
Biomass concentration of 0.15 g/L

As it can be expected, the higher incident irradiances, the higher the flux of photons along the radius of riser and downcomer compartments. At the low biomass concentration of 0.15 g/L , incident light flux energy of 500 and $1000 \mu\text{mol E E/m}^2.\text{s}$ implies high irradiances at the center of the reactor, even higher than the irradiance of compensation ($10 \mu\text{mol E E/m}^2.\text{s}$). In consequence, the working illuminated fraction is higher than one, demonstrating that a fraction of the light energy provided to the system is not utilized by the culture. Values of the working illuminated fraction, at the same biomass concentration of 0.15 g/L , are presented in Table III.2.

Table III.2. Working illuminated fraction for different irradiances

Light flux density ($\mu\text{mol E/m}^2.\text{s}$)	γ ($Cx = 0.15 \text{ g/L}$)
50	0.665
110	1
500	2.6
1000	6.2

As the biomass concentration increases in time, effects of absorption and scattering increase, thus there is less light energy available for photosynthesis, becoming a limiting factor. For this reason, the working illuminated fraction changes in time and, under specific incident irradiance, γ will change from being higher than one, equal to one and lower than one ($\gamma < 1$).

In this context, it is then interesting to study the variation of the light energy along the reactor according to several biomass concentrations. Figure III.7 shows the local irradiance in four radius of the reactor, including the riser and downcomer radiiuses with respective thickness (incident irradiance of $500 \mu\text{mol E/m}^2\cdot\text{s}$)

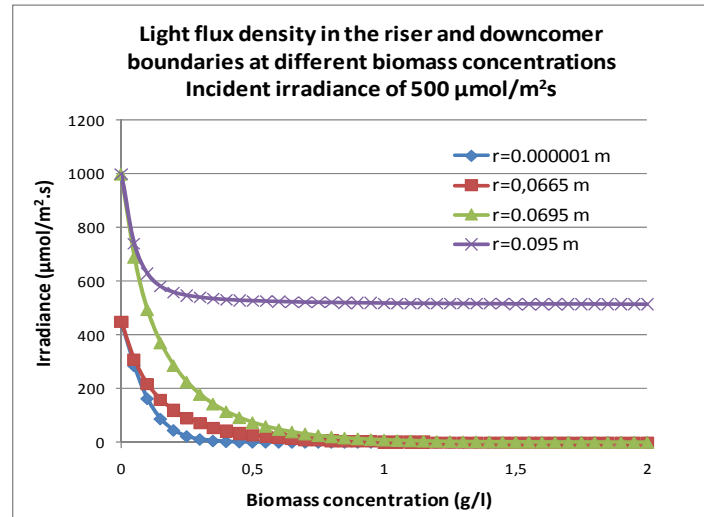


Figure III.7. Local light intensity in four different radius vs. biomass concentrations.

These results show that the highest light energy attenuation due to the augmentation of the biomass concentration occurs in the riser (from the radius of 0.0665 m to the center). For a biomass concentration of 0.45 g/L, the light energy is reduced to 96.3% in the riser and to 82.6% in the downcomer. The reason is the geometrical dimensions of the two compartments, since the riser has a cross sectional area larger than that of the downcomer. On the other hand, the light flux energy at the wall of the downcomer decreases until biomass concentrations reach 0.5 g/L then, the attenuation is almost zero.

These results illustrate that for microalgae culture in an IAL reactor, it is interesting to have a downcomer section slightly larger than the riser. First, the transmissivity of the draft tube determinates the light energy entering into the riser, reducing in a high percentage the energy already attenuated in the downcomer. Second, as the downcomer is the closest section to the incident irradiance, higher light intensities are incoming along its section compared to the riser (Figure III.7). However, two points have to be verified: the hydrodynamics of the system as well as the probability of photoinhibition due to high irradiances, as it is in the case of cultures exposed to mid-day light intensities.

From all results shown above, the optimal biomass concentration to avoid respiration at the center of the reactor can be determined for the four incident irradiances studied here (Figure III.8). As explained above, the interest is to find a working illuminated fraction equal to one, thus there are neither photons wasted nor photons required to avoid respiration.

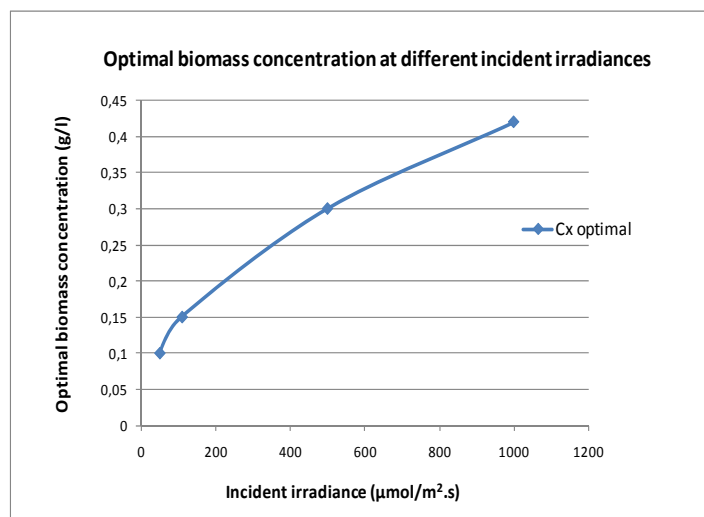


Figure III.8. Optimal biomass concentrations at four different irradiances.

Figure III.8 shows that, at higher irradiances, the optimal biomass concentration is higher. This is in accordance with results illustrated in Figures III.5 and III.6: the energy available for photosynthesis is higher for high incident irradiances and it diminishes when biomass concentration increases.

2.2.2 Microalgae culture under light-dark cycles

Light-dark cycles in an IAL reactor can be established in two situations. In the first, biomass concentration is too high so the light energy is strongly attenuated in the downcomer, thus there is very few or any photons reaching the riser. Second, the draft tube is constructed with very low transmissivity materials (e.g polyvinyl chloride) to make the riser opaque (Janssen et al., 2000; Wu and Merchuk, 2004).

Some experimental studies have found that it is interesting to have an opaque riser if algae are exposed to very high irradiances. According to several authors, some microalgae species require dark zones in the culture to repair the damages of the photon traps, once they have been exposed to high irradiances (Pruvost et al., 2002; Richmond, 2004). Responses of microalgae to a light/dark cycle depend on the species.

In both cases, it is necessary to avoid the appearance of dark zones in the downcomer, limiting the riser to be the only dark volume. Therefore, the objective is to guarantee a light flux density higher than the compensation irradiance at the external diameter of the draft tube. Figure III.9 illustrates the optimal concentrations to avoid respiration in the downcomer section, compared to those obtained when continuous illumination was assumed.

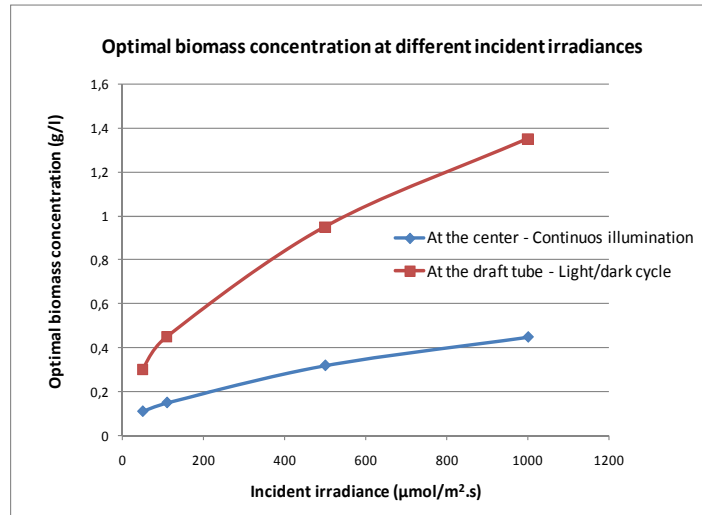


Figure III.9. Optimal biomass concentrations at the center and the draft tube.

By imposing a local irradiance at the draft tube higher than the compensation irradiance for a culture of *Chlamydomonas reinhardtii*, the optimal biomass concentrations for the four incident radiations are higher than those found previously. The difference among concentrations is larger when the incident irradiances are higher; e.g. 69% higher for an irradiance of 1000 $\mu\text{mol E/m}^2\cdot\text{s}$. Therefore, establishing light-dark cycles in an IAL reactor working in batch mode might increase the maximal biomass concentration at which the reactor can work. By guaranteeing the local light flux density higher than the irradiance of compensation, an increase in the biomass concentration might lead to an increase in the biomass productivity. However, these are qualitative results that do not take into account the effect that respiration might occur in the riser (depending on the circulation time in the section) reducing biomass productivities (Wu and Merchuk, 2004).

2.3 Estimation of the biomass production rate following Monod's law

In the first chapter, the specific growth rate was explained as the evolution of biomass concentration in time with respect to the initial biomass concentration. Then, the biomass production rate is a function of the biomass concentration and the specific growth rate. During microalgae culture, several correlations have been proposed to estimate the specific growth rate. In all correlations, it is generally agreed that the specific growth rate is a function of the light flux available inside the culture, considering light as one of limiting factors (Molina et al., 1999). On the other hand, it is usual to include nutrients evolution (e.g. nitrogen or sulfur) in specific growth rate estimation (Cornet et al., 1998; Nouals, 2000; Becerra, 2009).

In this study, it is considered that light is the only limiting factor thus, it is necessary to properly know its profile along the reactor to estimate reactor capacity to produce algal biomass. The most well known and employed method to estimate the specific growth rate is based on Monod's law (Molina et al., 1996; Jeon et al., 2005; Richmond, 2004; Wang et al., 2007). The correlation is a hyperbolic equation in the form of:

$$\mu = \frac{1}{C_x} \frac{dC_x}{dt} = \mu_{\max} \cdot \frac{G}{G + K_j} \quad (\text{III.10})$$

Where G is the local or the spatial averaged photon flux density, μ_{\max} is the maximum specific growth rate attainable at light saturation, and K_j is the half light saturation constant. The maximum growth rate and K_j change according to the incident irradiance since algae adapt their light harvested system to

light conditions. Consequently, the specific growth rate is estimated from applying the two flux method explained in the previous section, taking the corresponding optical properties of *Chlamydomonas reinhardtii*. As the local irradiance G varies radially from the downcomer wall to the reactor center, Equation III.10 is whether local or averaged along the reactor. If the ratio μ/μ_{\max} is defined as the normalized specific growth rate, its variation according to the local irradiances in the riser and downcomer is shown in Figure III.10.

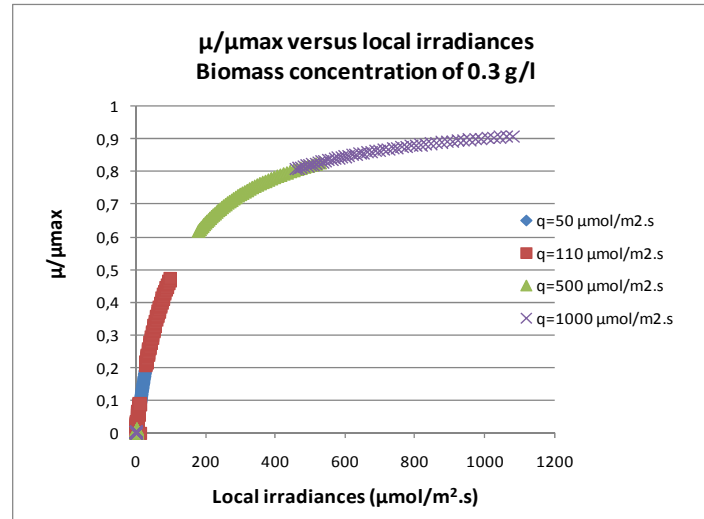


Figure III.10. Local and normalized specific growth rate in the reactor vs. local irradiances.

Figure III.10 shows that the local normalized specific growth rate increases very fast at low irradiances (between 0 and 200 $\mu\text{mol E/m}^2.\text{s}$) and gradually at higher irradiances, until it reaches the maximum attainable in the culture. As explained in Chapter I, at higher irradiances the phenomena of photoinhibition appears, thus the specific growth rate decays (Figure I.5). An empty space in the curve appears since there is no data of algae optical properties; for an incident irradiance that promotes local irradiances ranging from 115 to 170 $\mu\text{mol E/m}^2.\text{s}$.

To estimate the averaged specific growth rate along the reactor, two quantitative methods exist. The first consists in calculating the light flux density average over the reactor geometry. The second estimates the local specific growth rate corresponding to the local light flux density, integrating it over the reactor geometry (Molina et al., 1999). In this study, the averaged specific growth rate for *Chlamydomonas reinhardtii* is obtained from integrating Equation III.10 along the riser and downcomer compartments, once the local light flux density is known. Figure III.11 shows biomass concentration effects on the average specific growth rate, corresponding to the riser and downcomer compartments.

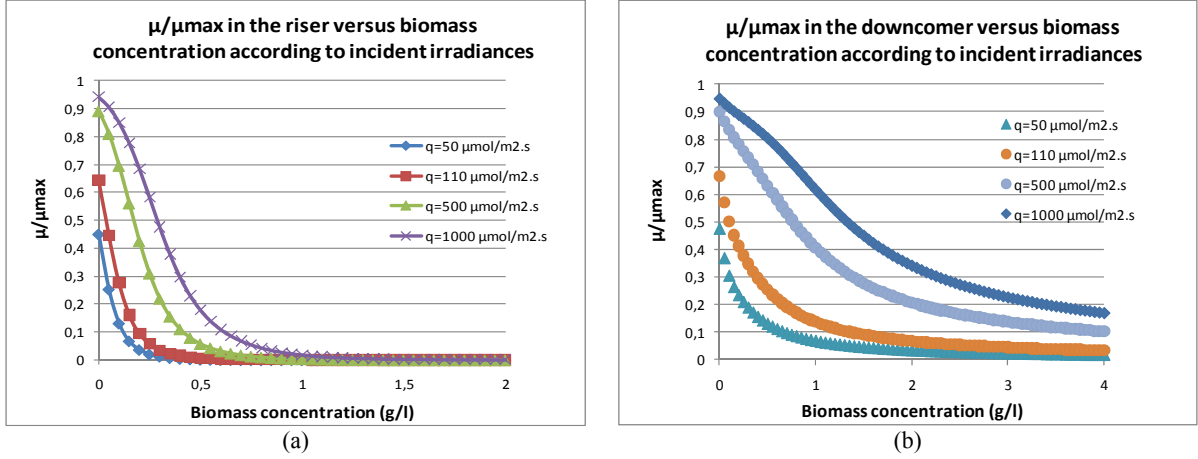


Figure III.11. Normalized specific growth rate integrated over reactor compartments vs. biomass concentration. a) in the riser, b) in the downcomer.

Results show that the averaged and normalized specific growth rates decrease if biomass concentrations increase since the local light flux density available for the culture diminishes. The mutual shading among cells becomes important, thus absorption and scattering phenomena increase inside the culture (Qiang and Richmond, 1994; Merchuk et al., 1998). The same tendency of the normalized specific growth rate was found by Pruvost et al. when the growth of *Chlamydomonas reinhardtii* was performed in a torus photobioreactor, working in batch mode with irradiances ranging from 100 to 1200 $\mu\text{mol E/m}^2.\text{s}$ and biomass concentrations between 0.72 and 2.77 g/L (Pruvost et al., 2008).

Since the highest light flux energy available for the culture, for all incident irradiances, is presented in the downcomer, the specific growth rate is therefore higher than in the riser. The specific growth rate in the riser is rapidly attenuated by the biomass concentration, reaching very low values at low biomass concentration such as 0.5 g/L. On the contrary, the effect of biomass concentration on the specific growth rate is less significant in the downcomer. Consequently, higher specific growth rate could be attained at higher biomass concentration. For irradiances of 500 and 1000 $\mu\text{mol E/m}^2.\text{s}$ and biomass concentrations even higher than 4 g/L, the normalized growth rate is still far from zero.

Once normalized specific growth rate is obtained according to incident irradiances and biomass concentrations, the next step is to determine the local biomass production rate, as follows (Richmond, 2004):

$$P_x(C_x, r) = C_x \mu_{\max} \frac{G(C_x, r)}{G(C_x, r) + K_j} \quad (\text{III.11})$$

Values of μ_{\max} for each incident irradiance and K_j are obtained from the experimental study performed by Takache et al. with *Chlamydomonas reinhardtii* (Takache et al., 2010). The local light flux densities G along the riser and downcomer compartments are evaluated for several biomass concentrations at four incident irradiances. Subsequently, the averaged biomass productivity results from integrating Equation III.11 along the limits of the riser and downcomer compartments (Cornet et al., 1995).

$$\langle P_x(C_x) \rangle = \left[\frac{C_x \mu_{\max}}{\Delta r_{\text{riser}}} \int_{\text{riser}} \frac{G(C_x, r)}{G(C_x, r) + K_j} dr \right] + \left[\frac{C_x \mu_{\max}}{\Delta r_{\text{downcomer}}} \int_{\text{downcomer}} \frac{G(C_x, r)}{G(C_x, r) + K_j} dr \right] \quad (\text{III.12})$$

Δr_{riser} is the difference between the center and the internal radius of the draft tube and $\Delta r_{\text{downcomer}}$ is the difference between the internal radius of the downcomer and the external radius of the draft tube. Results of biomass productivities, expressed in g/L.h, are shown in Figure III.12 for four incident irradiances.

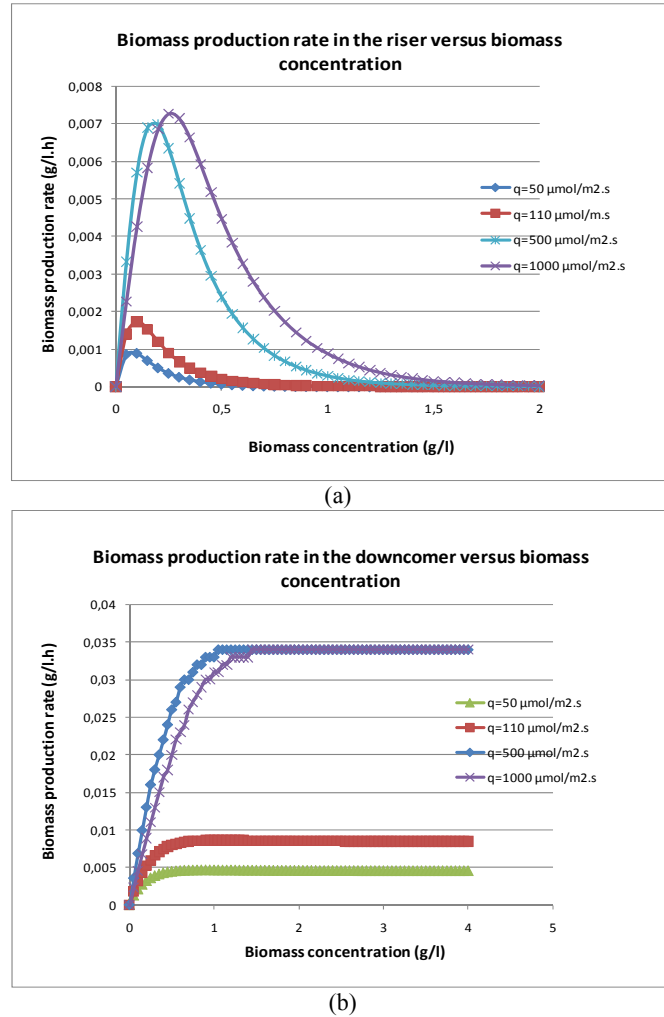


Figure III.12. Biomass production rate versus biomass concentration following Monod's model.
a) In the riser, b) in the downcomer.

In the riser, there is a sharp increase of the biomass productivity at low biomass concentrations, reaching a maximum and then, being progressively attenuated. At low incident irradiances of 50 and 110 $\mu\text{mol E}/\text{m}^2.\text{s}$, there is a very low or any productivity if biomass concentration is around 0.5 g/L. This is in concordance with results shown in Figure III.11 since the local irradiance is completely attenuated in the riser for this biomass concentration. This attenuation becomes more pronounced for higher irradiance. The reason is the compromise existing between the light flux density that it is attenuated due to the high biomass concentration and the increase of biomass concentration as well as the difference between μ_{max} values (0.082 and 0.05 1/h for 500 and 1000 $\mu\text{mol E}/\text{m}^2.\text{s}$ respectively).

In the downcomer, at low incident irradiances of 50 and 110 $\mu\text{mol E}/\text{m}^2.\text{s}$ the biomass production rates reach a constant value at low concentrations. This means that, if the algae growth is very fast the maximal biomass production rate will also be reached rapidly. Compared to the riser, the productivity is not attenuated from concentrations higher than 1 g/L. Instead, it appears that the biomass productivity reaches a constant value, even at very high biomass concentration. Quantitatively, this is due to the constant value of the light flux energy at the downcomer wall (Figure III.7) since

downcomer biomass productivity is obtained from the averaged integration of the Monod's law (Equation III.10) from the external to the internal radius. In reality, when microalgae culture is performed in photobioreactors, there is a biomass concentration at which productivity starts to decrease. Then, if algae concentration continues to increase, there is less light energy available for the cells implying degradation of biomass productivities (Wu and Merchuk, 2004).

Observing the values of biomass productivities in Figure III.12, they are similar to those obtained by Molina et al. when the culture of *Isochrysis galbana* was performed in a cylindrical bioreactor working in chemostat mode. The productivities ranged from 2.5 to 22.2 mg/L.h whereas in this study productivities range from 0 to 35 mg/L.h (Molina et al., 1996).

Regarding Figure III.12 and results shown above, it is clear that the optimal biomass productivity will be determined by the optimal biomass concentration in order to guarantee a light flux density profile higher than the compensation energy in the entire reactor. Therefore, the biomass productivity expression as a function of the optimal biomass concentration corresponding to each incident irradiance, is calculated by Equation III.11 and presented in Table III.3:

Table III.3. Biomass productivity under continuous illumination and according to optimal concentrations. Following Monod's law.

Light flux density ($\mu\text{mol E/m}^2.\text{s}$)	Optimal biomass concentration (g/L)	μ_{max} (1/h)	Biomass productivity (g/L.h)		
			Riser	Downcomer	Total
50	0.11	0.068	0.000855	0.00221	0.0015
110	0.15	0.063	0.00139	0.00467	0.003
500	0.32	0.082	0.00503	0.019	0.012
1000	0.45	0.05	0.00518	0.018	0.011

The total biomass productivity, expressed in g/L.h, is the result of averaging riser and downcomer productivities with respect to the volume of each compartment. Comparing riser and downcomer biomass productions, the contribution of the riser is not higher compared to that of the downcomer, since the riser produces approximately the fourth part of the downcomer biomass production.

At irradiances of 500 and 1000 $\mu\text{mol E/m}^2.\text{s}$, biomass productivities are very similar, both in the riser and downcomer. The reason is that, even though the local and the averaged irradiances are higher, the maximal specific growth decreases. In the study performed by Takache et al., the degradation of μ_{max} may be due to a reduction of biomass production since the irradiance is too strong, causing damages to photons traps (Takache et al., 2010).

Assuming that the riser is opaque, it was shown in Figure III.9 that optimal biomass concentrations to avoid respiration in the downcomer are higher than those obtained when the reactor works under continuous illumination. Taking these optimal biomass concentrations, the resulting productivities are as presented in Table III.4. These biomass productivities are true if there is no respiration occurring in the riser. If respiration occurs, there is consumption of biomass weight (e.g. carbohydrates) resulting in lower biomass net productivity. In this case, it will be interesting to experimentally study whether the residence time of algae cells in the riser is high enough to observe respiration (Richmond, 2004).

Table III.4. Biomass productivity having the riser opaque and according to optimal concentrations.
Following Monod's law.

<i>Light flux density</i> ($\mu\text{mol E/m}^2.\text{s}$)	<i>Optimal biomass concentration</i> (g/L)	μ_{max} (1/h)	<i>Biomass productivity</i> (g/L.h)
			<i>Downcomer</i>
50	0.3	0.068	0.00385
110	0.45	0.063	0.0077
500	0.95	0.082	0.033
1000	1.35	0.05	0.033

The next step is to determine the time of cultivation at which the optimal biomass concentrations are achieved under continuous illumination. Since the downcomer has the highest local irradiances, the optimal biomass concentration found for the entire reactor will be reached first in the downcomer and, in consequence, the cultivation time is governed by the evolution of the biomass concentration in this section (Figure III.13). Hydrodynamically, this biomass concentration is then traduced as a solid fraction that flows from the downcomer to the riser. Figures III.13 and III.14 show the evolution of biomass concentrations in the two reactor compartments by following Monod's law (Equation III.10).

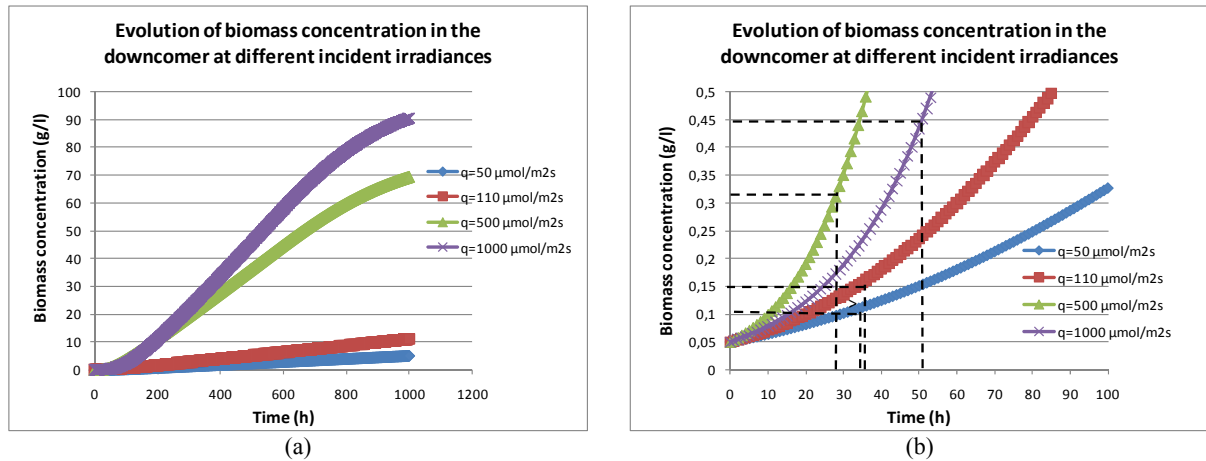


Figure III.13. Evolution of biomass concentration in the downcomer.
a) biomass concentration as a function of time; b) time to reach optimal biomass concentrations.

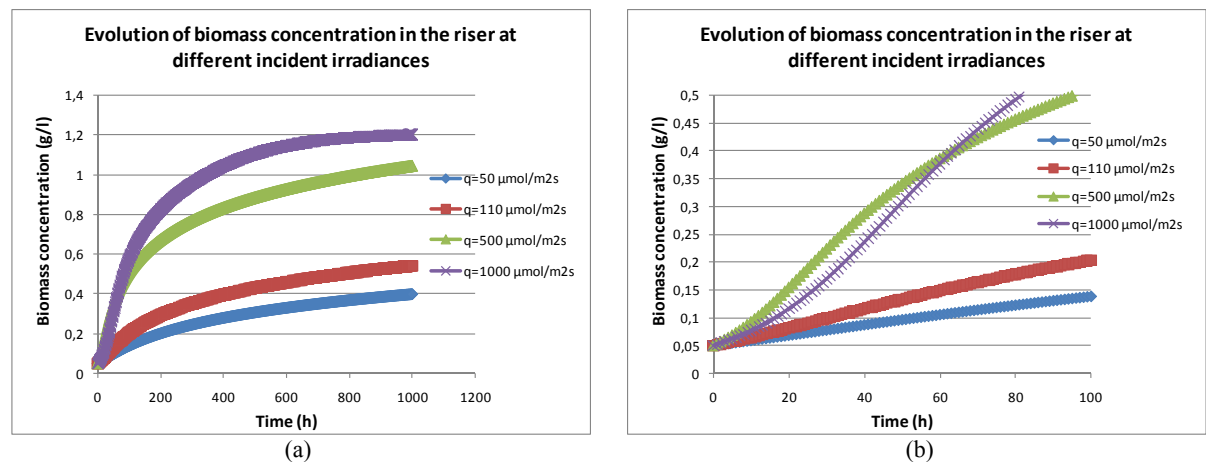


Figure III.14. Evolution of biomass concentration in the riser.
a) biomass concentration as a function of time b) biomass concentration up to 100 hours of cultivation.

In the downcomer and riser compartments, the exponential phase is longer at high irradiances. At the end of the exponential phase for an incident irradiance of $50 \mu\text{mol E/m}^2\text{s}$, the biomass concentration is the fourth part of that at $1000 \mu\text{mol E/m}^2\text{s}$, approximately. In microalgae culture, the biomass is usually harvested either during or at the end of the exponential phase, since the culture has generally attained an ideal biomass concentration (when light limitation is still minimal) (Zeng and Vonshak, 1998; Jeon et al., 2005; Haiduc et al., 2009).

Conversely, Figure III.14 shows that the biomass concentration reaches a constant and a maximum value in the riser faster than in the downcomer. In addition, these maximal biomass concentrations are much lower in the riser than in the downcomer. The reason, as it was explained before, is the low availability of the local light energy in the riser compared to that of the downcomer.

Regarding the time of cultivation to reach optimal concentrations, the range is between 35 and 51 hours approximately, for the incident irradiances employed here (Figure III.13b). Therefore, if it is desired to cultivate *Chlamydomonas reinhardtii* or other species with similar optical properties, it is expected that the highest productivities will be observed at these times (according to the incident irradiance applied over the reactor). At times longer than those corresponding to the optimal biomass concentrations, photorespiration probably will be observed as well as a decay of the biomass productivity.

On the other hand, if it is desired to establish a light/dark cycle inside the reactor, the time of cultivation changes according to the optimal biomass concentrations previously obtained (Table III.4). Figure III.15 presents corresponding results.

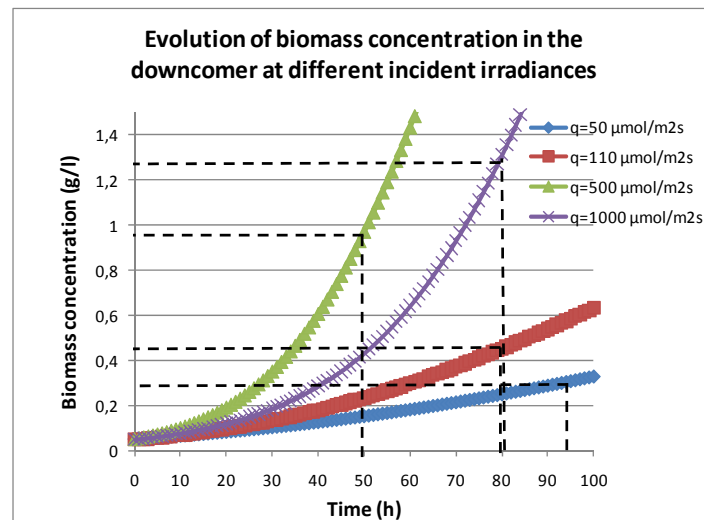


Figure III.15. Time to reach optimal biomass concentration having a light/dark cycle.

As expected, the time of cultivation will be longer, between 50 and 95 hours. As explained above, the cultivation time in this case is limited to avoid photorespiration in the downcomer ($\gamma = 1$), while it might occur in the riser section.

The times of cultivation obtained here, whether under continuous illumination or having light/dark cycles, results are very low. For reactors working in batch mode in experimental studies, it is usual to find times of cultivation around 15 days, having certain decay of biomass productivities (Travieso et al., 2001; Danesi et al., 2003; Kong et al., 2010). Assuming that the IAL reactor studied here is used to

cultivate *Chlamydomonas reinhardtii* under the highest irradiance, establishing a light/dark cycle during 15 days, probably photorespiration will be observed during the culture.

On the other hand, results show that if the residence time of microalgae culture in the riser is short enough not to observe respiration, it is more interesting whether to have the riser opaque or to reduce downcomer and riser diameters. The time of cultivation is longer than when continuous illumination is applied and higher biomass concentrations could be obtained (Figures III.13 and III.15).

2.4 Estimation of the biomass production rate following Cornet and Dussap's Model

The correlation formulated by Cornet and Dussap can be regarded as an equivalent expression of the Monod's law, conserving its hyperbolic tendency (Cornet and Dussap, 2009). Similarly to Equation III.11, the local biomass production rate is estimated as follows:

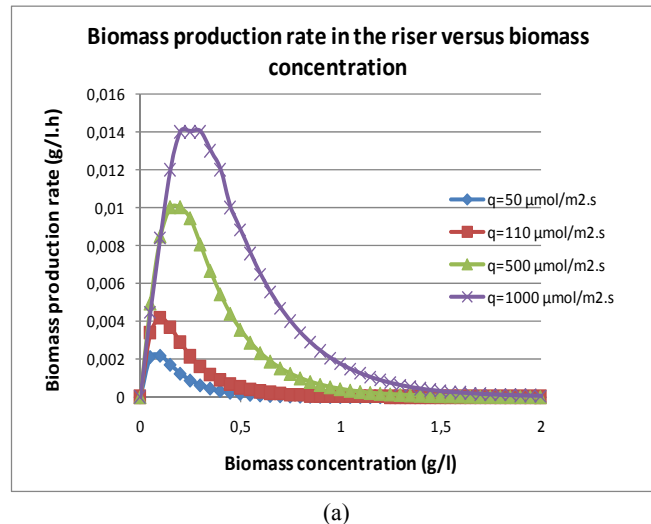
$$P_x(C_x, r) = C_x \beta \frac{G(C_x, r)}{G(C_x, r) + K_j} \quad (\text{III.13})$$

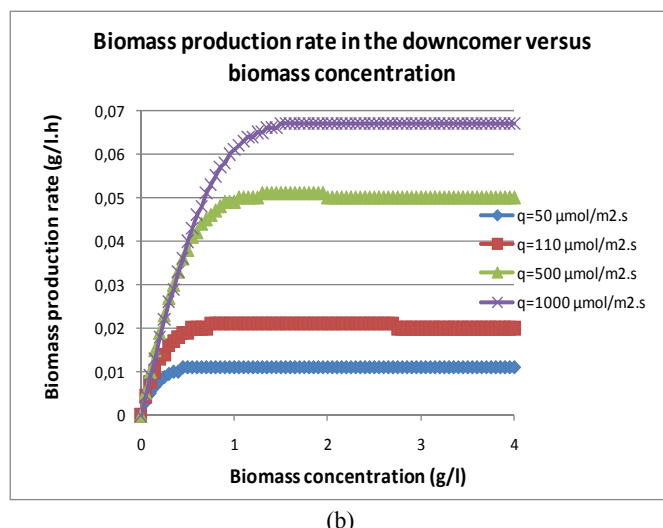
The term β is defined as:

$$\beta = \rho_m K_j \phi E_a \quad (\text{III.14})$$

Where ρ_m is the maximum energetic yield for photon conversion at the antenna level (where the algae pigments are presented). The term ϕ represents the mass quantum yields obtained from performing a stoichiometry analysis of photosynthesis while K_j and E_a are the half light saturation constant and the mass absorption coefficient, respectively.

Results of biomass productivities, following the model proposed by Cornet and Dussap are shown in Figure III.16. Figure III.16 shows same tendencies as in Figure III.12. There is an increase in the biomass production rate when incident irradiances are augmented. In the riser, the effect of biomass concentration is more important than in the downcomer since the biomass production rate decreases sharply. In both cases, when Monod's law and Cornet and Dussap's model were applied, the biomass production rate was completely reduced close to zero when biomass concentration reached 1.5 g/L. However, applying Monod's law results in biomass production rates lower than those when Cornet's model was used. The difference resides in the values of μ_{\max} and β , because the effect of light energy profile is the same in both cases (Equation III.11).





(b)
Figure III.16. Biomass production rate vs. biomass concentration following Cornet and Dussap's model.
a) in the riser, b) in the downcomer.

Since the local light energy profile and the optimal biomass concentrations remain the same, Tables III.5 and III.6 present the time at which optimal biomass concentrations are reached as well as biomass production rates obtained from applying Cornet and Dussap's model. Similarly, two situations are presented, when the reactor is considered completely transparent and when the riser is considered opaque.

Table III.5. Biomass productivity under continuous illumination and according to optimal concentrations following Cornet and Dussap's model.

Light flux density ($\mu\text{mol E/m}^2.\text{s}$)	Optimal biomass concentration (g/L)	Time to reach optimal biomass concentration (h)	Biomass productivity (g/L.h)		
			Riser	Downcomer	Total
50	0.11	14	0.0021	0.00544	0.0037
110	0.15	12.5	0.00336	0.011	0.0071
500	0.32	13.5	0.00747	0.028	0.0175
1000	0.45	14.5	0.01	0.036	0.0227

Table III.6. Biomass productivity having the riser opaque and according to optimal concentrations following Cornet and Dussap's model.

Light flux density ($\mu\text{mol E/m}^2.\text{s}$)	Optimal biomass concentration (g/L)	Time to reach optimal biomass concentration (h)	Biomass productivity (g/L.h)
			Downcomer
50	0.3	38	0.00947
110	0.45	30	0.019
500	0.95	23.5	0.049
1000	1.35	23	0.066

As expected, biomass production rates obtained at optimal concentrations are higher in both cases. By applying Cornet and Dussap's model, the difference can be between 1.47 and 2.45 times of those obtained Monod's law (Table III.7). This difference may be due to the underestimation of the μ_{\max} values that predicts low values of biomass production rates (Equation III.11). On the other hand, β is a function of the mass quantum yield ϕ that strongly depends on the nitrogen source provided to the culture (e.g. nitrate, ammonia, etc.) (Cornet and Dussap, 2009).

Since biomass production rates are higher than those obtained by applying Monod's law, the time to reach optimal concentrations are then lower. If the reactor is completely transparent and it is exposed to the irradiances studied here, in 12 hours of continuous illumination optimal biomass concentrations will be reached. If the riser is opaque, optimal concentrations will be then reached in one day.

Table III.7. Comparison between Monod and Cornet and Dussap models.

	Light flux density ($\mu\text{mol E/m}^2.\text{s}$)	Following Monod		Following Cornet and Dussap	
		Optimal biomass concentration (g/L)	Biomass productivity (g/L.h)	Optimal biomass concentration (g/L)	Biomass productivity (g/L.h)
Continuous illumination	50	0.11	0.0015	0.11	0.0037
	110	0.15	0.003	0.15	0.0071
	500	0.32	0.012	0.32	0.0175
	1000	0.45	0.011	0.45	0.0227
Riser opaque	50	0.3	0.00385	0.3	0.00947
	110	0.45	0.0077	0.45	0.019
	500	0.95	0.033	0.95	0.049
	1000	1.35	0.033	1.35	0.066

Even though biomass production rates estimated from applying Monod's law and Cornet and Dussap's model differ in their values, they are similar to those obtained today at large scale (assuming that the reactor produces biomass with these rates at 24 hours per day) (Travieso et al., 2001; Hall et al., 2002; Xu et al., 2002; Doucha and Livansky, 2006).

2.5 Determination of reactor efficiencies and productivities

The photosynthetic efficiency is defined as the energy stored in biomass produced during the culture per unit of light energy absorbed (Janssen et al., 2002). From the biomass production rates and the averaged light energy absorbed in the riser and downcomer compartments, the photosynthetic efficiency of *Chlamydomonas reinhardtii* culture, in the designed IAL reactor, can be calculated as follows:

$$PE = \frac{P_b H_g}{\langle A \rangle} \quad (\text{III.15})$$

Where P_b is the biomass productivity, H_g is the enthalpy, usually taken as 20.15 kJ/g of the dried biomass, and $\langle A \rangle$ is the spatial averaged volumetric radiant power density absorbed, whether in the riser or in the downcomer section (Hall et al., 2002). The averaged radiant energy absorbed is defined as a function of the local light energy density, the mass absorption coefficient, and the biomass concentration, as follows (Cornet and Dussap, 2009):

$$\langle A(C_x) \rangle = \left[\frac{C_x E_a}{\Delta r_{\text{section}}} \int_{\text{section}} G(C_x, r) dr \right] \quad (\text{III.16})$$

Figures III.17 illustrates photosynthetic efficiencies, averaged in the riser and downcomer compartments, obtained at biomass concentrations ranging from 0.05 to 4 g/L.

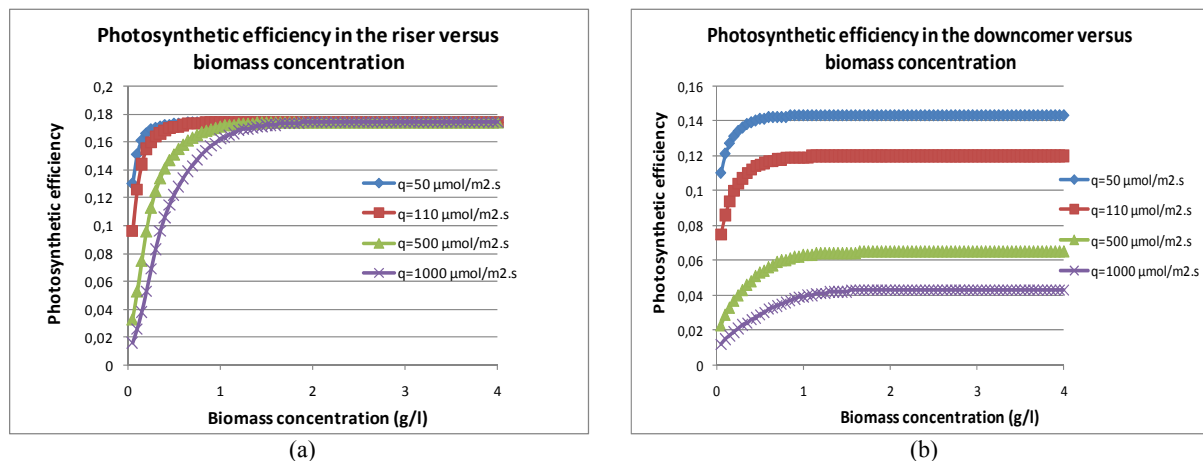


Figure III.17. Photosynthetic efficiency vs. biomass concentration
a) in the riser; b) in the downcomer

Results show that photosynthetic efficiencies decrease when incident irradiances are augmented. It appears that biomass production rates do not increase very much with respect to the energy absorbed and therefore, with the local light energy density. This is related to the optical properties of algae, directly linked to their pigment composition and the reactor design.

For all concentrations, highest photosynthetic efficiencies occur in the riser, achieving a constant value of 18% at high concentrations. In the downcomer, the highest photosynthetic efficiency is 14%. It appears, even though the lowest biomass production rate is observed in the riser (Figure III.16), that the local light energy is better benefited by algae to reproduce biomass in this compartment.

For optimal biomass concentrations, the PE ranges from 11.5% to 15.4% in the riser and from 2.7% to 12.2% in the downcomer. In both cases, the lowest PE corresponds to the highest irradiance and vice versa. In any case, the maximal values of PE obtained here are high since in experimental studies, punctual photosynthetic efficiencies have ranged between 1 and 16%, being 3, 4, and 6% the most common averaged efficiencies (Tredici and Chini Zittelli, 1998; Hall et al., 2003; Huntley and Redalje, 2006).

Apart from photosynthetic efficiencies, it is also of interest to analyze the areal productivity as well as the illuminated surface productivity, which are related to the reactor geometry and performance. The areal productivity is defined as the biomass production rate per unit of ground area occupied by the reactor. Since the external cylinder, that forms the downcomer, has an external diameter of 200 mm, a first approximation of the occupied area is 0.0314 m^2 . However, an occupied area of 0.79 m^2 is taken into account since the reactor was constructed over a rectangular metallic support.

On the other hand, the illuminated surface productivity is referred to the biomass productivity per unit of illuminated surface. In an IAL reactor, the illuminated surface is given by the external diameter of the downcomer section and the height of the liquid.

Table III.8 presents the areal and the illuminated surface productivity for the designed reactor cultivating *Chlamydomonas reinhardtii* under optimal concentrations, following Monod's law and under continuous illumination. It is assumed that the reactor works for 24 hours to calculate the daily biomass production rate.

Table III.8. Efficiencies and productivities of the designed IAL reactor.

<i>Light flux density</i> ($\mu\text{mol E/m}^2.\text{s}$)	<i>Optimal biomass concentration</i> (g/L)	<i>Areal productivity</i> ($\text{g/m}^2.\text{d}$)	<i>Illuminated surface productivity</i> ($\text{g/m}^2.\text{d}$)
50	0.11	4.88	7.87
110	0.15	9.29	15
500	0.32	23	37
1000	0.45	29.7	48

The estimated areal productivities are in the same order as those observed in open ponds, horizontal tubular, and helical bioreactors (Chapter I, Table I.4). In open ponds the average dried biomass productivity is between 10 and 25 $\text{g/m}^2.\text{d}$, having biomass concentrations in the range of 0.5 g/L. (Becker, 1998; Lee, 2001).

The specific illuminated area is another parameter that characterizes photobioreactors. It is defined as the ratio between the illuminated surface and the working volume. In an IAL reactor, specific illuminated area is given by $4/D$, where the term “D” is the external diameter of the downcomer (Richmond, 2007, Takache et al., 2010). In experimental studies, examples of specific illuminated area are 400 1/m and 49 1/m for horizontal-tubular photobioreactors (Carlozzi, 2000; Vonshak, 1997), 25 1/m for a torus PBR (Takache et al., 2010), and for internal airlift reactors 20.7 and 13.3 1/m (Sanchez et al., 2002; Xu et al., 2002). In this study, the specific illuminated area of the reactor is equal to 20 1/m, which is small compared to horizontal-tubular photobioreactors but in the range of those observed in IAL reactors. Generally, high specific illuminated area requires larger occupied land (Munoz and Guieyssen 2006).

On the other hand, in an IAL reactor the difference between riser and downcomer diameters can be regarded as the *optical path* (definition usually employed for flat plate photobioreactors). The optical path influences the local and the averaged light energy absorbed by the culture (Equation III.16). In this case, the optical path is equal to 5 cm. The energy absorbed by cells diminishes if the optical path is augmented (Muller-Feuga et al., 1998; Huntley and Redalje, 2006). Therefore, if the optical path is reduced in an IAL reactor, higher light energy will be available for cells while the culture volume will be reduced if the height is maintained. In this case, the specific illuminated area will be also reduced.

If all above parameters are grouped, the challenge to have an efficient photobioreactor is to have high illuminated surface that can provide high volumetric biomass productivities, occupying small surfaces.

3. Mass transfer in an Internal Airlift Reactor: experimental and modeling study

In an internal airlift reactor, the liquid circulation is generated by injecting gas at the bottom of the reactor. The injected gas, mainly air or CO_2 enriched air, is in direct contact with the liquid thus there is a mass exchange between phases. The exchange phenomenon is called *diffusion* and is expressed as:

$$\text{Mass transport rate} = k(\text{interfacial area})(\text{concentration difference}) \quad (\text{III.17})$$

This equation means that the mass flux is proportional to the concentration difference from the bulk of one phase to the gas-liquid interface and proportional to the interfacial area, a . This is in concordance with the *film theory*, which is one of the existing theories (e.g. penetration theory, surface renewal theory, etc.) to estimate the mass transport rate between phases with different solute concentrations.

In the *film theory*, the interface between two phases separates two stagnant films at which the mass transfer occurs by diffusion, as a consequence of the solute gradient. The stagnant films have a thickness e and it is a function of the flow conditions. The solute gradient has a linear profile in the stagnant film (Cussler, 2007; Roustan, 2003).

The proportionality in Equation III.17 refers to an *overall mass transfer coefficient* k , which groups the respective mass transfer coefficients of the liquid (k_L) and gas side (k_g) (Equation III.18).

$$k = \frac{1}{\frac{1}{k_L} + \frac{1}{k_g}} \quad (\text{III.18})$$

For a system working with gas and liquid phases, it has been observed that the mass transfer coefficient in the gas is considerably larger than that of the liquid. In consequence, the overall mass transfer coefficient is approximately equal to k_L (Bird, 2002; Cussler, 2007).

In airlift reactors, it is of interest to estimate the specific interfacial area and the overall mass transfer coefficient, since they are the key for mass transport. Generally, they are obtained theoretically and experimentally as the product of $k_L a$ (named here as the volumetric mass transfer coefficient) (Talvy et al., 2007).

3.1 Determination of the overall volumetric mass transfer coefficient $k_L a$

In the next section, the volumetric mass transfer coefficient is first calculated theoretically for the transport of oxygen from the injected air into the liquid, by employing different correlations. Subsequently, the volumetric mass transfer coefficient $k_L a$ is determined experimentally.

3.1.1 Theoretical determination of $k_L a$

The specific interfacial area a is defined as the ratio between the gas contact surface and the liquid volume. If it is assumed that gas bubbles are spherical, the specific interfacial area is then determined from the bubble diameter (d_B) and gas holdup (ε_g) (Contreras et al., 1999; Tobajas et al., 1999; Talvy et al., 2007):

$$a = \frac{6\varepsilon_g}{d_B(1-\varepsilon_g)} \quad (\text{III.13})$$

This means that the specific interfacial area depends indirectly on the air flow rate injected into the reactor, since the gas holdup depends on the air flow rate (Chapter II). On the other hand, this correlation affirms that there is a compromise between the gas holdup presented in the system and bubble sizes, thus the interest is to obtain high gas holdup with small bubble diameters (Chisti, 2000; Freitas and Texeira, 2001).

From results obtained in the second chapter, the specific interfacial area is then calculated by applying Equation III.13, for the riser and downcomer compartments (Figure III.18).

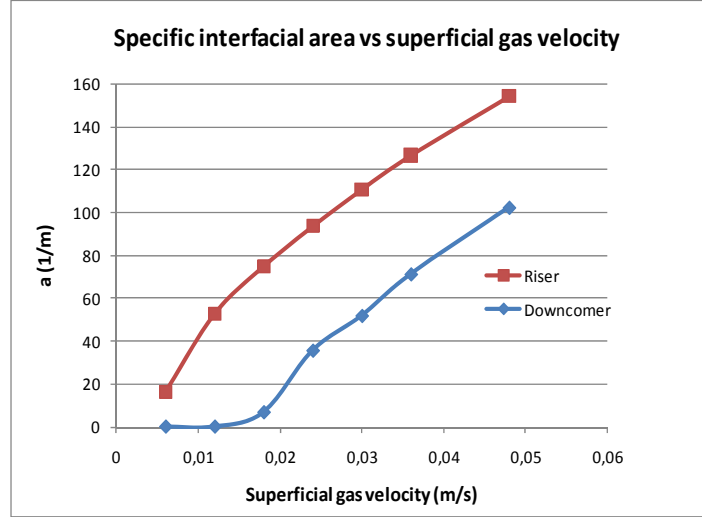


Figure III.18. Specific interfacial area vs. superficial gas velocities.

As results of the internal airlift reactor hydrodynamics, the specific interfacial area in the downcomer is lower than in the riser, since downcomer gas holdup is always lower than in the riser. Specific interfacial areas increase with superficial gas velocities since there is an augmentation of the gas holdup in both compartments. In the downcomer, it is assumed that bubble diameters are approximately the same as in the riser (Fan et al., 2008).

One method to determine the overall mass transfer coefficient (k_L) when bubbles are freely rising in a liquid is relating three dimensionless numbers: the Sherwood (Sh), the Schmidt (Sc), and the Grashof numbers (Gr). Together, they represent the conservation of mass, conservation of species, and momentum balances (Bailey and Ollis, 1986).

The Schmidt and the Grashof numbers are defined as:

$$Sc = \frac{\mu_L}{\rho_L D_L} \quad Gr = \frac{d_B^3 \rho_L (\rho_L - \rho_g)}{\mu_L^2} \quad (III.14)$$

These two numbers are function of liquid and gas properties, bubbles diameter, and the diffusion of the species in the liquid (D_L). The Sherwood number is a function of the Schmidt and Grashof numbers, involving k_L , as follows:

$$Sh = \frac{k_L d_B}{D_L} = f(Sc, Gr) \quad (III.15)$$

According to Calderbank and Moo-Young, the Sherwood number has two different forms depending on the gas bubble diameter. There is a critical bubble diameter that differentiates two regimes of bubble mass transfer. For bubbles diameter smaller than 2.5 mm, air bubbles behave as rigid bodies. For larger bubbles, bubble shapes change from spherical to ellipsoidal (Calderbank and Moo-Young, 1961):

For $d_B < d_c = 2.5$ mm, the Sh number is equal to:

$$Sh = 0.31 Gr^{1/3} Sc^{1/3} \quad (III.16)$$

While for $d_B > d_c$ the Sh number is:

$$Sh = 0.5Gr^{1/3}Sc^{1/2} \quad (\text{III.17})$$

These two expressions result in being independent of bubble diameters and slip velocity when they are applied together with Equation III.15. Values obtained for k_L are in the range from 6.2×10^{-5} to 2.6×10^{-4} m/s. The coefficient 0.5 in Equation III.17 has been employed for airlift reactors, while 0.42 is generally used (Bailey and Ollis, 1986; Calderbank and Young, 1961).

Lamont and Scott have proposed a relationship for airlift reactors to estimate the mass transfer coefficient assuming turbulent flow in the liquid, taking into account the Schmidt number (Talvy et al., 2007)

$$k_L = 0.4Sc^{-1/2} \left(\frac{\mu_L}{\rho_L} V_{sg} g \right)^{1/4} \quad (\text{III.18})$$

Results of mass transfer coefficients range from 3.3×10^{-4} to 5.5×10^{-4} m/s, which are in the same order of magnitude as those found by Talvy et al. (Talvy et al., 2007).

On the other hand, some authors have proposed relationships to determine $k_L a$ in airlift reactors as a function of the power input given by the gas per unit of liquid volume (P_g/V_L). They suggested an expression in the form of:

$$k_L a = \alpha (P_g / V_L)^\beta \quad (\text{III.19})$$

Chisti proposed values of α and β of 2.39×10^{-4} and 0.86 respectively for systems working with air and water (Chisti, 1989). Similarly to these values, Rubio et al. used α equal to 1.27×10^{-4} and β equal to 0.925 (Rubio et al., 2001). On the contrary of previous authors, Bello et al. included the ratio between riser and downcomer cross sectional areas in the following form (Bello et al., 1985):

$$k_L a = \frac{0.0005 (P_g / V_L)^{0.8}}{1 + A_d / A_r} \quad (\text{III.20})$$

Other authors have related the product $k_L a$ with superficial gas velocities since air flow rates affect the mass transfer. Van't Riet and Tramper proposed a relationship for bubble columns assuming coalescence and non-viscous flow, in the form of:

$$k_L a = 0.32 (V_{sg})^{0.7} \quad (\text{III.21})$$

Where values 0.32 and 0.7 were obtained empirically (Babcock et al., 2002).

Finally, Figure III.19 shows the results of volumetric mass transfer coefficients obtained from all correlations presented above.

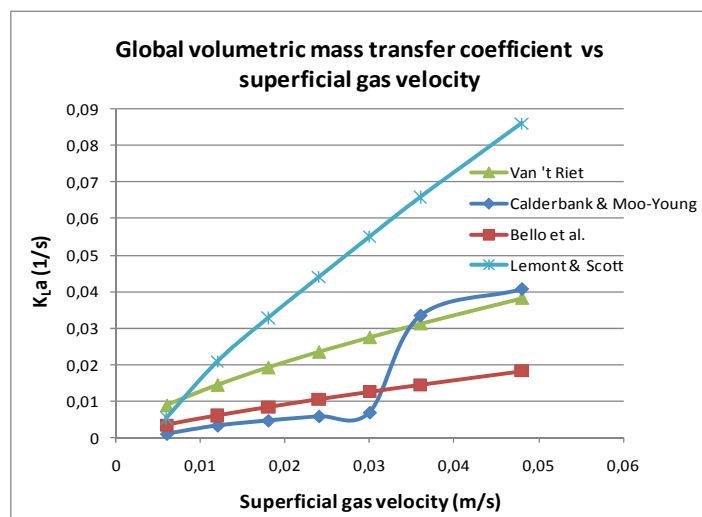


Figure III.19. Overall volumetric mass transfer for the riser according to several authors.

High discrepancies exist among calculated values of k_{La} . Comparing Lemont and Scott results with those obtained from using Bello et al. relationship, values differ between 49 and 87.5%. Contrarily, k_{La} values become similar at high superficial velocities when they were estimated from relationships proposed by Van't Riet and Calderbank and Moo-Young.

On the other hand, results found from using Calderbank and Moo-Young expression shows a sharply variation of k_{La} for superficial gas velocities higher than 0.03 m/s. The reason is the change of bubble diameter into sizes higher than the critical diameter, thus k_{La} values increase according to Equation III.17, obtaining k_{La} values as high as 4.3 times compared to those calculated using Equation III.16.

The following section presents overall volumetric mass transfer coefficients for oxygen obtained from experimental results in the designed IAL reactor. Then, relationships explained above are compared to experimental results.

3.1.2 Experimental determination of k_{La}

3.1.2.1 Materials and methods

The internal airlift reactor was filled with non-mineral water at 20°C until a level of 3 cm over the draft tube. Thus, the total water column height is 0.78 m. An oxygen electrode with a time of response of 20 s, was placed at the top of the riser and connected to a data acquisition system (Consort D130, multi parameters), which updates the data every 3 s. Particle concentrations of 2 and 5 g/L were added to the system in order to study their influence on the overall mass transfer coefficient.

Following the method of gassing-in and gassing-out, the overall volumetric mass transfer coefficient was obtained in the riser (Roustan, 2003, Loubiere et al., 2008). First, nitrogen gas was injected at the bottom of the reactor to strip the oxygen dissolved in the water. Once the dissolved oxygen reached a low and constant value, compressed air was injected into the riser at the desired flow rate. The evolution of dissolved oxygen in the water was then registered until it reached a constant value. This procedure was performed three times for air flow rates of 5, 10, 15, 20, 30, and 40 L_n/min.

3.1.2.2 Results

Figure III.17 shows the evolution of dissolved oxygen in the riser for four different air flow rates, after stripping the oxygen from water.

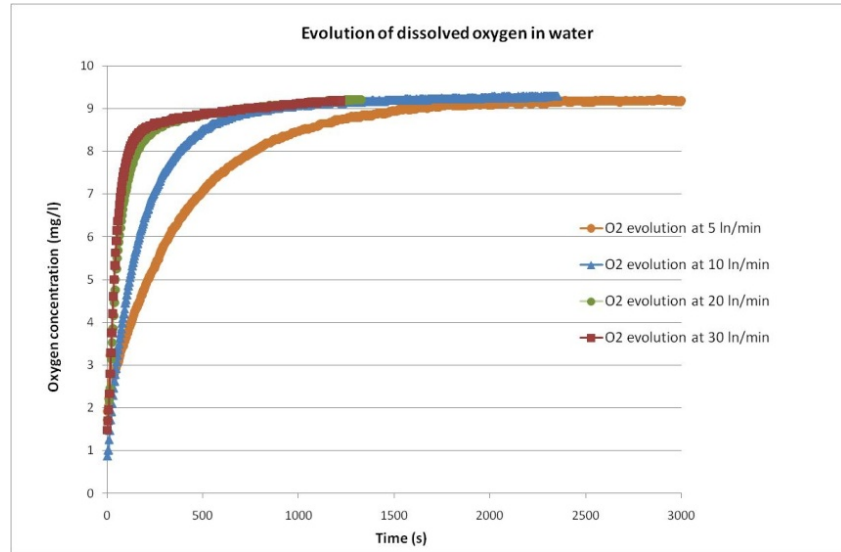


Figure III.20. Evolution of dissolved oxygen as a function of time vs. air flow rate.

Results show that the rate of dissolving oxygen into the water is higher when the air flow rate is increased in the riser. The mass transport is larger since gas holdups increase with superficial gas velocities (Cerri et al., 2008).

To estimate values of $k_L a$ for the oxygen in the riser at each air flow rate, it is assumed that the turbulence is sufficient in the liquid and the gas phases to achieve complete mixing in the bulk (the oxygen is diluted in both phases). As a first approximation, the reactor is considered as a continuous stirred tank, thus the dissolved oxygen evolution is expressed as follows (Babcock et al., 2002; Zhang et al., 2006):

$$\frac{dC_{O_2,L}}{dt} = (k_L a)_{O_2} (C_{O_2}^* - C_{O_2,L}) \quad (\text{III.22})$$

Integrating the equation above results in:

$$\ln \left(\frac{C_{O_2}^* - C_{O_2,L}^0}{C_{O_2}^* - C_{O_2,L}} \right) = (k_L a)_{O_2} (t - t^0) \quad (\text{III.23})$$

$C_{O_2}^*$ is the equilibrium dissolved oxygen in water and it is estimated by using Henry's law.

$$C_{O_2}^* = \frac{C_{O_2,g}}{He_{O_2}} \quad (\text{III.24})$$

$C_{O_2,g}$ is the oxygen concentration in the air while He is the dimensionless Henry's constant for the oxygen at 20°C ($He=31.5$ for O_2) (Perry et al., 1999; Babcock et al., 2002). In Equation III.23, the term $C_{O_2}^0$ is the initial dissolved oxygen in water, once nitrogen injection has been stopped to proceed with air injection. By plotting the left side of the equation versus time, the product of the overall mass

transfer coefficient with the interfacial area is the slope of the curve (Rubio et al., 2001; Jin et al., 2006; Giaveno et al., 2007). Figure III.21 shows the estimation of the volumetric mass transfer coefficient $k_L a$ for an air flow rate of 10 L_n/min.

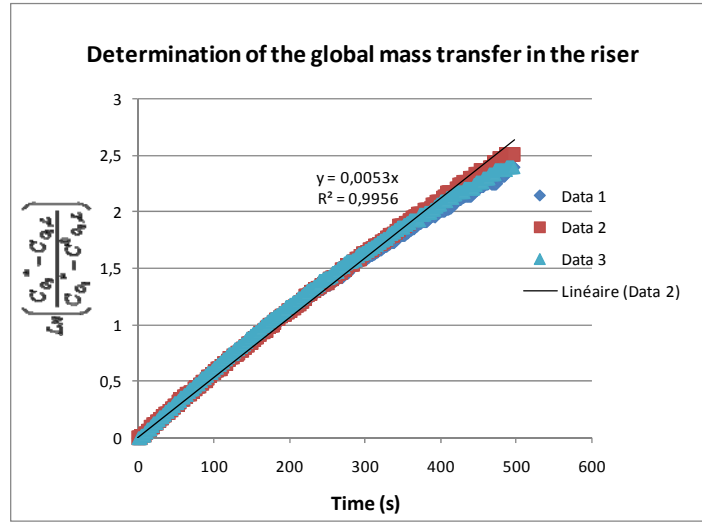


Figure III.21. Experimental determination of $k_L a$ in the riser for an air flow rate of 10 L_n/min.

By performing the same procedure for other air flow rates, values of volumetric mass transfer coefficients for the oxygen resulted in values ranging from 0.0024 to 0.02 1/s (8.64 to 72 1/h) (Figure III.22):

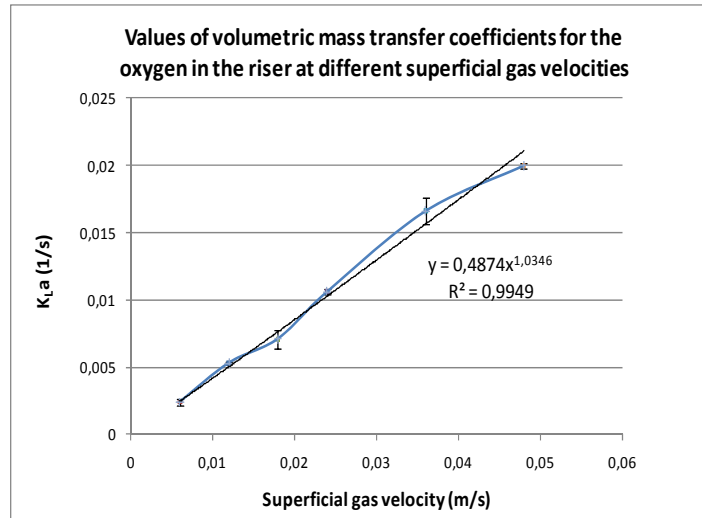


Figure III.22. Values of $k_L a$ in the riser vs. superficial gas velocity.
Experimental values have a maximal standard deviation of 11%.

On the other hand, it is important to compare electrode response time with the mass transfer characteristic time, which is defined as the inverse of the volumetric mass transfer (Loubiere et al., 2008). For the electrode, a similar procedure given by Equation III.23 was followed, given a time constant of 20 s. As some authors stand, this time constant can be negligible compared to values of mass transfer characteristic times ranging from 370 s to 94 s (corresponding to air flow rates of 5 and 20 L_n/min respectively) (Perry et al., 1999; Roustan, 2003; Wiesmann et al., 2007). However, for higher air flow rates, the mass transfer characteristic times are closer to the electrode time constant, thus the electrode time response might not be high enough to observe fast changes in oxygen concentrations.

From Figure III.22, results show that the overall mass transfer coefficient increases with superficial gas velocities (Jin et al., 2006). Similarly to the relationship proposed by Van't Riet and Tramper (Equation III.21), a mathematical regression of experimental results obtained in the riser, is:

$$k_L a = 0.487(V_{sg})^{1.035} \quad (\text{III.25})$$

To calculate $k_L a$ in the downcomer, the interfacial area is obtained from the gas holdup measured in this section. Then, it is assumed that the mass transfer coefficient k_L in the downcomer is equal to that in the riser, since the physical properties of the two phases are the same and it is considered that bubbles diameter are similar in both compartments. Other authors estimated k_L in the downcomer assuming 90% of that of the riser, alleging that downcomer gas holdup is lower than that of the riser (Rubio et al., 2001).

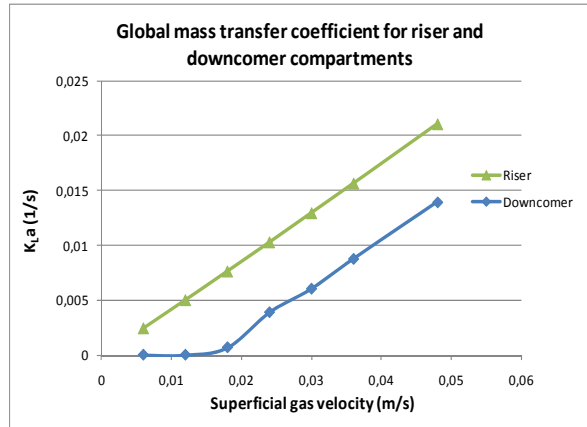


Figure III.23. Values of $k_L a$ in the riser and downcomer compartments

In the riser, values of the overall volumetric mass transfer are in the same range of those found by Contreras et al. and Jin et al. in an experimental study performed with an internal airlift bioreactor. In Contreras et al. study, tested superficial gas velocities were higher, reaching 0.2 m/s and observing a constant value of $k_L a$ once velocities were higher than 0.1 m/s. Similarly to this study, for superficial gas velocities up to 0.045 m/s, $k_L a$ values increase approximately linearly (Figure III.22) (Contreras et al., 1999; Jin et al., 2006). Experimental results provide good values of $k_L a$ since authors have considered that volumetric mass transfer coefficients around 0.001 1/s are low (Rubio et al., 1998).

Results in Figure III.23 imply that mass transport between phases is more important in the riser than in the downcomer, which is in concordance with specific interfacial areas and gas holdups. In the downcomer, $k_L a$ is null for superficial gas velocities between 0.006 and 0.018 m/s since the reactor works in regime I (there is no gas entering to the downcomer).

On the other hand, it is interesting to find the capacity of the reactor to promote mass exchange between phases. This is traduced into estimate the power input given by the gas (P_g) to generate gas holdup, liquid circulation and therefore, to promote mass transfer. In this sense, the specific power input defined as the power input given by the gas per unit of liquid volume is due to gas isothermal expansion along the riser height (Merchuk and Berzin, 1995; Fadavi and Chisti, 2007):

$$\left(\frac{P_g}{V_L}\right) = \frac{Q_g RT}{V_L} \ln\left(1 + \frac{\rho_L g H}{P_a}\right) \quad (\text{III.26})$$

In airlift reactor, it is usual to associate the riser gas holdup with the specific power input while the overall volumetric mass transfer coefficient is related to the gas holdup (Figure III.24) (Rubio et al., 1998).

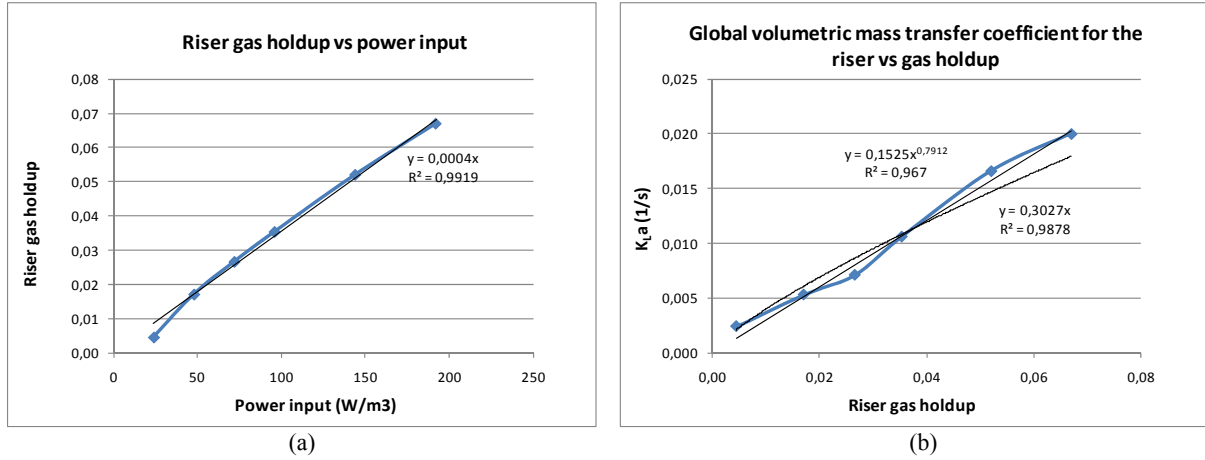


Figure III.24 Relationship among k_La in the riser, gas holdup, and power input.
a) Riser gas holdup vs. power input; b) Overall volumetric mass transfer vs. Riser gas holdup.

Results from Figure III.24 show that specific power input, gas holdup, and the volumetric mass transfer coefficient are related in the form of:

$$\varepsilon_{g,r} = 4 \cdot 10^{-4} \left(\frac{P_g}{V_L} \right) \quad (\text{III.27})$$

$$(k_La)_r = 0.153 (\varepsilon_{g,r})^{0.79} \quad (\text{III.28})$$

Where the specific power input is expressed in W/m^3 , ranging from 24 to 192 W/m^3 .

Constants in Equation III.27 are close to those obtained by Sanchez et al. working with a tubular photobioreactor of 57 liters and 200-m long, while having specific power input between 400 and 500 W/m^3 (Sanchez et al., 1999).

The specific power input given by the gas injected into the system is in concordance with other experimental studies performed with airlift reactors. Giaveno et al. estimated a power input ranging from 90 to 500 W/m^3 of an internal airlift reactor working with 10.5 liters (Giaveno et al., 2007). Ganzeveld et al. estimated lower specific power inputs (from 0 to 33 W/m^3) in a split-cylinder airlift reactor working with low volume of 1.75 liters (Ganzeveld et al., 1995). For a forced airlift reactor of 16.3 liters (liquid pump was added to the system), the specific power input ranged from 50 to 1000 W/m^3 approximately (Fadavi and Chisti, 2007). Values of specific power input in bubble columns range from 98 to 270 W/m^3 (Sanchez et al., 1999).

On the other hand, values of the overall volumetric mass transfer corresponding to riser gas holdup are in agreement with those obtained by Jin et al. for an internal airlift reactor of 19 liters (Jin et al., 2006). Figure III.24b shows that a linear and power regression can be established between the overall volumetric mass transfer and riser gas holdup, having proper correlation coefficients (R^2). Nicolella et al. proposed a linear relationship while Jin et al. stated a power regression (Nicolella et al., 1998; Jin et al., 2006).

Subsequently, if the volumetric mass transfer coefficient is directly related to the specific power input given by the gas, the following relationship is established:

$$(k_L a)_r = 9.10^{-5} \left(\frac{P_g}{V_L} \right)^{1.035} \quad (\text{III.29})$$

A correlation coefficient (R^2) of 0.99 is obtained. Values of constants are similar to those obtained by Rubio et al. for a split-cylinder airlift reactor of 156 liters. Comparing experimental results to the relationships presented in Section 3.1.1, values of $k_L a$ in the riser vary according to Figure III.25.

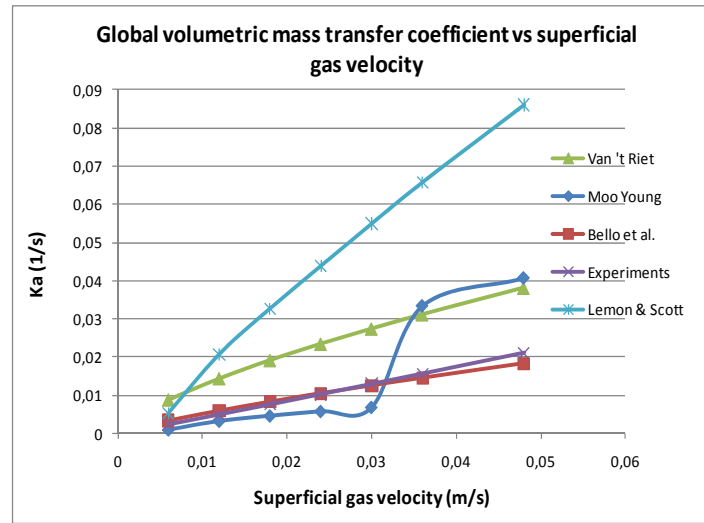


Figure III.25. Experimental and theoretical results of $k_L a$ vs. superficial gas velocity.

The correlation proposed by Van't Riet and Tramper for bubble columns overestimates $k_L a$ values, as high as 3.7 times compared to experimental results. On the contrary, the relationship among the dimensionless numbers proposed by Moo-Young underestimates $k_L a$ values, as lowest as 0.4 times compared with experimental values. The difference might reside in the estimation of bubble diameters, since they were calculated theoretically and not by direct measurement. In conclusion, the most well suited correlation to experimental results obtained in this study is the one proposed by Bello et al. with a maximal deviation of 37% for the lowest superficial gas velocity (Equation III.20).

Finally, to study the effect of solids on the overall mass transfer coefficient, concentrations of particles of 0, 2, and 5 g/L were added to the system. As explained above, oxygen was stripped from non-mineral water by injecting nitrogen, followed by air injection. Figure III.26 shows values of $k_L a$ for three particle concentrations for different air flow rates.

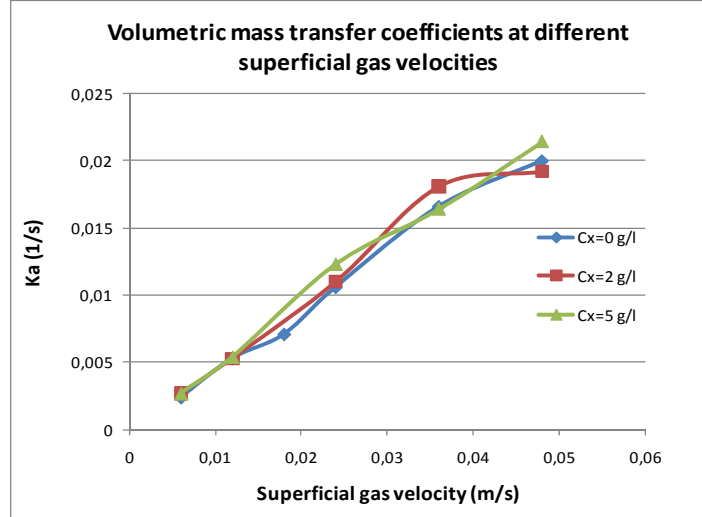


Figure III.26. Values of k_La at different particle concentrations.

From these results, it can be observed that dissolved oxygen evolution is slightly affected for the range of particle concentrations studied here. Similarly, authors such as Jin et al. and Nicolella et al. found that solid loading do not affect the overall volumetric mass transfer coefficient (Nicolella et al., 1998; Jin et al., 2006). Compared to other studies, results have shown that values of k_La decrease when solids were added in loadings of 5, 10, 15, 20, and 30 %v/v, essentially for riser superficial gas velocities higher than 0.075 m/s (Freitas and Texeira, 2001). In this study, the maximal deviation among k_La values is 10%. Therefore, the empirical correlation obtained for k_La at zero particles concentration can be employed, always for particle concentrations ranging from 0 to 5 g/L.

Once k_La values at different superficial gas velocities and particle concentrations have been obtained, the next step is to model the evolution of dissolved oxygen in non-mineral water in order to compare modeling results with experiments. Once the model is validated, the objective is to estimate the capacity of the reactor to release the oxygen and to absorb carbon dioxide if microalgae culture is performed under specific conditions of light intensities and microalgae species.

3.1.3 Oxygen evolution in the internal airlift reactor

The prediction of oxygen evolution along the reactor can be obtained by performing a mass balance in a differential column height (Δz) in the form of:

$$(\text{Accumulation}) = (\text{O}_2 \text{ flow in} - \text{O}_2 \text{ flow out}) + (\text{O}_2 \text{ absorption}) \quad (\text{III.30})$$

The term accumulation refers to an unsteady state problem since it is desirable to observe oxygen evolution in time, once air is injected into the O_2 -stripped water. Subsequently, the general transport equation for the oxygen in the liquid is in the form of:

$$\frac{dC_{O_2,i}}{dt} = D_z \frac{d^2 C_{O_2,i}}{dz^2} - V_L \frac{dC_{O_2,i}}{dz} + (k_L a)_{O_2} (C_{O_2}^* - C_{O_2,L}) \quad (\text{III.31})$$

(1) (2) (3) (4)

Terms (2) and (3) correspond to the axial dispersion and the convective transport of the solute, respectively. Term (4) is the oxygen transport between phases determined from applying the *film theory*, as it was mentioned above (Cussler, 2007).

The axial dispersion in the liquid and gas phases in photobioreactors might be neglected according to the geometry and the characteristics of the flow (e.g. velocity, physical properties). In bubble columns and airlift reactors, it is generally agreed that in the gas, the convective transport is dominant over the diffusive transport, since gas bubbles flow at high velocity and there is no reaction in the gas. In consequence, the second term in Equation III.31 can be neglected for the gas phase, being considered as *plug flow* (Froment and Bischoff, 1990; Talvy et al., 2007).

On the contrary, the oxygen in the liquid phase might have certain dispersion according to the reactor and the flow physical characteristics, thus the second term might not be neglected (Rubio et al., 1998; Burris et al., 2002; Sanchez et al., 2004; Talvy et al., 2007). Consequently, the liquid might be considered whether as *plug flow*, *axial dispersed plug flow* or *complete mixed flow*. To characterize the flow, the dimensionless Peclet number is usually employed. The Peclet number for the liquid phase is defined as:

$$Pe = \frac{V_{SL}H}{D_Z} \quad (III.32)$$

Where D_Z is the axial dispersion coefficient (second term in Equation III.31). In bubble columns and airlift reactors, the axial dispersion coefficient reflects the difference between the liquid flow in the bulk and that caused by the movement of the liquid behind the rising bubbles (Sanchez et al., 2004).

Regarding Equation III.32, if Peclet number is higher than 20, the flow is considered as plug while the opposite results in a complete mixed flow (Froment and Bischoff, 1990; Rubio et al., 1998; Babcock et al., 2002). Other authors define the same relationship as the Bodenstein number (Sanchez et al., 2004). In this study, the axial dispersion coefficient in the riser is calculated from different authors, who establish D_Z as a function of reactor geometry, properties of the fluid, and superficial gas velocities (Deckwer et al., 1974; Kawase et Moo-Young, 1986; Merchuk et al., 1997; Sanchez et al., 2004; Liu et al., 2010). These correlations are written in Table III.9.

Table III.9. Correlations to estimate the axial dispersion coefficient.

<i>Authors</i>	<i>Axial dispersion coefficient</i>
Merchuk et al., 1997	$D_Z = 0.94(D_{equiv})(V_{sg}/\varepsilon_g)^{1.11}$
Kawase and Moo-Young, 1986	$D_Z = 0.343(D_r)^{4/3}(gV_{sg})^{1/3}$
Deckwer et al., 1974	$D_Z = 2.7(D_r)^{1.4}(V_{sg})^{1/3}$
Liu et al., 2010	$D_Z = 3.2 \cdot 10^{-4}(\text{Re}_L)(\text{Re}_g)^{-0.5}$
Sanchez et al., 2004	$D_Z = \frac{V_{SL}H}{8.28(Fr^{1/3})^{1.364}}$

Correlations proposed by Deckwer et al. and Kawase and Moo-Young were obtained from testing air-water in bubble columns. These correlations are necessary to estimate the axial dispersion coefficient in the riser. The remaining equations were obtained for air-water in internal airlift reactors. Once the

axial dispersion coefficients are estimated, the corresponding Peclet numbers are calculated from Equation III.32 (Figure III.27).

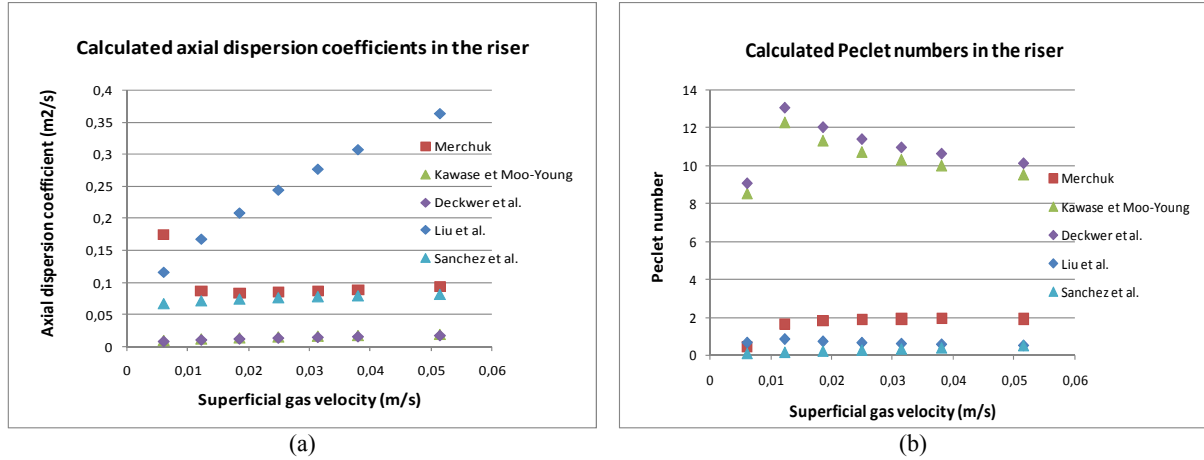


Figure III.27. Axial dispersion coefficient and Peclet number in the riser
a) Axial dispersion coefficient vs. superficial gas velocity; b) Peclet number vs. superficial gas velocity

Results show that in general, axial dispersion coefficients increase slightly with superficial gas velocities. The increase is more pronounced for the correlation proposed by Liu et al. Correlations proposed by Deckwer et al. and Kawase and Moo-Young result in very low axial dispersion coefficients, while other authors results in even 20 times higher. The two first correlations were estimated from testing bubble columns, in which may reside the difference among results (Deckwer et al., 1974; Kawase and Moo-Young, 1986). On the other hand, values calculated from using Merchuk correlation are similar to those obtained by Sanchez et al. one when tap water was employed in an internal airlift reactor with similar diameters (Sanchez et al., 2004).

Results from applying equations in Table III.7, lead to Peclet numbers ranging from 0.44 to 2 for the oldest correlations and from 8.6 to 13 for the most recent. For instance, the liquid in the riser cannot be considered as completely plug flow; instead it presents a certain degree of axial dispersion. Subsequently, the second term in Equation III.31 is considered in this study and the axial dispersion coefficient is calculated from Sanchez et al., which is a most recent correlation (Sanchez et al., 2004).

Referring to the downcomer, if the reactor works in regime I, there is no gas entering into this section, thus the liquid is considered in plug flow (Peclet number tends to be infinite). In regime II, superficial gas velocities are very low since bubbles seem not to move with respect to reactor wall. Consequently, Peclet number tends to be high and plug flow can be assumed.

In consequence, the model of oxygen evolution in the riser assumes that:

- The gas in the riser is taking as plug flow
- The liquid in the riser presents a certain degree of axial dispersion
- The liquid in the downcomer is assumed to be in plug flow.

The transport equation for the oxygen (Equation III.31) is then developed in finite volume method for the liquid phase:

$$\frac{dC_{O_2,L}}{dt} = D_z \frac{C_{O_2,L}^{j+1} - 2C_{O_2,L}^j + C_{O_2,L}^{j-1}}{2\Delta z} - V_{sl} \frac{C_{O_2,L}^j - C_{O_2,L}^{j-1}}{\Delta z} + (k_L a)_{O_2} (C_{O_2,L}^* - C_{O_2,L}^j) \quad (\text{III.33})$$

While for the gas phase:

$$\frac{dC_{O_2,g}}{dt} = V_{sg} \frac{C_{O_2,g}^j - C_{O_2,g}^{j-1}}{\Delta z} - (k_L a)_{O_2} (C_{O_2,L}^* - C_{O_2,L}^j) \quad (III.34)$$

The model was simulated in Dymola, an environment from the modeling language Open Modelica®. The model is developed inside a package, where riser and downcomer compartments are defined as two different models, connected by gas and liquid phases (Appendix I)

Figure III.28 shows a comparison between experimental and modeling results for an air injection of 5, 10, 15, and 20 L_n/min. Modeling results are developed for axial dispersion coefficients of 0.067, 0.071, 0.074, and 0.076 m²/s, which result from applying Sanchez et al. equation (Table III.7).

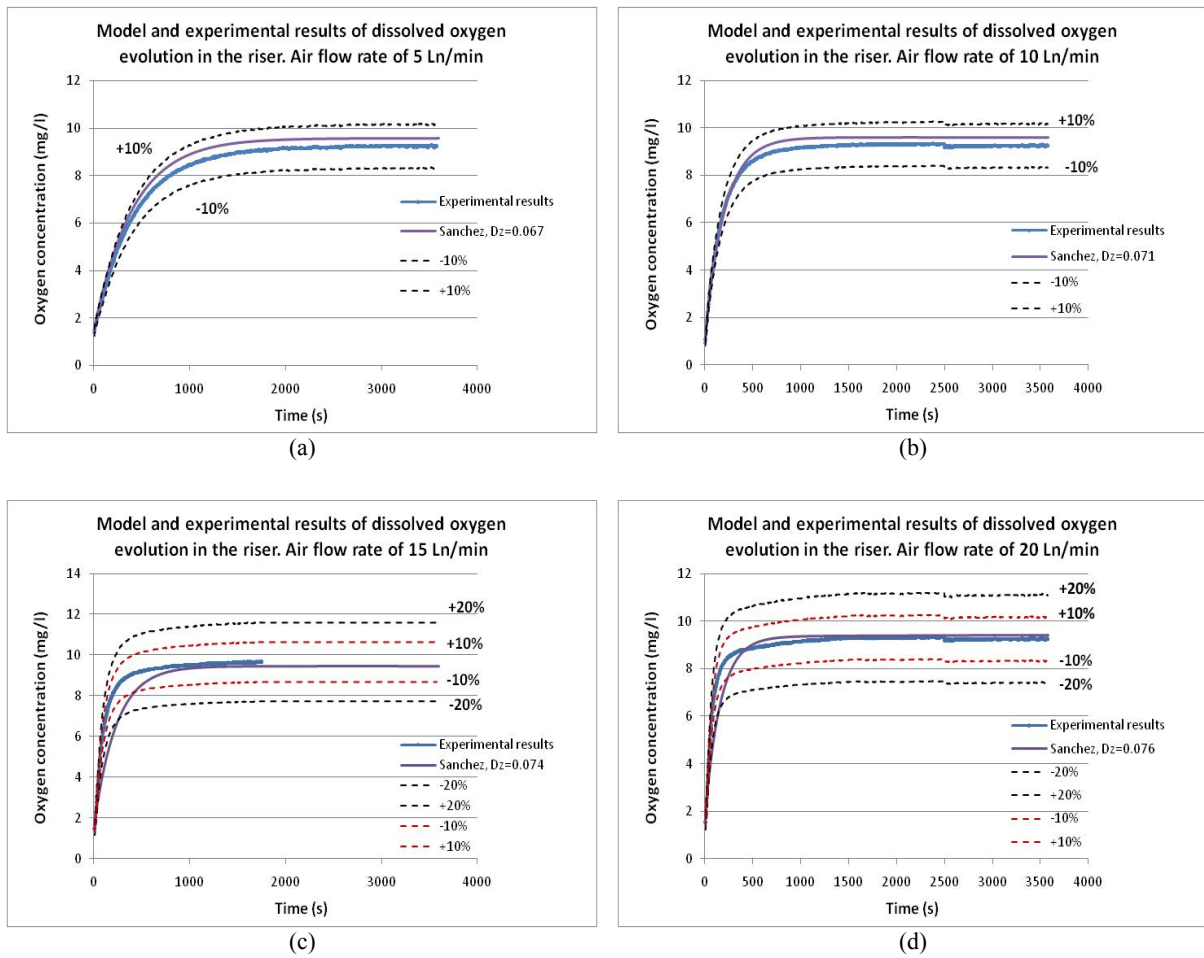


Figure III.28. Simulation and experimental results of dissolved oxygen in the riser.

a) Air flow rate of 5 L_n/min; b) Air flow rate of 10 L_n/min; c) Air flow rate of 15 L_n/min; d) Air flow rate of 20 L_n/min

Comparing experimental and modeling results, the best modeling approximation occurs for air flow rates of 5 and 10 L_n/min. Simulation values are in the range of 10% deviation from experimental values, being smaller at the beginning of air injection. For air flow rates of 15 and 20 L_n/min, the difference between experimental results and modeling results is higher, being close to 20% at the beginning of air injection. These deviations are reduced to less than 10% once the time is longer than 500 seconds for 15 and 250 seconds for 20 L_n/min (Figures III.28c and III.28d).

On the other hand, simulation results illustrate the same tendency found with experimental results: the rate of mass transport between phases is higher once the air flow rate is increased in the riser (Figure III.20).

These results allow continuing with the estimation of the reactor capacity to provide carbon dioxide to the culture and to release photosynthetic oxygen to the atmosphere if, for example, the culture of *Chlamydomonas reinhardtii* is performed in the reactor.

3.2 Modeling gas-to-liquid mass transfer in the IAL reactor performing microalgae culture

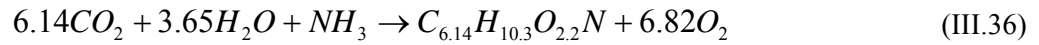
As microalgae perform photosynthesis, the biochemical conversion process is expressed quantitatively as the absorption of carbon dioxide and oxygen release. In both cases, the rate of production or absorption is directly related to the biomass productivity and the conversion yield coefficient ($Y_{S/X}$), obtained from the stoichiometry equation of photosynthesis (Cogne et al., 2001). Consequently, the term *production rate* represents the flux of O_2 or CO_2 per unit of liquid volume and time. In the case of oxygen:

$$R_{O_2} = P_{bio} (Y_{O_2/X}) \quad (III.35)$$

While for the carbon dioxide:

$$R_{CO_2} = P_{bio} (Y_{CO_2/X}) \quad (III.36)$$

According to Nouals, Myers proposed a general stoichiometry equation for algal biomass in the form of:



From which a value of $Y_{O_2/X}$ results in 51.2 mol O_2 /kg while a value of $Y_{CO_2/X}$ results in 46.1 mol CO_2 /kg. These values can then be estimated and used in this study (Nouals, 2000). This is in concordance with the ratio Y_{CO_2/O_2} of 1.11 ± 0.238 g CO_2 /g O_2 (0.811 mol CO_2 /mol O_2) proposed by Doucha and Livansky (Doucha and Livansky, 2006). Subsequently, reactants and products are carried to and from microalgae cells by transport processes that involve liquid and gas phases. Reconsidering the *film theory* as it was explained in the section above, the respective carbon dioxide and oxygen transports are illustrated in Figure III.29.

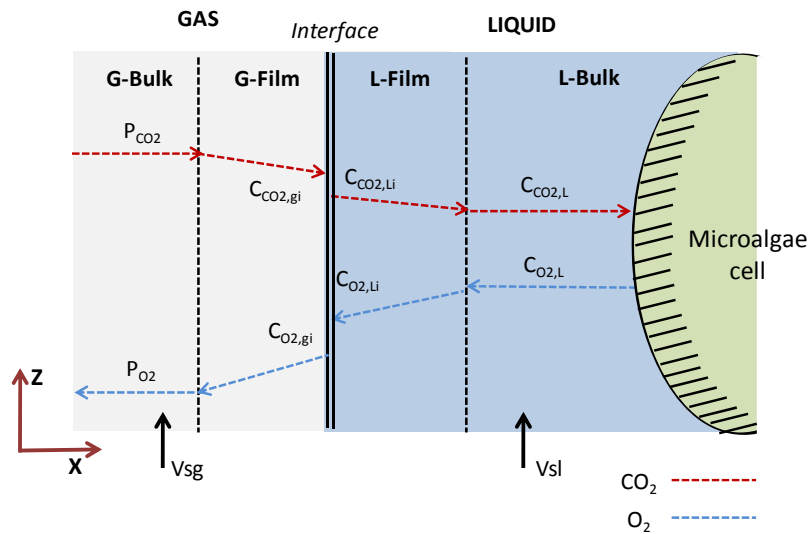


Figure III.29. Illustration of the film theory applied to microalgae culture

Here, it is assumed that the cell is completely submerged in the liquid and there is no resistance to mass transport in the film between the solid and the liquid. Subsequently, carbon dioxide and oxygen fluxes pass directly from the cell to the liquid.

As it was explained in Chapter I, the dissolved carbon dioxide forms part of the total inorganic carbon presented in algae culture. The carbon dioxide has to be in equilibrium with carbonic acid (H_2CO_3), carbonate (CO_3^{2-}), and bicarbonate (HCO_3^-), which are accompanied by pH changes. During photosynthesis reaction, the pH tends to increase due to OH^- release (Molina et al., 1999; Cogne et al., 2001; Richmond, 2007). The total inorganic carbon concentration (C_{tic}) is related to carbon dioxide concentration in the following form:

$$C_{tic} = K_{tic} (C_{CO_2}) \quad (III.37)$$

K_{tic} is a constant that depends on the dissociation equilibrium constants K_1 and K_2 and the culture pH. The constant K_{tic} is calculated as (Cogne et al., 2001; Roustan, 2003):

$$K_{tic} = 1 + \frac{K_1}{10^{-pH}} + \frac{K_1 K_2}{10^{-2pH}} \quad (III.38)$$

K_1 is the equilibrium constant between bicarbonate and carbon dioxide while K_2 is the equilibrium constant between carbonate and bicarbonate, both being dependent on the temperature. Table III.10 presents their respective values, estimated from correlations shown in Roustan et al. for 20°C (Roustan, 2003).

Table III.10. Equilibrium reactions among CO_2 , HCO_3^- , and CO_3^{2-}

Reaction	Equilibrium constants	Values* (mol/l)
$CO_2 + H_2O \longleftrightarrow HCO_3^- + H^+$	$K_1 = \frac{[HCO_3^-] \cdot [H^+]}{[CO_2]}$	$K_1 = 5.02 \cdot 10^{-5} e^{(-1462.7/T)}$ $K_1 = 3.42 \cdot 10^{-7}$
$HCO_3^- \longleftrightarrow CO_3^{2-} + H^+$	$K_2 = \frac{[CO_3^{2-}] \cdot [H^+]}{[HCO_3^-]}$	$K_2 = 7.83 \cdot 10^{-8} e^{(-2213/T)}$ $K_2 = 4.12 \cdot 10^{-11}$

* Calculated for 20°C

When the culture of *Chlamydomonas reinhardtii* is performed in closed systems, the best growth occurs under pH between 7 and 7.5 (Moroney and Tolbert, 1985; Oncel and Vardar-Sukan, 2009; Kong et al., 2010). In this study, it is assumed that a pH equal to 7 is maintained along the culture since the pH tends to increase due to photosynthesis and it can be regulated by CO_2 injection. To calculate K_{tic} , values of K_1 and K_2 are taken as those shown in Table III.10, resulting in K_{tic} equal to 4.42 (Roustan, 2003).

In the model developed here, the CO_2 volumetric fraction in the injected air is initially known and it varies as a function of time and along the reactor according to the biomass productivity. The dissolved carbon dioxide is then determined by Henry's law and in consequence, the total inorganic carbon evolves as a function of time and along the reactor (Fan et al., 2008; Becerra, 2009; Nouals, 2000).

In real microalgae culture, the pH changes continuously and it is regularly monitored. Subsequently, the relationship between the dissolved carbon dioxide and the total inorganic carbon is not constant as a function of time, as it is assumed here (Equation III.38). The total inorganic carbon concentration is

determined from Equations III.37-38 and performing a balance of protons (electroneutrality equation). In consequence, the total inorganic carbon evolves as a function of time, according to the pH and CO₂ concentration in air (Camacho et al., 1999; Nouals, 2009).

Subsequently, Equation III.31 is re-written for the oxygen and the total inorganic carbon, together with carbon dioxide, to represent the evolution of their concentrations along the riser and downcomer compartments. In this case, terms of O₂ production (R_{O2}) and CO₂ (R_{CO2}) are taken into account as representation of photosynthesis activity. Equations are presented in Table III.11.

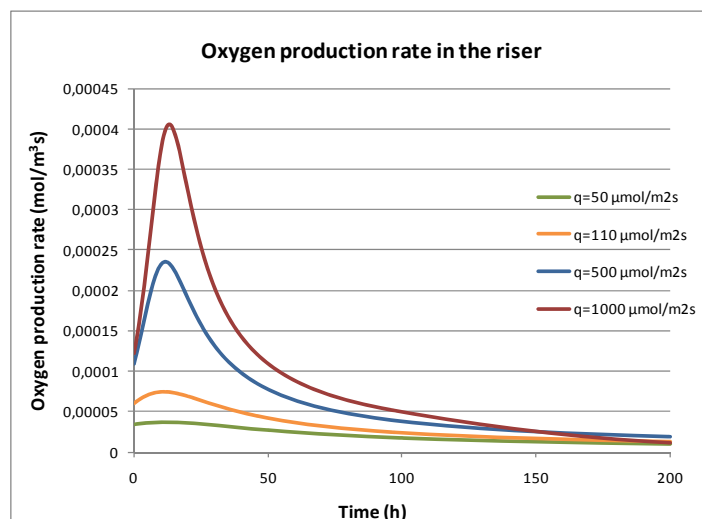
Table III.11. Expressions to estimate O₂ and CO₂ mass transport between phases in the IAL reactor.

<i>Riser</i>	<i>Downcomer</i>
For the oxygen in the liquid: $\frac{dC_{O_2}}{dt} = D_z \frac{d^2 C_{O_2}}{dz^2} - V_{sl,r} \frac{dC_{O_2}}{dz} + (k_L a)_{O_2,r} (C_{O_2}^* - C_{O_2,L}) + R_{O_2} (1 - \varepsilon_{g,r})$	For the oxygen in the liquid: $\frac{dC_{O_2}}{dt} = -V_{sl,d} \frac{dC_{O_2}}{dz} + (k_L a)_{O_2,d} (C_{O_2}^* - C_{O_2,L}) + R_{O_2} (1 - \varepsilon_{g,d})$
For the oxygen in the gas: $\frac{dC_{O_2}}{dt} = -V_{sg,r} \frac{dC_{O_2}}{dz} - (k_L a)_{O_2,r} (C_{O_2}^* - C_{O_2,L})$	For the oxygen in the gas: $\frac{dC_{O_2}}{dt} = -V_{sg,d} \frac{dC_{O_2}}{dz} - (k_L a)_{O_2,d} (C_{O_2}^* - C_{O_2,L})$
For the total inorganic carbon in the liquid: $\frac{dC_{TIC}}{dt} = D_z \frac{d^2 C_{TIC}}{dz^2} - V_{sl,r} \frac{dC_{TIC}}{dz} + (k_L a)_{CO_2,r} (C_{CO_2}^* - C_{CO_2,L}) - R_{CO_2} (1 - \varepsilon_g)$	For the total inorganic carbon in the liquid: $\frac{dC_{TIC}}{dt} = -V_{sl,d} \frac{dC_{TIC}}{dz} + (k_L a)_{CO_2,d} (C_{CO_2}^* - C_{CO_2,L}) - R_{CO_2} (1 - \varepsilon_g)$
For the carbon dioxide in the gas: $\frac{dC_{CO_2}}{dt} = -V_{sg,r} \frac{dC_{CO_2}}{dz} - (k_L a)_{CO_2,r} (C_{CO_2}^* - C_{CO_2,L})$	For the carbon dioxide in the gas: $\frac{dC_{CO_2}}{dt} = -V_{sg,d} \frac{dC_{CO_2}}{dz} - (k_L a)_{CO_2,d} (C_{CO_2}^* - C_{CO_2,L})$

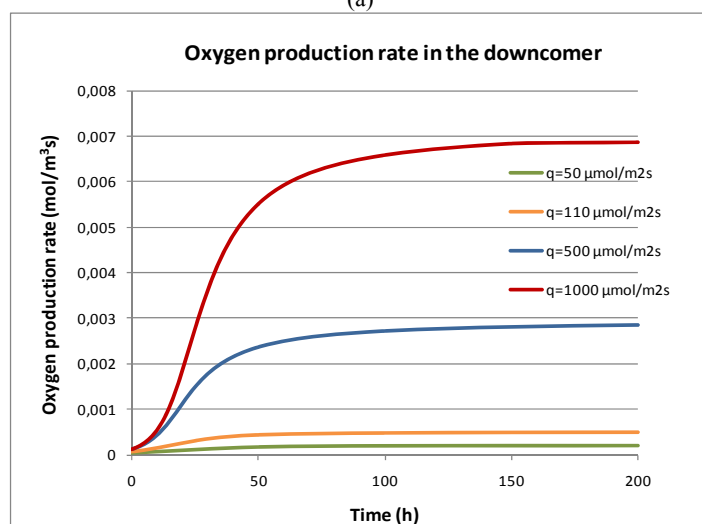
Discretizing equations in Table III.11, oxygen and carbon dioxide transportation and evolution are simulated in Dymola. The evolution of biomass concentration according to light energy available is added to the simulation as known values, already obtained in the first section. Respective conversion yield coefficients for oxygen and carbon dioxide are taken as Y_{O2/x} = 51.2 mol O₂/kg of biomass and Y_{CO2/x} = 46.1 mol CO₂/kg of biomass, respectively (Cogne et al., 2001; Babcock et al., 2002). Following sections present modeling results obtained from applying equations formulated in Table III.9.

3.2.1 Results: oxygen evolution

First results show the oxygen production rate as a function of time according to four incident light intensities. As it was explained above, biomass productivities depend on the incident light and the light energy available in each section of the reactor during the culture. Subsequently, oxygen production rates change in time according to these two parameters (Figure III.30). On the other hand, oxygen production rate does not depend on the air flow rate injected neither gas holdups. However, gas holdups affect oxygen transport from the cell to the liquid, as it is observed in the fourth term of Equation III.31 (Camacho et al., 1999; Molina et al., 1999).



(a)



(b)

Figure III.30. Evolution of oxygen production rate.
a) in the riser, b) in the downcomer

In agreement with results obtained in the first section (Figure III.16), the higher the incident irradiances, the higher the oxygen production rates. For this reason, O_2 production rates are higher in the downcomer than in the riser. Results in the downcomer are similar to those obtained by Camacho et al. in microalgae *Porphyridium cruentum* when it was exposed to sunlight irradiances (Camacho et al., 1999).

As the optimal biomass concentrations will be reached first in the downcomer, the maximal O_2 production rate occurs also in the downcomer after approximately 70, 100, 125, and 150 hours of cultivation for the incident irradiances considered in this study. Observing modeling results obtained from Monod's law and Cornet and Dussap's model, at these times optimal biomass concentrations will be already observed in both cases (Figure III.13, Tables III.5 and III.6). Therefore, if biomass continues to increase, dark zones might appear and thus photorespiration will be observed. In this case, the oxygen consumed will have to be subtracted from that produce during photosynthesis. A reduction of biomass growth rate might be observed.

Subsequently, the next step is to study the evolution of dissolved oxygen in each compartment in order to observe if high levels are reached and thus, if exist the risk of inhibiting photosynthesis. In the

liquid, initial conditions establish that oxygen in the air is in equilibrium with water at temperature of 20°C, according to Henry's law. Thus, the initial dissolved oxygen is estimated at 8.9 mg/L (0.278 mol/m³). In the air, the oxygen volume concentration is taken as 21%v/v as long as it is not modified according to CO₂ concentration. On the other hand, boundary conditions assume that the dissolved oxygen at the bottom of the riser is the same as in downcomer bottom. Similarly, at the top of riser and downcomer compartments, the dissolved oxygen concentration is identical.

Figure III.31 illustrates the dissolved oxygen evolution at the riser top and downcomer bottom, for air flow rates of 5, 10, 15, and 20 Ln/min and for an incident irradiance of 100 $\mu\text{mol E/m}^2\text{s}$.

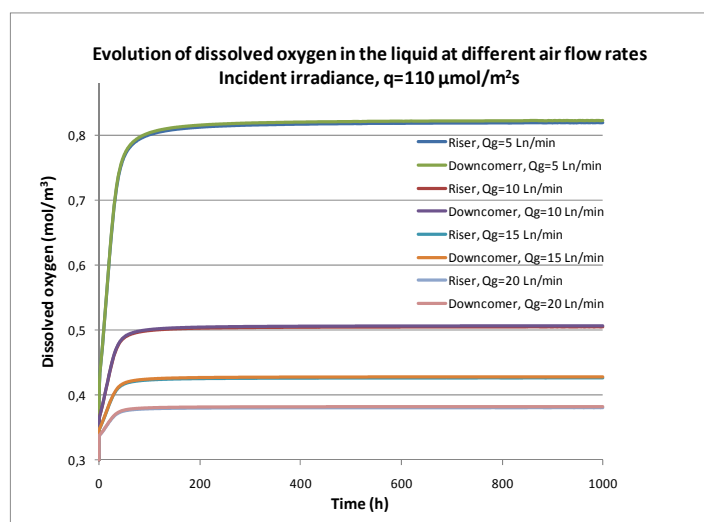


Figure III.31. Dissolved oxygen in the liquid vs. air flow rates
Incident irradiance of 110 $\mu\text{mol E/m}^2\text{s}$

Results demonstrate that dissolved oxygen in the liquid increases in time due to the production of photosynthetic oxygen in the entire reactor. At the riser top, the dissolved oxygen is lower than the dissolved oxygen at the bottom of the downcomer, meaning that oxygen is released in the riser thus there is less oxygen accumulated. The highest difference of dissolved oxygen between the two compartments is 0.44% and it occurs for an air flow rate of 5 Ln/min.

Comparing oxygen concentrations for different superficial gas velocities, it results that the lowest dissolved oxygen in the liquid is observed for the highest air flow rate, 20 Ln/min. This is in concordance with results obtained in Section 2.1.2 since the volumetric mass transfer coefficient is the highest for this air flow rate, thus having higher oxygen transport rate from the liquid to the gas (Figure III.22). To estimate the maximum value of dissolved oxygen attainable during microalgae culture, oxygen concentrations at four different incident irradiances are compared for the lowest air flow rate, 5 Ln/min.

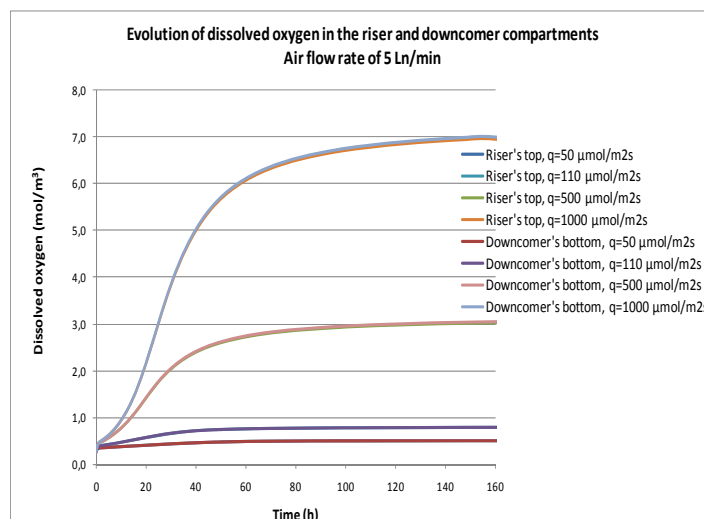


Figure III.32. Dissolved oxygen in the liquid vs. incident irradiance. Air flow rate of 5 Ln/min.

For all incident irradiances, oxygen concentrations at the bottom of the downcomer remain higher compared to the riser. As a consequence of having higher oxygen production rates at higher irradiances (Figure III.30), dissolved oxygen in the liquid is higher at higher irradiances. Increasing irradiances from 50 to 1000 $\mu\text{mol E/m}^2\text{s}$ leads to an increase of fourteen times the oxygen concentration in the liquid.

Several authors have observed a reduction of photosynthesis activity after a certain oxygen concentration in the liquid. According to Camacho et al., in the cultivation of *Chlorella vulgaris*, oxygen concentrations higher than 1.38 mol/m^3 reduced photosynthesis activity rate by 35% (Camacho et al., 1999). Jimenez et al. observed, in cultivation of *Spirulina platensis* in open ponds, a reduction of biomass once oxygen levels were higher than 25 mg/L (0.78 mol/m^3). In addition, Vonshak affirms that a maximum oxygen saturation of 300% (0.81 mol/m^3 considering 0.27 mol/m^3 air saturation at 20°C) avoided inhibition of photosynthesis, when *Spirulina platensis* was cultivated in ponds (Jimenez et al., 2003). According to Richmond, oxygen concentrations might reach 400% saturation at midday in low mixing raceway open ponds and 600% in tubular reactors (Richmond, 2007).

Modeling results show that O_2 concentration of 0.793 mol/m^3 (25.4 mg/L) is attainable when there is an incident irradiance of 110 $\mu\text{mol E/m}^2\text{s}$ over the reactor while lower O_2 concentrations are obtained for 50 $\mu\text{mol E/m}^2\text{s}$. These values are in the range between 100% and 177% air saturation for 50 $\mu\text{mol E/m}^2\text{s}$ and between 100% and 293.9% for 100 $\mu\text{mol E/m}^2\text{s}$, which are lower than those recommended by Vonshak. (Jimenez et al., 2003).

Similarly, Alias et al. obtained, in a bubble column working with *Phaeodactylum tricornutum*, oxygen concentrations always below 180% saturation with superficial gas velocities between 0.0087 and 0.017 m/s and under incident irradiances of 300 and 500 $\mu\text{mol E/m}^2\text{s}$.

In this study, incident irradiances of 500 and 1000 $\mu\text{mol E/m}^2\text{s}$ generate too high oxygen concentrations in the liquid, which will probably induce photosynthesis inhibition. In this case, it will be recommendable either to increase the volumetric mass transfer coefficient in the riser or not to perform *Chlamydomonas reinhardtii* culture under such high intensities.

Figure III.33 shows the change of dissolved oxygen with respect to saturation along the reactor height for light intensity of $110 \mu\text{mol E/m}^2\text{s}$.

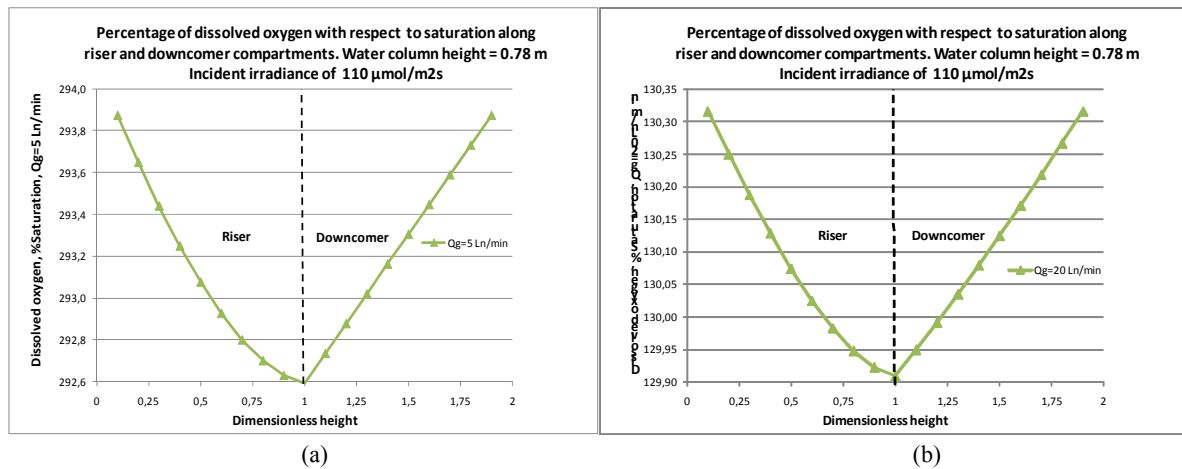


Figure III.33. Percentage of dissolved oxygen with respect to air saturation.
Incident irradiance of $110 \mu\text{mol E/m}^2\text{s}$
a) for an air flow rate of 5 Ln/min, b) for an air flow rate of 20 Ln/min

Results show that the highest variation of dissolved oxygen along the riser height occurs for an air flow rate of 5 Ln/min, decreasing 1.28% with respect to saturation, from the bottom to the top. On the contrary, for an air flow rate of 20 Ln/min, the oxygen concentration varies only 0.41% however; oxygen concentrations are lower compared to those obtained at 5 Ln/min. Variations of dissolved oxygen obtained here are low compared to those obtained in other studies. For example, Camacho et al. found that the oxygen accumulated in 100 m-tube decreases in an airlift device (3.5-m high) from 0.52 mol/m^3 (192.6% saturation) to 0.32 mol/m^3 (118.5%). These results demonstrate that, due to the hydrodynamical conditions and the geometry of the reactor established here, the desired dissolved oxygen depends more on the air flow rate injected than on the reactor height to release the oxygen, always maintaining low values of dissolved oxygen.

To confirm this, Figure III.34 shows the variation of oxygen concentrations assuming a water column height of 2 meters and taking the same hydrodynamical conditions of a water column height of 0.78 m. This assumption is valid for an air flow rate of 5 Ln/min, since it is more difficult to observe air bubbles flowing to the downcomer in a taller column. However, for an air flow rate of 20 Ln/min, this assumption will have to be verified since the reactor might not work under regime II, as it occurs in the presented study.

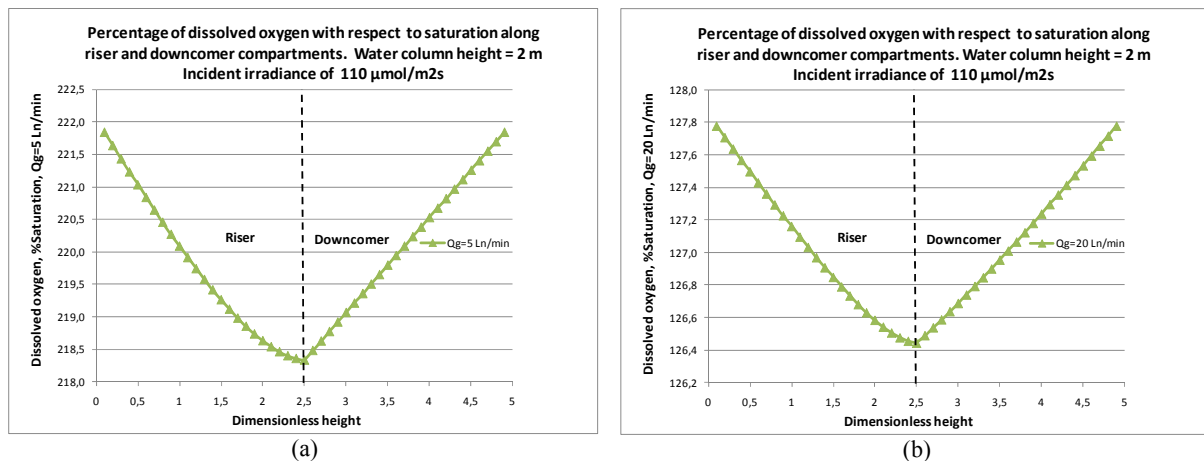


Figure III.34. Percentage of dissolved oxygen with respect to saturation assuming water column height of 2 m
Incident irradiance of $110 \mu\text{mol E/m}^2\text{s}$ - a) for an air flow rate of 5 Ln/min, b) for an air flow rate of 20 Ln/min

Comparing Figures III.33 and III.34, oxygen concentrations with respect to saturation are lower in the liquid supposing that the water column height is 2-m high. The difference between the two heights attains values of 72.5% saturation for 5 Ln/min and 13% for 20 Ln/min.

Figure III.34 shows that oxygen concentrations with respect to saturation decrease 3.5% from the bottom to the top when an air flow rate of 5 Ln/min is injected, which is higher than having a water column of 0.78 m. Similarly, for air flow rates of 20 Ln/min, oxygen concentrations decrease 1.33%. Regarding these results, it can be concluded that increasing column height benefits oxygen stripping from water, while culture volume increases. However, increasing column height to longer heights (e.g 22 times downcomer diameter) might carry some problems such as construction design (due to higher pressures) and accessibility to sterilize the system (Cascallo, 2000).

To complement the study of oxygen evolution in the reactor, Figure III.35 shows oxygen concentrations in the air at the top of the riser for four air flow rates.

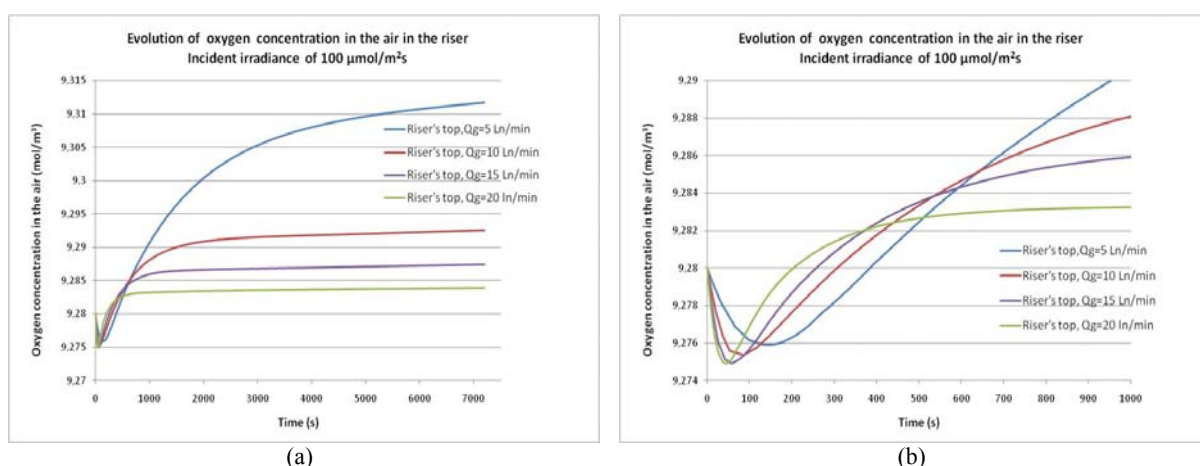


Figure III.35. Dissolved oxygen in the air vs. air flow rate.
Incident irradiance of 100 $\mu\text{mol E/m}^2\text{s}$

Results show that, according to the air flow rate, the oxygen concentration decreases in the air during the first seconds after starting air injection, reaching the lowest value of 9.275 mol/m^3 (296.8 mg/L) for air flow rate of 20 Ln/min. It seems that air provides oxygen to the liquid during the first seconds.

At low air flow rates, oxygen concentration maintains low values for a longer period of time. This is the consequence of lower volumetric mass transfer coefficient at lower air flow rates. Same results were obtained by Talvy et al. when air was injected in an airlift reactor after stripping dissolved oxygen with sodium sulfite (Talvy et al., 2007). Once oxygen concentrations reach the initial value in the gas, concentrations continue to increase as dissolved oxygen in the liquid is transported to the gas. Then, oxygen concentrations attain a constant value.

On the other hand, it is interesting to analyze the evolution of the mass-transfer driving force, defined as the difference between the equilibrium concentration and the oxygen concentration in the liquid, which is in charge of transporting oxygen between the phases (Molina et al., 2001; Hall et al., 2002).

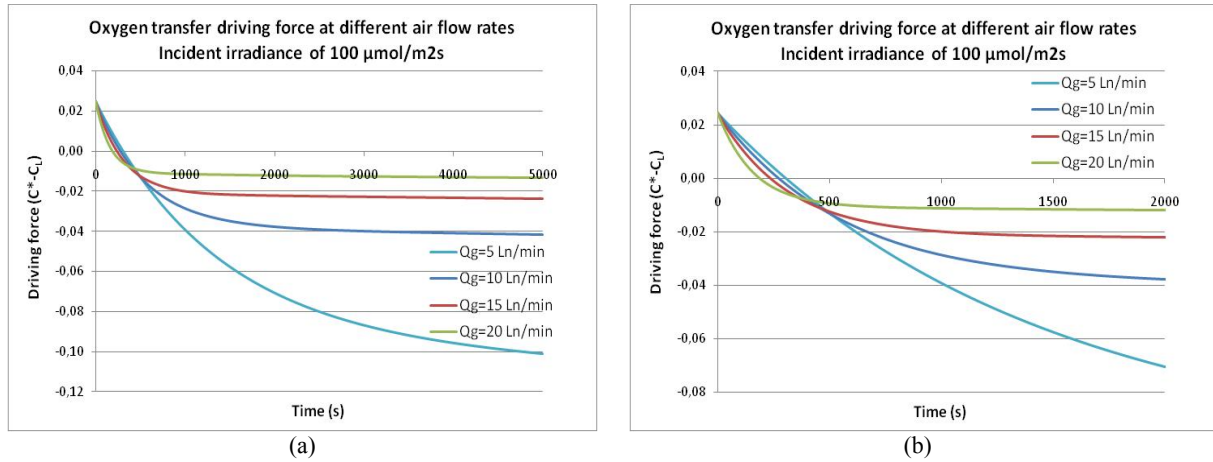
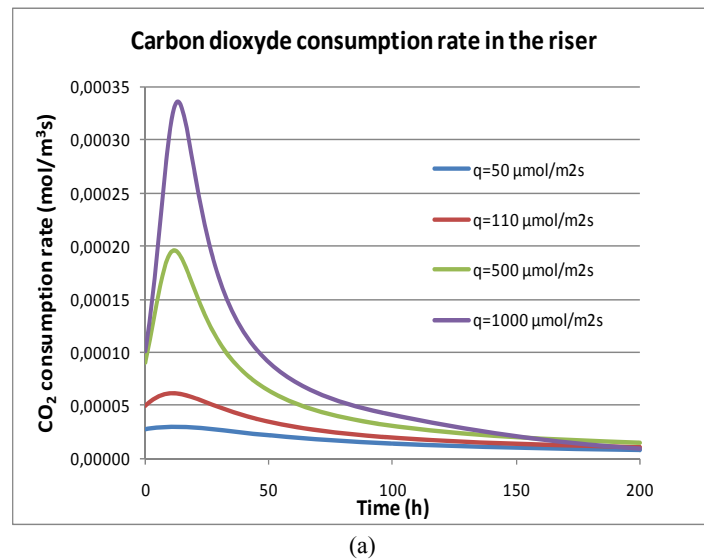


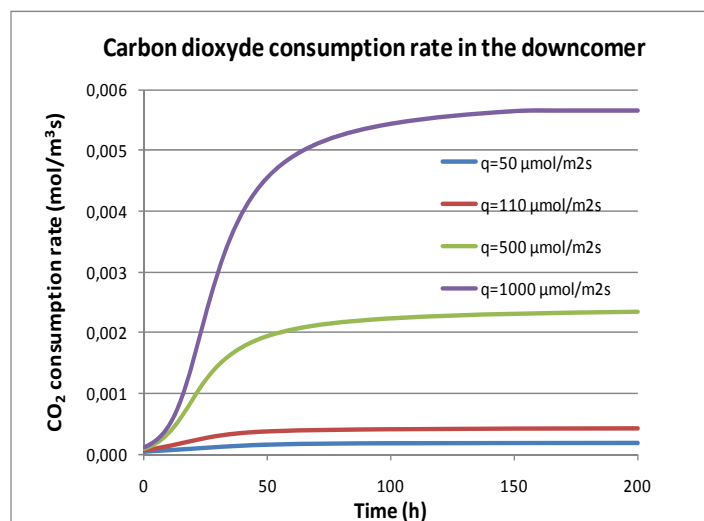
Figure III.36. Evolution of the oxygen transfer driving force vs. air flow rate
Incident irradiance of 100 $\mu\text{mol E/m}^2\text{s}$

Figure III.36 shows that the driving force ($C_{O_2}^* - C_{O_{2,L}}$) diminishes as a function of time since dissolved oxygen concentration in the liquid increases, due to photosynthesis. The driving force then reaches negatives values, indicating that the oxygen is then transported from the liquid to air. According to air flow rates, the driving force is less or more pronounced, reaching a constant value. At high air flow rates, the driving force is higher and it becomes constant faster compared to lower air flow rates. This is the reason of observing lower dissolved oxygen in the liquid when air flow rates are increased in the reactor.

3.2.2 Results: carbon dioxide evolution

First results show the carbon dioxide consumption rate as a function of time according to four incident light intensities.





(b)
Figure III.37. Evolution of carbon dioxide consumption rate.
a) in the riser, b) in the downcomer

As expected, the same tendency obtained for oxygen production rates is observed here for carbon dioxide consumption rate. The carbon dioxide consumption rate increases with incident irradiances as well as with biomass concentrations, being more important in the downcomer than in the riser. Values obtained for incident irradiances of 500 and 1000 $\mu\text{mol E/m}^2\text{s}$ are in the same order of magnitude as those obtained by Camacho et al. in a tubular photobioreactor (Camacho et al., 1999).

On the other hand, the carbon dioxide consumption rate is slightly lower than the oxygen produced during photosynthesis, if the ratio $Y_{\text{CO}_2/\text{O}_2}$ is established in mol CO_2 /mol O_2 (Doucha and Livansky, 2006; Cascallo, 2000; Nouals, 2000). As expected, maximal rates of CO_2 consumption in the riser and downcomer compartments are observed for the same time of cultivation at which maximal O_2 production rates were observed (Figure III.30).

The next step is to study the evolution of dissolved CO_2 and total inorganic carbon in each compartment of the reactor to examine whether carbon is high enough in the culture. If there is no source of carbon added to the growth medium of *Chlamydomonas* (e.g sodium carbonate, NaHCO_3 (Moroney and Tolbert, 1985)), the carbon dioxide presented in the air remains as the only carbon source. The presence of carbonates and bicarbonates depends on the carbon dioxide concentrations in the air as well as culture conditions. First results are estimated for a system working with natural air. If the pH of the growth medium is maintained at 7, constants K_{tic} , K_1 , and K_2 are taken as those presented in Table III.10. After that, initial values of dissolved CO_2 , HCO_3^- , and CO_3^{2-} as well as total inorganic carbon are estimated for four carbon dioxide concentrations in the injected air, usually employed to cultivate *Chlamydomonas reinhardtii* (Leon and Galvan, 1997; Oncel and Sukan, 2009; Kong et al., 2010) (Table III.12)

Table III.12. Initial concentrations of CO_2 , HCO_3^- and CO_3^{2-} and TIC for 0.038, 1, 3 and 5% CO_2 -enriched air.

%v/v CO_2 enriched air	Dissolved CO_2 (mol/m^3)	Dissolved HCO_3^- (mol/m^3)	Dissolved CO_3^{2-} (mol/m^3)	Total inorganic carbon (mol/m^3)
0.038	0.0157	0.053	2.21×10^{-5}	0.069
1	0.413	1.41	5.8×10^{-4}	1.82
3	1.24	4.23	1.75×10^{-3}	5.47
5	2.06	7.05	2.9×10^{-3}	9.12

Results for dissolved CO₂ and total inorganic carbon are presented in Figure III.35 if natural air is injected into the system.

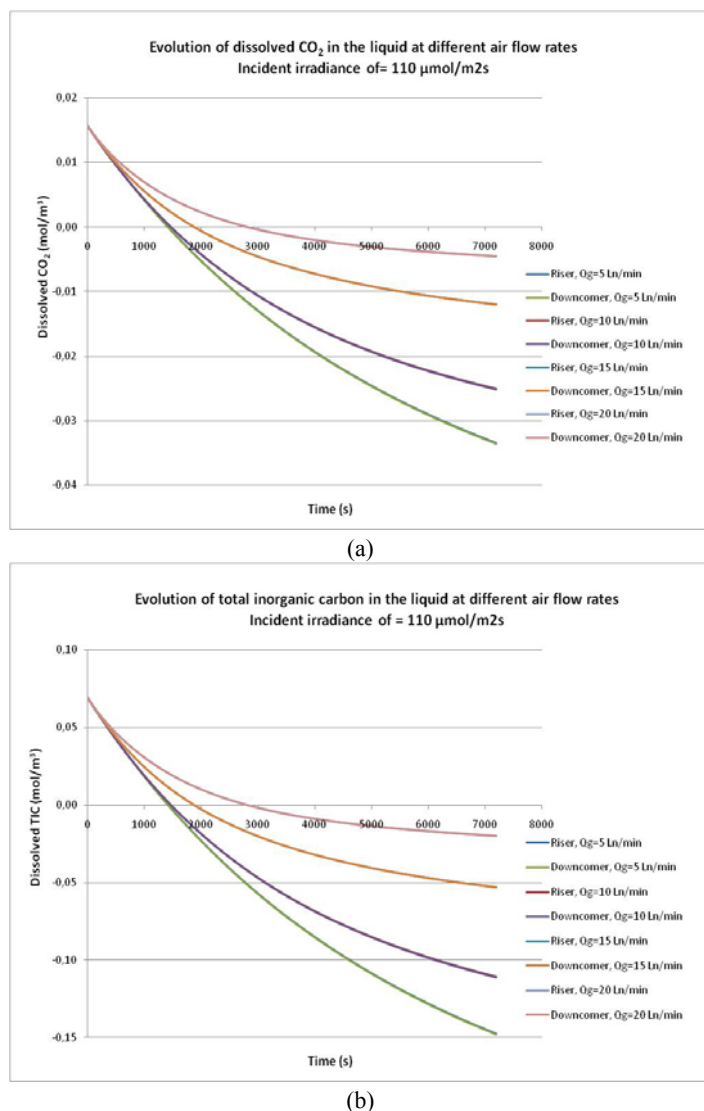


Figure III.38. Dissolved CO₂ and TIC in the liquid vs. air flow rate
Incident irradiance of 110 μmol E/m²s
a) dissolved CO₂ in the liquid, b) total inorganic carbon in the liquid

Dissolved carbon dioxide and total inorganic carbon in the liquid is slightly lower in the downcomer than in the riser. The reason is the higher CO₂ consumption in the downcomer compared to that in the riser, as higher light energy is available and higher biomass is produced in this section. For all flow rates, CO₂ and TIC becomes limited for the culture in less than one hour, which means that the CO₂ and TIC rate of consumption is higher than the flux transferred from the gas to the liquid (in the case of CO₂) and dissociated (in the case of carbonate and bicarbonate) in the culture. The higher the air flow rate injected in the reactor, the higher the concentration of CO₂ and TIC species in the liquid, both for the riser and downcomer compartments. This is complementary to results obtained for oxygen concentration in the liquid observing that, the higher the air flow rate, the lower the dissolved oxygen (Figure III.31). Both results are consequence of $k_L a$ increase with air flow rates, as shown in Figure III.22.

On the other hand, it is reasonable to think that the higher incident irradiances, the higher the CO₂ and TIC consumptions and thus, for the same air flow rate, these elements will be less available for algae.

Figure III.39 illustrates the evolution of dissolved CO₂ for air flow rates of 5 and 20 Ln/min if the volumetric mass transfer coefficient is increased, by using results obtained from applying Van't Riet and Tramper correlation (Equation III.21)

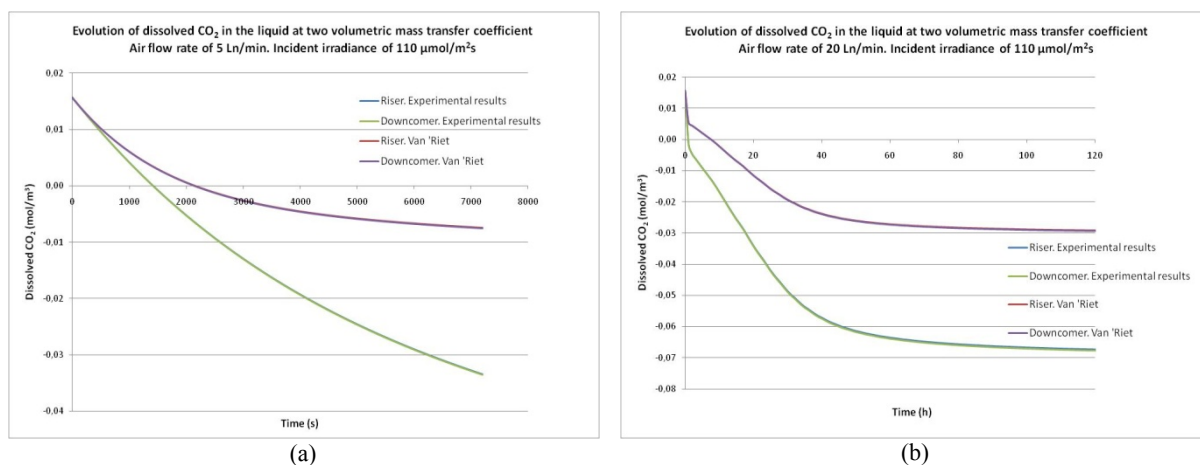
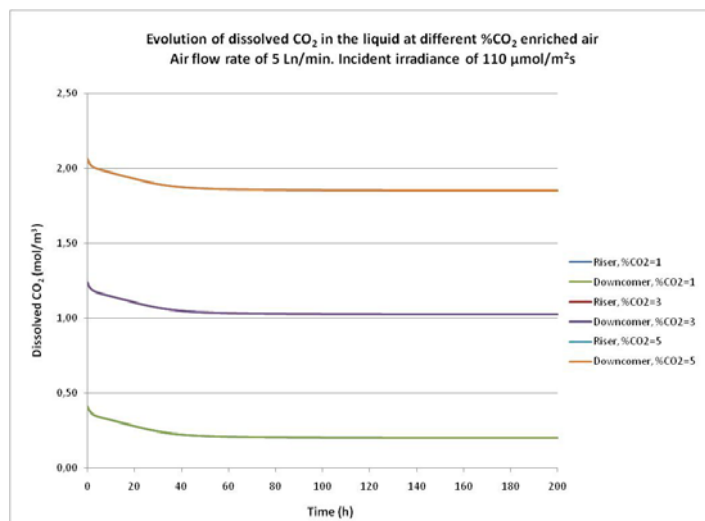


Figure III.39. Evolution of dissolved CO₂. Comparison between modeling results and Van't Riet correlation Incident irradiance of 100 μmol E/m²s

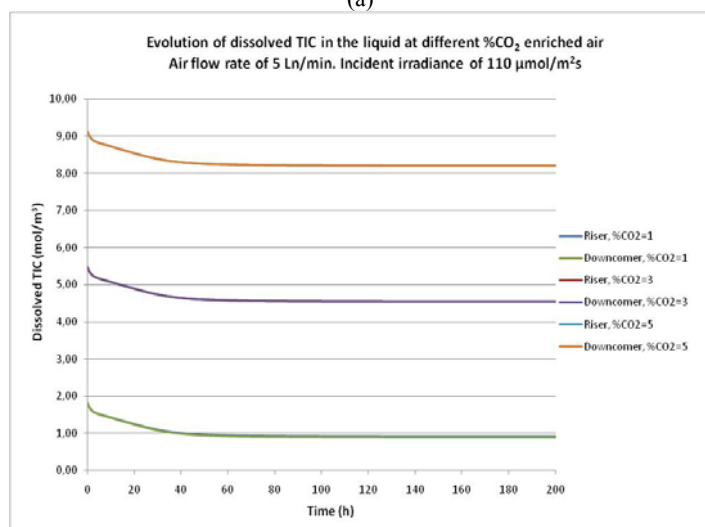
As expected, CO₂ concentrations in the liquid are higher if the volumetric mass transfer coefficient is increased. For air flow rate of 5 Ln/min, time difference between the two cases and at which CO₂ becomes limited is low (around 700 s). On the contrary, at air flow rate of 20 Ln/min, the difference in time is higher (less than 7 hours). However results show that even though the volumetric mass transfer coefficient is increased, the CO₂ is still a limiting factor. Even if the volumetric mass transfer coefficient is augmented to high values (0.01 1/s), CO₂ requirements are not satisfied for the culture (Camacho et al., 1999). If liquid and gas properties are maintained, the only method to increase the volumetric mass transfer coefficient is to reduce the diameter of bubbles, for a fixed air flow rate (Chisti, 2000; Freitas and Texeira, 2001). As an example, Camacho et al. observed very low volumetric mass transfer coefficient in tubular reactor since the flow was slug type, provoking low interfacial area (Camacho et al., 1999).

Several authors have used CO₂-enriched air to grow *Chlamydomonas reinhardtii*, observing an augmentation of the growth rate (Oncel and Sukan, 2009; Kong et al., 2010). Therefore, it is interesting to study whether CO₂-enriched air injected in the reactor, for the lowest air flow rate, does not become limited for the algae after a certain time of cultivation.

If natural air is injected in the system, the CO₂ concentration does not satisfy the CO₂ amount required by the culture (Figure III.38a), so it is necessary to enrich the air injected into the system. Concentrations of 1, 3, and 5% (v/v) are usually employed in microalgae culture of *Chlamydomonas reinhardtii* and according to the results obtained here, they appear to satisfy CO₂ requirements. Figure III.40 shows the evolution of CO₂ and TIC for 5 Ln/min for three CO₂ concentrations, under an incident irradiance of 110 μmol E/m²s.



(a)



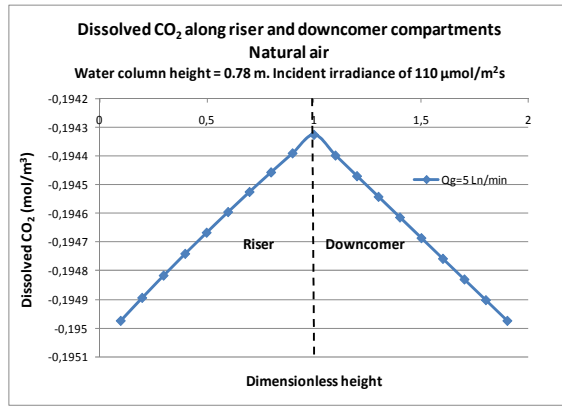
(b)

Figure III.40. Evolution of CO₂ and TIC at different %CO₂-enriched air.

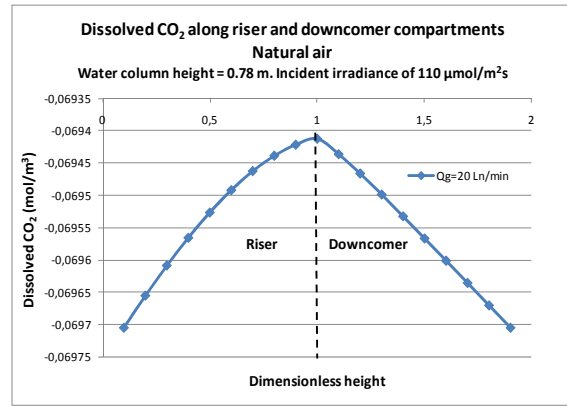
Results show that, even though the system is working at low air flow rate, CO₂ and TIC concentrations in the liquid are not limiting factors for microalgae. There is always dissolved CO₂ and TIC available for the culture while the biomass increases. In steady state regime, the dissolved CO₂ in the liquid augmented 195.2% when 1% CO₂-enriched air is compared to natural air injection. On the other hand, when CO₂ concentration in the gas is augmented from 1% to 5% (v/v), dissolved CO₂ increases nine times.

According to Camacho et al., there is a level of dissolved CO₂ at which photosynthetic activity might be inhibited. Lee and Hing denoted that CO₂ concentration of 1.5 mol/m³ in algae growth medium have inhibited certain microalgae (Camacho et al., 1999). Regarding the results presented here, the value of 1.5 mol/m³ is over passed when 5% CO₂-enriched air is injected into the system (Figure III.40a), which means that at this and higher CO₂ concentrations in the air might cause a decay of biomass growth rate. Similarly to CO₂ evolution, total inorganic carbon in the liquid increases when CO₂-enriched air is injected in the system and CO₂ concentration in the air is increased (Figure III.40b).

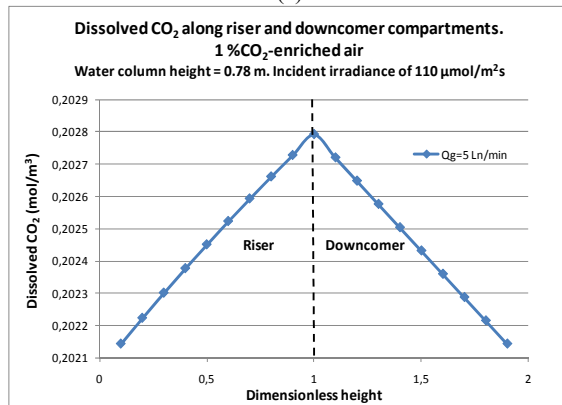
Figure III.41 illustrates the progress of dissolved CO₂ along riser and downcomer height whether natural air or CO₂-enriched air is injected in the riser



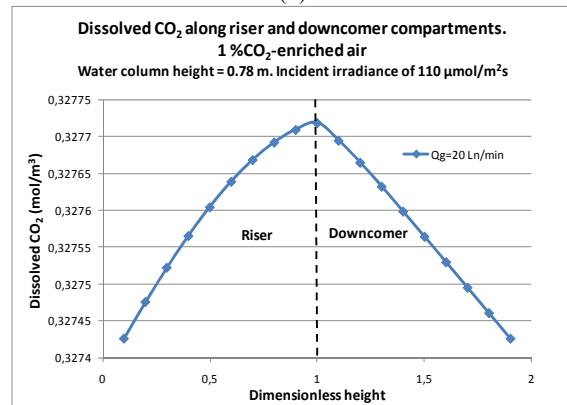
(a)



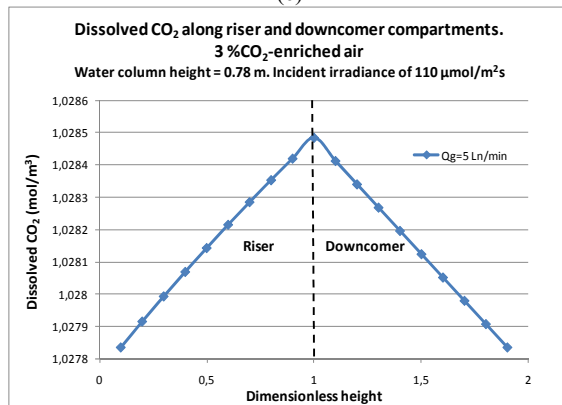
(b)



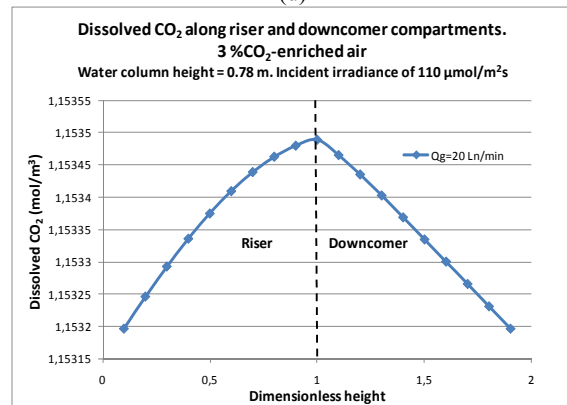
(c)



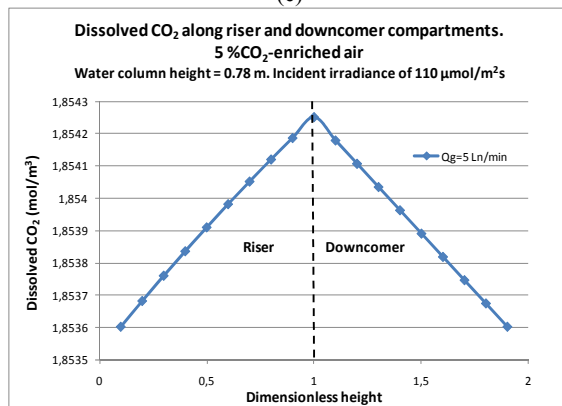
(d)



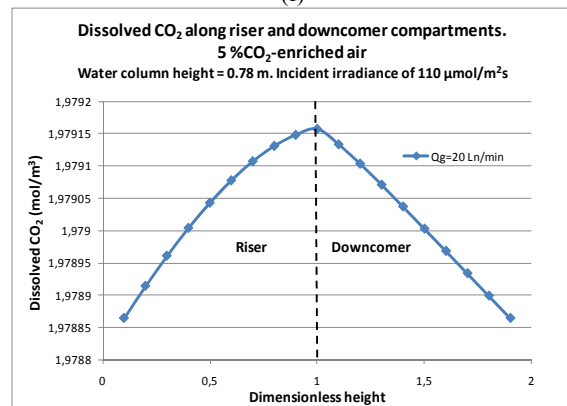
(e)



(f)



(g)



(h)

Figure III.41. Dissolved CO₂ in the reactor injecting natural air and 1%, 3%, and 5% CO₂-enriched air.

a) Natural air and air flow rate of 5 Ln/min, b) Natural air for and air flow rate of 20 Ln/min

c) 1%CO₂-enriched air and air flow rate of 5 Ln/min, d) 1%CO₂-enriched air for and air flow rate of 20 Ln/min

e) 3%CO₂-enriched air and air flow rate of 5 Ln/min, f) 3%CO₂-enriched air for and air flow rate of 20 Ln/min

g) 5%CO₂-enriched air and air flow rate of 5 Ln/min, h) 5%CO₂-enriched air for and air flow rate of 20 Ln/min

In figures III.41a and III.41b, dissolved CO_2 concentrations are negative since there is limitation of CO_2 at steady state, as it is observed in Figure III.38.

Contrary to results obtained for the oxygen, dissolved CO_2 in the riser increases from the bottom to the top and diminishes along the downcomer height, for all % CO_2 -enriched air simulated here. Both tendencies are in concordance with biomass production profile in the reactor, since it is higher in the downcomer than in the riser. As CO_2 concentration in the gas is augmented, higher CO_2 concentration is dissolved in the reactor because the non-consumed CO_2 by algae remains dissolved in the liquid. Similarly to results obtained for the oxygen, as the air flow rate is increased, higher CO_2 concentration is found in the liquid. Therefore, if it is desirable to maintain a limit of dissolved CO_2 less than 1.5 mol/m^3 but high enough to have CO_2 available for the culture, the best condition is injecting 3% CO_2 -enriched air at air flow rate of 20 Ln/min (Figure III.41f).

On the other hand, results of Figure III.41 show that dissolved CO_2 difference between the two compartments is small, as it is also observed in Figures III.38 and III.39. Nevertheless, it is important to compare dissolved CO_2 between the bottom and the top of riser and downcomer compartments, under different CO_2 concentrations in the gas, in order to observe riser capacity to absorb CO_2 as well as CO_2 consumption in the downcomer.

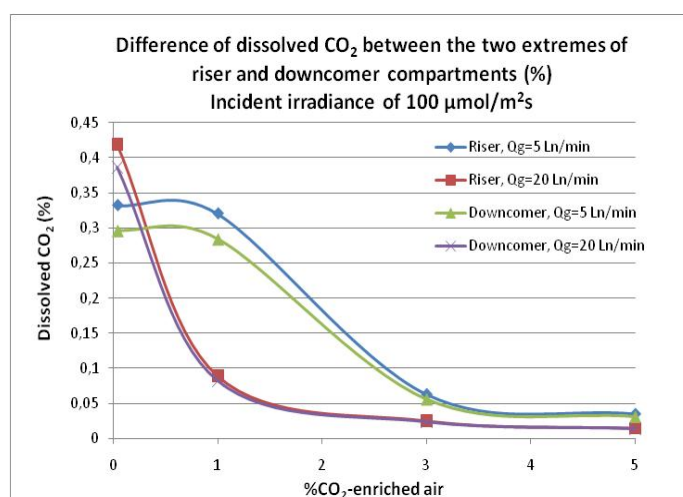


Figure III.42. Dissolved CO_2 in the reactor injecting natural air and 1%, 3%, and 5% CO_2 -enriched air.

Figure III.42 shows that dissolved CO_2 is more uniformly distributed along the reactor if the CO_2 concentration in the gas is augmented. The difference between the bottom and the top in both compartments becomes smaller as well as the difference of dissolved CO_2 between the compartments. On the other hand, an augmentation of air flow rates leads to diminish the difference of dissolved CO_2 between and along the compartments.

As CO_2 is dissolved in the liquid and consumed by the culture, it is interesting to estimate CO_2 losses in the system. This can be obtained from the difference between CO_2 concentration in the gas at the entrance and the exit of the riser compartment (Camacho et al., 1998; Doucha and Livansky, 2006). Figure III.43 shows CO_2 concentration in the gas along riser height for CO_2 concentrations mentioned above as well as for four air flow rates.

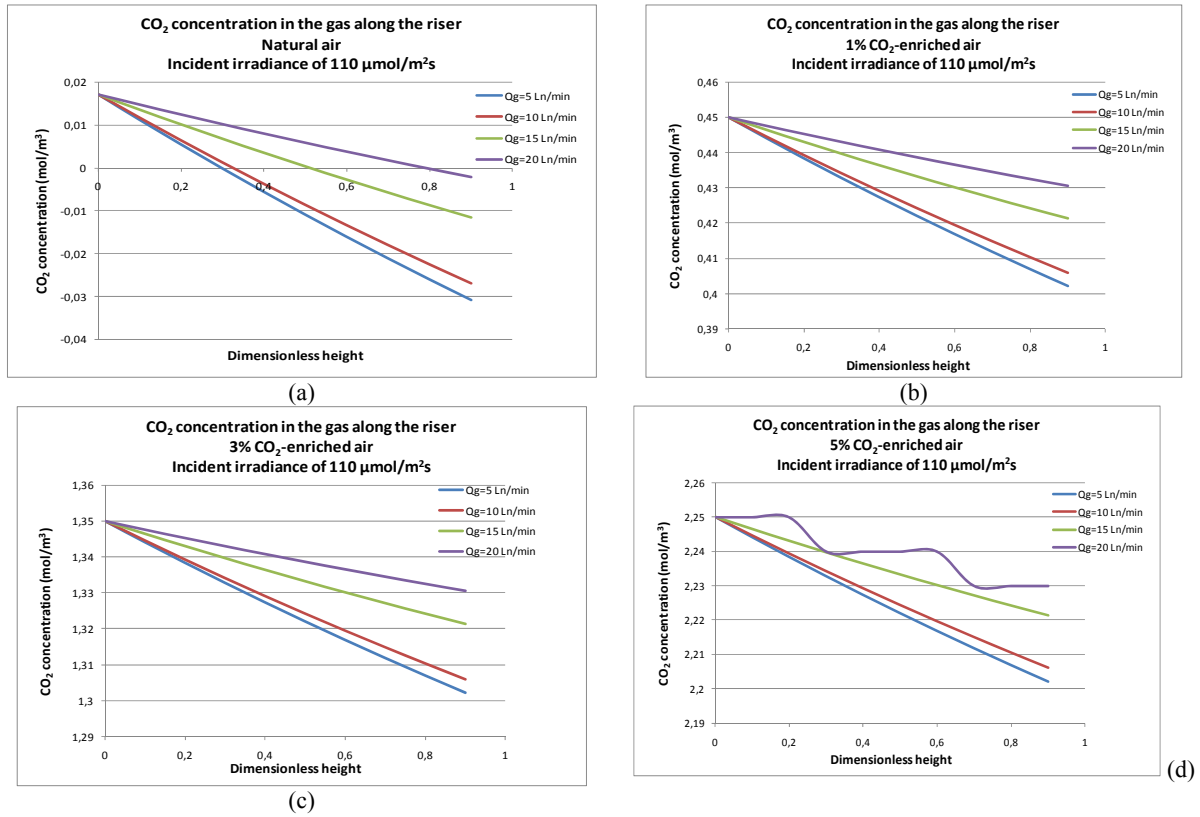


Figure III.43. CO₂ concentration in the gas along the riser vs. air flow rate
a) Natural air, b) 1% CO₂-enriched air, c) 3% CO₂-enriched air, d) 5% CO₂-enriched air

Results show that CO₂ concentrations in the gas diminish along the riser height, as there is CO₂ mass transport from the gas to the liquid, for all flow rates and CO₂ concentrations tested here. On the other hand results show that, if air flow rate is increased in the riser, CO₂ losses diminish in the reactor. This is valid for all percentages of CO₂-enriched air tested here. Results are in concordance with those obtained for dissolved CO₂ (Figures III.38, III.40, III.41) demonstrating that dissolved CO₂ in the liquid increase with air flow rates and thus CO₂ losses diminish, even though biomass increases as a function of time.

Regarding values of CO₂ concentrations at the gas exit, they are higher than those recommended by Doucha and Livansky to avoid CO₂ limitation in microalgae culture. According to these authors, CO₂ partial pressures of 0.1 to 0.2 kPa are necessary to avoid inhibition of microalgae growth (Doucha and Livansky, 2006). In this study, the lowest CO₂ partial pressure is 0.98 kPa observed when air is enriched with 1% CO₂ and injected at 5 Ln/min, which means that at higher CO₂ concentrations and higher air flow rates dissolved carbon dioxide is not a limiting element in the culture.

4. Conclusions

When microalgae culture is performed in photobioreactors, it is generally agreed that light energy is the first limiting parameter. Authors recommend diluting the light in the culture in order to increase the energy available inside the culture. In this sense, it is necessary to estimate the evolution of light energy profile in the reactor inside the entire culture. If all environmental conditions (e.g. temperature and pH) and nutrients are well controlled, the biomass concentration will evolve according to light

energy available. While biomass concentration reaches very high values, then zones with energy lower than the energy of compensation for photosynthesis appear. In consequence, there is a theoretical optimal biomass concentration at which there are no *dark zones* established in the reactor. As incident irradiances increase, the energy available for photosynthesis is higher along the two compartments of the reactor. In consequence, optimal biomass concentrations are more important at higher incident irradiances.

An internal airlift reactor can be designed to expose cells under continuous illumination or under light/dark cycles (e.g having an opaque riser). In the first case, it is necessary to avoid dark zones at the center of the reactor, thus the light attenuation is high since light energy has to travel from the downcomer to the draft tube and then transmitted to the center of the reactor. In consequence, optimal biomass concentrations are lower. Under continuous illumination, the optimal biomass concentration is determined by the downcomer since there is the highest energy available for photosynthesis.

In the second case, light/dark cycles are usually established in the reactor when it is desired to expose the culture to very high irradiances. Optimal concentrations are higher in order to avoid dark zones in the downcomer. In this case, it is necessary to have short times in the riser to avoid photorespiration and sufficient time to repair photon traps.

Comparing both cases, highest biomass productivities are obtained under light/dark cycles, always assuming that there is no biomass consumption due to photorespiration. In this case, it is necessary to perform an experimental study to determine whether the light/dark cycle does not promote respiration. These results demonstrate that it is interesting in IAL reactor to have a downcomer cross sectional area higher than that of the riser in order to obtain a larger volume exposed to high intensities and to avoid light attenuation caused by the draft tube. However, hydrodynamics of the entire reactor has to be well verified.

Regarding biomass productivities, they depend on the specific growth rate as well as the current biomass concentration. In this study, it is assumed that the specific growth rate is only a function of the light flux available in the culture. Therefore during biomass production, there is a compromise between the light flux density that it is attenuated due to the high biomass concentration and biomass increase.

Comparing results obtained by applying Monod's law and Cornet and Dussap's model, biomass productivities are higher in the second model. The difference resides in values of the maximal specific growth proposed by Monod's law and the relationship proposed by Cornet and Dussap's model among physical characteristics and optical properties. Results demonstrated that in the riser and for low irradiances, the biomass production rate is completely reduced at biomass concentration of 0.5 g/L while for higher irradiances, productivities are reduced at 1.5 g/L. In the downcomer, the biomass productivity increases with the biomass concentration until it reaches a constant and maximum value. At low incident irradiances, the maximum is reached at 0.5 g/L while at higher irradiances, it is reached at 1.5 g/L. In all cases, the contribution of the riser to produce biomass is not high compared to that of the downcomer, since the riser produces approximately the forth part of downcomer biomass production.

On the other hand, it is expected that biomass productivities are the highest for the optimal biomass concentration. When it is assumed that the reactor is completely transparent, the optimal biomass concentration is defined as to avoid dark zones in the riser while it will be first reached in the

downcomer. Then, the total biomass productivity will be given by the addition of both biomass productivities.

For all irradiances, the total biomass productivity is lower than that estimated when the riser is assumed opaque. The reason is that light attenuation is higher when the reactor is under continuous illumination than when the riser is opaque. When the reactor is under light/dark cycles, it is assumed that there is no biomass consumption in the riser.

Results show that biomass concentrations at which maximal productivities are attained are very low, even though they are in agreement with those observed in experimental studies with photobioreactors. On the other hand, regarding optimal cultivation times obtained here, whether the culture is exposed to continuous illumination or having light/dark cycles, results are very low compared to periods of experimental cultures. In this case, it might be necessary to dilute the culture in order to diminish shading among cells. This is typical of reactors working in batch mode since the light energy is limiting faster than when reactors are working continuously.

Regarding photosynthetic efficiencies, they are higher in the riser than in the downcomer. Photosynthetic efficiencies diminish with higher irradiances and that is the reason of having higher values in the riser than in the downcomer. These results demonstrate that biomass production rates do not increase very much with respect to the energy absorbed.

Furthermore, in studies of internal airlift reactors performing microalgae culture, it is necessary to estimate reactor capacity to absorb carbon dioxide and to release dissolved oxygen produced during photosynthesis. According to the light energy available and biomass productivities, there will be certain oxygen production rate and carbon dioxide consumption rate. In concordance with photosynthesis activity, both rates are higher when higher irradiances are available in the reactor; then the mass transport between phases becomes crucial. For this reason, the overall volumetric mass transfer, whether for O_2 or for CO_2 , is a key parameter in the hydrodynamics of the reactor. It depends on the gas holdup and bubble diameter, increasing at higher air flow rates and therefore, at higher power input.

As a consequence of the hydrodynamics in an internal airlift reactor, the overall volumetric mass transfer is higher in the riser than in the downcomer, since the gas holdup is higher in the first. The presence of particles, in the range up to 5 g/L, demonstrates not to affect values of mass transfer coefficients for the oxygen, in concordance with results obtained in the second chapter. Experimental results performed after stripping oxygen from water, show that dissolved oxygen increases when air flow rate is increased in the riser.

In order to create a model capable of simulate mass transport in the reactor, a transport equation was employed including axial dispersion, convective and diffusion transport. Referring to axial dispersion, it has been neglected in some studies while in this study it has been included and estimated by employing a recent relationship. Modeling results are close to those obtained experimentally. The best modeling approximation occurs for low air flow rates while at higher air flow rates, the discrepancy is higher (20% maximum).

Modeling photosynthetic activity in the reactor includes oxygen production rates and carbon dioxide consumption rate in the equation of mass transport. These two terms were estimated from the specific growth rate and biomass concentration, according to the model proposed by Cornet and Dussap's

model. The conversion coefficient yield for O_2 and CO_2 were obtained from a general stoichiometry equation formulated for algal biomass. Results show that dissolved oxygen concentration in the liquid increases with time due to photosynthetic oxygen production, until it reaches a maximal and constant value. Since photosynthetic activity is higher in the downcomer, the dissolved oxygen is higher in this section and it increases along the downcomer height. On the contrary, dissolved oxygen in the riser is slightly lower compared to dissolved oxygen in the downcomer and it diminishes along the riser height. As expected, the riser is the compartment in charge of stripping the photosynthetic oxygen generated. However, regarding results of dissolved oxygen along riser and downcomer heights, the difference from the bottom to the top is never significant.

Gas holdups and volumetric mass transfer coefficients are more important at higher air flow rates, so the dissolved oxygen in the liquid diminishes if air flow rate is increased. Therefore, at low air flow rates, it is necessary to identify the maximal dissolved oxygen that can be reached in the system. According to several experiences, there is a limit of dissolved oxygen in the culture to avoid photosynthesis inhibition (300%, 400% oxygen saturation in water). Modeling results show that dissolved oxygen for all the air flow rates and an incident irradiance of $110 \mu\text{mol E/m}^2\cdot\text{s}$ does not reach this limit (this incident irradiance was selected since it is usually employed in *Chlamydomonas* culture). However, at air flow rate of 5 Ln/min, values of dissolved oxygen are close to the limit. If incident irradiances are further augmented, photosynthesis probably will be inhibited.

On the other hand, results show that if the water column height is higher, the dissolved oxygen presented in the liquid is lower. Comparing results of dissolved oxygen along riser and downcomer heights when the column was 0.78 and 2-m high, the difference from the bottom to the top is never significant. Results demonstrate that, due to the hydrodynamical conditions and the geometry of the reactor established in this study, the desired dissolved oxygen depends more on the air flow rate injected to maintain low values of oxygen concentration than the height of the reactor to release oxygen.

In mass transfer studies, it is also of interest to analyze the mass transfer driving force along the time. For the oxygen, the mass transfer driving force is high some seconds after air injection, meaning that oxygen disengagement from the liquid is the highest in this period. As the slope of the driving force is more important for higher air flow rates, the oxygen disengagement is then more important at higher air flow rates.

To study CO_2 evolution, it is necessary to analyze its evolution together with the total inorganic carbon. Similarly to the oxygen production rates, CO_2 consumption rates increase with biomass productivities as well as with incident irradiances, being more important in the downcomer than in the riser.

If natural air is injected in the reactor, CO_2 and TIC becomes limiting for the culture, even for all air flow rates. This means that CO_2 and TIC consumption rates are higher than the flux rate transferred from the gas to the liquid.

To increase the dissolved CO_2 in the liquid, there are two options, either to increase volumetric mass transfer coefficient or to increase the CO_2 concentration in the gas. In the first case, the dissolved CO_2 increases but still is a limiting factor. In the second case, CO_2 concentrations of 1, 3, or 5% (v/v) in the gas, increase values of dissolved CO_2 and TIC that satisfy culture requirements, even when the reactor is working at low air flow rate.

On the other hand, as CO₂ concentration in the gas is augmented, higher is the dissolved CO₂ in the reactor since the non-consumed CO₂ remains dissolved in the liquid. However, attention must be paid since there is also a limit of dissolved CO₂ to avoid inhibition of photosynthesis. According to modeling results, the limit is over-passed if 5% CO₂-enriched air is employed in the culture. In addition, results show that dissolved CO₂ is more uniformly distributed along the reactor if the CO₂ concentration in the gas is augmented as well as air flow rates.

Regarding CO₂ losses, they diminish when air flow rates are increased in the reactor. This is in agreement with the discussed results since an augmentation of air flow rate leads to an increase in the gas holdup, volumetric mass transfer coefficient, and therefore dissolved CO₂ concentrations.

When microalgae culture is performed in photobioreactors, the pH should be continuously monitored since it increases during photosynthesis activity. For this reason, some authors decide to inject CO₂-enriched air intermittently whereas others inject it continuously. The higher the photosynthesis activity, the more frequent should be carbon dioxide injections. In this study, it is assumed that CO₂-enriched air is continuously injected while the pH is maintained. This might not be true if the biomass production rate changes frequently (e.g. during the day time), observing pH fluctuations and therefore, changes in total inorganic carbon composition.

Finally, comparing biomass productivities with microalgae culture, it appears that the designed reactor is capable of producing higher productivities than open ponds and similar to those observed in other photobioreactors. Results show that photosynthetic dissolved oxygen does not attain undesirable levels if incident irradiances are lower than 110 $\mu\text{mol E/m}^2\cdot\text{s}$, while it is necessary to inject CO₂-enriched air in the culture to avoid carbon limitations.

With these results, the culture of *Chlamydomonas reinhardtii* in internal airlift reactor avoids the risk of photosynthesis inhibition due to high light limitation and high levels of dissolved oxygen while having an equilibrated dissolved CO₂ concentration.

5. References

- Acien, F., García, J., Sánchez, J., Fernández, J., & Molina, E. (1997). A Model for Light Distribution and Average Solar Irradiance Inside Outdoor Tubular Photobioreactors for the Microalgal Mass Culture. *Biotechnology and Bioengineering* 55 , 701-714.
- Babcock, R., Malda, J., & Radway, J. (2002). Hydrodynamics and mass transfer in a tubular airlift photobioreactor. *Journal of Applied Phycology* 14 , 169-184.
- Bailey, J., & Ollis, D. (1986). *Biochemical engineering fundamentals*. MacGraw-Hill.
- Becerra, G. (2009). *Proposition des strategies de commande pour la culture de microalgues dans un photobioréacteur continu*. Paris: Ecole Centrale des Arts et Manufactures "Ecole Centrale Paris".
- Becker, E. (1994) *Microalgae: Biotechnology and microbiology*. New York: Cambridge University Press.
- Bello, R., Robinson, C., & Moo-Young, M. (1985). Gas holdup and overall volumetric oxygen transfer coefficient in airlift contactors. *Biotechnology and Bioengineering* 27 , 369-381.
- Bird, R., Stewart, W., & Lightfoot, E. (2002). *Transport Phenomena*. New York: John Wiley & Sons, Inc.
- Burris, V., McGinnis, D., & Little, J. (2002). Predicting oxygen transfer and water flow rate in airlift aerators. *Water Research* 36 , 4605-4615.
- Calderbank, P., & Moo-Young, M. (1961). The continuous phase heat and mass transfer properties of dispersions. *Chemical Engineering Science* 16 , 39-54.
- Camacho, F., Acien, F., Sanchez, J., Garcia, F., & Molina, E. (1999). Prediction of dissolved oxygen and carbon dioxide concentrations profiles in tubular photobioreactors for microalgal culture. *Biotechnology and Bioengineering* 62 , 71-86.
- Carlozzi, P. (2000). Hydrodynamic aspects and *Arthrospira* growth in two outdoor tubular undulating row photobioreactors. *Applied Microbiology and Biotechnology* 54 , 14-22.
- Cascallo, A. (2000). *Conception, contrôle et fonctionnement d'un photobioréacteur pour la culture en mode continu de la cyanobactérie Spirulina platensis*. Université de Technologie de Compiègne. Universitat Autònoma de Barcelona.
- Cerri, M., Futiwaki, L., Jesus, C., Cruz, A., & Badino, A. (2008). Average shear rate for non-Newtonian fluids in a concentric-tube airlift bioreactor. *Biochemical Engineering Journal* 39 , 51-57.
- Chisti, M. (1989). *Airlift bioreactors*. Elsevier Science Publishers Ltd, London.
- Chisti, M. (2000) Animal-cell damage in sparged bioreactors. *Trends in Biotechnology* 18, 420-432
- Cogne, G., Lasseur, C., Cornet, J., Dussap, C. & Gros, J., (2001). Growth monitoring of a photosynthetic micro-organism (*Spirulina platensis*) by pressure measurements. *Biotechnology Letters* 23, 1309–1314
- Contreras, A., García, F., Molina, E., Merchuk, J. (1999). Influence of sparger on energy dissipation, shear rate, and mass transfer to sea water in a concentric-tube airlift bioreactor. *Enzyme and Microbial Technology* 25, 820-830

- Converti, A., Lodi, A., del Borghi, A., & Solisio, C. (2006). Cultivation of *Spirulina platensis* in a combined airlift-tubular reactor system. *Biochemical Engineering Journal* 32 , 13-18.
- Cornet, J. (2010). Calculation of optimal design and ideal productivities of volumetrically lightened photobioreactors using the constructal approach. *Chemical Engineering Science* 65 , 985-998.
- Cornet, J., & Dussap, C. (2009). A simple and Reliable Formula for Assessment of Maximum Volumetric Productivities in Photobioreactors. *Biotechnology Progress* , 424-435.
- Cornet, J., Dussap, C., & Gros, J. (1995). A simplified monodimensional approach for modeling coupling between radiant light transfer and growth kinetics in photobioreactors. *Chemical Engineering Science* 50 , 1489-1500.
- Cornet, J., Dussap, C., & Gros, J. (1998). Kinetics and energetics of photosynthetic microorganisms in photobioreactors. *Advanced Biochemical Engineering Biotechnology* 59 , 153-224.
- Cussler, E. (2007). *Diffusion. Mass Transfer in Fluid Systems*. New York: Cambridge University Press.
- Danesi, E., Rangel, C., Carvahlo, J., & Sato, S. (2004). *Biomass and Bioenergy* 26 , 329-335.
- Deckwer, W., Burckhart, R., & Zoll, G. (1974). Mixing and mass transfer in tall bubble columns. *Chemical & Engineering Science* 29 , 2177-2188.
- Doucha, J., & Livansky, K. (2006). Productivity, CO₂/O₂ exchange and hydraulics in outdoor open high density microalgal (*Chlorella* sp.) photobioreactors operated in a Middle and Southern European climate. *Journal of Applied Phycology* 18 , 811-826.
- Fadavi, A., & Chisti, Y. (2007). Gas holdup and mixing characteristics of a novel forced circulation loop reactor. *Chemical Engineering Journal* 131 , 105-111.
- Fan, L., Zhang, Y., Zhang, L., & Chen, H. (2008). Evaluation of a membrane-sparged helical tubular photobioreactor for carbon dioxide biofixation by *Chlorella vulgaris*. *Journal of Membrane Science* 325 , 336-345.
- Freitas, C., & Texeira, J. (2001). Oxygen mass transfer in a high solids loading three-phase internal-loop airlift reactor. *Chemical Engineering Journal* 84 , 57-61.
- Froment, G., & Bischoff, K. (1990). *Chemical Reactor and Design*. New York: John Wiley & Sons, Inc.
- Ganzeveld, K., Chisti, Y., & Moo-Young, M. (1995). Hydrodynamic behaviour of animal cell microcarrier suspensions in split-cylinder airlift bioreactors. *Bioprocess Engineering* 12 , 239-247.
- Giaveno, A., Lavalle, L., Chiacchiarini, P., & Donati, E. (2007). *Microbial Processing of Metal Sulfides*. Dordrecht: Springer.
- Haiduc, A., Brandenberger, M., Suquet, S., Vogel, F., Bernier-Latmani, R., & Ludwig, C. (2009). SunCHem: an integrated process for the hydrothermal production of methane from microalgae and CO₂ mitigation. *Journal of Applied Phycology* .
- Hall, D., Acién, F., Canizares, E., Krishna, K., & Molina, E. (2003). Outdoor Helical Tubular Photobioreactors for Microalgal Production: Modeling of Fluid-Dynamics and Mass Transfer and Assessment of Biomass Productivity. *Biotechnology and Bioengineering* 82 , 62-73.
- Huntley, M., & Redalje, D. (2006). CO₂ mitigation and renewable oil from photosynthetic microbes: a new appraisal. *Mitigation and Adaptation Strategies for Global Change* 12 , 573-608.

- Janssen, M., Bresser, L., Baijnes, T., Tramper, J., Mur, L., Snel, J., et al. (2000). Scale-up aspects of photobioreactors: effects of mixing-induced light/dark cycles. *Journal of Applied Phycology* 12 , 225-237.
- Janssen, M., Janssen, M., de Winter, M., Tramper, J., Mur, L., Snel, J., et al. (2000). Efficiency of light utilization of *Chlamydomonas reinhardtii* under medium-duration light:dark cycles. *Journal of Biotechnology* 78 , 123-137.
- Jeon, Y., Cho, C., & Yun, Y. (2005). Measurement of microalgal photosynthetic activity depending on light intensity and quality. *Biochemical Engineering Journal* 27 , 127-131.
- Jimenez, C., Cossio, B., & Niell, X. (2003). Relationship between physicochemical variables and productivity in open ponds for the production of *Spirulina*: a predictive model of algal yield. *Aquaculture* 221 , 331-345.
- Jin, B., Yin, P., & Lant, P. (2006). Hydrodynamics and mass transfer coefficient in three-phase air-lift reactors containing activated sludge. *Chemical Engineering and Processing* 45 , 608-617.
- Kawase, Y., & Moo-Young, M. (1986). Theoretical prediction of gas holdup in bubble columns with Newtonian and non-Newtonian fluids. *Industrial & Engineering Chemistry Research* 26 , 933-937.
- Kong, Q., Li, L., Martinez, B., Chen, P., & Ruan, R. (2010). Culture of Microalgae *Chlamydomonas reinhardtii* in Wastewater for Biomass Feedstock Production. *Applied Biochemistry Biotechnology* 160 , 9-18.
- Lee, Y. (2001) Microalgal mass culture systems and methods: Their limitation and potential. *Journal of Applied Phycology* 13, 307-315.
- Leon, R., & Galvan, F. (1997). Analysis of effective light in different photobioreactors: its influence on growth, photosynthetic activity and glycerol production by the freshwater green alga *Chlamydomonas reinhardtii*. *World Journal of Microbiology & Biotechnology* 13 , 237-293.
- Liu, M., Lu, C., Shi, M., Yan, C., Fan, Y. (2010). Region-dependent mass transfer behavior in a forced circulation airlift loop reactor. *Powder Technology*, 93-103
- Loubiere, K., Olivo, E., Bougaran, G., Pruvost, J., Robert, R., & Legrand, J. (2008). A New Photobioreactor for Continuous Microalgal Production in Hatcheries Based on External Loop Airlift and Swirling Flow. *Biotechnology and Bioengineering* , 132-147.
- Merchuk, J., & Berzin, I. (1995). Distribution of energy dissipation in airlift reactors. *Chemical Engineering Science* 50 , 2225-2233.
- Merchuk, J., Ronen, M., Giris, S., & Arad, S. (1998). Light/Dark Cycles in the Growth of the Red Microalgae *Porphyridium* Sp. *Biotechnology and Bioengineering* 59 , 705-713.
- Molina, E., Acién, F., Garcia, F., & Chisti, Y. (1999). Photobioreactors: light regime, mass transfer, and scaleup. *Journal of Biotechnology* 70 , 231-247.
- Molina, E., Fernandez, J., Acien, F., & Chisti, Y. (2001). Tubular photobioreactor design for algal cultures. *Journal of Biotechnology* 92 , 113-131.
- Molina, E., Fernandez, J., Sanchez, J., & Garcia, F. (1996). A study on simultaneous photolimitation and photoinhibition in dense microalgal cultures taking into account incident and averaged irradiances . *Journal of Biotechnology* 45 , 59-69.
- Moroney, J., & Tolbert, N. (1985). Inorganic Carbon Uptake by *Chlamydomonas reinhardtii*. *Plant Physiology* 77 , 253-258.

- Muller-Feuga, A., Le Guédes, R., Hervé, A., & Durand, P. (1998). Comparison of artificial light photobioreactors and other production systems using *Porphyridium cruentum*. *Journal of Applied Phycology* 10 , 83-90.
- Munoz, R., & Guieysse, B. (2006). Algal–bacterial processes for the treatment of hazardous contaminants: A review. *Water research* 40 , 2799-2815.
- Nicolella, M., van Loosdrecht, M., van der Lans, R., & Heijnen, J. (1998). Hydrodynamic Characteristics and Gas–Liquid Mass Transfer in a Biofilm Airlift Suspension Reactor. *Biotechnology and Bioengineering* 60 , 627-635.
- Nouals, S. (2000). *Modélisation d'un photobioréacteur pilote pour la mise en oeuvre de microalgues*. Paris: Ecole Centrale des Arts et Manufactures "Ecole Centrale Paris".
- Ogbonna, J., Yada, H., & Tanaka, H. (1995). Light Supply Coefficient: A New Engineering Parameter for Photobioreactor design. *Journal of Fermentation and Bioengineering* 80 , 369-376.
- Oncel, S., & Vardar-Sukan, F. (2009). Photo-bioproduction of hydrogen by *Chlamydomonas reinhardtii* using a semi-continuous process regime. *International Journal of Hydrogen Energy* 34 , 7592-7602.
- Perry, R., Green, D., & Maloney, J. (1999). *Perry's Chemical Engineers's handbook*. United States of America: McGraw-Hill.
- Pruvost, J., Cornet, J., & Legrand, J. (2008). Hydrodynamics influence on light conversion in photobioreactors: An energetically consistent analysis. *Chemical Engineering Science* 63 , 3679-3694.
- Pruvost, J., Legrand, J., Legentilhomme, P., & Muller-Feuga, A. (2002). Simulation of Microalgae Growth in Limiting Light Conditions: Flow Effect. *Bioengineering, Food, and Natural Products* 48 , 1109-1120.
- Qiang, H., & Richmond, A. (1994). Optimizing the population density in *Isochrysis galbana* grown outdoors in a glass column photobioreactor. *Journal of Applied Phycology* 6 , 391-396.
- Radmann, E., Reinehr, C., & Costa, J. (2007). Optimization of the repeated batch cultivation of microalga *Spirulina platensis* in open raceway ponds. *Aquaculture* 265 , 118-126.
- Richmond, A. (2004). *Handbook of Microalgal Culture. Biotechnology and Applied Phycology*. Oxford: Blackwell Science.
- Roustan, M. (2003). *Transferts gas-liquide dans les procédés de traitement des eaux et des effluents gazeux*. Paris: TEC & DOC.
- Rubio, F., Garcia, J., Molina, E., & Chisti, Y. (2001). Axial inhomogeneities in steady-state dissolved oxygen in airlift bioreactors: predictive models. *Chemical Engineering Journal* 84 , 43-55.
- Sanchez, A., Ceron, M., Garcia, F., Molina, E., & Chisti, Y. (2004). Mixing in Bubble Column and Airlift Reactors. *Chemical Engineering Research and Design* , 1367-1374.
- Sanchez, A., Contreras, G., Garcia, F., Molina, E., & Chisti, Y. (1999). Comparative evaluation of compact photobioreactors for large-scale monoculture of microalgae. *Journal of Biotechnology* 70 , 249-270.
- Siegel, R., Howell, J. (2002) *Thermal Radiation Heat Transfer*. Taylor & Francis. New York, London

- Skjanes, K., Lindblad, P., & Muller, J. (2007). BioCO₂ – A multidisciplinary, biological approach using solar energy to capture CO₂ while producing H₂ and high value products. *Biomolecular Engineering* 24 , 405-413.
- Takache, H., Christophe, G., Cornet, J., & Pruvost, J. (2010). Experimental and theoretical assessment of maximum productivities for the microalgae *Chlamydomonas reinhardtii* in two different geometries of photobioreactors. *Biotechnology Progress* 26 , 431-440.
- Talvy, S., Cockx, A., & Liné, A. (2007). Modeling of Oxygen Mass Transfer in a Gas-Liquid Airlift Reactor. *American Institute of Chemical Engineers* 53 , 316-326.
- Tobajas, M., Garcia-Calvo, E., Siegel, M., & Apitz, S. (1999). Hydrodynamics and mass transfer prediction in a three-phase airlift reactor for marine sediment biotreatment. *Chemical Engineering Science* 54 , 5347-5354.
- Travieso, L., Hall, D., Rao, K., Benitez, F., Sanchez, E., & Borja, R. (2001). Ahelical tubular photobioreactor producing *Spirulina* in a semicontinuous mode. *International Biodeterioration & Biodegradation* 47 , 151-155.
- Tredici, M., & Chini Zittelli, G. (1998). Efficiency of Sunlight Utilization: Tubular versus Flat Photobioreactors. *Biotechnology and Bioengineering* 57 , 187-197.
- Vonshak, A. (1997). *Spirulina Platensis (Arthrospira): Physiology, Cell-biology and Biotechnology*. London: Taylor & Francis Ltd.
- Wang, C., Fu, C., & Liu, Y. (2007). Effects of using light-emitting diodes on the cultivation of *Spirulina platensis*. *Biochemical Engineering Journal* 37 , 21-25.
- Wiesmann, U., Choi, I., & Dombrowski, E. (2007). *Fundamentals of Biological Wastewater Treatment*. Weinheim: WILEY-VCH Verlag GmbH & Co.
- Wu, X., & Merchuk, J. (2004). Simulation of algae growth in a bench scale internal loop airlift reactor. *Chemical Engineering Science* 59 , 2899 – 2912.
- Xu, Z., Baicheng, Z., Yiping, Z., Zhaoling, C., Wei, C., & Fan, O. (2002). A simple and low-cost airlift photobioreactor for microalgal mass culture. *Biotechnology Letters* 24 , 1767-1771.
- Zeng, M., & Vonshak, A. (1998). Adaptation of *Spirulina platensis* to salinity-stress. *Comparative Biochemistry and Physiology Part A* 120 , 113-118.
- Zhang, T., Zhao, B., & Wang, J. (2006). Mathematical models for macro-scale mass transfer in airlift loop reactors. *Chemical Engineering Journal* 119 , 19-26.

Hydrodynamical study of a Helical-airlift photobioreactor

Nomenclature

A	Cross sectional area	m^2
C_r	Flux concentration or distribution parameter	
d	Diameter	m
D_c	Coil diameter	m
f	Friction factor	
g	Gravitational acceleration	m/s^2
H	Height	m
i	Compartment: riser, downcomer or helical section	
J	Superficial velocity of the mixture	$m^3/m^2.s$
K	Loss coefficient	
L	Length	m
n	Number of turns (curvatures) in the helical coil	
P	Pressure	Pa
P_a	Atmospheric pressure	Pa
P_g	Power input	W
Q	Volumetric flow rate	m^3/s
R	Universal gas constant	J/K.mol
R_b	Bubble radius	m
Re	Reynolds number	
S	Pitch	m
t_c	Circulation time	s
T	Temperature	K
U_{bt}	Terminal bubble velocity	m/s
V	Velocity	m/s
V_b	Volume of a bubble	m^3
V_L	Volume of the liquid	m^3
V_{sl}	Superficial liquid velocity	m/s
V_{sg}	Superficial gas velocity	m/s
V_∞	Terminal bubble velocity in an infinite vessel	m/s
X	Solids loadings	

Dimensionless numbers

Re Reynolds number

Greek letters

ε	Holdup
α	Proportional coefficient
β	Exponential coefficient

μ	Viscosity	Pa.s
ρ	Density	kg/m ³
σ	Surface tension	N/m

Subscripts

b	Bubble
c	Coil
c	Critical
d	Downcomer
g	Gas
h	Helical
i	Internal
i	Pipe fitting, valves
j	Reactor section: riser, downcomer or helical section
l	Liquid
m	Measured
loss	Losses
r	Riser
s	Solids
t	Total

Abbreviations

HAL	Helical airlift reactor
IAL	Internal airlift reactor
PMMA	Polymethyl methacrylate

1. Introduction

The following chapter presents the design and a hydrodynamic study of a photobioreactor based on airlift reactor design. The bioreactor combines the principle of internal and external airlift reactors, having a riser and downcomer compartments as well as one helical section.

In this study, a helical section is included into the bioreactor in order to control liquid velocities and to increase liquid circulation time. It is well known that helical wound pipes are advantageous in fluid transporting systems since fluid velocities can be manipulated according to helical geometry. On the other hand, they occupy small surfaces compared to straight pipes. Helical wound pipes have been largely employed in heat exchangers as well as in flow transportation in chemical industries (Xin et al., 1996). They have also been employed in a patented photobioreactor called BIOCOIL, where species such as *Phaeodactylum tricornutum*, *Spirulina platensis*, and *Chlorella* have been cultivated, reaching high cell densities (Borowitzka, 1999; Travieso et al., 2001; Hall et al., 2002).

In the concept to be presented here, helical wound pipes can be regarded as an extra section of the downcomer of an internal airlift reactor. Similar to the IAL reactor, the riser is a very important compartment since the process of gas-liquid exchange occurs. In this work, a complete hydrodynamic study is presented, including an experimental analysis as well as the formulation of a model. In the experimental study, two pipes with different diameters are tested in the helical section, measuring pressure losses, riser gas holdups, and liquid velocities. On the other hand, modeling results will be compared to experimental data, highlighting gas holdups and liquid velocities.

Finally, the hydrodynamics of the reactor is compared to the internal airlift reactor presented previously, emphasizing advantages and disadvantages of both reactors.

2. Equipment and methods

2.1 Equipment

The reactor is divided in three sections: the riser, the downcomer, and the helical section.

- *The riser* consists in a transparent cylinder, made of polymethyl methacrylate (PMMA), in which air is injected to provoke liquid circulation. Like the internal airlift reactor, the gas injection system (sparger) is designed in the form of a shower sprinkler with 24 holes of 2-mm diameter.
- *The downcomer* is constructed by superposing a larger cylinder at 112 cm of riser height, creating an annular space. At the bottom, a pipe fitting was installed to connect the downcomer to the helical section. The downcomer is built of PMMA, as well.
- *The helical section* consists of semi-transparent tubing called “tubclair”, which are wrapped helically around a frame structure. The spirals are superposed, thus the spiral pitch is equal to the pipe external diameter. The end of the helical section is connected to the riser bottom to close the loop.



Figure IV.1. Helical airlift reactor.

Two tubes of different diameters have been tested in the helical section: one with an internal diameter of 30 mm and the second with an internal diameter of 25 mm. Sizes were selected in order to obtain optical paths like those recommended for flat panel photobioreactors (Richmond, 2007). This would be in the case that artificial lamps are placed inside the section.

Both pipes are wound at the same frame external diameter of 63 cm, resulting in different coil diameters (figure IV.1).

Table IV.1 shows the dimensions corresponding to all sections in the reactor.

Table IV.1. Dimensions of the helical-airlift reactor (HALR).

	<i>Riser</i>	<i>Downcomer</i>	<i>Helical section</i>	
Internal diameter (m)	0.133	0.19	0.03	0.025
External diameter (m)	0.139	0.2	0.038	0.032
Height (m)	1.09	0.58	0.34	0.3
Frame External diameter (cm)			0.63	
Coil diameter (m)			0.71	0.69
Number of spires			9	10
Ar/Ad	1.053			
Curvature ratio d/D			0.041	0.034
Equivalent length			20	22
Total working volume (lt)			37	34

The equivalent length, which includes the effect of curvatures in the helical section, is calculated as (Hall et al., 2002)

$$L_{eq} = n\sqrt{s^2 + (\pi D_c)^2} \quad (IV.1)$$

To create liquid circulation in the reactor, compressed air is injected in the riser by using a gas flow controller with integrated regulator (Red-Y smart controller GSC with an accuracy of $\pm 1.5\%$). Air pressure is maintained at 200 kPa while air flow rates of 5, 10, 15, 20, and 25 Ln/min are varied. Tap water at ambient temperature is used as liquid phase.

To control the liquid circulation, three ball valves are installed between the helical section and the riser to feed and empty the entire system. A diaphragm valve is installed at the end of the helical section to regulate water flow rate if necessary.

Two pressure sensors, type Keller PR-33X with an analog signal ranging from 0 to 10 Volts and an accuracy of $\pm 0.1\%$, are installed in the riser to measure the corresponding pressure difference and therefore, gas holdups. In the helical section, a pressure sensor (type Rosemount 1151 with accuracy of $\pm 2\%$), is installed to measure the differential pressure between the entrance and the exit of the helical section.

An acquisition system composed of field points (FP-AI-110, National Instruments) allows transforming analog signals, sent by the three pressure sensors, into digital signals. Digital signals are then processed by an acquisition computer and a program conceived in LabWindows/CVI (a

computational environment for test and measurement developed by National Instruments). Figure IV.2 shows liquid circulation in the HAL reactor, using the interface utilized in CVI.

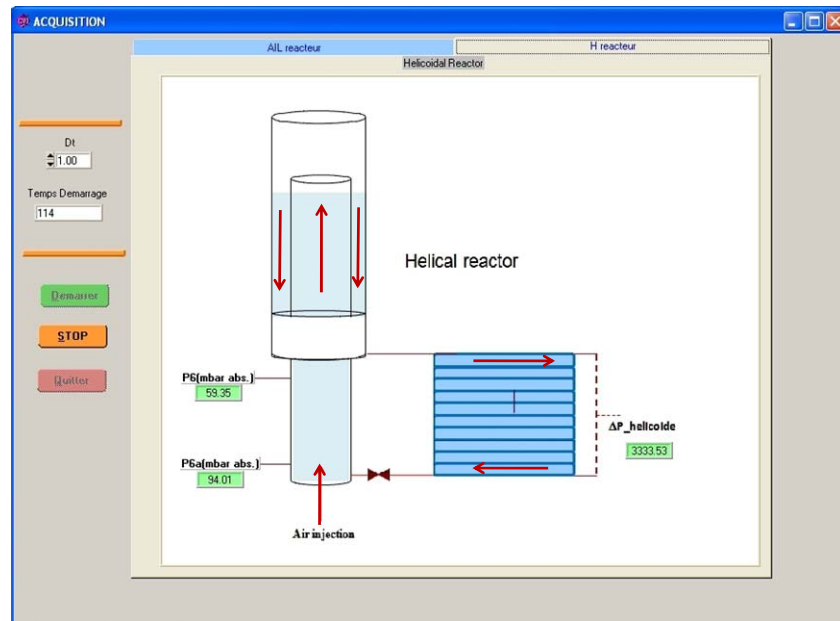


Figure IV.2. Flow circulation in the HAL reactor. Interface designed in CVI.

2.2 Methods

The experimental study performed in the HAL reactor can be divided in two steps. First, *total losses* in the helical section are measured for different liquid flow rates with aim to estimate the *total loss coefficient* in this section. Subsequently, pressure differences in the riser and the helical section are measured to obtain riser gas holdups and liquid flow rates in the helical section. Figure IV.3 shows a schematic diagram of the procedure followed in the experimental study.

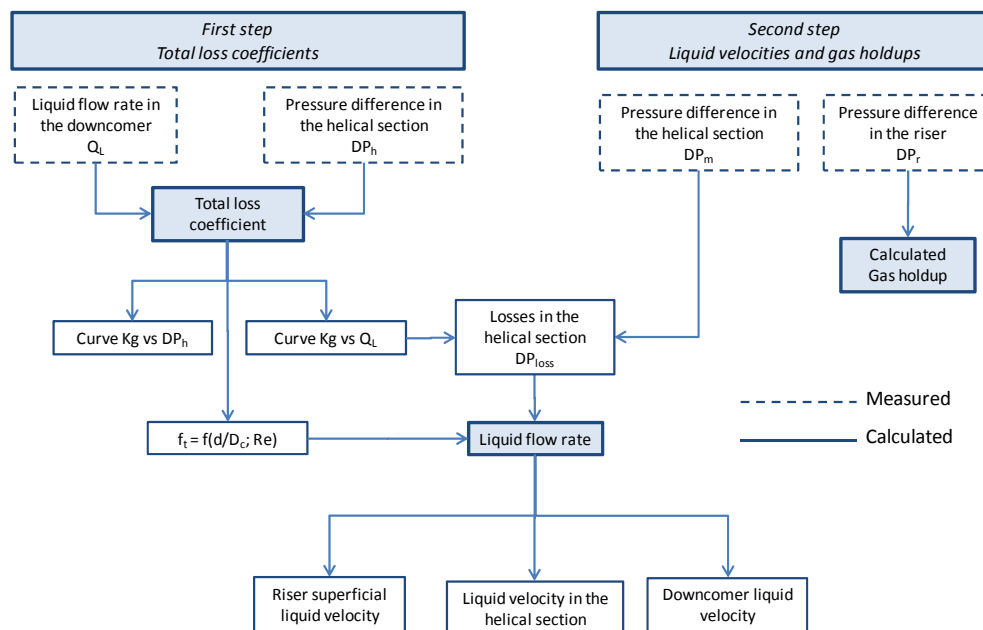


Figure IV.3. Steps to perform HAL experimental study.

In the first step, total loss coefficients are estimated as a function of volumetric flow rates. Tap water is sent in the helical section, through one of the draining pipes to the bottom of the helical coil. Then, the helical coil is filled carefully in order to avoid the formation of air pockets. Water continues to flow up until the downcomer is filled while differential pressure is measured in the helical coil. The pressure difference between the entrance and the exit of the helical section represents the total pressure, involving gravitational pressure and pressure losses.

In the downcomer, the time of the liquid to flow from one height to a second is measured, thus the volumetric flow rate can be calculated. This procedure was repeated at least 15 times for the two pipe diameters chosen here.

In the second step, gas holdups and liquid velocities are estimated according to results obtained in the first step. Riser and downcomer compartments are filled with water until it reaches a level of 4 cm under the top of the draft tube. Subsequently, air is injected into the riser at the desired air flow rate. The liquid in the riser overflows and there is a liquid circulation from the riser to the downcomer and then, to the helical section. The gas is completely released in riser, thus there is neither gas entering to the downcomer nor to the helical section.

Once air is injected into the system, differential pressures in the riser and the helical section are measured after reaching steady state (after 10 minutes approximately). Similarly to the internal airlift reactor, differential pressures in the riser lead to estimate gas holdups. In the helical section, differential pressures allow calculating liquid flow rates, by using the total loss coefficients previously estimated.

3. Experimental results

3.1 Estimation of the total loss coefficient in the helical section

Measuring the pressure difference between the entrance and the exit of the helical section leads to estimate pressure losses in the helical section. They are calculated from the difference between the measured pressure (ΔP_m) and the static pressure (ΔP_g) (Xin et al., 1995).

$$-\Delta P_{loss} = \Delta P_m - \Delta P_g \quad (IV.2)$$

Subsequently, total loss coefficients are calculated from pressure losses by applying Equation IV.3.

$$K_T = \frac{2\Delta P_{loss}}{\rho_L} \left(\frac{A_h}{Q_L} \right)^2 \quad (IV.3)$$

Equation IV.3 is the expression employed to represent losses in a system when Bernoulli's equation is applied along a streamline (Idelchik, 1996; Shaughnessy et al., 2005). Figures IV.4 and IV.5 show total loss coefficients at corresponding pressure losses and liquid flow rates, for the two pipe diameters tested here.

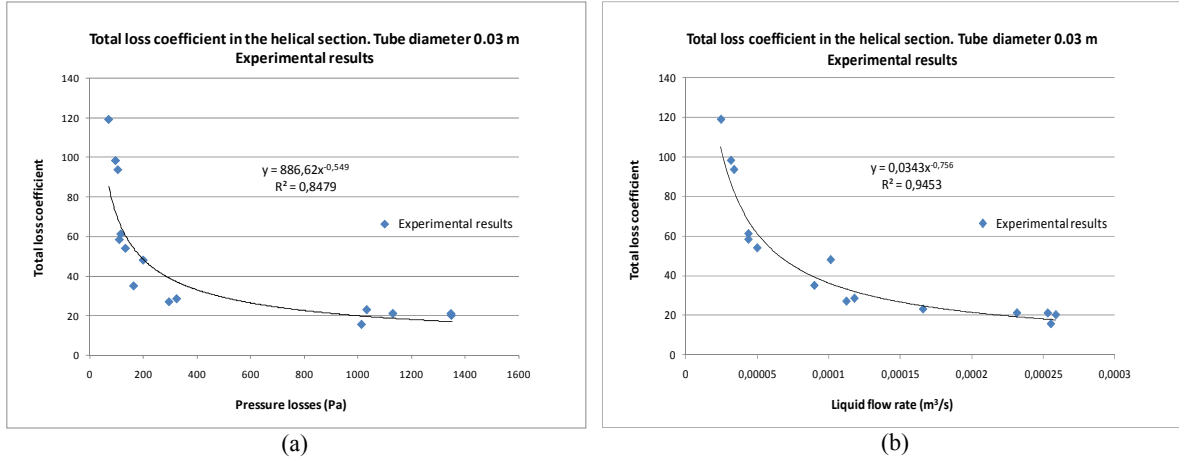


Figure IV.4. Total loss coefficients in the helical section for a pipe diameter of 30 mm
a) as a function of pressure losses; b) as a function of liquid flow rates.

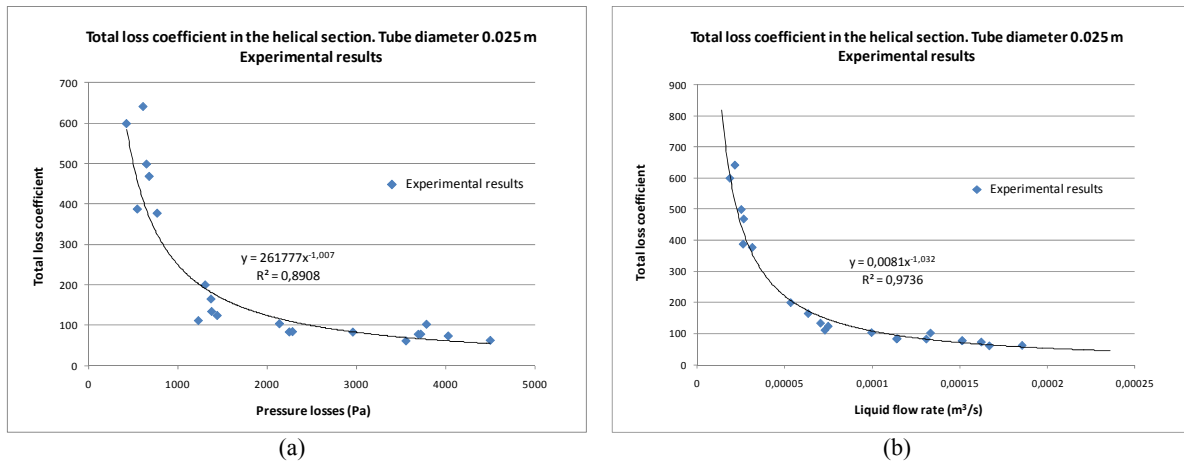


Figure IV.5. Total loss coefficients in the helical section for a pipe diameter of 25 mm
a) as a function of pressure losses; b) as a function of liquid flow rates.

For a pipe diameter of 30 mm, the measured liquid flow rate has a maximal uncertainty of 0.8% while for the total loss coefficient is of 4%. Results for a pipe diameter of 25 mm have a maximal uncertainty of 0.83% for the liquid flow rate and 3.7% for the total loss coefficient.

Figures IV.4 and IV.5 show that total loss coefficients are higher at low-pressure losses and liquid flow rates. The total loss coefficient involves frictional losses in the pipe as well as the effect of having spires to form the helical coil (Xin et al., 1996). These results have the same tendency as those presented in the Moody diagram (Shaughnessy et al., 2005), even though the total loss coefficient presented here involves pipe diameter and equivalent length. Total loss coefficients have the same tendency as those found by Coronel and Sandeep and Guo et al. The first worked with helical heat exchangers while the second used water in coiled tubes (Guo et al., 2001; Coronel and Sandeep, 2003).

On the other hand, equivalent length and pipe diameter (d_h) can be included in the definition of K_t to express the total loss coefficient in the form of Fanning equation (Tobajas et al., 1999):

$$K_T = f_h \cdot (L_{eq}/d_h) \quad (IV.4)$$

The term f_h can be regarded as a friction factor that represents frictional losses in the helical section. Results show that f_h ranges between 0.023 and 0.15 for a pipe diameter of 30 mm and it ranges from 0.084 to 0.73 for a pipe diameter of 25 mm.

Once the total loss coefficient is obtained for each differential pressure measured in the helical section, the next step is to estimate the liquid flow rate.

3.2 Liquid velocities in the reactor

Liquid velocities in the helical section are calculated from Equation IV.3 once total loss coefficients are estimated from the first step. For each differential pressure measured in this section, there is a corresponding pressure drop and thus, a total loss coefficient (Equations IV.2 and IV.3). Figure 6 shows average pressure losses corresponding to liquid flow rates, obtained in the second step.

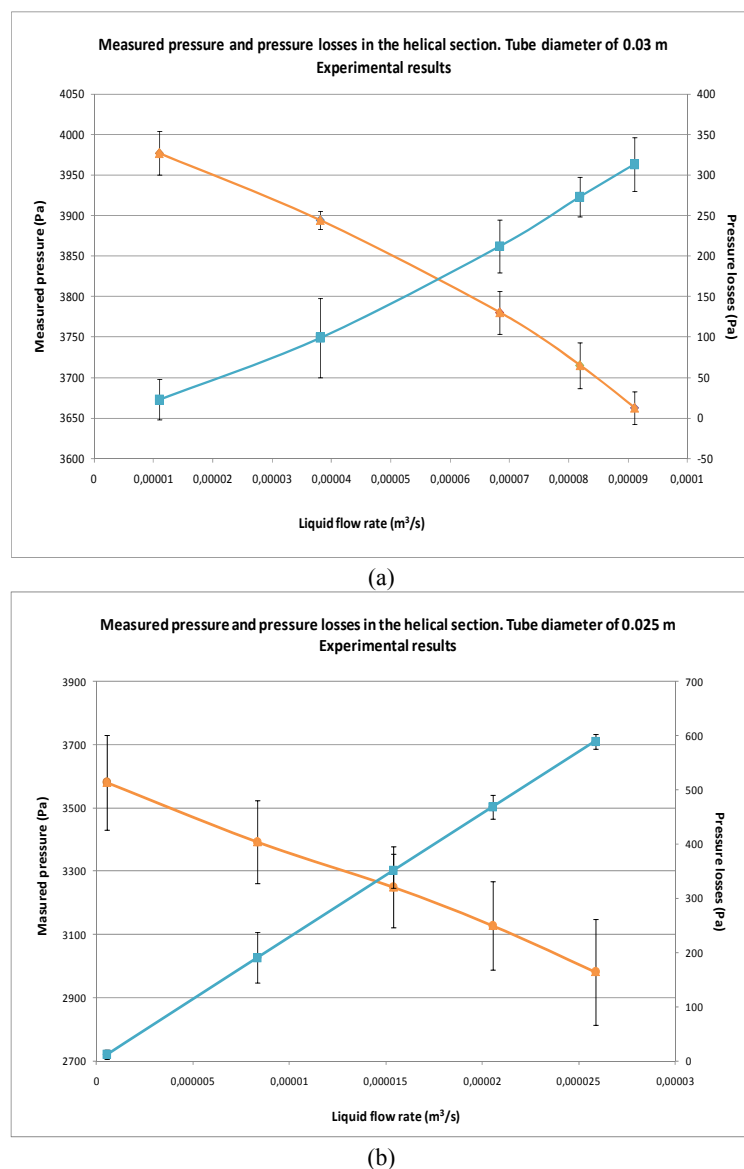


Figure IV.6. Measured pressure and pressure losses in the helical section
a) for a pipe diameter of 30 mm; b) for a pipe diameter of 25 mm
Orange lines correspond to measured pressure. Blue lines correspond to pressure losses
Vertical bars represent standard deviation

Experimental results show that measured pressures are lower than the static pressure, while they diminish at higher liquid flow rates. In concordance with these results, pressure losses increase with liquid flow rates.

Comparing losses between the two pipe diameters, the pressure drop is higher for the smallest pipe diameter, for the same liquid flow rate. The reason is that liquid finds higher resistance to flow due to smaller pipe cross sectional area. In concordance, measured pressures are lower for a pipe diameter of 25 mm compared to those obtained for a 30-mm pipe diameter.

Complementing results showed above, Figure IV.7 presents pressure losses as a function of Reynolds number.

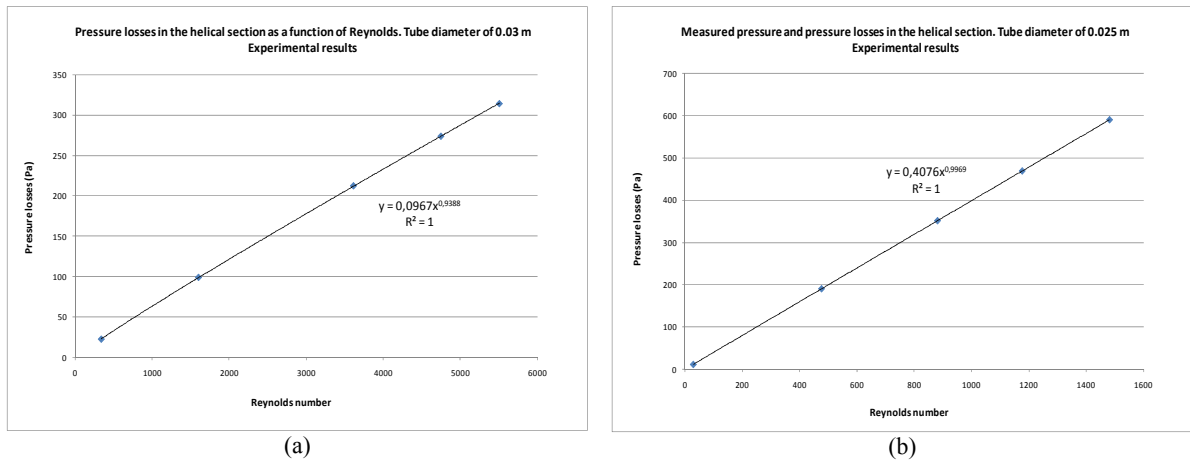


Figure IV.7. Pressure losses in the helical section as a function of Reynolds number
a) for a pipe diameter of 30 mm; b) for a pipe diameter of 25 mm.

From these results, a correlation between pressure losses and Reynolds number can be established.

For a pipe diameter of 30 mm:

$$\Delta P_{loss} = 0.00967(Re)^{0.939} \quad (IV.5)$$

For a pipe diameter of 25 mm:

$$\Delta P_{loss} = 0.408(Re)^{0.997} \quad (IV.6)$$

According to several authors, critical Reynolds number used to determine the transition from laminar to turbulent flow, changes in curvature pipes compared to straight tubes with same characteristics (Ali, 2001). In helical coiled pipes, critical Reynolds numbers can be estimated according to the relationship proposed by Srinivasan et al., as follows (Ali, 2001; Guo et al., 2001; Coronel and Dussap, 2002):

$$Re_c = 2100 \left[1 + 12(d/D_c)^{0.5} \right] \quad (IV.7)$$

Due to the geometrical characteristics of the helical section, the critical Reynolds number for the 30-mm pipe diameter is 7300 while it is 6900 for a 25-mm pipe diameter. Following this and results obtained above, it can be observed that the flow in the helical section is laminar for all gas air flow rates and the two pipes tested here (Figure IV.7).

Since the liquid flows in a closed loop, the liquid flow rate is equal along the entire reactor. In consequence, superficial liquid velocity in the riser as well as actual liquid velocities in the downcomer and helical section can be calculated according to the corresponding cross sectional area.

Since air injection promotes liquid circulation in the system, it is important to establish the relationship between superficial gas velocities and liquid velocities in all sections of the reactor. Figures IV.8 and IV.9 present liquid velocities as a function of superficial gas velocities in each section of the reactor.

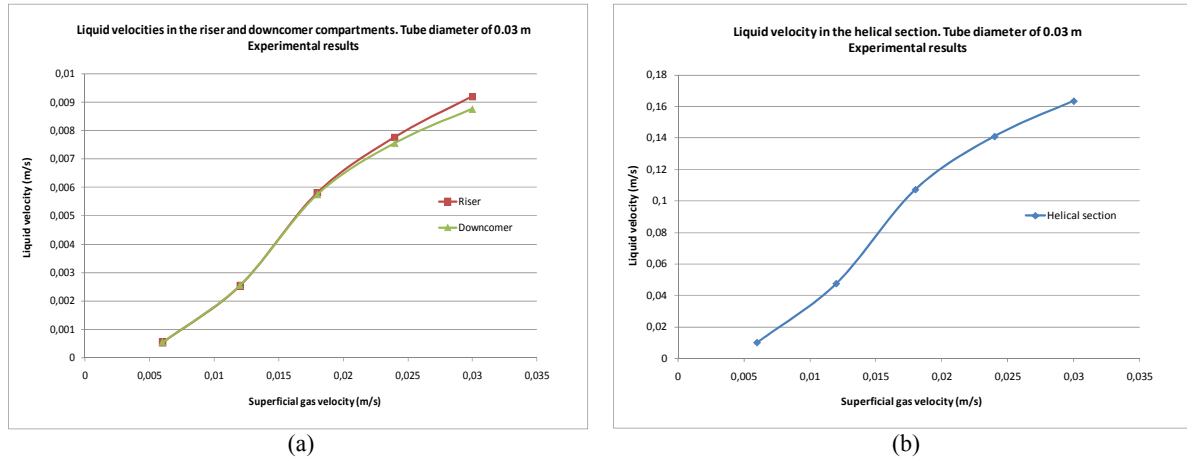


Figure IV.8. Liquid velocities in all sections of the reactor for a pipe diameter of 30 mm
a) riser and downcomer; b) helical section.

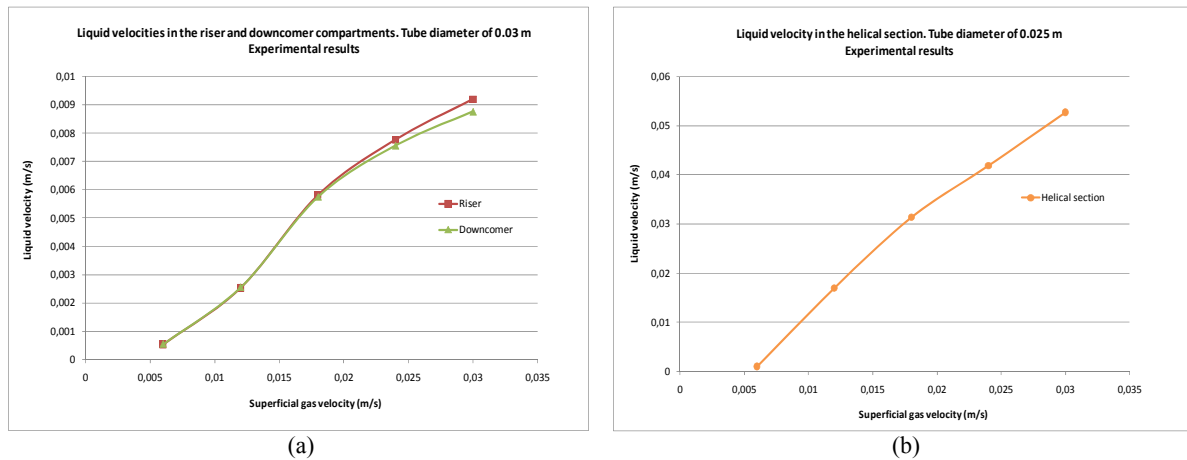


Figure IV.9. Liquid velocities in all sections of the reactor for a pipe diameter of 25 mm
F., Molina, E., & Merchuk, J. (1999). Infl.

Uncertainties of values presented above range between 0.67 and 7.2%, where the maximal uncertainty corresponds to a pipe diameter of 25 mm installed in the helical section.

Experimental results show that for both helical pipes tested here, liquid velocities are very low for an air flow rate of 5 Ln/min as well as pressure losses. This means that liquid circulation is close to zero. On the other hand, results show that liquid velocities in the riser and downcomer are very low compared to those in the helical section. Liquid velocities in the helical section can be as high as 27 times the liquid velocity in the riser (for a pipe of 30-mm diameter). The reason is that liquid velocity increases once the flow passes from one compartment with certain cross sectional area to a smaller one. The cross sectional area of the riser is much larger than that of the helical coiled pipes ($A_r/A_h = 28.3$). In this study, results of liquid flow rates are in the range of those employed by Fan et al. when

the culture of *Chlorella vulgaris* was performed in a membrane-sparged helical tubular photo-bioreactor (Fan et al., 2008).

On the other hand, liquid velocities in the riser and downcomer compartments are higher when a pipe diameter of 30 mm is installed in the helical section. In this case, pressure losses in the helical section are lower, thus the energy transferred to the riser is higher. The consequence is an increase in the riser liquid velocity and therefore, the downcomer liquid velocity.

Comparing riser and downcomer liquid velocities, the riser liquid velocity is slightly higher than in the downcomer. Here, it is important to note that riser liquid velocities shown in Figures IV.8 and IV.9 are the so-called *actual velocities* since the liquid flow rate gives the superficial gas velocity (Livingston and Zhang, 1992) (Equation II.2). From results shown previously, two relationships can be established to characterize the most crucial sections in the reactor. One between the riser liquid velocity as a function of the superficial gas velocity and the second between the liquid velocity in the helical section and the superficial gas velocity. The relationships have the form of $V_l = \alpha(V_{sg})^\beta$ as proposed by authors for internal airlift reactors (Chisti, 1989; Freitas et al., 1999; Babcock et al., 2002) (Table IV.2)

Table IV.2. Relationships between liquid velocities and superficial gas velocities.

<i>D (mm)</i>	<i>Helical section</i>	<i>Riser</i>
30	$V_{l,h} = 13.1(V_{sg})^{1.23}$	$V_{l,r} = 0.86(V_{sg})^{1.28}$
25	$V_{l,h} = 20(V_{sg})^{1.77}$	$V_{l,r} = 28.5(V_{sg})^{2.62}$

For the relationships presented above, the highest deviation occurs at air flow rates of 5 Ln/min. Regarding Figures IV.8 and IV.9, the tendency of the curves is to cut the abscissa showing that the liquid has a certain velocity even though there is no gas being injected into the riser. Since compressed air provides the energy to the liquid to flow, this cannot be possible. For this reason, equations shown in Table IV.2 are forced to pass to the origin, resulting in lower deviations for air flow rates higher than 5 Ln/min. Figure IV.10 shows liquid residence time in each compartment of the reactor, calculated from liquid velocities and respective dimensions. Liquid residence times correspond to air flow rates ranging from 10 to 25 Ln/min since it was observed that there is very low liquid circulating along the reactor for an air flow rate of 5 Ln/min.

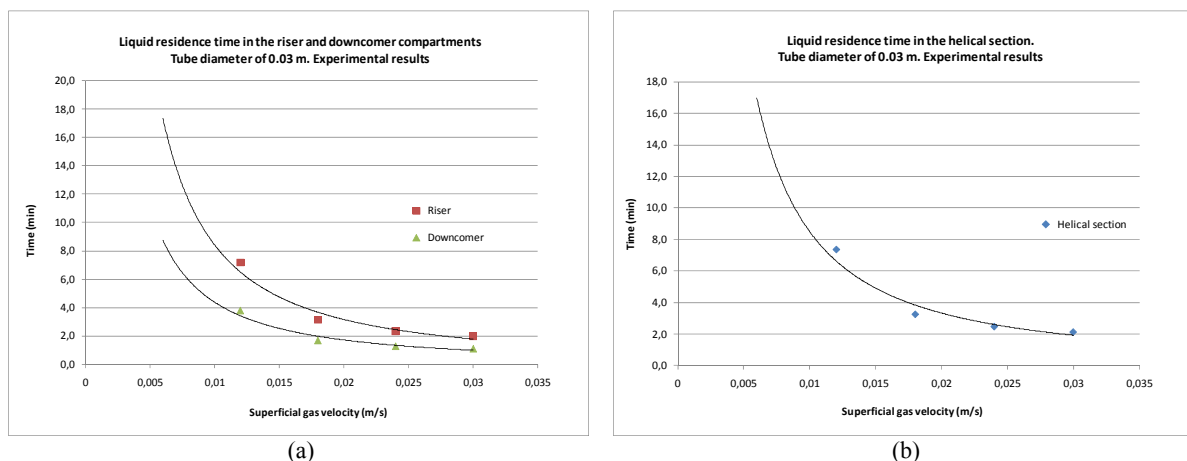


Figure IV.10. Liquid residence time in all sections of the reactor for a 30-mm pipe diameter
a) riser and downcomer; b) helical section.

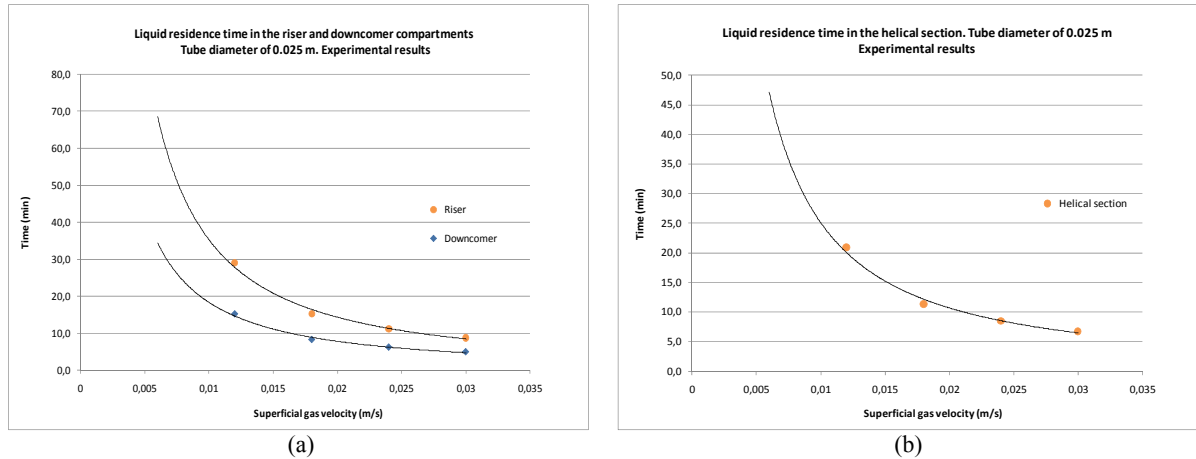


Figure IV.11. Liquid velocities in all sections of the reactor for a 25-mm pipe diameter
a) riser and downcomer; b) helical section.

Comparing results, liquid residence times are very similar in the riser and the helical section for a 30-mm pipe diameter of. For a 25-mm pipe diameter, the liquid residence time in the riser is 1.4 times of those found in the helical section. On the other hand, liquid residence times in all sections are higher for a coiled pipe of 25 mm. They are in the range of 65.2 and 20.4 minutes while they range between 16.2 and 6.6 minutes for a coiled pipe diameter of 30 mm.

Similar to liquid velocities, liquid circulation times (in minutes) can be related to superficial gas velocities in the form of (Freitas et al., 1999; Babcock et al., 2002):

$$t_c = 0.0376(V_{sg})^{-1.376} \quad (\text{IV.8})$$

With an uncertainty of 2.1% for a pipe diameter of 30 mm, and

$$t_c = 0.9(V_{sg})^{-0.83} \quad (\text{IV.9})$$

With an uncertainty of 1.25% for a pipe diameter of 25 mm.

3.3 Gas holdup and power input

Analogous to an internal airlift reactor, it is important to determine the gas holdup in the helical reactor as well as the power input given by the gas to the entire system. In the riser, the measured pressure difference leads to the estimation of gas holdup, in the form of:

$$\Delta P_r = gH_L(\rho_L(1-\varepsilon_g) + \rho_g\varepsilon_g) \quad (\text{IV.10})$$

Where H_L is the liquid height and ε_g is the gas holdup, both in the riser. Figure IV.12 presents values of gas holdups according to superficial gas velocities, both for pipe diameters of 30 and 25 mm in the helical section.

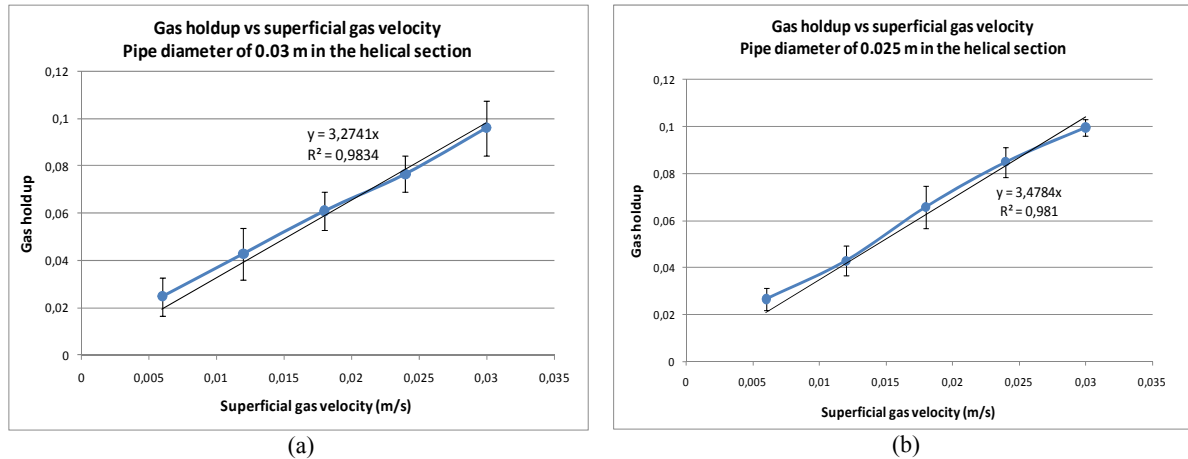


Figure IV.12. Gas holdup as a function of the superficial gas velocities
a) for a pipe diameter of 30 mm; b) for a pipe diameter of 25 mm
Vertical bars represent standard deviations.

A linear equation is the most appropriate mathematical regression found for the experimental data, which is simpler than those found by authors in internal airlift reactors (Van't Riet and Tramper, 1991; Heijnen et al., 1997).

Results in Figure IV.12 show that values of gas holdup change slightly when the pipe diameter in the helical section is reduced from 30 mm to 25 mm. This means that gas holdup is not affected by the change of liquid flow rates when the pipe diameter is modified in the helical section. For both pipe diameters, liquid flow rates are low in the reactor, which results in low superficial liquid velocities in the riser, particularly when they are compared to superficial gas velocities.

On the other hand, it is interesting to study the relationship between the power input given by the gas and resulting liquid flow rates. As it was explained in Chapter III, the power given by the gas is the result of its isothermal expansion along the riser height. Then, the specific power input defined as the power input per unit of liquid volume, is estimated in the form of (Merchuk and Berzin, 1995; Fadavi and Chisti, 2007):

$$\left(\frac{P_g}{V_L}\right) = \frac{Q_g RT}{V_L} \ln\left(1 + \frac{\rho_L g H_L}{P_a}\right) \quad (\text{IV.11})$$

Figure IV.13 presents gas holdups and liquid flow rates according to the specific power input.

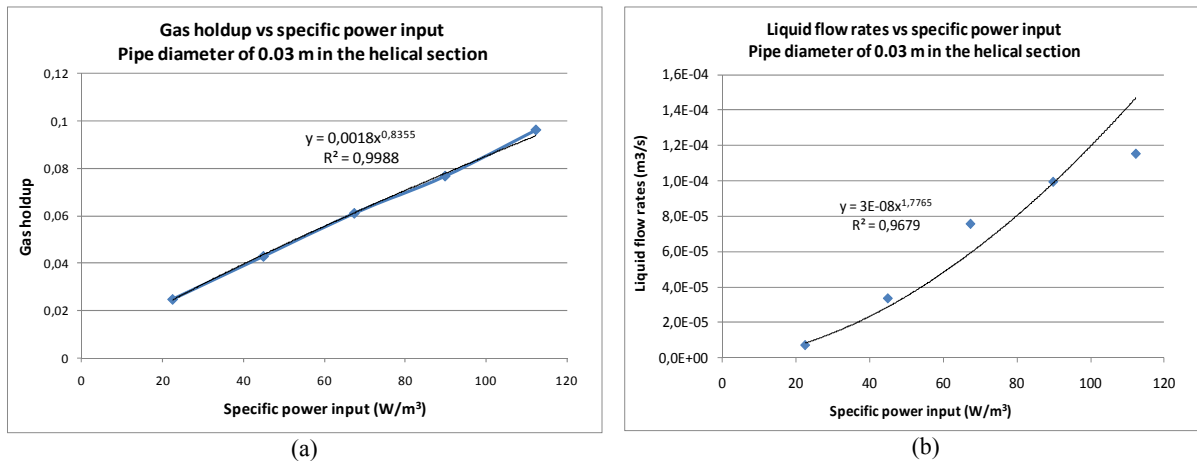


Figure IV.13. Gas holdups, liquid flow rates and specific power inputs. $D_h=30$ mm
a) Gas holdup vs. specific power input; b) Liquid flow rates vs. specific power input.

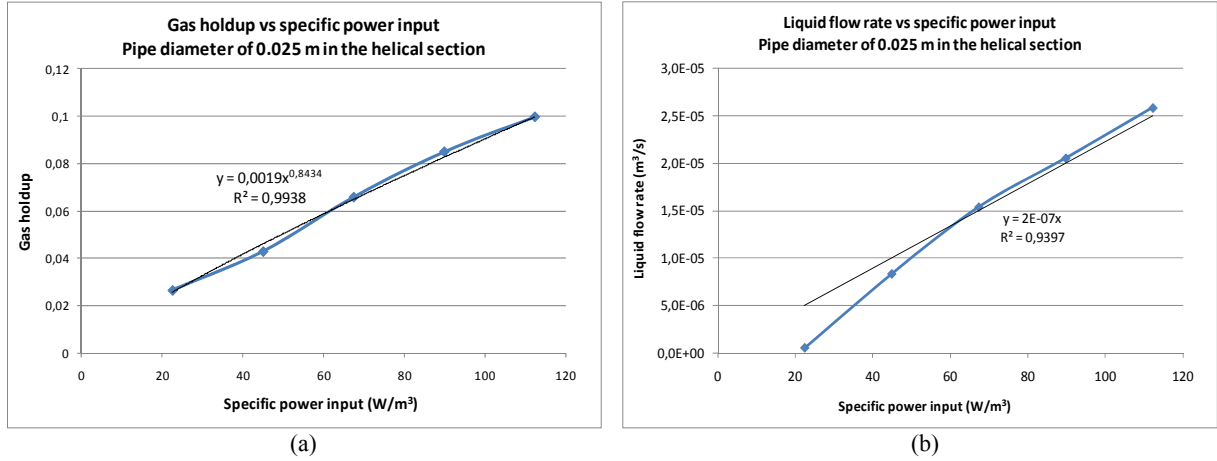


Figure IV.14. Gas holdups, liquid flow rates and specific power inputs. $D_h=25$ mm
a) Gas holdup vs. specific power input; b) Liquid flow rates vs. specific power input.

Since gas holdups change slightly for the two coiled pipes tested here, it is expected that the relationship between specific power inputs and gas holdups are practically the same in both cases (regressions in Figures IV.13a and IV.14a).

Results in Figures IV.13b and IV.14b show that it is necessary, for a coiled pipe diameter of 25 mm, to have higher power input from the gas to obtain the same liquid flow rates as those obtained when using a coiled pipe of 30 mm in the system. As it was observed above, pressure drops are higher for a 25-mm pipe diameter of compared to those for a 30-mm pipe diameter of (Figure IV.7).

4. Hydrodynamic model

Similarly to internal and external airlift reactors, the hydrodynamics in the riser compartment can be determined by employing the so-called *Drift-flux model* proposed by Wallis (Wallis, 1969; Livingston et al., 1993; Lu et al., 1995; Freitas et al., 1999). The mixture flow model proposes a relationship between the superficial velocities of phases and the gas holdup, in the form of:

$$V_{g,r} = \frac{V_{sg,r}}{\epsilon_{g,r}} = C_r (V_{sl,r} + V_{sg,r}) + U_{bt} \quad (IV.12)$$

Where C_r is the flux concentration or distribution parameter, usually ranging between 1.02 and 1.17 in internal airlift reactors (Livingston et al., 1993; Lu et al., 1995; Contreras et al., 1999). In the riser, the gas and the liquid flow in co-current flows. J_r is the superficial velocity of the mixture, covering velocities of each phase presented in the system. U_{bt} is the terminal bubble velocity assuming that bubbles do not interact (Lu et al., 1995; Contreras et al., 1999; Freitas et al., 1999).

The terminal bubble velocity is obtained from the characteristics of the sparger (e.g orifice diameter), air flow rate in the orifice as well as liquid and gas physical properties. To estimate the terminal bubble velocity, it is necessary to first determinate an average bubble diameter. According to Davidson and Amick, the volume (V_b) of a bubble formed in a non-viscous liquid is in the form of (Wallis, 1969; Levy 1999):

$$V_b = 1.138 \frac{(Q_{g,orifice})^{6/5}}{g^{3/5}} \quad (IV.13)$$

From bubble volume, the equivalent radius is obtained assuming that bubbles are spherical. In this study, it is assumed that bubbles have approximately the same diameter and they rise at uniform velocity.

According to Peebles and Gerber, there are four regions at which terminal bubble velocity in an infinite vessel can be calculated according to the bubble Reynolds number. Subsequently, it is necessary to perform an iterative process assuming a first value of the terminal bubble velocity, then obtaining the bubble Reynolds number and finally verifying the assumption according to the region. Table IV.3 shows mathematical expressions to calculate the terminal bubble velocity and the respective regions (Wallis, 1969).

Table IV.3. Terminal bubble velocity in an infinite vessel
(Wallis, 1969).

<i>Regions</i>	<i>Terminal velocity</i>	<i>Range of applicability</i>
Region 1	$V_{\infty} = \frac{2R_b^2(\rho_l - \rho_g)g}{9\mu_l}$	$Re_b < 2$
Region 2	$V_{\infty} = 0.33g^{0.76}\left(\frac{\rho_l}{\mu_l}\right)^{0.52}R_b^{1.28}$	$2 < Re_b < 4.02G_1^{-2.214}$
Region 3	$V_{\infty} = 1.35\left(\frac{\sigma}{\rho_l \cdot R_b}\right)^{0.5}$	$4.02G_1^{-2.214} < Re_b < 3.1G_1^{-0.25}$ or $16.32G_1^{0.144} < G_2 < 5.75$
Region 4	$V_{\infty} = 1.18\left(\frac{g\sigma}{\rho_l}\right)^{0.25}$	$3.1G_1^{-0.25} < Re_b$ $5.75 < G_2$

G_1 and G_2 are dimensionless group defined as:

$$Re_b = \frac{2\rho_l \cdot V_{\infty} \cdot R_b}{\mu_l} \quad G_1 = \frac{g \cdot \mu_f^4}{\rho_l \cdot \sigma^3} \quad G_2 = \frac{g \cdot R_b^4 \cdot V_{\infty}^4 \cdot \rho_l^3}{\sigma^3} \quad (IV.14)$$

It has to be noted that, in the fourth region, the terminal velocity is not longer dependent on bubble diameters; instead it depends on the liquid properties (Wallis, 1969). This means that, at air flow rates higher than 15 Ln/min, when the bubble Reynolds number is higher enough to be in region 4, the bubble diameter is not longer important.

Once the terminal bubble velocity in an infinite vessel has been determined, the next step is to take into account the influence of walls in a finite vessel. According to Wallis, terminal bubble velocities in an infinite vessel are higher than those estimated when they are flowing in a tube of internal diameter, D_i . Collins established the following relationships according to the ratio between the bubble diameter and the vessel internal diameter (Table IV.4) (Wallis, 1969).

Table IV.4. Terminal bubble velocity in a finite vessel
(Wallis, 1969)

<i>Terminal velocity</i>	<i>Range of applicability</i>
$U_{bt} = V_{\infty}$	$\frac{d_b}{D} < 0.125$
$\frac{U_{bt}}{V_{\infty}} = 1.13e^{-\frac{d_b}{D}}$	$0.125 < \frac{d_b}{D} < 0.6$
$\frac{U_{bt}}{V_{\infty}} = 0.46 \left(\frac{d_b}{D} \right)^{-1/2}$	$0.6 < \frac{d_b}{D}$

Figure IV.15 presents terminal bubble velocities in the riser according to superficial gas velocities and the estimated bubble diameter.

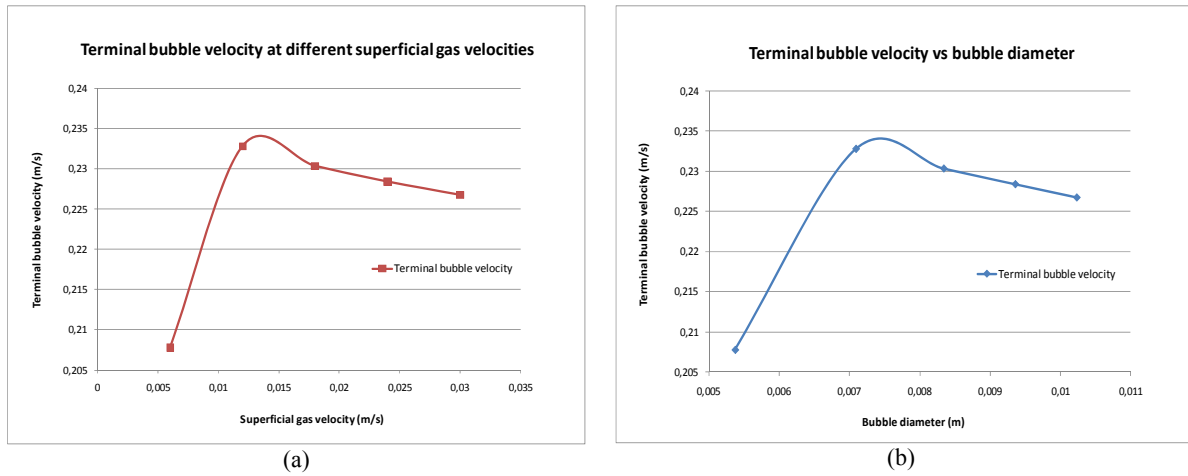


Figure IV.15. Bubble diameter and terminal rise velocity of bubbles in the riser
a) terminal bubble velocity vs. superficial gas velocity; b) terminal bubble velocity vs. bubble diameter.

Results show that terminal bubble velocities are in the range from 20.55 to 23.25 cm/s for the superficial gas velocities treated here. As mentioned in Chapter II, the terminal bubble velocities are usually assumed to be between 25 and 40 cm/s (Livingston et al., 1993; Heijnen et al., 1997), which are in the same order of magnitude of those found here. For instance, the terminal bubble velocity in the riser increases if air flow rates are from 5 to 10 L/min, then it decreases slightly. Figure IV.15b presents the same tendency as that found by Haberman and Morton in a system working with air bubbles in distilled water, demonstrating that there is a bubble diameter at which the terminal velocity diminishes. According to Levy, drag forces increase due to changes in bubbles shape, causing velocities decrease (Levy, 1999).

Once the terminal bubble velocity in a finite vessel is calculated, the liquid velocity in the riser can be determined by applying Equation IV.12 if the riser gas holdup is known. On the contrary, if the riser gas holdup is unknown, it is necessary to perform a macroscopic energy balance in the reactor.

4.1 Macroscopic energy balance in the HALR

Similarly to an internal airlift reactor, the liquid circulation in the helical airlift reactor is caused by the difference of hydrostatic pressure between the downcomer (ΔP_d), the helical section (ΔP_h), and the hydrostatic pressure in the riser (ΔP_r).

$$\Delta P = (\Delta P_d + \Delta P_h) - \Delta P_r \quad (\text{IV.15})$$

The hydrostatic pressure in the riser is given by Equation IV.7, which involves the variation of the water column height due to the gas holdup. The hydrostatic pressure in the downcomer is given by the water column height of 53 cm, since the gas injected in the riser is released completely to the atmosphere. In this reactor, there is no gas entering into the downcomer as it was sometimes observed in the internal airlift reactor. The hydrostatic pressure in the helical compartment is given by the height resulting from the superposition of all spires (Table IV.1). Therefore, Equation IV.15 can be re-written as:

$$\Delta P = [\rho_L g H_{L,d} + \rho_L g H_{L,h}] - [g H_{L,r} (\rho_L (1 - \varepsilon_g) + \rho_g \varepsilon_g)] \quad (\text{IV.16})$$

The difference of pressure heads among the compartments equals the pressure losses in the entire system (Lu et al. 1994; Freitas et al., 1999; Livingston et al., 1993).

$$\Delta P = -\Delta P_{loss} \quad (\text{IV.17})$$

Total pressure losses in the system are composed of the friction losses in each section of the reactor (first term of the right side of Equation IV. 18) as well as losses due to pipe fittings and valves in the circuit (second term of the right side of Equation IV.18). The last are calculated according to their type and sizes (Fox et al., 2004)

$$\Delta P_{loss} = \sum \frac{1}{2} \rho_L f_j \left(\frac{H_{L,j}}{D_j} \right) \left(\frac{Q_L}{A_j} \right)^2 + \sum \frac{1}{2} \rho_L K_i \left(\frac{Q_L}{A_j} \right)^2 \quad (\text{IV.18})$$

The subscript j represents the section in the reactor whether the riser, the downcomer or the helical section. The term f is the Darcy friction factor estimated according to the flow characteristic, either laminar or turbulent (Shaughnessy et al., 2005). In the riser and downcomer compartments, friction factors are determined according to Equations IV.19 and IV.20:

$$f = 64/\text{Re} \quad \text{For laminar flow (Re} < 2100) \quad (\text{IV.19})$$

$$f = 0.316/\text{Re}^{0.25} \quad \begin{array}{l} \text{Blasius equation for turbulent flow (Re} \leq 10^5) \\ \text{Smooth pipes} \end{array} \quad (\text{IV.20})$$

In the helical section, pressure losses are given by the total loss coefficients obtained experimentally in Section 3.1. Since it is usual to find in the literature the total loss coefficient as a function of a friction factor (Equation IV.4), an expression for f_h can be formulated as a function of curvature ratio d/D_c and Reynolds number, in the form of:

$$\ln(f_h) = -204.6 + 219.6e^{-(d/D_c)} - 1.075 \ln(\text{Re}) \quad (\text{IV.21})$$

The relationship is obtained by employing the program *TableCurve 3D* in order to find the best fitting equation for the empirical data. The corresponding coefficient of determination is $R^2 = 0.977$.

Expression IV.21 is applicable for the two curvature ratios tested in this study and Reynolds number ranging from 1100 to 10700. The resulting expression shows the dependency of the friction factor on

Reynolds number and geometrical characteristics, as it has been proven by authors (Ali, 2001; Naphon and Wongwises, 2006).

Finally, to solve Equations IV.15 to IV.21, it is necessary to perform an iterative process. Figure IV.16 illustrates the algorithm followed in this study to estimate gas holdups in the riser as well as liquid flow rates.

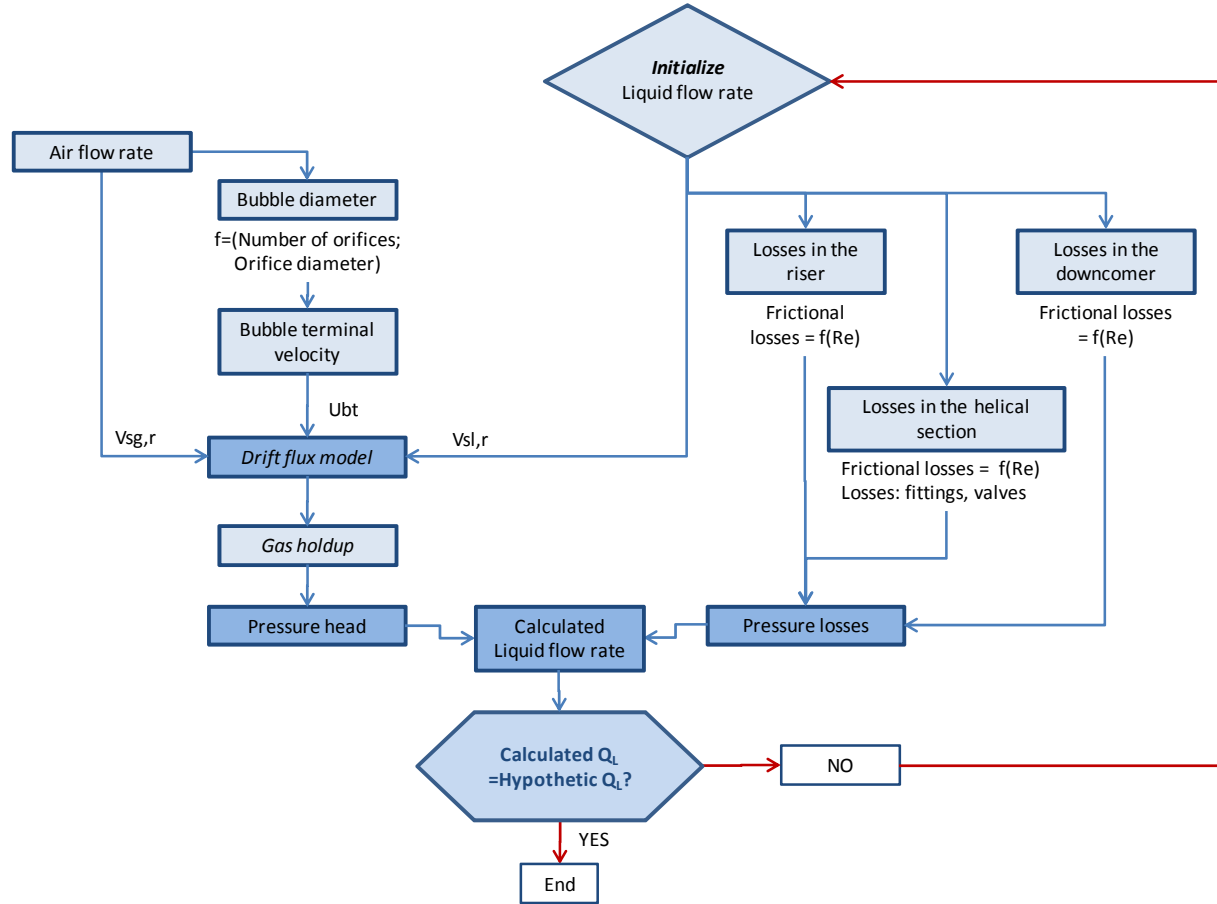


Figure IV.16. Algorithm to model the hydrodynamics of the helical airlift reactor.

First, a value of liquid flow rate is assumed in order to have liquid velocities in each section and according to the cross sectional area. Subsequently, pressure losses are estimated in each section of the reactor. At the same time, a second iterative process is performed to calculate the terminal bubble velocity, as shown in Tables IV.3 and IV.4. Knowing the riser superficial liquid velocity and the terminal bubble velocity, the next step is to determine the riser gas holdup (Equation IV.12) and the available pressure (Equation IV.7). Then, the liquid flow rate is calculated from total pressure losses and the available pressure in the riser (Equation IV.16). Finally, the calculated liquid flow rate is compared to the assumed value, minimizing the error. On the other hand, calculated gas holdups are compared to experimental results.

4.2 Modeling results

Following experimental results shown in Section 3.1, it is interesting to compare the tendency of total loss coefficients obtained in step 1 as well as those obtained after applying the mathematical regression (Equations IV.3 and IV.21). Figure IV.17 presents total loss coefficients obtained in steps 1 and 2 as a function of liquid flow rates.

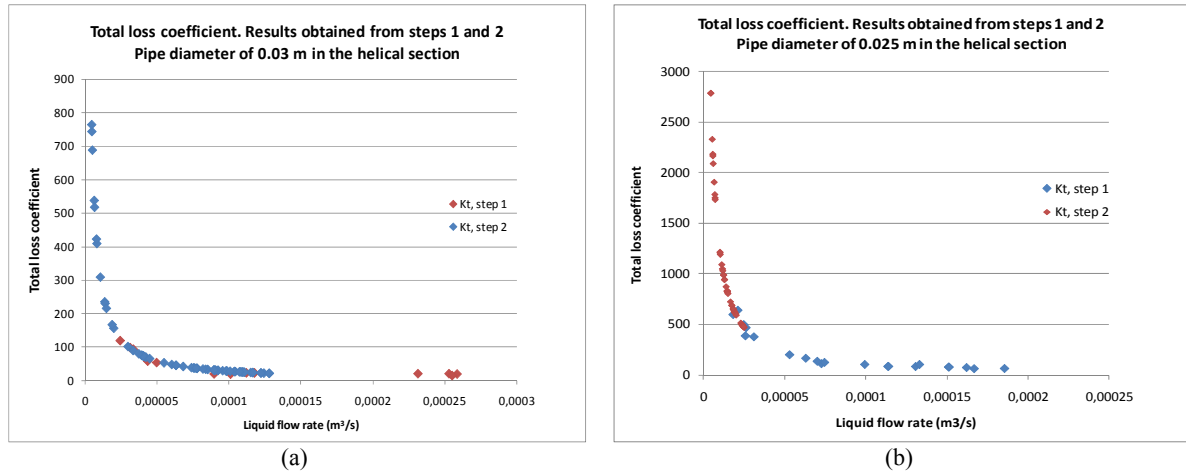
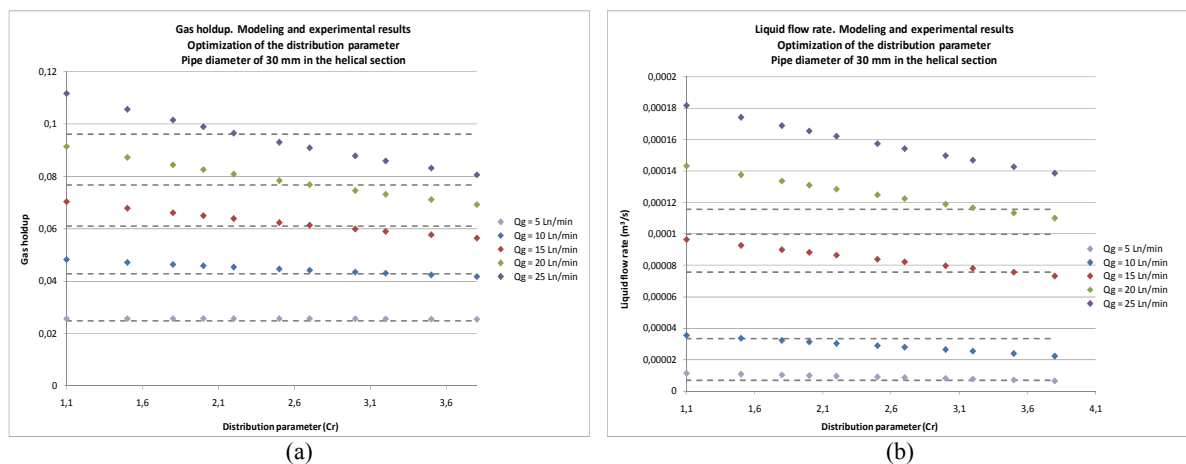


Figure IV.17. Total loss coefficients estimated in steps 1 and 2
a) For a pipe diameter of 30 mm; b) for a pipe diameter of 25 mm.

Results show that the mathematical regression presented in Equation IV.21 gives an appropriate approximation of frictional losses and thus, of the total loss coefficient in the helical section. The exponential tendency is maintained, as observed in Section 3.1, and it is valid for both pipe diameters tested in the helical section.

The next step is to estimate gas holdups and liquid flow rates by applying the iterative process presented in Figure IV.16. In order to obtain low deviations among modeling and experimental results, it is necessary to perform an optimization procedure to find the most appropriate distribution parameter presented in the Drift Flux Model (Equation IV.12). For that, two criteria are established: the averaged standard deviations among experimental and modeling values of gas holdups, and liquid flow rates have to be lower than 15%, both at the same distribution parameter.

Figure IV.18 shows values of gas holdups and liquid flow rates at different air flow rates, corresponding to several distribution parameters. Gray and pointed lines correspond to average experimental values.



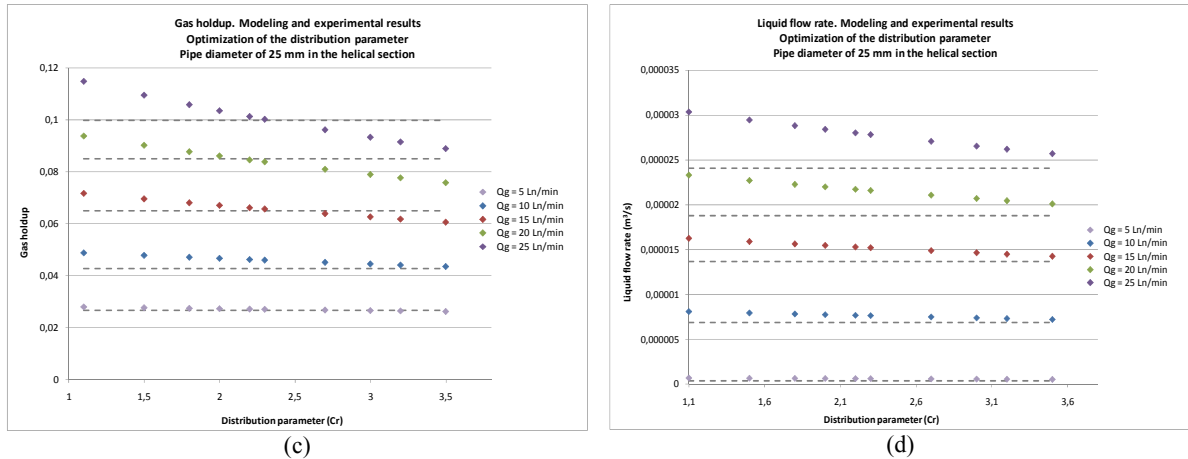


Figure IV.18. Liquid velocities in all sections of the reactor for a pipe diameter of 25 mm
a) Gas holdup, pipe diameter of 30 mm; b) Liquid flow rate, pipe diameter of 30 mm
c) Gas holdup, pipe diameter of 25 mm; d) Liquid flow rate, pipe diameter of 30 mm.

Results show that deviations among experimental and modeling results diminish once the distribution parameter increases from 1.1. Deviations are lower for values of gas holdups compared to liquid air flow rates (averaged deviations are 9 and 6% for gas holdups while deviations are around 15% for liquid flow rates).

Comparing values of liquid flow rates for the two pipe diameters, the highest deviation occurs for the pipe diameter of 30 mm installed in the helical section. An appropriate value of $Cr = 3.8$ is chosen since the averaged deviation is lower than 15% for the liquid flow rate and around 9% for the gas holdup. In this case, the highest uncertainty occurs for an air flow rate of 25 Ln/min (Figure IV.18b). On the other hand, a Cr value of 3.5 is preferred for the pipe diameter of 25 mm since the averaged deviation is 14% for liquid flow rates and 5.7% for gas holdups.

Figure IV.19 presents a comparison between modeling and experimental results of gas holdups. For air flow rates of 5 and 10 Ln/min, deviations are very low among experimental and modeling results for the two pipe diameters tested here. At higher air flow rates, the model seems to underestimate averaged values of gas holdup but still they are under the range of 15% deviations. This means that the model is suitable to estimate gas holdups in the riser.

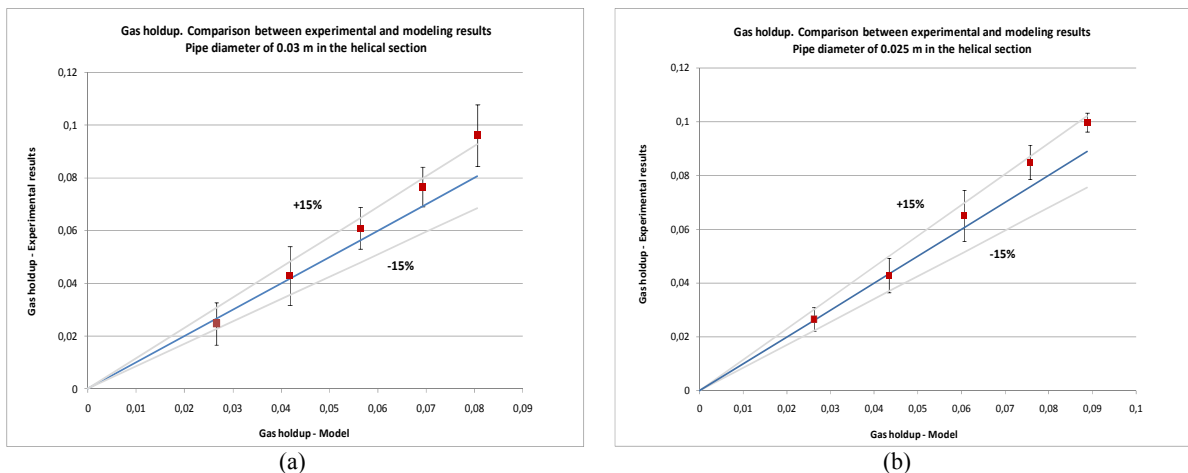


Figure IV.19. Riser gas holdup. Comparison between experimental and modeling results
a) for a pipe diameter of 30 mm; b) for a pipe diameter of 25 mm
Vertical bars represent standard deviation.

Figure IV.20 shows modeling and experimental values of liquid flow rates found for the two pipe diameters tested in this study.

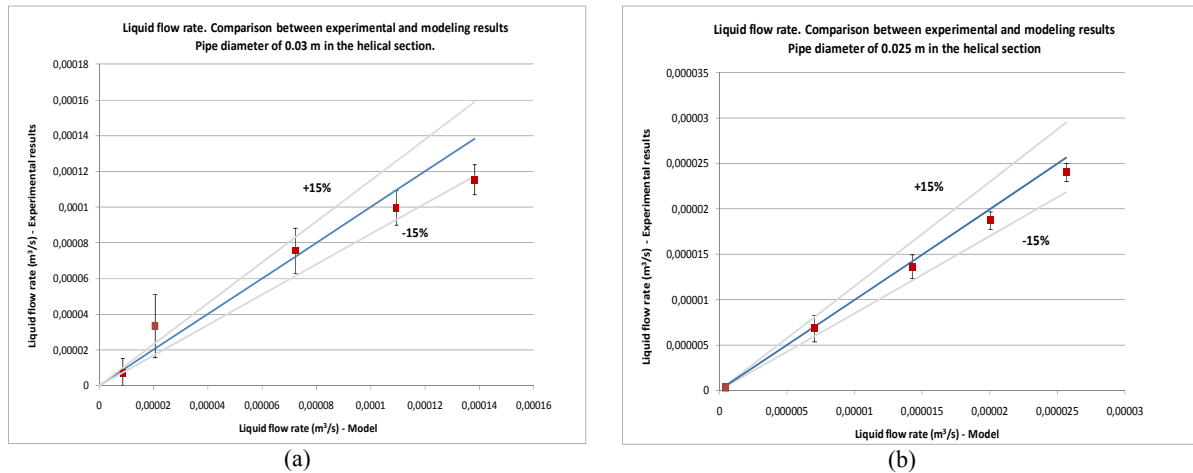


Figure IV.20. Liquid flow rates. Comparison between experimental and modeling results
a) for a pipe diameter of 30 mm; b) for a pipe diameter of 25 mm
Vertical bars represent standard deviation.

Figure IV.20a shows that the highest deviation between averaged experimental results and the model occurs for an air flow rate of 15 Ln/min, being higher than 15%. At air flow rates of 20 and 25 Ln/min, the model overestimates experimental results. On the contrary, for a pipe diameter of 25 mm, experimental average values are very close to modeling results (Figure IV.20b). Moreover, respective standard deviations of experimental results are in the range of 15% model deviations.

The reason of divergences observed in Figures IV.19 and IV.20 might be due to the estimation of bubble diameters and bubble rise velocities. Bubble diameters and velocities probably change due to coalescence and their random movement, and these factors are not taken into account in the expression proposed in the Drift-Flux model (Equation IV.12) (Wallis, 1969).

5. Comparison between the IAL and HAL reactors

The internal airlift reactor and the helical airlift reactor work under the same hydrodynamics principle: liquid circulation is the consequence of the pressure difference existing between the riser and the downcomer (plus the helical section in the HAL reactor) compartments, created by the air injection in the riser. In this sense, four fundamental parameters of the hydrodynamics are considered: gas holdup, liquid velocities, liquid circulation times, and power inputs.

Gas holdups depend on the air flow rate injected in the riser and thus, on superficial gas velocities. For the same air flow rates, gas holdups in the riser are higher in the HAL reactor compared to those obtained in the IAL reactor. They range from 2.4 to 9.6% in the HAL reactor and from 0.7 to 3.7% in the IAL reactor, at superficial gas velocities ranging from 0.6 to 3 cm/s. The reason is that liquid velocities in the riser are much higher in the IAL reactor than those obtained in the HAL reactor, meaning that a more important volume of gas is displaced to the atmosphere, resulting in lower gas holdup.

If gas holdups are more important in the HAL reactor, then specific interfacial areas should be higher if bubble diameters are identical. Estimating bubble diameters according to Davidson and Amick

results in bubble diameter being dependent on the number of sparger orifices (Equation IV.13). As sparger characteristics are maintained identical in the two reactors, interfacial areas are theoretically higher in the HAL reactor. This will result in having higher volumetric mass transfer coefficients compared to those obtained in the IAL reactor and in consequence, higher mass exchange between liquid and gas phases.

On the other hand, the main advantage of the HAL reactor is the riser height, which is 44 cm higher than in the IAL reactor. As studied in Chapter III, taller columns result in having lower levels of dissolved O₂ and higher CO₂ absorption along the column. Since the equivalent length in the helical section is higher than the downcomer height in the IAL reactor, the residence time of the liquid is much longer in the first. In consequence, the risk of reaching high levels of dissolved O₂ in the helical section is higher compared to the levels estimated in the downcomer of the IAL reactor. In the same manner, there is a higher risk of observing CO₂ limitation in the helical section.

Comparing liquid velocities, they result being higher in the IAL than in the HAL reactor. Liquid velocities change slightly when the air flow rate is increased in the HAL reactor, which is the opposite of that observed in the IAL reactor. For the low air flow rate of 5 Ln/min, the liquid circulation is low or zero in the HAL reactor.

In the helical section, the pipe diameter as well as the fact of having curvature pipes result in higher pressure losses compared to those in the downcomer of the IAL reactor, thus liquid flow rates are lower in the helical reactor. The advantage of the HAL reactor is that liquid flow rates in the helical section can be easily varied by modifying the curvature ratio (d/D_c) and the number of spires. In the IAL reactor, liquid velocities can be varied by varying draft tube diameter, which can be technically more complicated than modifying the helical geometry.

Table IV.5 show a comparison of liquid velocities between the two reactors studied here and reactors presented in the literature. Liquid velocities are referred to those in the illuminated section: in the IAL, liquid velocities correspond to the downcomer whereas in the helical reactor, they correspond to the helical section.

Table IV.5. Comparison among IALR, HALR and other experimental reactors

<i>Type of reactor</i>	<i>Working volume (L)</i>	<i>Superficial gas velocity (m/s)</i>	<i>Liquid velocity (m/s)</i>	<i>Circulation time</i>	<i>References</i>
IALR	21	0.006-0.048	0.11-0.25	6-14 (s)	This study
HALR, d=30 mm	37	0.006-0.048	0.047-0.16	5.2-18 (min)	This study
HALR, d=25 mm	34	0.006-0.048	0.014-0.049	22-79 (min)	This study
IALR	60	0.01-0.497	0.05-0.3	7-23 (s)	Freitas et al., 1998
IALR	100	0.001-0.01	0.017-0.078	20-90 (s)	Xu et al., 2002
IALR	11.3	0.0027-0.22	0.046-0.2	7.5-32.5 (s)	Contreras et al., 1999
Helical tubular	21	n.d.	0.193	5.2 (min)	Travieso et al., 2001

Regarding power inputs given by the gas and the total volume of the reactor, the power input is slightly higher in the helical airlift reactor than in the internal airlift reactor. Then, it is worth to analyze the relationship existing between the power input given by the gas and liquid velocities gained in the illuminated section (e.g. the downcomer in the IAL reactor and the helical section in the HAL reactor). Comparing both reactors, the energy given by the gas in the IAL reactor is better transferred

to the downcomer since higher velocities are observed in this section. On the contrary, much lower liquid flow rates are observed in the helical section while similar power inputs exist between the reactors. This means that, if it is desired to have liquid velocities in the helical section similar to those observed in the IAL reactor, higher power inputs are needed.

Finally, both reactors can be compared according to the surface occupied and the working volume. The purpose is to obtain the lowest ratio since it is desired to achieve the highest working volume in a small occupied surface. The helical section in the HAL is an external compartment that occupies larger surface compared to the IAL reactor and it depends on the coil diameter. For the two curvature ratios studied here, the surface-to-volume ratio are 24.6 and 26.7 1/m for pipe diameters of 30 and 25 mm, respectively. The highest ratio corresponds to the IAL reactor, being equal to 37 1/m.

6. Conclusions

In this work, a hydrodynamic study of a helical airlift photo-bioreactor has been presented. The reactor design is based on the concept of airlift as well as on the liquid circulation in coiled wound pipes. The work includes an experimental study, testing two different pipe diameters in the helical section, as well as the formulation of a hydrodynamic model.

The experimental study was performed in two parts. In the first, total loss coefficients in the helical section were estimated according to liquid flow rates and pressure losses. Results have shown that the total loss coefficient diminishes at higher liquid flow rates while pressure losses increase. As the total loss coefficient can be also expressed as a function of the friction factor, a correlation was proposed as a function of the curvature ratio and Reynolds number. The correlation, together with further measured differential pressures, has been used to estimate liquid flow rates in the second part of the experimental study. Results demonstrate that liquid velocities in the helical section are much higher than those in the riser and downcomer compartments.

Comparing liquid velocities between the two pipes tested in the reactor, they diminished when a 25-mm pipe diameter was installed. In consequence, liquid residence times were longer for this pipe diameter than for a 30-mm pipe diameter. The reason of lower liquid velocity and higher liquid residence time for a 25-mm pipe diameter is the increment of pressure losses due to the reduction of the pipe cross sectional area. On the other hand, results show that liquid velocities are lower than those observed in the IAL reactor and vice versa for liquid residence times. In both reactors, liquid velocities and residence times were related to the riser superficial gas velocities.

On the other hand, gas holdups were measured in the riser and they were related to superficial gas velocities and specific power inputs given by the gas. Results demonstrate that gas holdups are not affected by changing pipe diameters from 30 to 25 mm. Compared to the internal airlift reactor, gas holdups are higher since riser liquid velocities are low to displace an important gas volume. Referring to power inputs, results demonstrated that it is necessary to increase the power given by the gas, if it is desired to reduce pipe diameter in the helical section and to obtain higher liquid velocities.

The hydrodynamic model proposes the utilization of the Drift Flux Model and to perform a macroscopic energy balance of the reactor. The distribution parameter in the drift flux model has been modified in order to have small deviations among experimental and modeling results. For the two

pipes tested here, the fitted distribution parameter resulted in 3.5 for a 25-mm pipe diameter and 3.8 for a 30-mm pipe diameter, being higher than those usually employed to model internal airlift reactors.

The model proposed here is capable of predicting gas holdups and liquid velocities for superficial gas velocities ranging from 1.2 to 3 cm/s and pipe diameters of 25 and 30 mm in the helical section.

The designed helical airlift reactor presents several advantages over the studied internal airlift reactor: 1) riser gas holdup is higher, which means higher mass exchange between liquid and gas phases; 2) liquid flow rates can be easily modified as a function of pipe and coil diameter as well as the number of spires; 3) a light system supply can be installed inside the helical section, thus energy losses are lower.

On the other hand, if microalgae culture is performed in the HAL reactor, it is necessary to estimate theoretically the biomass production rate according to the light intensity reaching the helical section. Since the equivalent length of the coiled pipe is important, high levels of dissolved oxygen can be observed as well as carbon dioxide limitation. In addition, small pipe diameters in the helical section can bring the problem of bio-fouling, which limits light energy transport to the culture and demands constant cleaning.

7. References

- Ali, S. (2001). Pressure drop correlations for flow through regular helical coil tubes. *Fluid Dynamics Research* 28 , 295-310.
- Babcock, R., Malda, J., & Radway, J. (2002). Hydrodynamics and mass transfer in a tubular airlift photobioreactor. *Journal of Applied Phycology* 14 , 169-184.
- Borowitzka, M. (1999). Commercial production of microalgae: ponds, tanks, tubes and fermenters. *Journal of Biotechnology* 70 , 313-321.
- Chisti, M. (1989). *Airlift Bioreactors*. London: Elsevier.
- Contreras, A., Garcia, F., Molina, E., & Merchuk, J. (1999). Influence of sparger on energy dissipation, shear rate, and mass transfer to sea water in a concentric-tube airlift bioreactor. *Enzyme and Microbial Technology* 25 , 820-830.
- Coronel, P., & Sandeep, K. (2003). Pressure drop and friction factor in helical heat exchangers under nonisothermal and turbulent flow conditions. *Journal of Food Process Engineering* 26 , 285-302.
- Fadavi, A., & Chisti, Y. (2007). Gas holdup and mixing characteristics of a novel forced circulation loop reactor. *Chemical Engineering Journal* 131 , 105-111.
- Fan, L., Zhang, Y., Zhang, L., & Chen, H. (2008). Evaluation of a membrane-sparged helical tubular photobioreactor for carbon dioxide biofixation by *Chlorella vulgaris*. *Journal of Membrane Science* 325 , 336-345.
- Fox, R., McDonald, A., & Pritchard, P. (2004). *Introduction to Fluid Mechanics*. United States of America: John Wiley & Sons, Inc.
- Freitas, C., Fialova, M., Zahradnik, J., & Teixeira, J. (1999). Hydrodynamic model for three-phase internal- and external-loop airlift reactors. *Chemical Engineering Science* 54 , 5253-5258.
- Guo, L., Feng, Z., & Chen, X. (2001). An experimental investigation of the frictional pressure drop in steam-water two-phase flow in helical coils. *International Journal of Heat and Mass Transfer* 44 , 2601-2610.
- Hall, D., Acién, F., Canizares, E., Krishna, K., & Molina, E. (2003). Outdoor Helical Tubular Photobioreactors for Microalgal Production: Modeling of Fluid-Dynamics and Mass Transfer and Assessment of Biomass Productivity. *Biotechnology and Bioengineering* 82 , 62-73.
- Heijnen, J., Hols, J., van der Lans, R., van Leeuwen, H., Mulder, A., & Weltevrede, R. (1997). A simple hydrodynamic model for the liquid circulation velocity in a full-scale two-and three phase internal airlift reactor operating in the gas recirculation regime. *Chemical Engineering Science* 52 , 2527-2540.
- Idelchik, I. (1996). *Handbook of Hydraulic Resistance*. New York: Beggel House, Inc.
- Levy, S. (1999). *Two-phase flow in complex systems*. New York: John Wiley & Sons.
- Livingston, A., & Zhang, S. (1993). Hydrodynamic behaviour of three-phase (gas-liquid-solid) airlift reactors. *Chemical Engineering Science* 48 , 1641-1654.
- Lu, W., Hwang, S., & Chang, C. (1995). Liquid velocity and gas holdup in three-phase internal loop airlift reactors with low-density particles. *Chemical Engineering Science* 50 , 1301-1310.

- Merchuk, J., & Berzin, I. (1995). Distribution of energy dissipation in airlift reactors. *Chemical Engineering Science* 50 , 2225-2233.
- Naphon, P., & Wongwises, S. (2006). A review of flow and heat transfer characteristics in curved tubes. *Renewable and Sustainable Energy Reviews* 10 , 463-490.
- Richmond, A. (2004). *Handbook of Microalgal Culture. Biotechnology and Applied Phycology*. Oxford: Blackwell Science.
- Shaughnessy, E., Katz, I., & Schaffer, J. (2005). *Introduction to fluid mechanics*. New York: Oxford University Press.
- Tobajas, M., Garcia-Calvo, E., Siegel, M., & Apitz, S. (1999). Hydrodynamics and mass transfer prediction in a three-phase airlift reactor for marine sediment biotreatment. *Chemical Engineering Science* 54 , 5347-5354.
- Travieso, L., Hall, D., Rao, K., Benitez, F., Sanchez, E., & Borja, R. (2001). A helical tubular photobioreactor producing Spirulina in a semicontinuous mode. *International Biodeterioration & Biodegradation* 47 , 151-155.
- Van't Riet, K., & Tramper, J. (1991). *Basic Bioreactor Design*. New York: Marcel Dekker.
- Wallis, G. (1969). *One-Dimensional Two Phase Flow*. New York: McGraw-Hill.
- Xin, R., Awwad, A., Dong, Z., & Ebadian, M. (1996). An investigation and comparative study of the pressure drop in air-water two phase flow in vertical helicoidal pipes . *International Journal of Heat and Mass Transfer* , 735-743.

*Microalgae culture: integration and potential environmental impacts***Nomenclature****Abbreviations**

CO	Carbon monoxide
CO ₂	Carbon dioxide
GMO	Genetically modified organisms
LCA	Life Cycle Assessment
NO _x	Generic term for the mono-nitrogen oxides NO and NO ₂
N ₂ O	Nitrous oxide
PBR	Photobioreactor
PET	Polyethylene terephthalate
PUFA	Polyunsaturated fatty acids
PVC	Polychlorure de vinyle
SO _x	Generic term for the sulfur oxides like SO, SO ₂ , SO ₃
VOC	Volatile organic compound
WW	Wastewater

1. Introduction

The interest to cultivate microalgae for energy production is constantly increasing. Nowadays the main objective is to perform microalgae culture at large scale. Parallel to this idea, some studies appeared to identify potential advantages, disadvantages, and constraints of microalgae culture as well as upstream and downstream processes. The main subjects have been potential greenhouse gas emissions, energy consumption, and environmental impacts, trying to identify the *bottlenecks* of the entire process.

In the following sections, the culture of microalgae is presented as a process with requirements to be satisfied as well as products and co-products to be allocated. This process might produce wastes that have to be minimized. For this reason, the integration of microalgae culture in industrial processes is considered here, highlighting the use of wastewaters and the incorporation of transformation processes like anaerobic digestion.

In this context, the potential environmental impacts of microalgae cultivation are presented, emphasizing nutrients utilization, water consumption, and other elements that might alter the sustainability of the process. Here, the aim is to understand the transformations presented in the entire process, under the concept of industrial ecology, indentifying energy and materials flows as well as potential impacts to natural systems.

2. Integration of microalgae culture in industrial processes

2.1 The process of microalgae culture

The exploitation of algal biomass is a process that involves microalgae culture as well as their further treatment to obtain final products and manage the waste and effluents. To complete the information presented in Chapter I, Figure V.1 illustrates the whole process of microalgae culture, including forms of energy and required materials. Upstream processes supply fertilizers, energy in the form of electricity, heating, and cooling as well as water and carbon dioxide. On the other hand, downstream processes include all biomass treatments after cultivation (harvest, dewatering, drying, cell disruption, biodiesel production, anaerobic digestion, fermentation, etc). Effluents and waste management are also to be considered.

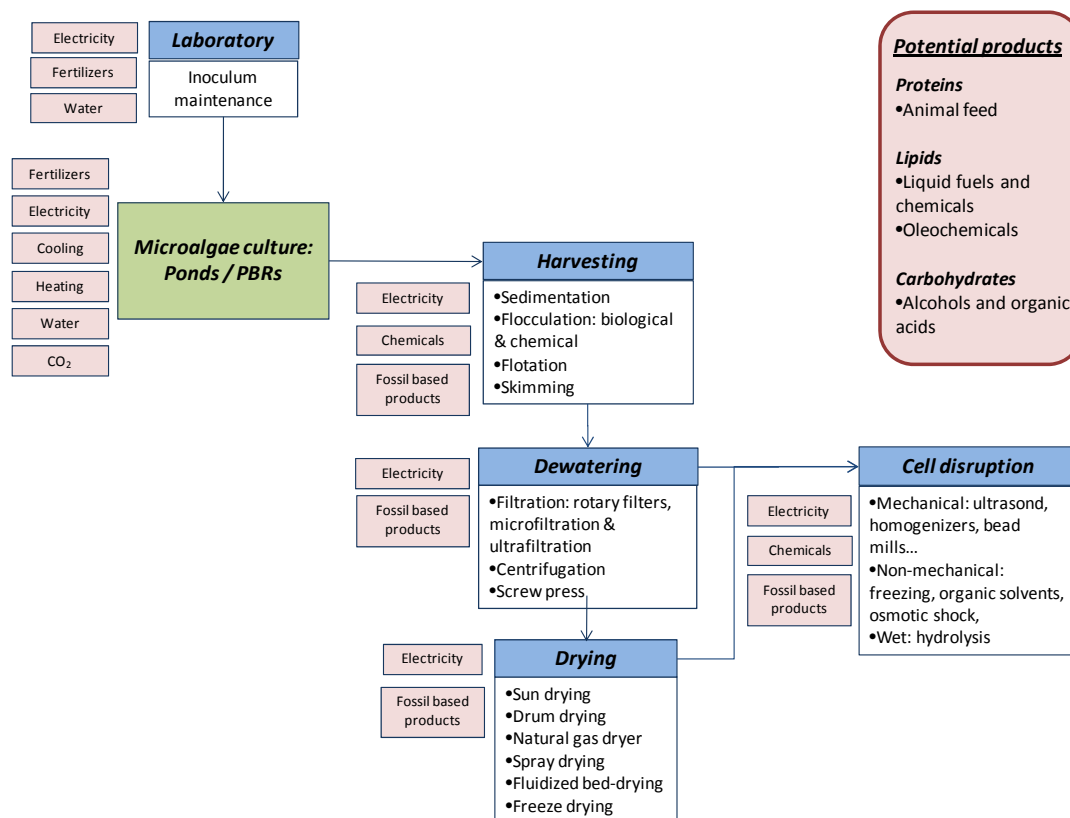


Figure V.1. Microalgae culture and biomass processing. Energy input and materials.

Cultivation of microalgae starts with inoculums of the species. To preserve the inoculums, it is necessary to have a well-cleaned chamber with appropriate temperature and light intensities. Sometimes laboratory vessels (e.g. erlen meyers), containing microalgae and the growth medium, are installed inside sterilized chambers to avoid any types of contamination. Here, electricity is the main energy consumption.

Subsequently, the cultivation system (open pond or photobioreactor) requires energy to create liquid circulation and mixing as well as to maintain the proper temperature. In raceway ponds, electricity is required to turn the paddle wheel while in photobioreactors, electricity is needed for liquid pumping, CO₂ transport, air compressing and/or mechanical stirring. Some fossil-based products, like lubrication products are needed here for pumps, compressors, etc. Depending on the location and the season, a heating/cooling system may be provided, increasing energy demand. On the other hand, all nutrients and carbon dioxide are supplied here.

Current harvesting methods are based on those employed in wastewater treatment plants. In open ponds, the most common methods are flocculation, sedimentation, flotation, and skimming. In flocculation, substances such as aluminum sulfate, ferric sulfate, and chitosan have been employed. Flocculation is advantageous for species with very small sizes like *Chlorella* and *Scenedesmus* (1 to 5 µm in diameter) and it is more efficient if biomass concentrations are higher (Richmond, 2007; Lardon et al., 2009). In sedimentation, a settling pond can be installed next to the culture, obtaining a more concentrated biomass at the bottom of the vessel. Generally, between 85 and 95% of the biomass is deposited at the bottom, composed of 3% dry algae (Richmond, 2007; FAO, 2009). Settling ponds are practical for managing large culture volumes. Dissolved air flotation, contrary to sedimentation, requires compression and thus energy, to promote biomass flotation.

In dewatering, the most well-known employed equipments are centrifuges and filters. In recent literature, the following centrifuges are the most recommended: decanter centrifuges, separator nozzle centrifuges, and self-cleaning plate separator centrifuge (Sadaznoff, 2006; Sander and Murthy, 2010; Stephenson et al., 2010). Centrifugation is a high-energy demand process, especially if the culture is very diluted (Wijffels and Barbosa, 2010). On the other hand, centrifugation is one of the preferable dewatering methods since high biomass concentrations can be reached. Current centrifuges are easy to clean and sterilize (Richmond, 2007). Referring to filters, rotary filters and chamber filters press are the most currently mentioned filtering equipments to dewater algal biomass (Lardon et al., 2009; Sander and Murthy, 2010).

Drying is an optional step that depends on the product desired to recover from algae. Similarly, the most appropriate equipment to dry biomass depends on the quality of the final product. If the aim is to extract lipids from algae, it is necessary to dry algae down to 9% of moisture in order to employ n-hexane (Sheehan et al., 1998a; Sander and Murthy, 2010). For that, belt dryer, drum dryer, and natural gas-fired filter have been proposed, reaching moistures between 3 and 4% (Richmond, 2007).

Several populations have dried biomass in the sun with food purposes. Sun dried species like *Spirulina platensis* have been largely consumed in Asia (Habib et al., 2008). Currently, it is questionable if algal biomass destined to produce lipids can be dried in the sun, since it appears that lipids loss their stability (Lardon et al., 2009). Sun drying depends on the culture location and it is a slow process that is not feasible at large scale (Becker, 1994; Brennan and Owende, 2010).

Figure V.2 illustrates different combinations of methods to harvest, dewater, and dry algal biomass. These examples are based on recent publications that have evaluated the feasibility of microalgae exploitation.

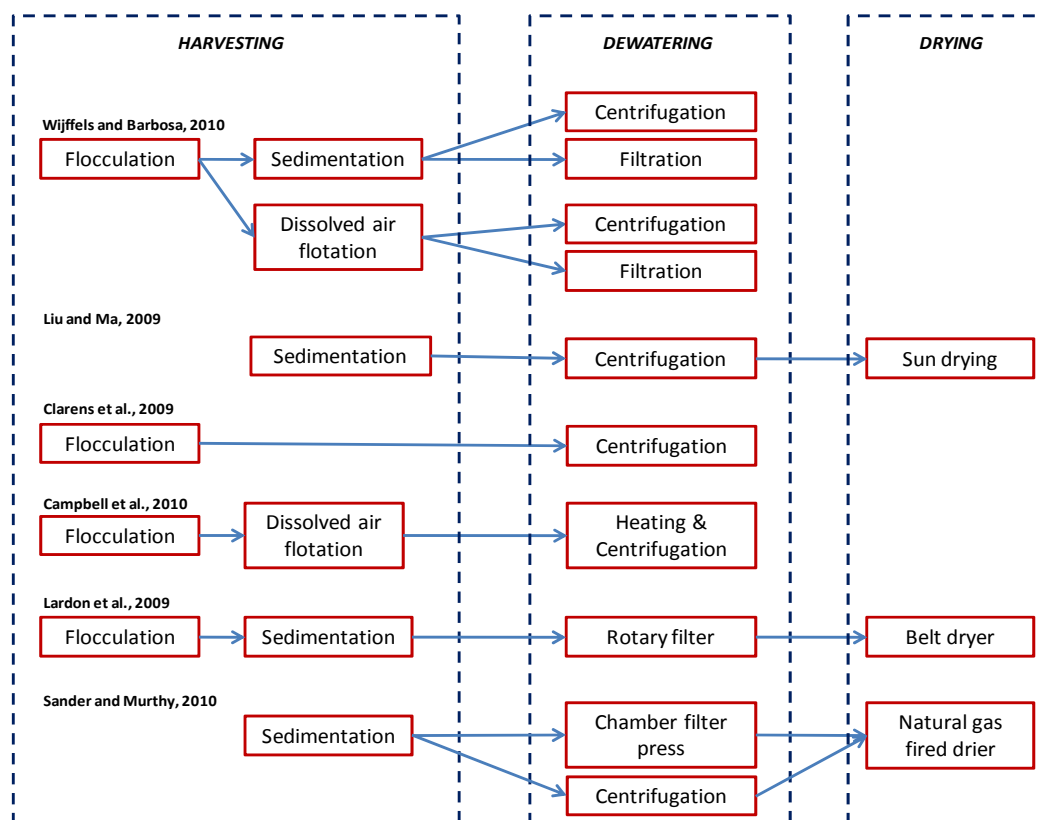


Figure V.2. Combinations of techniques for harvesting, dewatering and drying algae

From studies showed above, it appears that flocculation is a common method to start harvesting, facilitating sedimentation and flotation. Generally, after sedimentation or flotation, dry biomass is in the order of 3% in the algae slurry. The next step is to dewater algal biomass, as much as possible. Suggested equipments for dewatering do not handle very high liquid volumes, especially centrifuges.

After centrifugation, solid concentrations can reach 12 to 30% of dry algae matter (high concentrations have been observed in nozzle centrifuges) (Becker, 1994). The main advantage of rotary filters is that they are a total enclosed system, which preserves biomass composition. Compared to filter press, the dryness is higher. Dewatering is necessary if it is desired to increase dryness efficiency. Belt dryer is capable of producing a biomass paste with 90% of solids (Lardon et al., 2009). As mentioned previously, sun drying depends on the required product quality. If the algae paste is exposed in very thin layers, shorter times of exposition might be reached (Becker, 1994).

Microalgae cultivation and biomass treatment require energy and materials. For this reason, it is reasonable to think that integrating microalgae culture into an industrial process leads to energy savings, materials reuse, and minimizing wastes.

2.2 Industrial integration

Until nowadays, the sustainability of microalgae culture has been evaluated by few studies. Tools such as Life Cycle Assessment (LCA) and Environmental Impact Assessment (EIA) have been used to give an overview of constraints and advantages of the process. Most of these studies have been focused on microalgae cultivation in open ponds (Campbell et al., 2010; Sandy and Murthy, 2010), while studies about cultivation in photobioreactors are just beginning (Stephenson et al., 2010).

Results have demonstrated that, until nowadays, microalgae culture cannot be an isolated process (Clarens et al., 2009; FAO, 2009; Ferrel and Sarisky-Reed, 2010). The utilization of fertilizers implies high-energy consumption and costs. The energy consumed such as electricity, heat, cooling as well as the energy invested in harvesting, dewatering, and drying are not in agreement with the energy produced (Lardon et al., 2009; Sander and Murthy, 2010). Microalgae culture has to be integrated in production lines existing in facilities such as power plants, paper, cements and leather-processing industries. It is necessary to construct a closed-loop production system based on the principle of clean production where *“nothing is perceived as waste”*. In this context, the concept of biorefinery is pertinent:

“Biorefinery is based on converting series of renewable biomass streams via biochemical and thermochemical conversion pathways into an optimal range of products: biofuels, power and heat, biomaterials and green platform and bulk chemicals. All this must be achieved in as efficient a manner as possible by integrating conversion processes. In this sense, biorefining is analogous to the operations at refineries in the petrochemical industry.” (Biopact, 2007)

Therefore, it is indispensable to perform a detailed study in two complementary directions. In the first one, potential products, co-products, and wastes to be obtained should be well defined. In the second one, co-products and wastes of the industrial process should be studied in order to satisfy culture requirements. In this sense, several authors claim that a very appropriate option to reduce emissions and energy consumption consists in using wastewaters as source of nutrients and performing anaerobic digestion or fermentation to further produce energy (Sander and Murthy, 2010; Stephenson et al.,

2010). Until nowadays and according to recent studies, the most efficient integrated process for microalgae culture appears to be based on wastewater utilization, lipids extraction, and anaerobic digestion. The aim is to reduce energy consumption, fertilizers utilization, and greenhouse gas emissions (Yen and Brune, 2007; Lardon et al., 2009; Ras et al., 2010; Stephenson et al., 2010). Following this proposal, the next section presents advantages and disadvantages of utilizing wastewaters in microalgae culture.

2.2.1 Wastewater treatment and microalgae culture

The utilization of wastewaters in microalgae culture is, nowadays, a very attractive idea to reduce fertilizers consumption and therefore, the energy invested to produce these materials. On the other hand, this idea is attractive for wastewater treatment plants because it reduces the use of chemicals and it might result in energy savings (Clarens et al., 2010). The utilization of wastewaters in microalgae culture is limited by water characteristics since not every algae species can survive with high nutrient concentrations or the presence of other substances (e.g. organic acids, phenolic compounds, etc.). For example, high concentrations of medicines, disinfectants, and bacteria can inhibit microalgae growth (FAO, 2009).

Generally, wastewaters can be classified according to their source as domestic or industrial wastewaters. Domestic wastewaters include all waters coming from households. They contain carbohydrates, fats, soaps, detergents, proteins, and their decomposition products (FAO, 1992). Their urea content is an attractive source of nitrogen, in the form of ammonia, for algae. It has been proved that urea is an attractive nutrient for *Spirulina platensis*, *Chlorella pyrenoidosa*, and *Chlamydomonas snowiae* (Danesi et al., 2002; Lin et al. 2007; Richmond, 2007). However, it has been observed that algae have certain tolerance to ammonia. *Chlorella pyrenoidosa* and *Chlamydomonas snowiae* have resisted ammonia concentrations as high as 135 mg/L while other species like *Scenedesmus obliquus* are inhibited at ammonia concentrations higher than 34 mg/L (Lin et al., 2007). In some experimental studies, wastewaters had to be diluted since ammonia concentrations are too high for algae. Dilutions are in the range of 5 to 10% v/v (Lin et al. 2007; Hodaifa et al., 2009; Levine et al., 2010).

On the other hand, industrial wastewaters differ in their composition since they can come from all types of industrial plants, like steel producing companies, food industries, pharmaceutical laboratories, etc. In the ideal case, each industry has its own wastewater treatment plant, according to their liquid and sludge composition, to process the water to minimal concentrations of nutrients and metals imposed by the municipal wastewater treatment plant.

Treatment of wastewaters by algae is usually performed in stabilization ponds, in the tertiary treatment. Stabilization ponds can be constructed with depths ranging from 1 to 6 m (generally used to treat organic matter and pathogens) and with very short depths, around 30 cm (aiming at reducing nutrient concentrations). Water residence times vary from 4 to 10 days in high rate ponds while it can take from 20 to 100 days in conventional ponds (Ferrel and Sarisky-Reed, 2010). Examples of microalgae employed in stabilization ponds are *Chlorella* sp., *Scenedesmus*, *Micractinium* sp., and *Chlamydomonas* (Richmond, 2007).

As mentioned in Chapter I, heavy metals such as cadmium, lead, and mercury are toxic to organisms, even at low concentrations. Since microalgae are sensitive to free ion metals, they have been employed as pollution detectors in waters. In the process, microalgae first adsorb metal ions by using cell-wall components or extracellular cell-associated materials. Then, metal ions are absorbed and

bound with intracellular components, such as proteins. One the metal ions are bound, their toxicity diminishes. The entire process depends on algae species, type of heavy metal, biomass concentration, pH, temperature, and light intensities. Studies have demonstrated that some algae species are capable of sequestering metal ions such as copper, cadmium, nickel, gold, and chromium. Their performance is higher in waters with low concentrations of metals ions (Table V.2) (Richmond, 2007).

Experiences in wastewater treatment have demonstrated that it is very convenient to treat wastewater by a combination of bacteria and algae. Incorporating microalgae provides oxygen to bacteria, which are in charge of treating organic matter. The final products of oxidative bacteria and carbon dioxide are then taken by algae to perform photosynthesis. Bacteria are capable of degrading materials such as polycyclic aromatic hydrocarbons, phenolics, and organic solvents (Munoz and Guieysse, 2006, Ferrel and Sarisky-Reed, 2010). However, the resistance of algae to these compounds depends on microalgae species. Lin et al. found that, combined system with bacteria and algae (*Chlorella pyrenoidosa* and *Chlamydomonas snowiae*) results in higher nitrogen removal efficiencies than treating wastewater with only algae (Lin et al., 2009).

On the other hand, microalgae culture can produce negative effects on bacteria growth: pH increases during photosynthesis (since microalgae absorbs CO₂) as well as dissolved oxygen concentration and temperature. Additionally, bacteria might excrete metabolites that are algacides. In this combination, bacteria and algae growth rates should be in direct proportion in order to avoid limitation of whether O₂ or CO₂. A very low microalgae growth rate will limit oxygen available for bacteria while very low bacteria growth rate will limit CO₂ available for algae (Munoz and Guieysse, 2006).

In this sense, it is necessary to perform an in-depth study of algae and bacteria interaction as well as the characteristics of the water to be treated. In addition, it is mandatory to study effects of pH and temperature. pH promotes ammonia volatilization as well as precipitation of orthophosphate while temperature might increase or inhibit microalgae growth (Munoz and Guieysse, 2006).

Table V.I presents some experimental studies performed with different wastewaters treated by algae.

Table V.1. Experimental studies of wastewaters treated by microalgae.

<i>Algae specie</i>	<i>Type of wastewater</i>	<i>General composition</i>	<i>Conclusions</i>	<i>References</i>
<i>Scenedesmus obliquus</i>	Olive-oil mill wastewater	Vegetable water, olive and olive-oil washing waters	Algae assimilated nutrients contained in WW. High carbohydrates content due to nitrogen limitation	Hodaifa et al., 2009
<i>Chlamydomonas reinhardtii</i>	Three types of WW coming from different stages of the plant	Ranges of concentrations NH ₃ = 8.78-67 mg/L and total P = 1.25 to 120.6 mg/L	Removing rates: N = 55.8 mg/L.d; P=17.4 mg/L.d. Maximum algae productivity = 2 g/L.d	Kong et al., 2009
<i>Botryococcus braunii</i>	Secondarily treated sewage from domestic WW	NH ₃ = 15 mg/L, Phosphates = 11.5 mg/L	Lipids content was 7% higher in biomass when was growth in WW (compared with synthetic medium)	Orpez et al., 2009

Table V.1. Experimental studies of wastewaters treated by microalgae (cont'd).

<i>Algae specie</i>	<i>Type of wastewater</i>	<i>General composition</i>	<i>Conclusions</i>	<i>References</i>
<i>Chlorella vulgaris</i> and <i>Scenedesmus dimorphus</i>	Agro-industrial WW of a dairy industry & pig farming	NH ₃ = 36.3 mg/L and total P = 118.2 mg/L	Removing efficiencies NH ₃ : <i>Chlorella</i> : 30-95%, <i>Scenedesmus</i> : 55-95%. Phosphorus: approximately the same for both algae: 22-55%	Gonzalez et al., 1997
Algae: <i>Chlorella vulgaris</i> and bacteria: <i>Azospirillum brasilense</i>	Municipal WW: effluent of initial aerobic activated sludge	NH ₃ = 0.1-4.26 mg/L and total P = up to 5 mg/L	Removing efficiencies up to 100% ammonium, 15% nitrate, and 36% phosphorus	de-Bashan et al., 2003
<i>Neochloris oleoabundans</i>	Effluent of anaerobic digester using dairy manure	NH ₄ = 2100 mg/L. Different dilution ratios	Maximal assimilation of 90 to 95% of nitrate & ammonium. Fatty acid methyl esters 10 to 30% wt	Levine et al., 2010

Similarly, Table V.2 illustrates some examples of metal removing rates by algae.

Table V.2. Experimental studies of metals absorbed by microalgae

<i>Algae specie</i>	<i>Compound</i>	<i>Absorption removal rate</i>	<i>References</i>
<i>Scenedesmus obliquus</i>	Cobalt	0.82 mg/L.d	Travieso et al., 2002
<i>Chlorella vulgaris</i>	Zinc	114.2 mg/L.d	Travieso et al., 1999
<i>Scenedesmus acutus</i>	Chromium	3.5 mg/L.d	Travieso et al., 1999
<i>Chlorella vulgaris</i> /Alcaligenes sp.	Phenol	90 mg/L.d	Essam et al., 2006

Some disadvantages of treating wastewaters with algae can be enumerated as follows:

- The construction of stabilization ponds requires more land than chemical and mechanical treatment technologies (Ferrel and Sarisky-Reed, 2010).
- Since wastewater treatment with algae generally needs long residence times, it is possible that dissolved CO₂ would become a limiting factor. If it is desired to treat wastewaters only by algae, authors suggest proper monitoring of dissolved CO₂ and eventually, to inject CO₂ during wastewater treatment (Lin et al., 2007; Ferrel and Sarisky-Reed, 2010).
- Experimental studies have demonstrated that algae do not resist very high concentrations of nutrients. Instead, wastewaters have to be diluted in order to avoid growth inhibition (Lin et al. 2007; Hodaifa et al., 2009). This might result in a disadvantage since it would be necessary to add water to the system before treating with algae (this implies larger quantity of fresh water consumption). It would be necessary to perform further studies to find wastewaters that can be mixed with more concentrates in order to reduce fresh water consumption.

On the other hand, wastewater treatment with algae has the following potential benefits:

- Energy and cost savings since wastewater utilization might imply reduction of fertilizer consumption (Clarens et al., 2009). However, a detailed energy balance has to be performed if mechanical and chemical treatments are substituted by treatment with algae culture. If the

same mechanical equipment has to be employed in harvesting microalgae, energy and cost savings might not be reduced (Ferrel and Sarisky-Reed, 2010).

2.2.2 Anaerobic digestion and microalgae culture

Figure V.3 presents a flow diagram of energies and materials and the synergy among microalgae culture, wastewater utilization, biodiesel production, and anaerobic digestion.

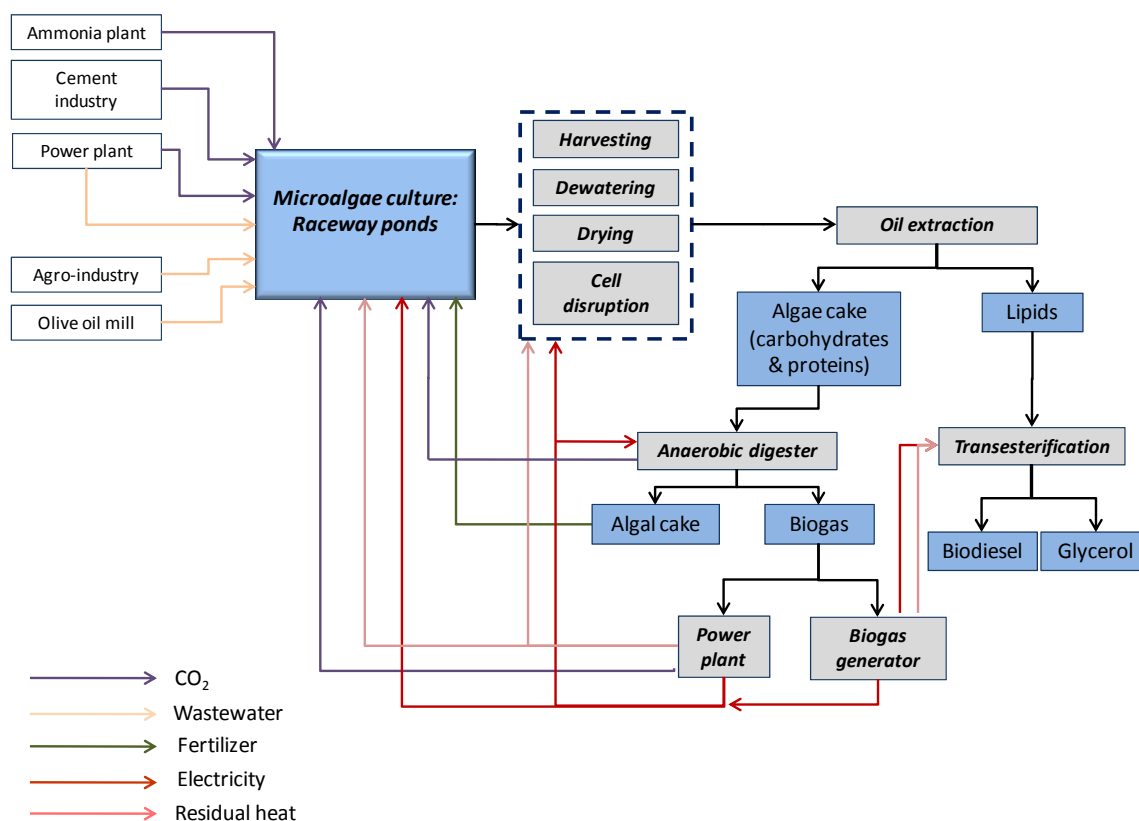


Figure V.3. Synergy among wastewaters, microalgae culture, biodiesel, and anaerobic digestion.

According to microalgae species, the inlet wastewater can be recovered from facilities such as cheese production plant, olive-oil mill, dairy industry, and pig farming (Gonzalez et al., 1997; Richmond, 2007; Hodaifa et al., 2009). The carbon dioxide can be obtained from ammonia and ethanol production plants, power plants, refineries, and cement industries. According to Sheehan et al., it is less expensive to recover CO₂ from ammonia and ethanol plants compared to others (Sheehan et al., 1998; Kadam, 2002; Campbell et al., 2010).

In microalgae culture and downstream processes (harvesting, dewatering, drying, and cell disruption), electricity is necessary for operating the equipments. Electricity can be obtained from the line (e.g. electricity coming from hydropower, nuclear...) or from a power plant next to the culture. Another alternative is to use a biogas generator (e.g. using a turbine, gas engine), if anaerobic digestion from algae residues is performed. On the other hand, chemicals are probably needed for flocculation.

Steam (residual heat) might be necessary for drying (e.g. to heat centrifuges) and it can be recovered from a power plant or another production plant next to the culture (Munoz and Guieysse, 2006).

According to the cultivated species, lipids can be extracted from the biomass to produce biodiesel. For this step, water is necessary to wash biodiesel from glycerol. The remaining biomass, mainly composed of carbohydrates and proteins, is sent to an anaerobic digester to produce biogas. One option is to separate methane from CO₂ (e.g. by performing water scrubbing), but this will add energy and water consumption. Then, carbon dioxide can be used in microalgae culture. If there is excess of CO₂ produced in the entire process, it can be used in industries that produce plastics, materials of construction, solvents, and others.

Table V.3 presents representative productivities of products and co-products of the system illustrated in Figure V.3. Values and assumptions are based on the work performed by Stepan et al., Cadoret and Bernard and Campbell et al. (Stepan et al., 2002; Cadoret and Bernard, 2008; Campbell et al., 2010). The assumptions are, as follows:

- The cultivation is performed in 200 raceway ponds of 5000 m², resulting in a total surface of 100 hectares,
- Two examples of lipids contents are taken into account: 30%wt of lipids (like the species *Phaeodactylum tricornutum*) and 70%wt of lipids (like *Dunaliella tertiolecta*) (Sheehan et al., 1998),
- The biomass productivity ranges from 10 and 200 ton of dry matter per hectare per year,
- The facility works 330 days during the year,
- The efficiency of oil extraction with hexane is 90%,
- The biodegradable volatile solids represent 65% of the dry biomass. In anaerobic digestion, this is completely transformed into methane while the rest forms an algae cake,
- The ratio of methane to carbon dioxide is 6:4.

Table V.3. Representative values of products and co-products from a closed system.

<i>References</i>	<i>Biomass productivity (g/m².d)</i>	<i>Biomass Productivity (ton/ha.y)</i>	<i>Biomass Production (ton/d)</i>	<i>Algal oil (30%wt) (ton/d)</i>	<i>Algal oil (70%wt) (ton/d)</i>	<i>Biodiesel (30%wt) (ton/d)</i>	<i>Biodiesel (70%wt) (ton/d)</i>	<i>Glycerol (30%wt) (ton/d)</i>	<i>Glycerol (70%wt) (ton/d)</i>	<i>Algae cake¹ (30%wt) (ton/d)</i>	<i>Algae cake¹ (70%wt) (ton/d)</i>
Sheehan et al., 1998	3.03	10	3.03	0.8	1.9	0.7	1.7	0.1	0.2	2.2	1.1
Stepan et al., 2002	9.09	30	9.09	2.5	5.7	2.2	5.2	0.2	0.5	6.6	3.4
Lardon et al., 2009	30.30	100	30.30	8.2	19.1	7.4	17.2	0.7	1.7	22.1	11.2
Cadoret and Bernard, 2008	60.00	200	60.00	16.2	37.8	14.6	34.0	1.5	3.4	43.8	22.2

¹Algae cake obtained after lipids extraction. Feedstock for anaerobic digestion.

<i>References</i>	<i>Biogas² (30%wt) (ton/d)</i>	<i>Biogas² (70%wt) (ton/d)</i>	<i>Methane (30%wt) (ton/d)</i>	<i>Methane (70%wt) (ton/d)</i>	<i>CO₂ (30%wt) (ton/d)</i>	<i>CO₂ (70%wt) (ton/d)</i>	<i>Algae cake³ (30%wt) (ton/d)</i>	<i>Algae cake³ (70%wt) (ton/d)</i>
Sheehan et al., 1998	1.4	0.7	0.9	0.4	0.6	0.3	0.8	0.4
Stepan et al., 2002	4.3	2.2	2.6	1.3	1.7	0.9	2.3	1.2
Lardon et al., 2009	14.4	7.3	8.6	4.4	5.8	2.9	7.7	3.9
Cadoret and Bernard, 2008	28.5	14.4	17.1	8.7	11.4	5.8	15.3	7.8

²Algal biomass transformed during anaerobic digestion into biogas (65%wt)

³Algae cake obtained after anaerobic digestion

Results show that the ratio between the produced oil and the dried algal biomass is of 0.24 (in mass) considering one microalga species containing 30% lipids. On the contrary, for species containing 70% lipids, the ratio increases to 0.6. This means that the energy produced from biodiesel ranges between 9.2 and 21 MJ/kg of algae dry biomass per day, according to lipid concentrations. If it is considered that biogas is directly used in a power plant or an engine (with thermal energy of 16.2 MJ/m³ (Goswami and Kreith, 2008)), the potential energy produced by algae in 100 hectares of cultivation ranges between 3.2 and 6.3 MJ/kg per day. On the other hand, the ratio between the biomass resulting after performing anaerobic digestion and the dried algal biomass is of 0.13 for algae containing 70%wt lipids and 0.26 for algae containing 30%wt lipids.

In experimental studies performed until nowadays, authors have suggested the utilization of algae, together with materials like vegetable and fruits wastes, chicken manures, and waste paper, to enhance the production of methane in anaerobic digestion. Generally, algae sludge has low C/N ratio which reduces anaerobic digestion performance. By adding rich carbon wastes, higher methane production rates can be reached (Yen and Brune, 2007). It is important to mention that not all species are easy to decompose in anaerobic digestion. The process performance depends on the characteristics of microalgae cell walls. If cell walls are already broken after extraction of lipids, the access to the organic material is easier, thus higher yields could be reached (Sialve et al., 2009).

Integration of microalgae culture in production chains involves several issues and requirements. Referring to the case showed in Figure V.3, some of these issues are as follows:

- Climate: location of microalgae culture according to the sunlight, rainfall, and evaporation,
- Land availability and conditions: whether it is desired to install the culture next to a production facility. Soil type is important if ponds are going to be utilized (study of permeability, materials of construction best adapted to the soil). Land is also required for downstream microalgae conditioning,
- Selection of the most appropriated microalgae specie, adapted to environmental conditions and capable of producing high lipid yields,
- Access to water (fresh or seawater) as well as wastewaters: this involves the installation of equipment for further conditioning of wastewaters, if necessary,
- Close access to flue gases: this includes the installation of equipments required to treat flue gases before CO₂ is sent to the culture. Since CO₂ transportation requires compression to liquid state, it implies an addition of energy consumption. In consequence, it is interesting to have access to carbon dioxide as close as possible,
- Easy access to electricity,
- Close access to heat and cooling sources: heat is necessary for drying. Cooling and heating are necessary to maintain culture temperature (especially if PBRs are employed).

According to the analysis presented by Chisti, three main aspects can be considered to improve microalgae culture: 1) to employ the *biorefinery* approach; 2) to optimize microalgae physical composition through genetic engineering; 3) design of photobioreactors with new advances (Chisti, 2007; Demirbas, 2010).

3. Potential environmental impacts of microalgae culture

From the experience obtained by performing microalgae culture in open ponds, following recent pilot projects and experimental studies, it is clear that alga cultivation has few controversial aspects with respect to environmental impacts. Similarly to agriculture, the addition of fertilizers in important quantities and high water consumption brings several questions about the sustainability of the process. The following section presents a general panorama about potential environmental impacts of carrying microalgae culture at large scale.

3.1 Nutrients

To perform intensive microalgae culture, it is necessary to provide the nutrients corresponding to the species. As mentioned in Chapter I, the most important nutrients are nitrogen and phosphorus. Generally, algae contain nitrogen in a range of 5 to 10% of dry weight and it is typically provided in the form of ammonium nitrate (NH_4NO_3), sodium nitrate (NaNO_3), ammonium chloride (NH_4Cl), and other elements such as $[(\text{NH}_4)_6\text{Mo}_7\text{O}_{24}, 4\text{H}_2\text{O}]$, $[\text{Cu}(\text{NO}_3)_2, 6\text{H}_2\text{O}]$. On the other hand, phosphorus content in dry biomass weight is lower, around 1%. It can be supplied in the form of potassium dehydrogen phosphate (KH_2PO_4), dipotassium phosphate (K_2HPO_4) and super phosphate ($\text{Ca}(\text{H}_2\text{PO}_4)_2$) (Becker, 1994; Kadam, 2002; Aslan and Kapdan, 2006; Richmond, 2007; Loubiere et al., 2008; FAO, 2009; Wijffels and Barbosa, 2010).

Considering that microalgae biomass has a composition of $\text{CO}_{0.48}\text{H}_{1.83}\text{N}_{0.11}\text{P}_{0.01}$ (Richmond, 2007, Sialve et al., 2009), nitrogen and phosphorus requirements can be estimated according to biomass productivities. Figure V.4 presents results following biomass productivities estimated nowadays. Here it is assumed that all nutrients provided to the culture are entirely absorbed by algae.

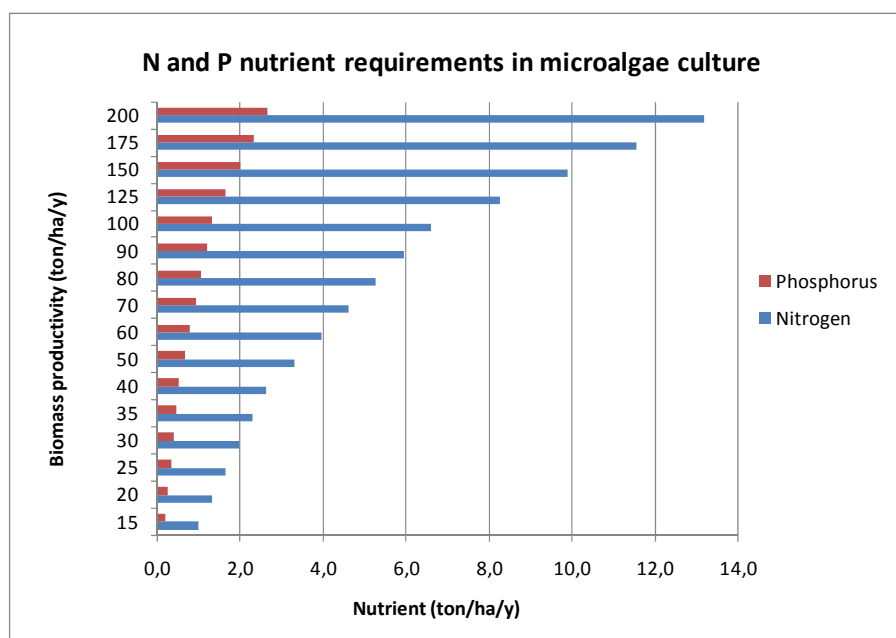


Figure V.4 Nitrogen and phosphorus requirements in microalgae culture.

According to Sialve et al., microalgae culture requires between 8 and 16 tons of nitrogen per hectare per year, which is true for biomass productivities higher than 125 ton/ha.year. Considering a biomass productivity of 25 g/m².d (approximately 82 ton/ha.year), nitrogen and phosphorus requirements are 5.4 and 1.1 ton/ha.year, respectively.

The high utilization of fertilizers affects the energy balance of microalgae culture (Lardon et al., 2009). The production of fertilizers is an energy intensive process, reaching levels of 50% of the total energy consumed in upstream algae culture, according to “cradle-to-gate boundary” study performed by Clarens et al. (Clarens et al., 2009). Nitrate production requires high energy while phosphates are exploited from mines (FAO, 2009).

Regarding gas emissions, intensive microalgae culture can release substances such as ammonia (NH_3) and nitrous oxide (N_2O) to the atmosphere, similarly to those observed in crop cultivations (FAO, 2009; Liu and Ma, 2009). Emissions might especially occur in ponds, since they are opened to the atmosphere. The volatilization of ammonia depends on environmental factors such as pH and temperature as well as mixing conditions and ammonium concentrations. High pH provokes the conversion of ammonium into ammonia, which is further volatilized. In an algae-based pond for waste water treatment, Zimmo et al. observed ammonia emissions ranging from 7.2 to 37.4 $\text{mg/m}^2\cdot\text{d}$ (Zimmo et al., 2003). Free ammonia contributes to rain acidification, vegetation damage, and it can be farther deposited onto the soil in the form of particulate ammonium, nitric acid, and oxides of nitrogen (FAO, 2009; Liu and Ma, 2009; EPA, 2010).

On the other hand, nitrous oxide is formed from the volatilization of ammonia and NO_x . Following the Kyoto Protocol, N_2O emissions are equivalent to 310 times CO_2 emissions in a time horizon of 100 years (Campbell et al., 2010). Studying potential environmental impacts from microalgae culture in open ponds to produce methanol, Liu and Ma found that 1.14 g of N_2O (353 g of CO_2 Eq.) are released per 1000 kg of dry microalgae. According to Campbell et al., these emissions are low compared to those observed in cultivation of crops for biodiesel production (Liu and Ma, 2009; Campbell et al., 2010). N_2O release in agriculture represents the second more important emissions, after methane emissions (Marta et al., 2010).

If nutrients rich wastewaters are not properly handled, instead they are rejected to the soil (being in direct contact with underground water), to lagoons or the sea, increasing the risk of promoting eutrophication in waters. Eutrophication occurs when there is an extraordinary growth of phytoplankton and other aquatic plant as consequence of an unbalance of nutrients (nitrogenous and phosphoric compounds) in waters. As the oxygen concentration is consequently altered, animal biodiversity is affected (de-Bashan and Bashan, 2004; Richmond, 2007). It has been largely observed in confined and coastal waters, like in the Baltic Sea, as consequence of discharging waters with high nutrient contents (e.g. waters coming from aquaculture, fertilizers production facilities and manure). According to Clarens et al. the potential of provoking eutrophication, taking into account fertilizers production and nutrient discharge from algae ponds, is lower than in cultivation of crops (Clarens et al., 2009). The reason is that algae are cultivated in ponds or in photobioreactors, thus there is no direct contact between the water and the soil, as it occurs in agriculture. There are more possibilities to prevent polluting discharges if it is required. However in ponds, there is a higher risk of observing water filtrations compared with photobioreactors, especially if ponds are not properly isolated or constructed with resistant materials.

To avoid eutrophication potential, it is necessary to perform an appropriated treatment of wastewaters (e.g. coming from harvesting, dewatering or drying), if they cannot be further employed in other processes. On the contrast, if wastewaters in downstream processes could be recycled, it would be necessary to perform an in-depth study about nitrogen and phosphorus required, consumed by the culture, and present in the system after evaporation. The objective is to estimate the availability of

nutrients as well as addition of further nutrients (Nouals, 2000; Sazdanoff, 2006; Wijffels and Barbosa, 2010).

Moreover, authors have suggested the utilization of the algae cake resulting from the anaerobic digestion of remaining biomass after lipids extraction. Generally, this algae cake is rich in nutrients, in the form of ammonium and phosphates (Lardon et al., 2009; Campbell et al., 2010).

On the other hand, high nitrogen concentrations in water and algae biomass can inhibit further conversion processes. In anaerobic digestion, it is well known that high nitrogen concentrations result in high free ammonia that inhibits methanogen bacteria, reducing the performance of the process. However, the inhibition degree depends on the substrate, acclimation period, and operating conditions. (Lardon et al., 2009; Sialve et al., 2009).

As some microalgae species have demonstrated that lipid contents increase under nitrogen starvation, the utilization of fertilizers associated to these species is lower. In consequence, potential impacts like acidification and eutrophication are less important and thus more favorable than in cultivation of other microalgae species (Lardon et al., 2009). In this sense, it is necessary to evaluate eutrophication potential according to the species to be cultivated and thus, according to required nutrients.

Concluding, it is very important to control adequately nutrients required by algae and those available in wastewaters. First, algae appear to be sensible to nutrient concentrations, defining their productivities and their final composition. Second, improper handling of fertilizers is associated with negative environmental impacts such as acidification, abiotic depletion, and toxicity (Liu and Ma, 2009). And third, there are nutrients available in wastewaters, which increase the importance of performing microalgae culture.

3.2 Water consumption

Water consumption in microalgae culture depends on several factors, starting by the type of cultivation system utilized. As explained previously, in open ponds water losses are high due to evaporation, whereas this problem is less accentuated in photobioreactors. According to Vonshak, water evaporation in open ponds can be as high as 5 and 6 mm per day. In the study performed by Sander and Murthy, evaporation in open ponds was estimated as 10% of the total volume during four days of cultivation (Sander and Murthy, 2010).

As suggested by Lardon et al., rainfall can be collected to be used in cultivation. In the Mediterranean climate, the balance between water evaporation and rainfall results in 0.8 mm water losses per day (Lardon et al., 2009). Assuming the same dimensions of an open pond proposed by these authors (10-m wide, 100-m long and 30-cm deep), water losses results in 0.27% of the pond volume, which is lower than that proposed by Sander and Murthy (table V.4) (Sander and Murthy, 2010). To collect rainfall for microalgae culture, it is necessary to prepare the water with the most appropriated nutrients, pH, and temperature. The balance between water evaporation and rainfall depends greatly on the culture location, as consequence of the local radiation, temperature, and rain frequency and volume.

On the other hand, rain water can be utilized to dilute wastewaters if the nutrients are too concentrated for the algae species. In the study performed by Lardon et al., they assumed that open ponds have to be washed every two months. The washing frequency might depend on the evaporation rate since

salts and other elements can be more concentrated and deposited in the pond (Ferrel and Sarisky-Reed, 2010). According to the species, algae might be more or less sensible to salts and other elements concentrations (e.g. CaCO_3), thus washing becomes more frequent. In this case, rain water can supply the water used for washing. Wastewaters resulting after flashing might contain traces of elements and non-negligible salt concentrations.

Some authors suggest that water after algae harvesting (e.g. water remaining in settling ponds) can be recycled back to the culture (Stepan et al., 2001; Sadaznoff, 2006). Enterprises like PetroAlgae affirm that 98% of the water employed in closed ponds is recycled. However, Lardon et al. claimed that waters remaining after harvesting cannot be recycled, estimating that the total water loss in the culture system, including water to produce CO_2 , fertilizers and electricity, is of 4 L/kg of dry algae (Lardon et al., 2009)

When photobioreactors are utilized in microalgae culture, losses due to evaporation are very low. Filtrations in the system results in water losses, however this should be constantly monitored. Since photobioreactors are closed systems that might have small sections and corners (like in flat panel), the formation of biofilm (algae attached to reactor wall) might result in increasing washing frequencies, thus increasing water consumption.

One method to control temperature in photobioreactors placed outdoors is spraying cool or hot water over bioreactor surface, as it is in the case of the pilot photobioreactor constructed by Thallia Pharmaceuticals S.A. (Nouals and Isambert, 2000). This increases total water consumption if it is not collected and reused in the system. According to Stephenson et al., if water is sprayed to tubular photobioreactor in a hot weather, evaporation losses are estimated to be between 1 to 2 liters of water per day per m^2 tube surface (Stephenson et al., 2010). In a pilot scale proposed by Camacho et al., the solar receiver was submerged in a pool placed outdoors for temperature control. The water was maintained at determinate temperature by cooling (Camacho et al., 1999). In this case, water evaporation has to be added to the total water consumed in the photobioreactor, which will probably result in very high water consumption (especially in zones like Cartagena, Spain).

Wijffels et al. talked about the utilization of sea water to cool closed microalgae culture, as it is used today in power plants (Wijffels et al., 2010). In this case, it will be necessary to respect municipal policies about water composition, the presence of trace metals as well as water temperature, before it is sent back to the sea.

Table V.4 presents results of water consumption from some studies. Values shown here are mostly for water evaporation. To extrapolate given values to other unit references, it was assumed that:

- there is a dry biomass productivity of $25 \text{ g/m}^2 \cdot \text{d}$,
- open ponds have a surface of 5000 m^2 and 0.3-m depth,
- oil extraction efficiency is 90%,
- algal biodiesel has a heating value of 41.6 MJ/kg ,
- density of algae biodiesel is 870 kg/m^3

Table V.4. Water consumption and losses in microalgae culture

<i>Assumptions</i>	<i>Water consumption</i>	<i>Water losses (L/kg biomass)</i>	<i>Water losses (L/MJ biodiesel)</i>	<i>References</i>
Open ponds	Evaporation: 2.5% of the total volume culture per day	193.2	5.1	Sander and Murthy, 2010
Open ponds	Evaporation: 6 mm per day (2% of pond volume)	240	6.3	Vonshak, 1997
Rainfall is recuperated and used in the pond	Total water losses in the pond: 300 mm/year (0.27% of pond volume per day)	32.8	0.87	Stephenson et al., 2010
Open ponds	Total water losses: back to the sea	472.5	11.34	Campbell et al., 2010
Open ponds	Total water losses: from microalgae culture to distribution and marketing of biodiesel	33.43-685.5 (average 225.7)	0.88-18.1 (average 5.95)	Harto et al., 2010
Closed systems: PBRs		31.34-65.83 (average 46)	0.82-1.73 (average 1.2)	

Results of water losses shown for open ponds are in the range of those proposed by Harto et al. As it is expected, water losses are lower in closed systems than in open ponds. If rainfall is collected and used in open ponds, water losses are very similar to the minimal losses found in closed systems (Harto et al., 2010).

Regarding these studies, it is reasonable to think that further research is needed. In-depth studies are required about water consumption in upstream and downstream process like fertilizers production, drying, heating, cooling, biodiesel production, and facility construction.

3.3 Other sources of environmental impacts

Similar to an industrial process, the cultivation of microalgae has other sources of environmental impacts that are directly and indirectly related to the process. It is obvious that installation of open ponds and photobioreactors do not require arable-land thus it is feasible to occupy surfaces as roof facilities. However, the production of algal biomass on large scale in open ponds and photobioreactors require large surfaces that might be difficult to have on roofs or close to an industrial facility.

Authors propose performing microalgae culture in confined waters like lakes, lagoons and in closed surfaces in coastal areas (Wijffels and Barbosa, 2010, NASA, 2009). This might result in an alteration of sea water composition since intensive microalgae culture requires addition of nutrients such as nitrogen and phosphorus. In addition, this might result in uncontrolled algae blooms that provoke eutrophication of the confined waters, damaging biodiversity. Environmental problems can even induce cluttering of confined waters.

If the aim is to perform microalgae culture in photobioreactors, it is important to study the availability of transparent materials that can accomplish it with high transmissivity. These materials have to be recyclable as well as to have positive energy and GHGs balances, including a proper lifetime. As an example of materials utilized in photobioreactors, the enterprise “Strategic Science Consult GmbH” uses polyethylene terephthalate (PET) to construct inclined flat panels. Other materials such as

polymethyl metacrylate (PMMA or Perspex) are considered to build photobioreactors (Stephenson et al., 2010; Wijffels and Barbosa, 2010)

The utilization of substances such as aluminum sulphate, ferric chloride, and ferric sulphate in flocculation can be absorbed by the biomass which, if the final end is to feed animals, can be toxic for those that accumulates aluminum (Richmond, 2007). The presence of excessive metals in algae might transport the problem to other elements. For example, if pyrolysis of biomass with high metals concentrations is performed, the resulting oil can contain non-negligible concentrations of metals and some of them might be volatilized (Menendez et al., 2005, Stals et al., 2010). Therefore, it is important to study methods to promote bioflocculation (e.g. by modifying pH or CO₂ injection), which is specific of the species (Munoz and Guieysse, 2006).

The solvent n-hexane has been largely used for oil extraction from soybean. During the process of oil extraction, n-hexane releases have increased emissions of hydrocarbons. After the extraction, certain concentrations have been observed in crushing plants (Sheehan et al., 1998a). Therefore in oil extraction from algae, the question resides whether there are important n-hexane emissions to the atmosphere or there is high residual quantity in the algal paste after the extraction of lipids. n-hexane is a solvent derived from petroleum that has shown negative effects in humans, especially in the respiratory, optical, and nervous system (OEHHA, 2010). According to Lardon et al., if the process of soybean oil extraction is considered similar to that of algal based oil, 2 g of hexane are lost per one kilogram of algal biomass. Stephenson et al. state that the ratio of hexane to algae slurry is of 0.5 (Lardon et al., 2009; Stephenson et al., 2010).

Other substances such as VOC's, NO_x, CO, SO_x, and particulate matters can be also emitted to the atmosphere. Potential sources are flue gases from industrial facilities (if they are integrated to the process of microalgae), production of fertilizers (if they are required), electricity generation, and transportation (e.g. from on-site culture to biodiesel production facility). Solid wastes may include wastes from wastewater treatment (whether wastewaters are treated before being used in microalgae culture), waste oil, and grease skimmed from biodiesel conversion process (Liu and Ma, 2009; Sander and Murthy, 2010).

The utilization of substances such as peroxyacetic acid solution and ethanol to sterilize photobioreactors implies proper disposal (Loubiere et al., 2008). If these waters are rejected to the soil, confined waters or the ocean, further problems related to composition and biodiversity might occur. On the other hand, materials employed in piping like PVC also imply proper handling. It is well known that seawater can be corrosive to many materials for pipelines. In consequence, it is necessary to observe if trace particles are carried by the water.

To improve the efficiency of microalgae culture, authors propose the cultivation of genetically modified algae. Until nowadays, cyanobacteria are the most studied genetically. The aim of altering algae genetics is mainly to increase accumulation of lipids, H₂ production and photosynthesis efficiency (by minimizing chlorophyll antennae) (Skjanes et al., 2007; Cadoret and Bernard, 2008; Melis, 2009). In this context, these algae must be cultivated in photobioreactors to avoid any intromission to natural systems that can affect local biodiversity. Mutant and modified algae might affect the equilibrium of the species.

Finally, it is well known that environmental impacts and energy consumption are proportional, as to those which are related to the energy processes. Therefore if a specific microalgae cultivation system

implies high energy demand, the potential negative impact on the environment will be greater as well (Lardon et al., 2009; Stephenson et al., 2010). For this reason, it is indispensable to develop parallel studies including potential environmental impacts and energy consumption, aiming at obtaining positive balances over the entire system.

4. Conclusions

The exploitation of algal biomass involves microalgae culture as well as upstream and downstream processes. To accomplish each step, it is necessary to provide some types of energy and materials: electricity, cooling, and heating are mostly the forms of energy consumed while fertilizers, water, carbon dioxide, and some fossil based products are the materials needed for the culture.

To fulfill the need of fertilizers, wastewaters are considered today as potential sources. Depending on their provenance, they can contain nitrogen and phosphorus concentrations demanded by algae. While some algae species absorb these nutrients, they treat wastewaters promoting energy savings and avoiding greenhouse gas emissions by wastewater-treatment plants. If they are coupled with bacteria, the performance of the treatment can increase. However, microalgae can be very sensible to high nutrient concentrations thus; it might be necessary to either pre-treat wastewaters or to dilute them.

Downstream processes of microalgae culture include harvesting, dewatering, drying, and cell disruption. The addition of chemical substances in flocculation increases harvesting efficiencies in sedimentation and dissolved air flotation. In dewatering, techniques like filtration, centrifugation, and filter press are employed, either separately or in combination. The choice depends on the physical characteristics of the species and the desired quality of final products. To dry, equipments such as natural gas drier and belt drier have been employed while sun drying remains as the simplest option.

At the present time, authors propose that microalgae culture be integrated in production lines existing in industrial facilities. To achieve a low-energy-demand process, it is necessary to promote an exchange among products, co-products, and wastes between the facility and microalgae culture. It is essential to apply the concept of biorefinery and the principles of industrial ecology and cleaner production.

Some studies agree that coupling biodiesel production and anaerobic digestion, while employing wastewaters as fertilizers, is a promising example of integrating processes. Once algal biomass is dried, algal oil can be extracted and transformed into biodiesel. The remaining biomass, rich in proteins and carbohydrates, can be exposed to anaerobic digestion to produce biogas for electricity generation. Algae cake might be reused in microalgae culture. In this synergy products such as biodiesel, biogas (or eventually methane), glycerin and potentially algae cake can be valuable feedstock for transportation, electricity generation, and feed for animals. Different forms of energy like electricity and heating can be reused in the process while diminishing energy demand and greenhouse gas emissions.

Regarding potential environmental impacts, high concentration of nutrients in open waters can lead to ammonia volatilization and N₂O emissions. The risk is higher in open ponds compared to photobioreactors. If high nutrient concentrations are present in wastewaters and are not properly handled, environmental problems such as eutrophication might occur in confined waters nearby.

Water consumption in microalgae culture accounts for the water consumed in upstream (e.g. fertilizers production), cultivation, and downstream processes. Most of studies performed until nowadays only take into account the water consumed during microalgae culture. Cultivation in open ponds appears to require more water than photobioreactors due to evaporation. Evaporation rates depend on the climate, thus is a local and seasonable parameter.

Several questions and issues still remain open in the process of microalgae culture. It is necessary to perform in-depth studies about:

- The best microalgae species to exploit the desired components. As products require further transformation, their characteristics have to be suitable for conditions of processes. If no further transformation is performed, then it is necessary to evaluate its potential utilization in the market
- The effect of environmental conditions on microalgae species and the culture, especially if it is outdoors. Here, the effect of wastewater composition on microalgae is included.
- Industrial facilities capable of providing microalgae culture requirements.
- Methods to recycle/reused water and nutrients as well as to avoid pollution and energy consumption as much as possible.

The challenge is to construct an integrated process which could guarantee a positive balance with respect to energy consumed-produced, greenhouse gas emissions emitted-saved and zero environmental impacts.

5. References

- Aslan, S., & Kapdan, I. (2006). Batch kinetics of nitrogen and phosphorus removal from synthetic waste water by algae. *Ecological Engineering* 28 , 64-70.
- Becker, E. (1994). *Microalgae: biotechnology and microbiology*. New York: Cambridge University Press.
- Benemann, J., Van Olst, J., Massingill, M., Weissman, J., & Brune, D. (s.d.). The Controlled Eutrophication Process: Using Microalgae for CO₂ Utilization and Agricultural Fertilizer Recycling. *Biopact*. (2007) An in-depth look at biorefinery concepts [online] Available from: <http://news.mongabay.com/bioenergy/2007/07/in-depth-look-at-biorefinery-concepts.html> [Accessed october 2010]
- Brennan, L., & Owende O. (2010). Biofuels from microalgae - A review of technologies for production, processing, and extractions of biofuels and co-products. *Renewable Sustainable Energy Review*, 14 , 557-577.
- Cadoret, J., & Bernard, O. (2008). La production de biocarburant lipidique avec des microalgues : promesses et défis. *Journal de la Société de Biologie* 202 , 201-211.
- Camacho, F., Acien, F., Sanchez, J., Garcia, F., & Molina, E. (1999). Prediction of dissolved oxygen and carbon dioxide concentrations profiles in tubular photobioreactors for microalgal culture. *Biotechnology and Bioengineering* 62 , 71-86.
- Campbell, P., Beer, T., & Batten, D. (2010). Life cycle assessment of biodiesel production from microalgae in ponds. *Bioresource Technology* , in Press .
- Chisti, J. (2007). Biodiesel from microalgae. *Biotechnology Advances* , 25, 294–306.
- Clarens, A., Resurreccion, E., White, M., & Colosi, L. (2009). Environmental Life Cycle Comparison of Algae to Other Bioenergy Feedstocks. *Environmental Science and Technology*, in Press .
- Danesi, E., Rangel, C., Carvalho, J., & Sato, S. (2004). Effect of reducing the light intensity on the growth and production of chlorophyll by *Spirulina Platensis*. *Biomass and Bioenergy* 26 , 329-335.
- de-Bashan, L., & Bashan, Y. (2004). Recent advances in removing phosphorus from wastewater and its future use as fertilizers. *Water Research* 38 , 4222-4246.
- Dermibas, A. (2010). Use of algae as biofuel sources. *Energy Conversion and Management* 51 , 2738-2749.
- EPA. (2010). *Nitrous Oxide*. [online] Available from: U.S. Environmental Protection Agency: <http://www.epa.gov/nitrousoxide/sources.html> [Accessed September , 2010]
- Essam, T. M. (2006). Biological treatment of industrial wastes in a photobioreactor. *Water Science Technology* 53 , 117–125.
- FAO. (1992). *FAO Irrigation and Drainage Papers*. [online] Available from: Wastewater characteristics and effluent quality parameters: <http://www.fao.org/docrep/t0551e/t0551e03.htm> [Accessed September 2010]
- FAO. (2009). *Algae-based biofuels: A Review of Challenges and Opportunities for Developing Countries*. Rome: Food and Agriculture Organization of the United Nations.
- Ferrel, J., & Sarisky-Reed, V. (2010). *National Algal Biofuels. Technology Roadmap*. Maryland: U.S. Department of Energy. Office of Energy Efficiency and Renewable Energy.

- Gonzalez, L., Canizares, R., & Baena, S. (1997). Efficiency of ammonia and phosphorus removal from a Colombian agroindustrial wastewater by the microalgae *Chlorella vulgaris* and *Scenedesmus dimorphus*. *Bioresource Technology* 60 , 259-262.
- Goswami, Y., & Kreith, F. (2008). *Energy Conversion*. Boca Raton: Taylor & Francis Group.
- Habib, M., Parvin, M., Huntington, T., & Hasan, M. (2008). *A review on culture, production and use of Spirulina as food for humans and feeds for domestic animals and fish*. Rome: Food and Agriculture Organization of the United Nations (FAO).
- Hodaifa, G., Martinez, M., & Sanchez, S. (2008). Use of industrial wastewater from olive-oil extraction for biomass production of *Scenedesmus obliquus*. *Bioresource Technology* 99 , 1111-7.
- Kadam, K. (2002). Environmental implications of power generation via coal microalgae. *Energy* 27 , 905-922.
- Kong, Q., Li, L., Martinez, B., Chen, P., & Ruan, R. (2010). Culture of Microalgae *Chlamydomonas reinhardtii* in Wastewater for Biomass Feedstock Production. *Applied Biochemical and Biotechnology* 160 , 9-18.
- Lardon, L., Helias, A., Sialve, B., Steyer, J., & Bernard, O. (2009). Life-Cycle Assessment of Biodiesel production from Microalgae. *Environmental Science and Technology* , 6475-6481.
- Levine, R., Costanza, M., & Spatafora, G. (2010). *Neochloris oleoabundans* grown on anaerobically digested dairy manure for concomitant nutrient removal and biodiesel feedstock production. *Biomass and Bioenergy*, in Press .
- Lin, L., Chan, G., Jiang, B., & Lan, C. (2007). Use of ammoniacal nitrogen tolerant microalgae in landfill leachate treatment. *Waste Management* 27 , 1376-1382.
- Liu, J., & Ma, X. (2009). The analysis on energy and environmental impacts of microalgae-based fuel methanol in China. *Energy Policy* 37 , 1479-1488.
- Loubiere, K., Olivo, E., Bougaran, G., Pruvost, J., Robert, R., & Legrand, J. (2008). A New Photobioreactor for Continuous Microalgal Production in Hatcheries Based on External Loop Airlift and Swirling Flow. *Biotechnology and Bioengineering* , 132-147.
- Mata, T., Martins, A., & Caetano, N. (2010). Microalgae for biodiesel production and other applications: A review. *Renewable and Sustainable Energy Reviews* 14 , 217-232.
- Melis, A. (2009). Solar energy conversion efficiencies in photosynthesis: Minimizing the chlorophyll antennae to maximize efficiency. *Plant Science* 177 , 272-280.
- Menendez, J., Dominguez, A., Inganzo, M., & Pis, J. (2005). Microwave-induced drying, pyrolysis and gasification (MWDPG) of sewage sludge: Vittrification of the solid residue . *Journal of Analytical and Applied Pyrolysis* 74 , 406-412.
- Munoz, R., & Guieysse, B. (2006). Algal-bacterial processes for the treatment of hazardous contaminants: A review. *Water Research* 40 , 2799-2815.
- NASA (2009). *NASA Envisions "Clean Energy" From Algae Grown in Waste Water* [Online] Available from: NASA News & Events. Ames Home. Features 2009: http://www.nasa.gov/centers/ames/news/features/2009/clean_energy_042209.html [Accessed December 2009]
- Nouals, S., & Isambert, A. (2000). *Modelling of a photobioreactor for microalgae piloting*. Chatenay-Malabry: Ecole centrale des arts et manufactures.

- OEHHA. (2010). *Chronic Toxicity Summary: n-Hexane*. [Online] Available from: Office of Environmental Health Hazard Assessment: http://oehha.ca.gov/air/chronic_rels/pdf/110543.pdf [Accessed September 2010]
- Orpez, R., Martinez, M., Hodaifa, G., El Yousfi, F., Jbari, N., & Sanchez, S. (2009). Growth of the microalgae *Botryococcus Braunii* in secondarily treated sewage. *Desalination* 246 , 625-630.
- Richmond, A. (2004). *Handbook of Microalgal Culture. Biotechnology and Applied Phycology*. Oxford: Blackwell Science.
- Sander, K., & Murthy, G. (2010). Life cycle analysis of algae biodiesel. *International Journal of Life Cycle Assessment* 15 , 704-714.
- Sazdanoff, N. (2006). *Modeling and Simulation of the Algae to Biodiesel Fuel Cycle*. Ohio: Department of Mechanical Engineering. The Ohio State University.
- Sheehan, J., Camobreco, V., Duffield, J., Graboski, M., & Shapouri, H. (1998a). *Life Cycle Inventory of Biodiesel and Petroleum Diesel for Use in an Urban Bus*. Colorado: National Renewable Energy Laboratory.
- Sheehan, J., Dunahay, T., Benemann, J., & Roessler, P. (1998b). *A Look Back at the U.S. Department of Energy's Aquatic Species Program—Biodiesel from Algae*. Colorado: National Renewable Energy Laboratory.
- Shimamatsu, H. (2004). Mass production of *Spirulina*, an edible microalga. *Hydrobiologia* , 39-44.
- Sialve, B., Bernet, N., & Bernard, O. (2009). Anaerobic digestion of microalgae as necessary step to make microalgal biodiesel sustainable. *Biotechnonology Advances* 27 , 409-416.
- Skjanes, K., Knutsen, G., Kallqvist, T., & Lindblad, P. (2008). H₂ production from marine and freshwater species of green algae during sulfur deprivation and considerations for bioreactor design. *International Journal of Hydrogen Energy* 33 , 511-521.
- Skjanes, K., Lindblad, P., & Muller, J. (2007). BioCO₂ – A multidisciplinary, biological approach using solar energy to capture CO₂ while producing H₂ and high value products. *Biomolecular Engineering* 24 , 405-413.
- Stals, M., Carleer, R., Reggers, G., Schreurs, S., & Yperman, J. (2010). Flash pyrolysis of heavy metal contaminated hardwoods from phytoremediation: Characterisation of biomass, pyrolysis oil and char/ash fraction. *Journal of Analytical and Applied Pyrolysis* , 22-29.
- Stepan, D., Shockey, R., Moe, T., & Dorn, R. (2002). *Substak 2.3 - Carbon dioxide sequestering using microalgal systems*. Dakota: U.S. Department of Energy.
- Stephenson, A., Kazamia, E., Dennis, J., Howe, C., Scott, S., & Smith, A. (2010). Life-Cycle Assessment of Potential Algal Biodiesel Production in the United Kingdom: A Comparison of Raceways and Air-Lift Tubular Bioreactors. *Energy Fuels* 24 , 4062-4077.
- Travieso, L. P. (2002). BIOALGA reactor: preliminary studies for heavy metals removal. *Biochemical Engineering Journal* 12 , 87-91.
- Travieso, L., Canizares, R., Borja, R., Benitez, F., Dominguez, A., Dupeyron, R., et al. (1999). Heavy metal removal by microalgae. *Bulletin of Environmental, Contaminant and Toxicology* 62 , 144-151.
- USDE (2010). *National Algal Biofuels Technology Roadmap*. Biomass Program. U.S. Department of Energy. Energy Efficiency & Renewable Energy.

Vonshak, A. (1997). *Spirulina Platensis (Arthrospira): Physiology, Cell-biology and Biotechnology*. London: Taylor & Francis.

Wijffels, R., & Barbosa, M. (2010). An Outlook on Microalgal Biofuels. *Science* 329 , 796-799.

Yen, H., & Brune, D. (2007). Anaerobic co-digestion of algal sludge and waste paper to produce methane. *Bioresource Technology* 98 , 130-134.

Nowadays, microalgae are considered as an attractive organic resource to many scientists and industrials. Microalgae are photosynthetic organisms that require light, carbon dioxide, nutrients and water as well as precisely controlled environmental conditions such as temperature and pH. These organisms are able to produce energy as well as valuable co-products. Some species have been cultivated for food, feed, nutritional components or pharmaceutical products, bringing experience about their cultivation. Open ponds are today the best known cultivation system; however, difficulties such as occupation of large surfaces, poor controlled environmental conditions, water evaporation, and low biomass concentrations and productivities have been observed in these systems. The utilization of open ponds is limited to some species since the risk of contamination is very high.

Photobioreactors are closed systems to which more and more attention is paid. With respect to open ponds, photobioreactors allow, on the contrary, to control parameters such as temperature, dissolved oxygen, nutrient concentrations and water losses. In addition, the culture is separated from other organisms and ecosystems. Many configurations exist, such as tubular photobioreactors, flat panels, plastic bags, and columns photobioreactors. Each configuration presents its own advantages and disadvantages compared to others, referring to hydrodynamics, dissolved oxygen release, carbon dioxide absorption as well as light distribution and availability. At laboratory scale, these reactors have attained high productivities compared to open ponds. Nevertheless, some questions are remaining with respect to hydrodynamics and to light energy available at high biomass concentrations. Columns- photobioreactors present large potential since they occupy small surfaces compared to other photobioreactors. These reactors can be found in many configurations such as bubble, annular columns, and airlift bioreactors.

In the first part of this work, an internal airlift photobioreactor was selected to perform an experimental and theoretical hydrodynamic study, regarding the effect of typical algal concentrations currently found in cultivation. An internal airlift reactor of 21-liter capacity was built by placing two transparent cylinders concentrically. To study the effect of biomass concentrations on the hydrodynamics, particles of 10 μm in diameter were added to the system, in concentrations ranging from 0.15 to 5 g/L. In parallel to the experiments, a hydrodynamic model was developed, based on the Drift Flux model and performing a macroscopic energy balance over the system.

Results have shown that gas holdups and PHL velocities increase with superficial gas velocities. In regimes II and III, the relationship between riser and downcomer gas holdups was obtained experimentally. Results demonstrate that a linear relationship can be established. In the range of particle concentrations used in this study, gas holdups, liquid velocities and solids holdups were not affected. The linear relationship between riser and downcomer gas holdups was neither affected.

It was considered of interest to study the distribution of light energy inside the reactor as well as its evolution according to biomass concentration. The two flux method proposed by Siegel, Howell and Cornet was employed to estimate light availability in the reactor. Results demonstrated that, for a determined biomass concentration, the light availability inside the reactor is highly attenuated from the wall to the center. According to the light intensity imposed to the reactor, there is an optimal biomass concentration at which “dark” zones (where photosynthesis becomes limited) are not observed. As incident-irradiance increases, the energy available for photosynthesis is higher along the two

compartments of the reactor. In consequence, optimal biomass concentrations are more important at higher incident irradiances. On the other hand, the effect of having an opaque riser, establishing light/dark cycles, demonstrates that higher optimal concentrations could be obtained. It was assumed that biomass residence time in the riser was not sufficient to observe respiration, which means that there is no biomass consumption. Modeling results demonstrate that it is interesting that the downcomer cross sectional area to be higher than that of the riser, in order to obtain a larger volume exposed to high intensities and to avoid light attenuation caused by the draft tube. In this case, hydrodynamics of the entire reactor has to be validated.

To estimate biomass productivities, it was assumed that it only depends on the light flux available in the culture, the biomass concentration and the affinity of algae for light. Models proposed by Monod's law and Cornet and Dussap's were used to estimate biomass productivities of the algae *Chlamydomonas reinhardtii*. Results show that Monod's law predicts higher biomass productivities. The differences are found in the maximal growth rate and the optical properties of algae.

By applying the two mentioned models, it was observed that the riser contribution to biomass production is one quarter of the biomass produced in the downcomer. In the riser, biomass production rate was completely offset at 0.5 g/L concentration when low irradiances were applied over the reactor; at high irradiances, productivities were offset at 1.5 g/L. These biomass concentrations are low; however they are in concordance with those found in experimental studies. Modeling results demonstrate that the photosynthetic efficiency, defined as the ratio between the biomass production rate and the absorbed energy, is higher in the riser than in the downcomer.

From biomass productivities, it was of interest to estimate reactor capacity to absorb carbon dioxide and to release dissolved oxygen produced during the culture. For that, it was necessary to determine the overall volumetric mass transfer coefficient which establishes the mass transfer rate between the CO₂ or O₂ and the liquid phase. The overall volumetric mass transfer coefficient was first obtained experimentally in the riser. Results showed that overall volumetric mass transfer increases with air flow rates since it depends on gas holdup and bubble diameters. In consequence, it is higher in the riser than in the downcomer. On the other hand, volumetric mass transfer coefficients were not affected by the presence of particles, fitting with the results obtained in the second chapter.

The mass transport equation was formulated including axial dispersion, convective and diffusion transport. Then, it was compared to the experimental evolution of oxygen in the riser, and low discrepancies were observed. These results allowed the formulation of a model to represent photosynthesis activity in the reactor. The CO₂ or O₂ absorption and production rates were estimated from specific growth rates, formulated from the model proposed by Cornet and Dussap. Results demonstrate that dissolved O₂ increases along the height of riser and downcomer compartments while CO₂ availability decreases. Dissolved O₂ was always higher in the downcomer as consequence of having higher light intensities. In concordance, CO₂ concentrations in the liquid were always lower in the downcomer than in the riser.

The maximal dissolved O₂ was estimated and compared to the maximal values accepted by algae (300% saturation). For an intermediate light intensity, dissolved O₂ never reached maximal values at the tested air flow rates; however, at higher intensities, dissolved O₂ reached maximal acceptance at the lowest air flow rate. Comparing two columns of different heights, modeling results showed that values of dissolved O₂ were lower along the entire height while CO₂ availability was higher.

However, it was observed that the influence of air flow rates on dissolved concentrations was more important than increasing reactor height.

The evolution of total inorganic carbon was estimated together with CO₂ evolution. Both are related according to the pH of the culture. Results demonstrated that if natural air is injected in the reactor, TIC and CO₂ act as limiting factors for microalgae culture, even at the highest air flow rate. On the contrary, when air enriched with 1, 3 and 5% CO₂, is injected into the reactor, values of TIC and CO₂ increase, satisfying culture requirements, even at the lowest air flow rate. Increasing CO₂ concentrations in the air, from 1 to 5%, results in higher dissolved concentrations in the liquid. At 5% concentration dissolved CO₂ provokes inhibition of the photosynthesis. Modeling results demonstrate that the internal airlift reactor proposed here is capable of producing higher productivities than open ponds, while they are similar to other photobioreactors. According to the conditions established here, the reactor is able to release oxygen if light intensities are lower than 110 $\mu\text{mol/m}^2 \cdot \text{s}$ while it is necessary to enrich the air injected to avoid photosynthesis inhibition.

In this work, a second photobioreactor was presented in order to develop a hydrodynamic study. The design was based on the concept of airlift circulation and liquid circulation in a helical wound pipe. Two pipe diameters (25 and 30 mm) were tested in the helical section in order to estimate liquid velocities and liquid residence times. A relationship between the friction factor, the Reynolds number and the curvature ratio was proposed from experimental results. From this correlation, liquid velocities were further obtained in the entire reactor. Results demonstrated that liquid velocities in the helical section are higher than those in the riser and downcomer compartments for all flow rates tested in the reactor.

Comparing results after testing the two pipe diameters, pressure losses were higher in the smaller pipe diameter. Consequently, liquid velocities were lower and liquid residence times higher. Comparing liquid velocities between the two bioreactors, results showed that liquid velocities in the helical section were lower than those in the downcomer of the IAL reactor. Because it was assumed that the downcomer and the helical section are the compartments to be exposed to light, it was necessary to estimate liquid residence time in both sections. Results showed that liquid residence times were much lower in the downcomer of the IAL reactor than in the helical section. The geometry of the HAL reactor allows varying liquid flow rates as a function of pipe and coil diameter as well as the number of spires.

Regarding gas holdups, their values were not affected by changing pipe diameter from 30 to 25 mm. They result to be higher in the HAL reactor than in the IAL reactor for the same air flow rate. The reason is that liquid velocities in the HAL reactor are low to displace the volume of gas. This means that higher mass exchange between the liquid and gas phases would probably occur in the HAL reactor rather than in the IAL reactor. In concordance with these results, it was observed that the power input has to be increased if it is desired to reach similar liquid velocities, while reducing pipe diameter in the helical section.

The model proposed for the HAL reactor was formulated by starting from performing a macroscopic energy balance and using the Drift Flux model. The distribution parameter in the Drift Model was modified in order to have low discrepancies with experimental results. Distribution parameters were different for the two pipes tested here, being higher than the distribution parameter used in the internal airlift reactor.

If microalgae culture is performed in the HAL reactor, a light system supply can be installed inside the helical section. In this case, it would be necessary to estimate oxygen production rates as well as carbon dioxide absorption rates. Since the equivalent length of the coiled pipe is longer than the IAL reactor height, higher levels of dissolved oxygen can be observed as well as carbon dioxide limitation. In consequence, it would be necessary to evaluate if gas holdups and bubble diameters in the riser are able to release the dissolved oxygen accumulated in the helical section.

The exploitation of algal biomass involves not only cultivation but also upstream and downstream processes. To extract valuable products, co-products and wastes from the whole process, it is necessary to provide electricity, cooling and heating as well as nutrients, water, carbon dioxide, and some fossil based products. Nutrients include mainly nitrogen and phosphorus which, according to experimental studies, might be obtained from wastewaters. Carbon dioxide can be provided by flue gases after proper conditioning.

The feasibility of microalgae cultivation depends on the energy and greenhouse-gas-emission balances. Studies performed up until the present have shown that microalgae cultivation has to be integrated in production lines existing in industrial facilities. One example is the combination of microalgae culture with biodiesel production, anaerobic digestion, and the utilization of wastewater use. The valuable products are biodiesel, biogas, glycerin and algae cake while electricity and heat can be exchanged among the processes.

Potential environmental impacts are associated to this process. If waters in open ponds are enriched with nutrients, risks of ammonia volatilization and N_2O emissions exist. In addition, if waters are not properly handled, ground and confined waters can be polluted, causing environmental damages such as eutrophization. On the other hand, water consumption is a controversial issue in microalgae cultivation. Cultivation in open ponds requires more water than photobioreactors due to evaporation, which depends largely on culture location. Since harvesting is frequently performed, it is necessary to determine whether water can be recycled back to the culture or not, and the volume fraction wasted each time. Upstream and downstream processes of microalgae culture require water as well. If wastewaters and/or rain water are used in microalgae cultivation, water consumption will probably decrease.

Results of this work demonstrate that it is indispensable to develop a preliminary study of the entire process. It is essential to find best microalgae species able to produce desired compounds and that can survive under the specific environmental conditions. Then, the most appropriated system for cultivation must be selected according to the physical characteristics of algae, e. g. affinity for light, physical structure to resist high turbulences, maximal acceptance of CO_2 concentrations, nutrients concentrations required, etc. This must be evaluated together with the hydrodynamic of the reactor or pond. Microalgae cultivation can be then integrated into an industrial facility able to provide microalgae requirements like CO_2 and/or nutrients, while water consumption is minimized.

The challenge is to build a biorefinery based on an integrated process, capable of producing valuable products. This concept must integrate the principles of industrial ecology, guaranteeing an energy positive balance while having nearly zero greenhouse gas emissions and environmental impacts.

In the first part of this work, the hydrodynamic study of an internal airlift reactor was based on the Drift Flux model while performing a macroscopic energy balance over the system. To apply the Drift Flux model, it was necessary to estimate the bubble diameter and the terminal bubble velocity. To validate the relationships proposed by Davidson, Schüler and Wallis, it would be useful to determine bubble diameter and terminal bubble velocity experimentally. Authors generally assumed bubble velocities without taking into account liquid and gas properties. It would be of interest to measure these two parameters in microalgae growth medium, to verify at what extent the liquid properties affect the bubble diameter and the terminal bubble velocity.

To evaluate hydrodynamic performance of the internal airlift reactor, it is highly recommended to perform microalgae culture. It is necessary to evaluate the maximum air flow rate that does not damage the cells. Some microalgae cells do not have rigid walls at all, being thus very sensible to turbulences. For this reason, it would be helpful to know previously the physical characteristics of the specie (e.g. composition of cell walls). Also the air flow rate has to be well coupled with liquid residence time, in each section of the reactor, if it is desired to expose microalgae to light/dark cycles.

With respect to the light distribution study, the model could be improved by taking into account the presence of bubbles in the reactor. Bubbles provoke dispersion of light, which will vary according to bubble sizes, trajectories, and velocities. On the other hand, it will be interesting to evaluate the feasibility of introducing reflecting materials inside the reactor, as it has been proposed by Richmond. However, this might alter the hydrodynamics of the system or even increase the frequency of bio-fouling. To complement this study, it is recommendable to evaluate light distribution around the reactor. If the reactor is placed indoors, working under artificial light, it could be useful to install reflecting walls that can reduce light energy losses, reducing the number of lamps and thus, reducing electricity consumption. On the other hand, if the reactor installed outdoors, the light distribution will have to be evaluated according to the location, season, and time of the day.

Regarding the microalgae growth model, it will be necessary to validate results with the cultivation of *Chlamydomonas reinhardtii* in the internal airlift reactor. For that, same conditions of light intensity, temperature, and growth medium have to be established according to Cornet and Dussap. Similarly, dissolved O_2 and CO_2 will have to be measured in order to validate modeling results regarding reactor capacity to absorb CO_2 and release O_2 .

Concerning the helical airlift reactor proposed here, the connection of the helical tube with the riser should be reconsidered, in order to obtain much energy as possible from the sparger. As for internal airlift reactor, the performance of the reactor will have to be validated with microalgae culture. Cultivating *Chlamydomonas reinhardtii*, at the same environmental conditions will allow to compare the performances of both helical airlift reactor with internal airlift reactor. Moreover, it will be necessary to determine the maximum number of spires in the helical section which prevents accumulation of dissolved oxygen to toxic levels. This has to be coupled to the riser capacity to release the oxygen.

Moreover, if the helical airlift reactor is installed indoors and exposed to artificial light, the light profile should be modeled when lamps are placed inside the helical section. In this case, it might be

reasonable to install a small pipe diameter in the helical section. However, attention must be paid not increase the risk of bio-fouling increase.

Concerning the hydrodynamics of the helical airlift reactor, it would be useful to examine whether the applicability of the friction factor correlation obtained in this study could be extended. In this perspective, different curvature ratios can be tested in the helical section. This would spread the range of liquid velocities at which the reactor could operate.

Finally, it will be interesting to study the feasibility of these two reactors at a larger scale. It is therefore necessary to first to establish the desired biomass production level, working volume, land surface, and environmental conditions, in order to design the most appropriated arrangement of reactors to constitute the cultivation system. Here, the cultivation of natural microalgae species (non genetically modified algae able to grow in wastewaters), should be a priority. Subsequently, the system could be placed in a specific production process, studying potential synergies, including inflows and outflows, specifically gaseous, liquids, and solids resulting wastes. This analysis should include total energy and water consumptions as well as greenhouse gas emissions associated to the complete chain process. In parallel, a technical-economical analysis should be performed under the established conditions.

I.1. Mass transferring modeling

Dymola is a solver compatible with open Modelica®. The riser and downcomer compartments are two different models connected by gas and liquid phases (Figure 1). In the riser and downcomer compartments, mass transport equations are developed in Modelica text.

To obtain oxygen generation and carbon dioxide absorption rates, it is necessary to estimate the biomass productivity in each section as a function of the incident irradiance. Biomass productivity is the variation of biomass concentration along the time. The derivative is calculated (function `der`) from the data contained in a database (type `CombiTable`). The database comprises the biomass concentration as a function of the light intensity.

Oxygen generation and carbon dioxide absorption rates are then introduced into the mass transport equation (Table III.11). Knowing volumetric mass transfer coefficients and initial conditions, the dissolved O_2 and CO_2 profiles along the reactor and along the time are obtained. Final results are then extracted from Modelica to the Workspace of the programming language Matlab®.

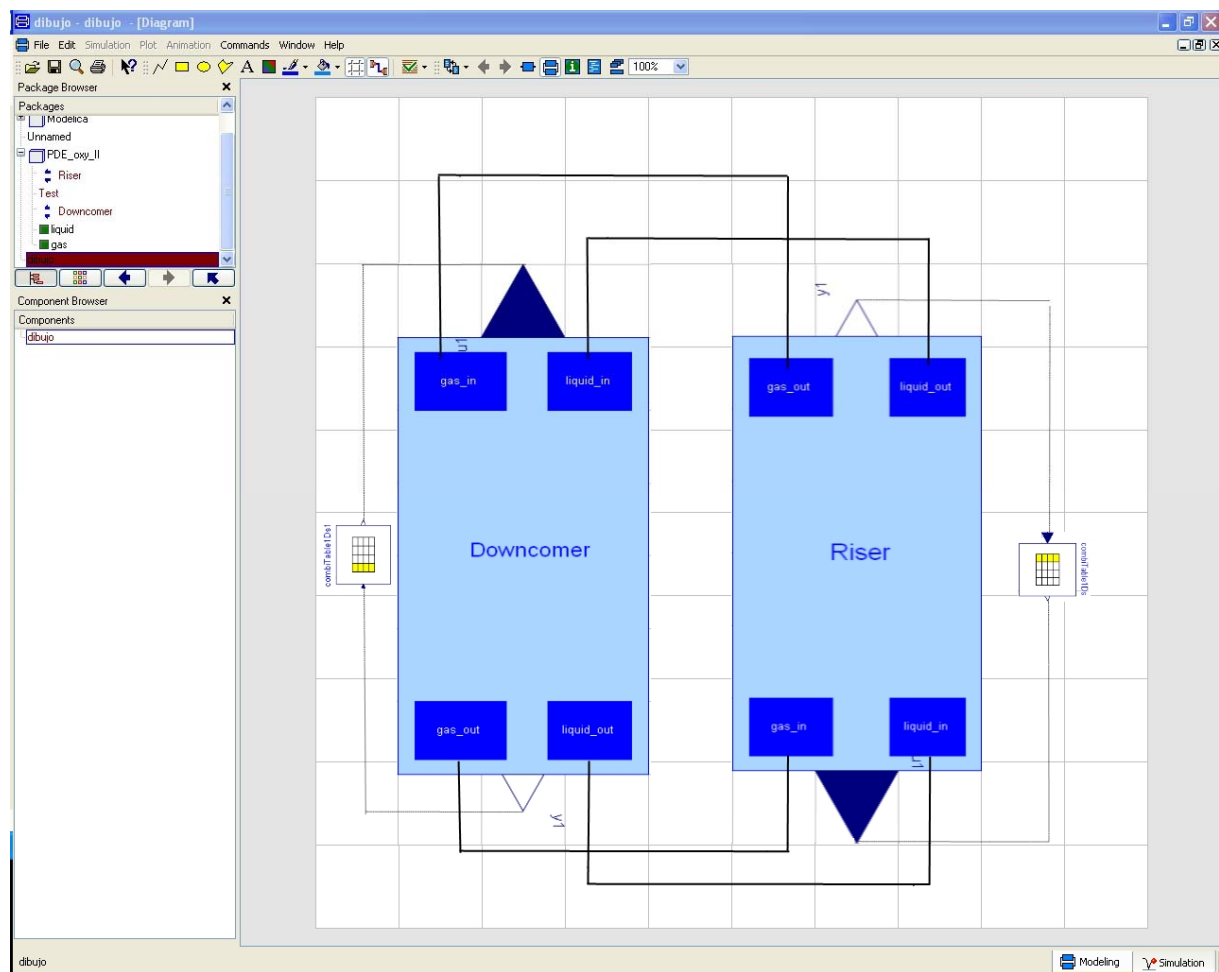


Figure 1. Dymola interface. Simulation of transport equation for the O_2 and CO_2 .

Conception et analyses énergétique et environnementale d'un bioréacteur à microalgues pour la production d'énergie

RESUME : Les microalgues sont des organismes photosynthétiques considérés pour la production d'énergie. Les photobioréacteurs sont des systèmes fermés avec des productivités plus importantes que les bassins ouverts. Cette étude concerne l'expérimentation et la modélisation d'un réacteur du type « airlift à circulation interne ». Des microparticules sont ajoutées pour modéliser les concentrations d'algues dans le réacteur. Les fractions du gaz et les vitesses du liquide ne sont pas affectées par la présence de microparticules. La distribution de la lumière dans le réacteur est calculée en considérant les concentrations de la biomasse et les propriétés optiques des algues. La lumière est atténuée de la paroi jusqu'au centre du réacteur et cette atténuation augmente avec la concentration de la biomasse. Les productivités de biomasse, estimées en utilisant deux modèles biologiques, montrent que celles obtenues dans les photobioréacteurs sont plus élevées que celles obtenues dans les bassins ouverts. La capacité du réacteur pour absorber du CO_2 et produire de l' O_2 est évaluée selon les productivités obtenues. A intensités lumineuses modérées, l' O_2 dissout n'atteint pas le niveau d'intoxication, même pour de faibles débits d'air. Le CO_2 et le CIT deviennent limitant si de l'air naturel est injecté dans le bioréacteur. Il est donc nécessaire d'injecter de l'air enrichi en CO_2 . L'hydrodynamique d'un réacteur airlift hélicoïdal est également présentée. Deux diamètres de tuyaux sont testés dans la section hélicoïdale. Une corrélation est proposée pour estimer le coefficient de frottement en fonction du Reynolds et le rapport entre le diamètre d'enroulement et le diamètre de tuyau.

Pour réaliser la culture de microalgues à l'échelle industrielle, il est indispensable d'obtenir un bilan énergétique positif et de faibles émissions de GES. Pour cela, il faudra intégrer la culture dans des procédés de transformation tels que la production de biodiesel et la digestion anaérobie.

Mots clés : microalgue, photobioréacteur, hydrodynamique, réacteur airlift de circulation interne, réacteur airlift hélicoïdal, intégration de la culture de microalgues

Energy and environmental analysis of a bioreactor for microalgae culture for energy production

ABSTRACT: Microalgae are photosynthetic organisms considered today for energy production. Photobioreactors are closed systems that present higher productivities than open ponds. In this study, a hydrodynamic model is developed for an internal airlift reactor and validated experimentally. Microparticles are added to the reactor at concentrations found in current microalgae cultures. Results show that gas hold-up and liquid velocities are not affected by the presence of particles. Light distribution and availability in the internal airlift reactor is calculated, taking into account biomass concentrations and algae optical properties. Light is attenuated from the wall to the reactor center while this attenuation increases with biomass concentrations. Based on two biological models, biomass productivities achieved in photobioreactors are higher than in open ponds. From biomass productivities, the reactor capacity to absorb CO_2 and to release O_2 is estimated. Results show that at moderate irradiances, dissolved O_2 levels do not reach intoxication at low air flow rates. If natural air is injected into the reactor, CO_2 and TIC become limiting therefore, it is necessary to inject CO_2 -enriched air. The hydrodynamics of a helical airlift reactor is also presented. Two pipe diameters are tested in the helical section. A mathematical correlation is proposed to estimate the friction factor as a function of the Reynolds number and curvature ratios.

To perform microalgae culture at large scale, it is necessary to obtain a positive energy and GHGs balance. Therefore, microalgae culture has to be integrated in a system where conversion processes such as biodiesel production and anaerobic digestion are performed.

Keywords : microalgae, photobioreactor, hydrodynamic, internal airlift reactor, helical airlift reactor, microalgae culture integration